Metabolic Regulation via a Nuclear Receptor/miRNA Pathway

Lillian J. Eichner

Department of Biochemistry
McGill University
Montréal, Québec, Canada

December 2012

A thesis submitted to McGill University in partial fulfillment of the requirements of the degree
of
Doctor of Philosophy

TABLE OF CONTENTS

ABSTRACT

Cancer cell metabolism is often characterized by a shift from an oxidative to a glycolytic bioenergetic pathway, a phenomenon known as the Warburg effect. miR-378* is embedded within *PPARGC1b* which encodes PGC-1β, a transcriptional regulator of oxidative energy metabolism. We show that miR-378* acts as a molecular switch involved in the orchestration of the Warburg effect in breast cancer cells via interference with the PGC-1β/ERRγ bioenergetics transcriptional pathway. Moreover, we identify that the expression of miR-378* is regulated by the breast cancer oncogene ERBB2, and that its expression in human breast cancer correlates with disease progression. Furthermore, we uncover that CAMKK2, the upstream kinase of the cellular energy sensor AMPK, is a functional direct target of miR-378* in breast cancer cells, through which miR-378* represses AMPK pathway activity.

We have identified that modulation of the relative availabilities of the Estrogen-Related Receptor (ERR) isoforms ERRα and γ is capable of inducing the Warburg effect. We then turned to an *in-vivo* system to further investigate the role of ERR in breast cancer. We found that the absence of ERRα delays ERBB2-induced mammary tumor onset but accelerates disease progression after onset. Moreover, tumor bearing ERRα-/- mice exhibit signs of cancer cachexia, including failure to maintain normal body weight, heightened inflammation, and metabolic derangements such as elevated serum amino acids, molecular markers in the skeletal muscle and adipose tissue, and reduced adipose mass. Together, we identify that systemic ablation or inhibition of ERRα may render the host more susceptible to cancer cachexia, a disease characterized by elevated inflammation, metabolic derangements and tissue atrophy.

The absence of mir-378 mouse models limited such *in-vivo* study of the functionally-related miRNA. Therefore, we produced mir-378 conditional and total knockout mouse models, which revealed thermogenesis-related phenotypes in the brown adipose tissue (BAT).

RÉSUMÉ

Le métabolisme des cellules cancéreuses est souvent caractérisé par une utilisation préférentielle de la voie de la glycolyse, au détriment de la phosphorylation oxydative, un phénomène connu sous le nom d'effet de Warburg. Le microARN miR378* est situé dans le gène *PPARGC1b*, qui code pour la protéine PGC-1β, un régulateur transcriptionel du métabolisme oxidatif. Nous avons démontré que le miR378*, en interférant ERRγ, est impliqué dans l'orchestration de l'effet de Warburg dans les cellules tumorales du sein. De plus, nous avons identifié que l'expression du miR378* est régulée par l'oncogène ERBB2 et corrèle avec l'agressivité du cancer du sein chez l'humain. Nous avons aussi établi que CAMKK2 est une cible directe du miR378* dans les cellules cancéreuses du sein, via laquelle miR378* réprime l'activité d'AMPK.

Nous avons observé que la disponibilité relative des isoformes α et γ du récepteur associé au récepteur des estrogènes (ERR) était capable d'induire l'effet de Warburg. Ceci nous a amené à explorer le rôle d'ERR dans le développement du cancer du sein. Nous avons observé, dans un modèle de tumeur mammaire, que l'absence d'ERRα ralentissait l'apparition du cancer, mais augmentait la vitesse de la croissance tumorale une fois la tumeur établie. De plus, les souris *knock-out* pour ERRα ayant une tumeur montre des signes cachexie, incluant une perte de poids, la présence d'inflammation et des désordres métaboliques tels qu'un niveau élevé d'acides aminés dans le sérum et une réduction de la masse adipeuse. Dans l'ensemble, nos résultats démontrent que l'inhibition d'ERRα rend les animaux plus susceptible à la cachexie cancéreuse, une maladie caractérisée par un niveau élevé d'inflammation, des dérangements métaboliques et une atrophie tissulaire.

Finalement, nous avons développé un modèle de souris *knock-out*, total ou conditionnel, pour le mir378. Nos résultats suggèrent notamment une implication pour le mir378 dans des tissus adipeux bruns.

PUBLICATIONS

ARISING FROM THE WORK OF THE THESIS

- **Eichner LJ**, Perry MC, Dufour CR, Bertos N, Park M, St-Pierre J, Giguère V. miR-378* Mediates Metabolic Shift in Breast Cancer Cells via the PGC-1β/ERRγ Transcriptional Pathway. *Cell Metabolism*. 2010 Oct 6; 12(4): 352-361.

- **Eichner LJ**, Giguère V. Estrogen-related receptors (ERRs): A new dawn in transcriptional control of mitochondrial gene networks. *Mitochondrion*. 2011 July; 11(4): 544-552. Review.

- **Eichner LJ*,** Wang SRX*, Chaveroux C, Tsang DWK, Giguère V. miR-378* Regulates the AMPK Pathway in Breast Cancer Cells Through Direct Control of CAMKK2. *To be submitted shortly.*
*Equal contribution.

- **Eichner LJ**, Chaveroux C, Perry MC, Dufour CR, El-Attar M, Sinitsyn M, Muller WJ, Giguère V. Systemic ablation of ERRα predisposes the host to cancer cachexia. *To be submitted shortly.*

- **Eichner LJ**, Zhao X, Chaveroux C, Dufour CR, Perry MC, Wang S, Giguère V. A Knockout Mouse Model Reveals Essential Roles for miR-378/378* in Brown Adipose Tissue Function. *To be submitted shortly.*

OTHER PUBLICATIONS

- Charest-Marcotte A, Dufour CR, Wilson BJ, Tremblay AM, **Eichner LJ**, Arlow DH, Mootha VK and Giguère V. The homeobox protein Prox1 is a negative modulator of ERRα/PGC-1α bioenergetic functions. *Genes & Development*. 2010 Mar 15; 24(6): 537-42.

- Dufour CR, Levasseur MP, Pham NH, **Eichner LJ**, Wilson BJ, Charest-Marcotte A, Duguay D, Cermakian N, Giguère V. Genomic Convergence among ERRα, PROX1 and BMAL1 in the Control of Metabolic Clock Outputs. *PLoS Genetics*. 2011 June; 7(6): e1002143.

- Giguère V, Dufour CR, **Eichner LJ**, Deblois G, Cermakian N. Estrogen-Related Receptor α, the Molecular Clock, and Transcriptional Control of Metabolic Outputs. *Cold Spring Harbor Symposia on Quantitative Biology*. 2011 Dec 16, 76:57-61.

- Chaveroux C, **Eichner LJ***, Dufour CR*, Shatnawi A, Fonseca BD, Bourque G, Sonenberg N, Giguère V. Molecular and Genetic Crosstalks Between mTOR and ERRα are Key Determinants of Rapamycin-induced Non-Alcoholic Fatty Liver. *In Review.*
*Equal contribution.

- Perry MC, **Eichner LJ,** Dufour CR, Tsang, D.W.K., Muller WJ, Giguère V. Trastuzumab induces cardiotoxicity via ablation of an ErbB2-E2F-1 molecular axis. *To be submitted shortly.*

ACKNOWLEDGEMENTS

I am grateful to my supervisor, Vincent Giguère, for all the opportunities for learning and growth that he provided. This doctoral work was an invaluable learning experience for me that provided a solid and well-rounded foundation of knowledge, ability and confidence that will stay with me for the rest of my scientific career, and I am very thankful to Vincent for everything.

I am grateful to all lab members who have contributed to my work and my training. To Cathy and Marie-Claude for their positive and motivating attitudes. To Cathy, Marie-Claude and Cedric for their invaluable help and contstructive discussions. To Cathy for critical reading of this thesis. To Majid for the encouragement and support. To Marie-Claude and Cedric for patience through my long process of learning to work with animals. To Xinhao for putting up with me when it was truly the blind leading the blind. To Sarah for being the best undergrad ever. I am grateful to all for helpful discussions.

I am grateful for the constructive and productive opportunity to collaborate with Julie St-Pierre. As my first collaborative experience, it raised the bar and brought fresh ideas and energy to the project at a challenging time. I am also thankful for the excellent and stimulating breast cancer research environment in the Rosalind and Morris Goodman Cancer Research Centre, which allowed me to obtain valuable suggestions and access to materials, without which my work could not have been published as well.

I would like to thank Maxim for his unending support through everything, his enjoyment of my excitement about science and my research, his patience for listening through every single practice talk, and

his company during the late-at-night lab trips. A shout-out to Felix for unending purrs despite never getting any lab mice for his own enjoyment.

I would like to thank my friends and family for their support. I am thankful to my parents for instilling in me an unending curiosity, for allowing me the luxury to follow what interests me, and for being content with whatever I choose to do (including, if necessary, being a barista at Starbucks). A word of thanks to my Grandfather for his >100 years of respect and appreciation for science, my Grandmother who is still so happy to hear that I graduated from High School, and Mutti who kindly and supportively feigned excitement and interest over my English-language publications despite them being fundamentally incomprehensible to her due to the language.

I am thankful to the FRSQ and the MUHC for funding.

CONTRIBUTION OF AUTHORS

Chaveroux, Cédric: Participated in the design and execution of the ES cell screen. Aided with animal husbandry, sample collection from animal models and some tumor volume measurement, as well as generation of the mir-378 stable cell clones.

Dufour, Catherine: Aided with ERRγ ChIP, sample collection from animal models, primer design for Chapters IV and V, and IPA analysis of tumor microarray.

El-Attar, Mayssun and Sinitsyn, Maxim: Performed the statistical analysis on the mouse weight data throughout mammary tumorigenesis.

Giguère, Vincent: Lab director, general guidance.

Muller, William: Provided the NMuMG and NT2196 cell lines, and the MMTV-NeuNDL2-5 mouse model.

Perry, Marie-Claude: Performed siERBB2 experiments and subsequent *PPARGC1b* detection in Chapter II, also western blots on siERR samples (Fig. 2.4B). Aided with tumor volume measurement and some tumor palpation. Processed samples for electron microscopy.

Park, Morag and Bertos, Nick: Provided the Tissue Microarray slide.

St-Pierre, Julie: Provided training for measuring oxygen consumption. Participated in discussions about metabolic experiments and manuscript revision.

Tsang, David: Participated in luciferase validation of CAMKK2 predicted target site.

Wang, Sarah: Performed most experiments in Chapter II and participated in manuscript preparation.

Zhao, Xinhao: Participated in planning the targeting strategy for the mir-378CKO mice, and cloned the targeting vector.

LIST OF FIGURES

Chapter I

Chapter II

Chapter III

Chapter IV

Chapter V

Appendix

LIST OF TABLES

Chapter II

Appendix

LIST OF ABBREVIATIONS

2HG	2-hydroxyglutarate
3’ UTR	3’ untranslated region
ACC	acetyl-coenzyme a carboxylase
ACL	ATP-citrate lyase
AMPK	5' AMP-activated protein kinase
AMP	adenosine monophosphate
ATP	adenosine triphosphate
BAT	brown adipose tissue
CAMKK2	Calcium/calmodulin-dependent protein kinase kinase 2
cDNA	complementary DNA
ChIP	chromatin immunoprecipitation
CS	citrate synthase
DCIS	ductal carcinoma *in situ*
DNA	deoxyribonucleic acid
ER	estrogen receptor
ERBB2	Human epidermal growth factor receptor 2
ERR	estrogen-related receptor
ERRE	ERR response element
ES cells	embryonic stem cells
FAO	fatty acid oxidation
FAS	fatty acid synthase
FDG-PET	^{18}F-deoxyglucose positron emission tomography
FH	fumarate hydratase
FISH	fluorescence *in situ* hybridization
GABPA	GA-binding protein alpha chain
GLS	glutaminase
H&E	hematoxylin and eosin
HDAC	histone deacetylase
HER2	human epidermal growth factor receptor 2
IDH	isocitrate dehydrogenase

IFN	interferon
IRF	IFN-regulatory factor
KO	knockout
LDH	lactate dehydrogenase
LKB1	liver kinase b1
LMF	lipid-mobilizing factor
miRNA	microRNA
Neo	neomycin
NRF-1	Nuclear respiratory factor 1
NR	nuclear receptor
O-GlcNAc	O-linked N-acetylglucosamine
OGT	*O*-linked *N*-acetylglucosamine transferase
OXPHOS	oxidative phosphorylation
PCAF	p300 coactivator associated factor
PCR	polymerase chain reaction
PEP	phosphoenolpyruvate
PGC-1	peroxisome proliferator activated receptor γ coactivator-1
PIF	proteolysis-inducing factor
PK	pyruvate kinase
PPAR	peroxisome proliferator activated receptor
PR	progesterone receptor
PROX1	homeobox protein prospero-related homeobox 1
RIP140	receptor interacting protein 140
RNA	ribonucleic acid
ROS	reactive oxygen species
SDH	succinate dehydrogenase
SIRT	sirtuin homolog
SRC	steroid receptor coactivators
TCA cycle	tricarboxylic acid cycle
TMA	tissue microarray
UDP-GlcNAc	Uridine diphosphate N-acetylglucosamine

WAT	white adipose tissue
WT	wildtype

CHAPTER I: Introduction

1.1 The Nuclear Receptor Superfamily

Nuclear receptors are a group of transcription factors which are typically inducible by small lipophilic hormones, vitamins and metabolites to directly regulate their target gene expression (Evans, 1988). Forty eight receptors comprise the human nuclear receptor superfamily, and these can be separated into subgroups based on the current understanding of each receptors' ligand: receptors with known ligands, receptors discovered without any known endogenous ligand correspondingly named Orphan Receptors, and the Adopted Orphan Receptors for which ligands were identified after the receptors' original discovery (Mangelsdorf et al., 1995). Nuclear receptors in all groups have been implicated in an extensive range of physiological functions and disease states including, of particular interest throughout this thesis, metabolic function. One major group of nuclear receptors implicated in metabolic regulation and control are the Estrogen-Related Receptors, or ERRs, a subfamily of orphan receptors comprised of ERRα (NR3B1), ERRβ (NR3B2) and ERRγ (NR3B3) (Giguere, 2008b).

1.2 Estrogen-Related Receptors

1.2.1 Fundamentals

The ERRs, as their name implies, are members of the superfamily of nuclear receptors that share close structural kinship with estrogen receptors α (ERα, NR3A1) and β (ERβ, NR3A2) (Giguere, 2002; Giguere et al., 1988; Tremblay and Giguere, 2007). However, the ERRs do not bind natural estrogens nor do they recognize ER binding sites in the intact chromatin (Deblois et al., 2009b; Giguere et al., 1988). So far, regulation of the transcriptional activity of the ERRs has not been associated with any endogenous hormones or metabolites and the three ERR isoforms are

still considered orphan receptors. Nonetheless, several synthetic compounds have been identified or developed that possess the ability to influence the function of the ERRs as transcription factors (Busch et al., 2004; Chao et al., 2006; Coward et al., 2001; Duellman et al., 2010; Takayanagi et al., 2006; Tremblay et al., 2001a; Tremblay et al., 2001b; Yu and Forman, 2005; Zuercher et al., 2005). These compounds, as most ligands of nuclear receptors, modulate the transcriptional activity of the ERRs by either promoting or inhibiting the interaction of the ERRs with specific coactivator or corepressor proteins. In particular, the ERRs have been shown to serve as a primary conduit for the action of the members of the PPARγ coactivator-1 (PGC-1) family (Gaillard et al., 2006; Huss et al., 2002; Kamei et al., 2003; Laganiere et al., 2004a; Mootha et al., 2004; Schreiber et al., 2004). In this respect, PGC-1α and β are often considered as protein ligands for the ERRs. The interaction of the ERRs with the PGC-1s and other coregulatory proteins are discussed in more detail below.

1.2.2 Patterns in tissue expression: hinting at a role in energy metabolism

While ERRα is ubiquitously expressed, its transcript generally displays high expression levels in tissues with elevated metabolic demands such as the heart, kidney, skeletal muscle, intestine, and brown adipose tissue (Giguere et al., 1988; Sladek et al., 1997b). Similarly, the ERRβ transcript can be found predominantly in the heart and kidneys as well as in the eye but at lower levels in a few other tissues that include the trophoblastic lineage in the developing placenta, mouse embryonic stem cells and the inner ear (Chen and Nathans, 2007; Luo et al., 1997; Onishi et al., 2010; Pettersson et al., 1996; Xie et al., 2009). ERRγ is also selectively expressed, its relevance in metabolic contexts confirmed by its high expression in tissues such as the embryonic and adult heart, stomach and kidneys (Alaynick et al., 2007a; Alaynick et al., 2010). Both ERRα and

ERRγ are also expressed in the brain, although their roles in that context are largely unexplored. Extensive expression profiling for all members of the superfamily of nuclear receptors in 39 mouse tissues validated the preferential expression of the three ERRs in metabolic tissues (Bookout et al., 2006).

1.2.3 ERRs interact with coregulatory proteins involved in metabolic control

Coregulator proteins have the ability to impart specific transcriptional properties to their nuclear receptor partners and this molecular mechanism of action is exceptionally pertinent to the biological functions of the ERRs (Feige and Auwerx, 2007). In particular, the transcriptional activity of the ERRs has been extensively linked to the members of the PGC-1 family of coactivators (Hock and Kralli, 2009). Members of the peroxisome proliferator activated receptor (PPAR) γ coactivator-1 (PGC-1) family (PGC-1α, PGC-1β and PPRC1) of transcriptional coactivator proteins are themselves essential regulators of cellular energy metabolism (Lin et al., 2005). The coactivation of the ERRs by the PGC-1 proteins has been studied to varied degrees, with most focus to date on PGC-1α. The PGC-1 proteins not only display similar tissue expression patterns to that of the ERRs, mostly in tissues with high metabolic demands, but have also been directly implicated in the control of energy homeostasis including mitochondrial functions such as OXPHOS, FAO, ROS production and mitochondrial biogenesis (Arany et al., 2005; Knutti et al., 2001; Leone et al., 2005; Lin et al., 2005; Lin et al., 2004; Mootha et al., 2004a; Rodriguez-Calvo et al., 2006; Rohas et al., 2007; Sonoda et al., 2007c; Sonoda et al., 2007d; Uldry et al., 2006). Indeed, much of the function of the PGC-1s depends on the presence of one or more ERR isoform which physically interact with PGC-1 through a specific nuclear receptor interaction motif (Gaillard et al., 2007; Gaillard et al., 2006; Huss et al., 2002; Ichida et al., 2002; Kamei et al., 2003; Laganiere

et al., 2004b; Schreiber et al., 2003; Sonoda et al., 2007a).

Important differences between the PGC-1s have also been uncovered. PGC-1α was originally identified from brown fat as a nuclear receptor coactivator dramatically elevated upon cold exposure of mice (Puigserver et al., 1998), and later found to be induced by other short-term physiological stimuli including exercise (Baar et al., 2002; Goto et al., 2000; Norrbom et al., 2004) and fasting (Lehman et al., 2000). Intriguingly, despite the largely parallel basal tissue expression of PGC-1α and PGC-1β (Kressler et al., 2002), while PGC-1β was induced in the liver upon fasting in parallel to PGC-1α induction (Lin et al., 2002), PGC-1β was not found to respond to cold exposure (Lin et al., 2002) or exercise (Mortensen et al., 2007) in a manner similar to the PGC-1α response. This suggests that, at least in certain physiological contexts, PGC-1α may be responsible for carrying out more short-term responses, whereas the relative stability of PGC-1β levels may indicate more of a role in the maintenance of longer-term metabolic homeostasis. Furthermore, studies of skeletal muscle cells have demonstrated precise differences in PGC1-α and -β function within the same physiological context. These two proteins were shown to have both overlapping and different effects on the expression of genes important for skeletal muscle fiber transition (Mortensen et al., 2006). Functionally, PGC-1α and -β were shown to increase mitochondrial metabolism, but PGC-1β, which uniquely induces the expression of several genes involved in reactive oxygen species scavenging, does not induce proton leak to the same extent as PGC-1α (St-Pierre et al., 2003b). Together, this evidence suggests different physiological functions for these two PGC-1 family members, although the thorough investigation of these differences has yet to be completed.

Other coactivators including steroid receptor coactivators (SRC)-1, -2 and -3 also associate with the ERRs in order to regulate hepatic metabolism, fat storage and energy balance (Jeong et al., 2006; Louet et

al., 2006; Picard et al., 2002; Wang et al., 2006) and these proteins also directly interact with the ERRs (Hong et al., 1999; Xie et al., 1999). Receptor interacting protein 140 (RIP140) is an ERR corepressor which interacts with ERRα (Augereau et al., 2006; Castet et al., 2006; Debevec et al., 2007; Sanyal et al., 2004) and regulates important metabolic pathways including OXPHOS (Christian et al., 2006; Leonardsson et al., 2004; Seth et al., 2007). More recently, Yang et al. (Yang et al., 2009) identified Bcl3 as a coactivator of ERRα, and showed that it interacts with and synergizes with ERRα and PGC-1α on the PDK4 promoter in cardiac myocytes. Our group has recently identified the homeobox protein prospero-related homeobox 1 (Prox1) as a factor that can counteract the action of PGC-1α on the transcriptional activity of ERRα (Charest-Marcotte et al., 2010a). Prox1 physically interacts with both ERRα and PGC-1α, occupies the promoter regions of metabolic genes on a genome-wide scale, and inhibits the activity of the ERRα/PGC-1α complex on these promoters. As expected from these observations, ablation of Prox1 and ERRα was shown to have opposite effects on the respiratory capacity of liver cells. The biological relevance of Prox1 in metabolic control was further validated by the concurrent finding from a large genetic study of glycemic traits that identified Prox1 as type 2 diabetes risk loci (Dupuis et al., 2010).

1.2.4 Post-transcriptional regulation

Activity of the ERRs is also controlled by post-translational modification. ERRα is a heavily phosphorylated protein (Sladek et al., 1997b). Phosphorylation of ERRα has been shown to promote selective regulation of target genes (Barry and Giguere, 2005; Tremblay et al., 2008). Furthermore, ERRα and γ are sumoylated in a phosphorylation-dependent manner (Tremblay et al., 2008; Vu et al., 2007). ERRα also interacts with and is acetylated by p300 coactivator associated factor (PCAF). Coexpression of PCAF reduced the transcriptional activity of

ERRα and, reciprocally, the histone deacetylase 8 (HDAC8) and sirtuin 1 homolog (Sirt1) enhanced ERRα transcriptional function (Wilson et al., 2010). These results showed that ERRα is an acetylated protein and demonstrated the existence of a dynamic acetylation/ deacetylation switch involved in the control of ERRα transcriptional activity on the promoters of genes such as *Got1* and *Cycs*. Altogether, post-translational modifications provide a mechanism through which different signaling events can promote unique and precise target gene regulation programs through the ERRs. However, despite action on individual metabolic genes, it remains to be investigated how these post-translational modifications could influence broad ERR-dependent metabolic gene programs.

miRNAs are short endogenous RNAs which inhibit protein translation of their mRNA targets (expanded upon below) and have recently been shown to play a role in ERR-dependent genetic programs. ERRγ has been shown to control the expression of two miRNAs known as miR-433 and miR-127 (Song and Wang, 2008, 2009). A role for miR-433 and miR-127 in metabolic control remains to be investigated. Two further studies, published after Chapter II of this thesis, extend the knowledge of miRNA direct control of ERRγ (Belleannee et al., 2012) and ERRα (Zhao et al., 2012), the former in the context of the human epididymis, the latter in the context of breast cancer cells. While it is clear that miRNA play an important role in the regulation of ERR activity, it is also evident that our current understanding of the miRNA/ERR molecular networks leave much to be revealed.

1.2.5 ERRs in metabolic regulation

1.2.5.1 Phenotypes of knock-out mouse models implicate ERRs in metabolic regulation

ERR-null mice have allowed for the identification of the biological relevance of the ERRs as well as the identification of several isoform-

specific functions. Indeed, ERRα-null mice are viable and fertile (Luo et al., 2003b), ERRβ-null mice are embryonic lethal (Luo et al., 1997) and ERRγ-null mice die shortly after birth (Alaynick et al., 2007a). In-depth studies of these mouse models with a focus on specific tissue contexts have solidified the importance of the ERRs for metabolic function.

ERRα-null mice were first reported to display reduced body weight and peripheral fat deposits, and to be resistant to high-fat diet-induced obesity (Luo et al., 2003b). However, no differences in food consumption, energy expenditure, or blood chemistry were observed. Upon closer examination of white adipose tissue, reduced lipogenesis was identified. Furthermore, ERRα-null mice were found to be unable to maintain body temperature in response to cold exposure (Villena et al., 2007). This was attributed not to an impaired thermogenesis transcriptional response but to a failure of mitochondrial biogenesis and oxidative capacity, and a corresponding inadequate supply of the energy necessary for thermogenesis in brown adipose tissue. This effect was attributed to ERRα's regulation of mitochondrial gene expression both directly and through other transcription factors including NRF-1 and GABPA. Intestinal epithelial cells from ERRα-null mice exhibited decreased β-oxidation activity relative to their wildtype counterparts, and fat malabsorption was observed in ERRα-null pups (Carrier et al., 2004). ERRα-null hearts subjected to pressure overload also exhibit signs of heart failure including chamber dilation and reduced left ventricular fractional shortening, in addition to abnormal phosphocreatine depletion and maximal ATP synthesis rates (Huss et al., 2007). Studies with ERRα-deficient macrophages showed that the receptor is required for induction of mitochondrial reactive oxygen species (ROS) production and efficient clearance of bacteria in response to interferon γ (IFN-γ) (Sonoda et al., 2007c). Consequently, mice lacking ERRα are susceptible to bacterial infection, a phenotype that can be traced to bone marrow-derived cells. Furthermore, it was found that IFN-γ-induced activation of ERRα depends

on PGC-1β.

Phenotypic analyses of the ERRβ-null mice have yet to demonstrate a direct role for this receptor in metabolic control. This is primarily due to the fact that ERRβ plays a crucial role in placental development resulting in early lethality of ERRβ-null embryos (Luo et al., 1997). However, ERRβ-null mice generated by aggregation of Esrrb mutant embryos with tetraploid wild-type cells, which contribute exclusively to extra-embryonic tissues, were shown to be viable (Luo et al., 1997; Mitsunaga et al., 2004). An inducible ERRβ knock-out mouse is now available and analyses of these mice have already shown an important role for ERRβ in inner ear and eye function (Chen and Nathans, 2007; Onishi et al., 2010). This model will offer the opportunity in the near future to study whether ERRβ cooperates with ERRα and ERRγ in the control of metabolic functions in the heart and kidneys, two tissues expressing relatively high levels of ERRβ.

ERRγ-null mice die shortly after birth due to a spinal cord dysfunction and to the inability of the heart to switch from a dependence on carbohydrates to a reliance on oxidative metabolism (Alaynick et al., 2007a). Before death, ERRγ-null mice exhibit lactatemia, electrocardiographic abnormalities and impaired mitochondrial function. Interestingly, since ERRα is also expressed in the embryonic heart, direct compensation by ERRα is not sufficient to produce the metabolic shift necessary after birth suggesting that ERRα, as a transcription factor, does not perform the same function as ERRγ.

1.2.5.2 Functional genomics links ERR target genes to metabolic pathways

The development of powerful chromatin immunoprecipitation (ChIP)-based techniques during the last decade has allowed for genome-wide discovery of nuclear receptor target genes (Deblois and Giguere, 2008). In the absence of specific/high affinity pharmacological tools to

study the ERRs, application of this approach was particularly effective in order to associate biological functions with the orphan ERRs in several tissues. One common trend emerging from these studies is that the primary role of the ERRs is to regulate metabolic gene networks, including those associated with mitochondrial biogenesis and function. Although other more indirect approaches have been used to identify ERR target genes (Gaillard et al., 2006; Mootha et al., 2004; Schreiber et al., 2004; Stein et al., 2008), we limited the next sections to the review of studies that allowed for the identification of large numbers of direct targets.

Location analyses by ChIP-on-chip across different metabolic tissues that include mouse heart (Dufour et al., 2007a), macrophages (Sonoda et al., 2007c), kidney (Tremblay et al., 2010a) and liver (Charest-Marcotte et al., 2010a) well as human breast cancer cells (Deblois et al., 2010; Deblois et al., 2009b) have identified a very large set of genes which implicate ERRα as a master regulator of metabolism. In particular, this network of metabolic genes includes a common set of mitochondrial genes implicated in all aspects of mitochondrial functions from energy production to amino acid metabolism and nucleotide biosynthesis. Perhaps the most dramatic finding was the discovery that, in the mouse liver, ERRα occupies the extended promoter region of all genes encoding enzymes and proteins participating in the TCA cycle, pyruvate metabolism and OXPHOS/ electron transport, thus defining a rare eukaryotic transcriptional regulon (Charest-Marcotte et al., 2010a). In addition, the ERRα regulon also includes all genes encoding enzymes involved in the glycolytic pathways, thus integrating two main energy-generating pathways under the control of a common transcription factor.

ERRα also recognizes the promoter regions of genes central to lipid metabolism (including *ACADM*, *FASN*, *DECR1*, *CPT1A*, and *HADHA*), heme synthesis (*FECH*) and AMPK signaling (including *ACC2*, *AK2*, and *CPT2*) implicating the receptor in an extensive range of metabolic functions. ERRα also binds the promoters of genes involved in free radical

scavenging (e.g. *UCP2* and *SOD2*), DNA replication, recombination and repair such as *POLG* and *POLDIP2*, protein synthesis, particularly ribosomal proteins such as *RPL10A* and *RPS14*, protein trafficking including several members of the family of translocase of inner mitochondrial membrane proteins (*TIMM8B, TIMM9*, etc.), calcium handling/apoptosis, represented by *SLC16A*1 and *BAK1* as well as propanoate metabolism (*MCEE*). Together, these findings illustrate the wide range of mitochondrial pathways controlled by ERRα.

Given that ERRβ is essential for proper trophoblast stem cell differentiation and can function as a reprogramming factor in stem cell biology (Feng et al., 2009), genome-wide identification of ERRβ target genes has recently been performed using ChIP-sequencing technology on chromatin isolated from mouse embryonic stem cells (Chen et al., 2008), a rare cell type that expresses the receptor *in vitro*. While the focus of the study was to identify gene networks involved in the reprogramming of fibroblasts into induced pluripotent cells, examination of the datasets generated by this group revealed that ERRβ most likely regulates the same metabolic gene networks as the two other ERR isoforms. Indeed, our own assessment of the ERRβ bound DNA segments in the chromatin of mouse embryonic stem cells reveals that a large fraction (71%) of mitochondrial genes identified as ERRα targets in the studies cited above are also targeted by ERRβ. In fact, our analysis of this dataset using a cut-off of +/−10 kb from the transcriptional start site revealed that, of the ~1100 proteins localized to the mitochondrion, 580 were bound by ERRβ in this context, indicating the vast regulation of mitochondrial programming imparted by this factor. One caveat to this study is that the authors used an antibody raised against the entire ligand binding domain of ERRβ. Thus, this antibody likely recognizes all three ERR isoforms. However, ERRβ is expressed at a much higher level than ERRα and ERRγ in mouse embryonic stem (Xie et al., 2009).

ERRγ not only binds the same regulatory sites as ERRα within

target promoters but also can do so as both homo- or heterodimeric species with ERRα (Dufour et al., 2007a). Therefore, the repertoire of ERRγ direct target genes has been shown to be essentially the same as that of ERRα in the tissue studied to date, the mouse heart (Alaynick et al., 2007a; Dufour et al., 2007a). However, the functional output of the ERRs binding the same genomic regions has yet to be thoroughly investigated.

1.2.5.3 Integrated control of metabolism by the ERRs

By also regulating the expression of transcription factors themselves implicated in metabolic control, ERR can influence the activity of metabolic gene networks in an integrated manner. In particular, the nuclear receptors PPARα and PPARγ, implicated in the expression of uncoupling proteins as well as in the control of fatty acid oxidation and lipid and glucose metabolism, were shown to be direct targets of ERRα, thus imparting regulation of various PPAR-dependent pathways on ERRα (Charest-Marcotte et al., 2010a; Cresci et al., 2010; Dufour et al., 2007a; Huss et al., 2004). Furthermore, the α subunit of NRF-2 (GABPA), is also directly regulated by ERRα and γ (Deblois et al., 2009b; Dufour et al., 2007a; Mootha et al., 2004). ERRα was also found to occupy the promoter regions of the gene encoding TFB2M, an initiation factor required for transcription of genes encoded within the mitochondrial genome (Charest-Marcotte et al., 2010a), and ChIP-sequencing results show ERRβ binding to the genomic region encoding the mitochondrial transcription factor TFAM (Chen et al., 2008). Thereby, ERRα has the ability to control in both direct and indirect manners the entire complement of the mitochondrial gene expression program. Fig. 1.1 outlines the transcription factor regulatory hubs which are ERR direct targets and themselves directly regulate genes responsible for major mitochondrial functions.

Figure 1.1

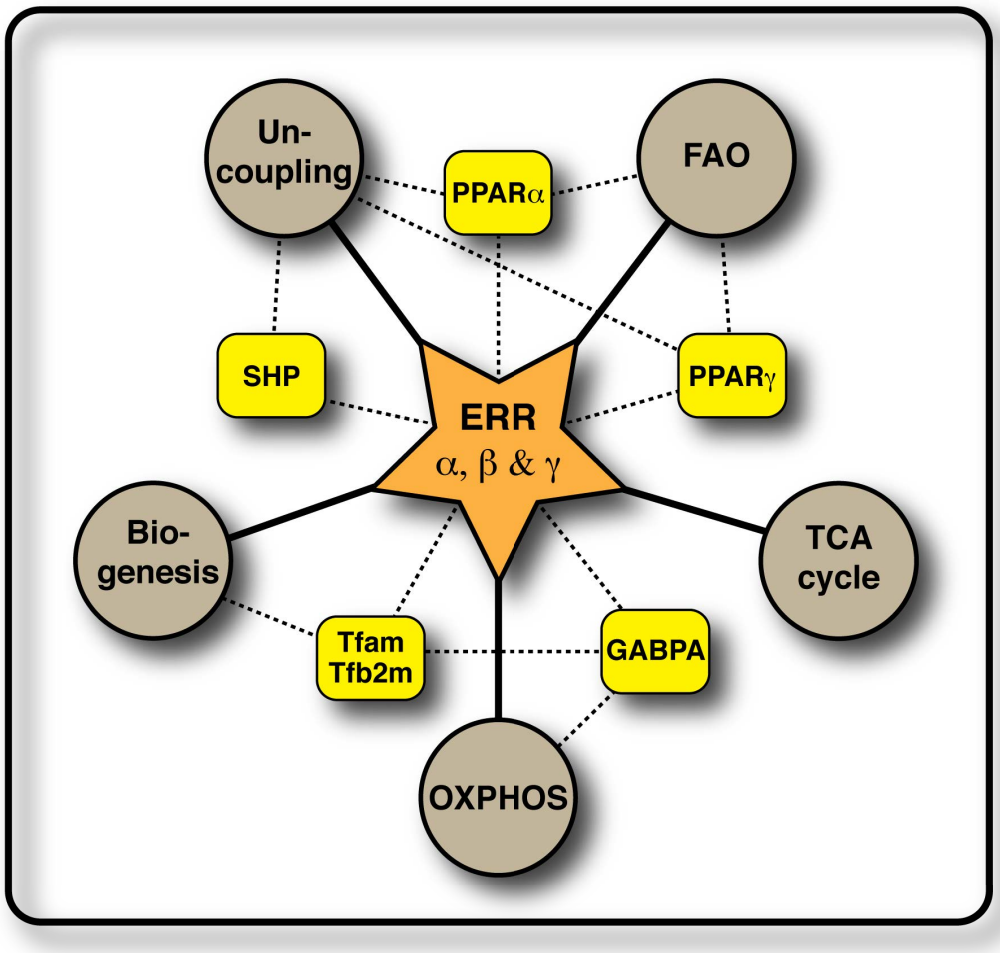

Fig. 1.1. The ERR regulatory hub of major mitochondrial functions. Transcription factors known to be involved in controlling the expression of mitochondrial genes and shown to be direct targets of ERR are represented by yellow boxes, and major mitochondrial functions are represented by gray circles. Solid lines radiating from the hub indicate direct regulation of mitochondrial functions by ERR while dashed lines indicate the action of ERR on these functions through other transcription factors. FAO — fatty acid oxidation, OXPHOS — oxidative phosphorylation, and TCA cycle — tricarboxylic acid cycle. (Figure from Eichner and Giguère, *Mitochondrion*, 2011)

1.2.5.4. Linking gene regulation and function

Studies of metabolic function and organization indicate that the regulation of mitochondrial gene expression by the ERRs does in fact translate into alterations of metabolic function. For example, C2C12 cells treated with XCT790, a synthetic ERRα inverse agonist, exhibit a blunted increase in total cellular respiration and uncoupled respiration in response to the addition of PGC-1α (Mootha et al., 2004). Others have reported a decrease in both basal and maximal cellular respiration in response to XCT790 alone, which is accompanied by an alteration of the metabolic organization measured by oligomycin sensitivity, as well as a decrease in COX and citrate synthase activity (Mirebeau-Prunier et al., 2010). Another group has shown that XCT790 increases ROS production and basal glucose uptake, and decreases mitochondrial membrane potential (Chen and Wong, 2009). Correspondingly, HepG2 cells with siRNA-depleted ERRα display impaired mitochondrial function in that their maximum respiratory capacity is lower than that of control cells (Charest-Marcotte et al., 2010a).

PDK4, a negative regulator of glucose oxidation which promotes a switch to fatty acid oxidation, is regulated by ERRα and ERRγ, indicating the ability of ERR to control metabolic substrate selectivity and pyruvate metabolism (Araki and Motojima, 2006; Wende et al., 2005; Zhang et al., 2006). Additionally, ERR has been implicated in the repression of gluconeogenesis through its negative regulation of *PEPCK* (Herzog et al., 2006; Ichida et al., 2002). ERRα was shown to affect lipid accumulation in cardiac myocytes and to promote palmitate oxidation, providing evidence that ERRα directly influences mitochondrial fatty acid oxidation (Huss et al., 2004). It was also shown that the expression of the lipid droplet protein CIDEA, a regulatory factor in adipose cell function and obesity, is regulated by ERRα in a manner modulated by the corepressor RIP140 and PGC-1α (Hallberg et al., 2008). As a last example, ERRα is also

responsible for controlling the mitochondrial network through its control of mitofusin 2 (Mfn2), a protein that regulates mitochondrial biogenesis and architecture (Cartoni et al., 2005; Soriano et al., 2006).

Taken together, functional genomic studies have revealed that, collectively, the three ERR isoforms recognize the proximal regulatory regions of genes encoding 705 unique proteins which have been reported to be functional components of the mitochondrion proteome. Indeed, these genes encode proteins involved in all aspects of mitochondrial biogenesis and function. A schematic representation of a mitochondrion with examples of genes associated with some of these functions is shown in Fig. 1.2. Given that most of these studies have been limited to the promoter regions of genes, it can be safely assumed that the ERR-controlled mitochondrion gene set is far from complete. Therefore, the recently described ERR regulon that comprises all genes encoding enzymes at every step in the glycolytic pathway, pyruvate metabolism, and TCA cycle is just the tip of an iceberg representing a huge metabolic gene network (Charest-Marcotte et al., 2010a). This undoubtedly positions the three ERRs as genuine master regulators of energy metabolism.

1.2.6 ERR-dependent transcriptional pathways and metabolic diseases

Mitochondrial dysfunction has been implicated in a wide array of human pathologies including insulin resistance and cardiomyopathies (Huss and Kelly, 2005; Morita et al., 2005). Interestingly, single nucleotide polymorphisms in the ERR coregulator protein PGC-1α are linked to susceptibility to insulin resistance and diabetes (Andrulionyte et al., 2004; Ek et al., 2001; Hara et al., 2002; Oberkofler et al., 2004). In muscle of diabetic patients, PGC-1α-responsive OXPHOS genes are downregulated in human diabetes (Mootha et al., 2004), and this gene expression modulation is attributed to the transcriptional regulation imparted by ERRα

Figure 1.2

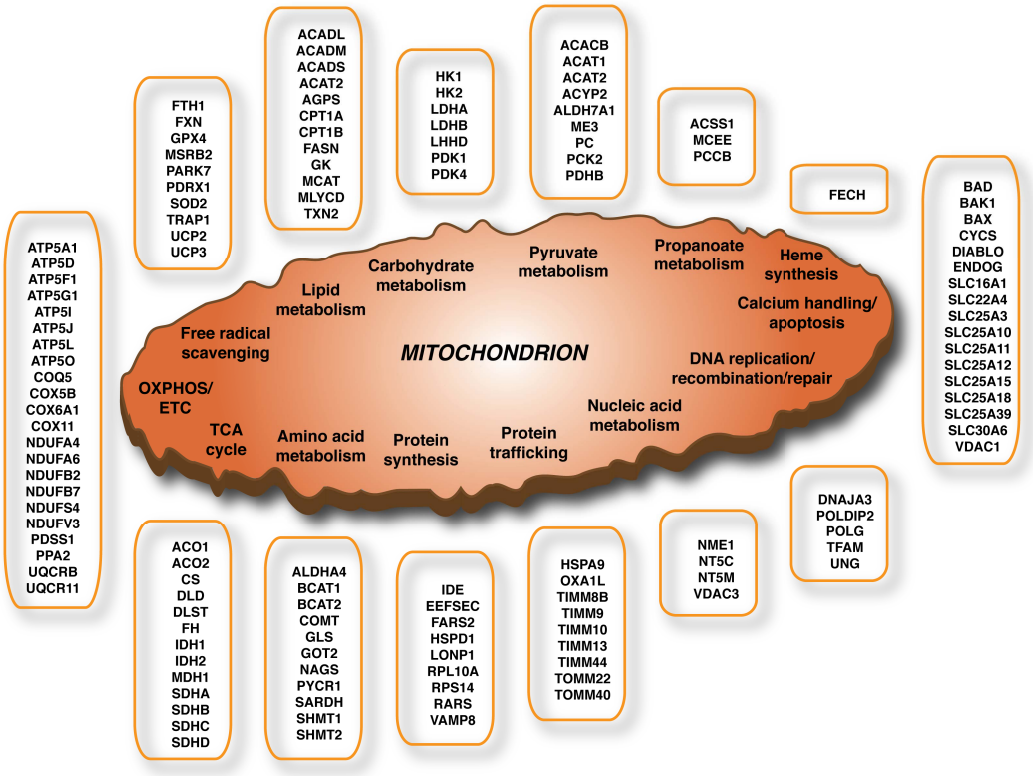

Fig. 1.2. Schematic representation of a mitochondrion illustrating that the three ERR isoforms have the potential to regulate all aspects of mitochondrial biogenesis and function.

Examples of functions and associated genes whose regulatory regions are directly targeted by one or more ERR isoforms are shown within boxes that are associated with diverse biological functions. To date, 705 nuclear-encoded mitochondrial genes have been shown to recruit one or more ERRs near their transcriptional start site. (Figure from Eichner and Giguère, *Mitochondrion*, 2011)

(Mootha et al., 2003). Furthermore, ERRα mRNA expression in human adipose tissue correlates with energy expenditure and insulin sensitivity (Rutanen et al., 2010). ERRγ and ERRα, and their regulation of mitochondrial functions, are required for proper cardiac bioenergetics and adaptation to pressure overload in mice (Alaynick et al., 2007a; Huss et al., 2007). Recently, it was reported that PGC-1α and ERRα target gene down-regulation, including the expression of ERRα itself, is a signature of the failing human heart (Sihag et al., 2009). Interestingly, the role of the PGC-1/ERR mitochondrial metabolism pathway in the heart could be downstream of inflammatory cascades (Palomer et al., 2009; Sonoda et al., 2007c; Yang et al., 2009), suggesting that ERR could play a role not only in basic transcriptional maintenance but also in the inflammatory response implicated in cardiac disease. In addition, ERRα regulation of mitochondrial function has been implicated in osteoclastogenesis, suggesting a role for ERRα in bone diseases such as osteoporosis and arthritis (Teyssier et al., 2009; Wei et al., 2010).

1.2.7 ERRs in cancer

While the Estrogen-Related Receptors (ERRs) are predominantly known for their role in regulating metabolic function and related gene expression programs (Eichner and Giguere, 2011; Giguere, 2008a), important roles for the ERRs in cancer have become increasingly apparent. In fact, the ERRs have been linked to many cancers including endometrial (Gao et al., 2006; Watanabe et al., 2006), lung (Wang et al., 2010), cervical (Mori et al., 2011), ovarian (Fujimoto et al., 2007; Permuth-Wey et al., 2011; Salzman et al., 2011; Sun et al., 2005), prostate (Fujimura et al., 2010; Fujimura et al., 2007; Yu et al., 2008a), and uterine (Fujimoto and Sato, 2009) cancers. However, a large body of research linking ERR to cancer has come from breast cancer research (Deblois and Giguere, 2011).

Breast cancer has been established to be a heterogeneous disease which can be subdivided into at least four different sub-types based on gene expression profiles, including two luminal-like, one basal-like and one ERBB2-overexpressing subtype (Sorlie et al., 2003), and these subtypes correlate with different predictions about patient outcome. ERRα and ERRγ were identified to correlate as unfavourable and favourable biomarkers, respectively (Ariazi et al., 2002b), immediately suggesting fundamentally different roles for these receptors in this disease. Multiple studies went on to confirm and expand upon the role of ERRα as a marker of poor prognosis (Deblois et al., 2009b; Fradet et al., 2011; Heck et al., 2009; Suzuki et al., 2004b). Furthermore, ERRα target gene expression was identified to predict clinical outcome, and to recapitulate the established breast cancer subtype classifications (Deblois et al., 2009b). ERRα expression correlates with the aggressive ERBB2-overexpressing sub-type of breast cancer (Suzuki et al., 2004b), which describes 20-30% of primary human breast cancer cases, and corresponds to poor patient survival (Slamon et al., 1989). ERRα activity was also shown to be modulated by the epidermal growth factor (EGF)/ERBB2 signalling pathway (Ariazi et al., 2007; Barry and Giguere, 2005), placing ERRα activity downstream of this oncogenic signalling. The role of ERRα as an oncogene contributing to the onset of ERBB2-induced mammary tumorigenesis was further validated using a mouse model of this disease (Deblois et al., 2010). Another indicator of ERR activity is the presence of the PGC-1 coactivators. Two studies have shown that low expression of PGC-1α in breast cancer corresponds to poor outcome (Jiang et al., 2003; Watkins et al., 2004), whereas PGC-1α expression was found to promote the growth of ERBB2-induced mammary tumors by regulating nutrient supply (Klimcakova et al., 2012). These studies yet again point to the complexity underlying PGC-1/ERR involvement in breast cancer signalling and regulation, and highlight the need for further study of this molecular intersection between cancer and metabolism.

Although functional studies in cell culture and animal models have unmistakably shown that the ERRs play key roles in controlling cellular metabolism, the exact contribution of each ERR isoform to the expression of each individual target gene remains to be demonstrated. In particular, a close examination of these studies suggests that, while targeting the same gene set, ERRα and ERRγ may have opposite effects on cellular bioenergetics in cell- and context-specific manners. It will be particularly important to decipher the molecular mechanisms and signaling pathways underlying these observations, especially if the goal of current research endeavors is to convert the ERRs into effective therapeutic targets against metabolic diseases or even cancer.

1.3 Metabolism and Cancer

Warburg observed long ago that, even under normal oxygen conditions, cancer cells rely more on glycolysis than OXPHOS to meet their cellular energy demands (Warburg, 1956a). This shift from aerobic, oxidative metabolism to glycolytic metabolism is now a well-recognized hallmark of cancer cells called the Warburg Effect. To utilize glucose for energy, cells metabolize glucose to pyruvate, which, under normal oxygen conditions, is processed by the tricarboxylic acid (TCA) cycle to reducing equivalents. Oxidative phosphorylation then produces ATP from the reducing equivalents, resulting in the production of cellular energy. In hypoxic conditions, pyruvate does not enter the TCA cycle, but instead is converted to lactic acid. This process of glycolytic metabolism produces much less energy per molecule of glucose consumed, but occurs more rapidly than OXPHOS. Under normal oxygen conditions, cancer cells exhibit a heavy reliance on glycolysis despite its energetically less efficient nature, favoring instead the faster energy source.

As the idea of oncogenes and tumor suppressors took hold, the metabolic component to cancer was put on the sidelines and, if considered, was attributed as a downstream side effect of oncogenic

transformation rather than a central component of this disease. Meanwhile, ^{18}F-deoxyglucose positron emission tomography (FDG-PET) scans established themselves as powerful clinical tools for cancer diagnosis and monitoring, extending the application of Warburg's observation concretely into the modern day and providing solid evidence that cancer cells are fundamentally metabolically different from normal cells. Furthermore, recent work indicated that targeting metabolic pathways could be a powerful method to inhibit cancer growth and progression, suggesting that metabolic pathways could have value as therapeutic targets. Indeed, inhibiting lactate dehydrogenase A (LDH-A), the enzyme which mediates the processing of pyruvate to lactate, the final step of glycolysis, enhanced oxidative phosphorylation and respiration while it suppressed cell growth and tumorigenicity in *ERBB2*-initiated mammary epithelial tumor cell lines (Fantin et al., 2006). This directly linked cellular proliferative ability to the switch between oxidative and anaerobic metabolism, and indicates the significance of the regulation of glucose metabolism for cancer cell maintenance and progression.

Recent work has established that the metabolic alterations observed in cancer also serve as an important avenue through which cancer cells are able to meet the anabolic requirements corresponding to rapid growth and division (Ward and Thompson, 2012). Metabolic reprogramming in cancer allows the cell to procure sufficient nucleotides, proteins and lipids for proliferation. These cells need materials for biosynthetic reactions more so than efficient ATP production and, therefore, exhibit mitochondrial reprogramming that allows for the redirection of enzymes involved in oxidative metabolism pathways away from ATP production and into roles in biosynthetic reactions. Different variations of how cancer cells hijack metabolic pathways in this fashion have already started to come to light, and the complexity and extensive impact of deregulating such key pathways is quickly becoming apparent. Key examples will be discussed below.

Several important molecules with established roles in cancer have been shown to directly regulate cancer cell metabolism. Dominant examples of this include PI3K/Akt and Myc. PI3K/Akt activation has been established in many cancers, and the result of this activation includes enhanced glucose uptake and glycolysis (Buzzai et al., 2005; Elstrom et al., 2004) as well as promoting glucose flux into biosynthetic pathways. Akt does so directly by phosphorylating ATP-citrate lyase (ACL) with the effect of diverting citrate from the TCA cycle by transforming it into acetyl-CoA (Ward and Thompson, 2012). The oncogenic transcription factor Myc promotes gene expression and mitochondrial biogenesis (Li et al., 2005) and this was attributed at least in part to its transcriptional control of PGC-1β (Zhang et al., 2007), yet it also promotes glutamine utilization by increasing glutaminase (GLS) expression, suggesting that myc contributes to mitochondrial reprogramming which promotes glutamine addiction (DeBerardinis et al., 2007; Fan et al., 2010; Gao et al., 2009; Wise et al., 2008; Yuneva et al., 2007).

The AMPK pathway is a well-recognized junction between metabolism and cancer cell development. A Ser/Thr kinase, AMPK acts as a cellular energy sensor to regulate glucose and lipid metabolism in response to nutrient availability and metabolic stress. When the AMP:ATP ratio is high, AMPK undergoes a conformational change that enables its activation by phosphorylation on the α subunit (Thr-172) by an AMPK kinase (Luo et al., 2005). The activity of AMPK is largely considered to be conferred by Liver Kinase B (LKB1) (Shackelford and Shaw, 2009), however the Calmodulin-Dependent Protein Kinase Kinase 2 (CAMKK2) also functions as an important upstream AMPK kinase (Hawley et al., 2005; Woods et al., 2005). The role of LKB1 as a tumor suppressor, which is inactivated in some cancers, functionally links AMPK activity to cancer (Ollila and Makela, 2011). Repression of AMPK activation leads to a series of effects on downstream networks, including stimulation of the mTOR pathway (Shaw, 2009) and reduced cell cycle regulation by p53 and p21,

thus promoting cell proliferation and survival (Motoshima et al., 2006). Reduced AMPK activity also induces upregulation of fatty acid and lipid synthesis through Acetyl-Coenzyme A Carboxylase Alpha (ACC) and Fatty Acid Synthase (FAS) activity, a metabolic change increasingly associated with cancer development (Swinnen et al., 2006).

There is accumulating evidence of the involvement of metabolic genes themselves in the progression of cancer. Studies have identified specific genes within the TCA cycle whose expression is important for inhibiting cancer cell proliferation. Succinate dehydrogenase (SDH) and fumarate hydratase (FH) were reported not only to be necessary for normal OXPHOS but also to possess tumor suppressor activity (Cervera et al., 2008; King et al., 2006), thus providing evidence that the oxidative metabolic switch is not only correlated with rates of cell proliferation but that these pathways are linked at a molecular level. Loss-of-function mutations in these genes were found to occur in various cancers, and the understanding of the impact of the TCA cycle truncation induced by these mutations was soon after expanded. In fact, accumulation of the metabolites, succinate and fumarate, just upstream of these two mutated enzymes leads not only to reduced TCA cycle function but also to the inhibition of α-ketoglutarate-dependent dioxygenases, resulting in the alteration of epigenetic modifications (Xiao et al., 2012).

Several other metabolic enzymes were also found to be mutated or amplified in cancer. For example, phosphoglycerate dehydrogenase amplification in breast cancer and melanoma allows for greater flux through the serine/glycine synthesis pathway (Locasale et al., 2011; Possemato et al., 2011). The enzyme isocitrate dehydrogenase 1, IDH1, was found in glioma and acute myeloid leukemia to exhibit a specific heterozygous missense mutation at arginine 132 (Mardis et al., 2009; Parsons et al., 2008). This modification is a loss-of-function mutation for isocitrate and α-ketoglutarate interconversion, and instead causes α-ketoglutarate to be converted into 2-hydroxyglutarate (2HG) (Dang et al.,

2009). IDH2 mutations at R140 or R172 also induced 2HG production (Gross et al., 2010; Ward et al., 2010). Correlation with tumor production of 2HG and IDH mutations identified 2HG as an oncogenic metabolite with clinically-relevant potential. Moreover, 2HG functions to inhibit TET family enzymes, which participate in DNA methylation, extending the range of function of this small onco-metabolite to the regulation of DNA methylation (Figueroa et al., 2010; Turcan et al., 2012; Xu et al., 2011).

Furthermore, pyruvate kinase (PK), the enzyme that produces pyruvate from phosphoenolpyruvate (PEP), was shown to be alternatively spliced by cancer cells. The M1 isoform of (PK) is the predominant form in non-proliferating cells, but cancer cells exhibit dominant expression of the M2 isoform (Mazurek, 2011). The M2 isoform displays a growth advantage, which corresponds to its reduced enzymatic activity forcing the accumulating upstream glycolytic intermediates into alternative anabolic pathways (Mazurek, 2011).

Taken together, it has become evident that metabolic reprogramming is a central component of cancer. Cancer cells reprogram cellular metabolism to shift away from catabolic, energy-efficient oxidative metabolism and promote instead reliance on glycolysis and related anabolic pathways. This modulation can be induced through modulation of metabolic enzymes or their upstream regulators, including through preferential isoform selection, mutation or amplification, resulting in modulation of corresponding metabolite levels. Considering their control of epigenetic programs, it is already evident that the consequences of metabolite misregulation on cellular metabolic networks are vast. To properly understand and treat cancer, it will be crucial to better understand cancer cell metabolism.

1.4 miRNA

1.4.1 Fundamentals

MiRNA are short, endogenous non-coding RNAs of ~22nt in length which post-transcriptionally regulate their mRNA targets, with the functional output of controlling target protein levels (Fabian and Sonenberg, 2012). miRNA, which are found in eukaryotes from plants to mammals, typically recognize their targets through imperfect sequence base-pairing to the 3' untranslated regions (UTRs) and function to suppress their specific mRNA targets by inhibiting translation initiation or promoting mRNA degradation (He and Hannon, 2004).

miRNA are transcribed from the genome by RNA polymerase II first as longer primary transcripts called pri-miRNAs (Lee et al., 2004), which have a 5' cap and a 3' poly-A-tail (Cai et al., 2004). The primary transcript folds to allow the formation of miRNA stem-loop structures, where the mature miRNA comprises the imperfectly paired double-stranded stem region of the structure. A multi-protein processing complex recognizes these stem-loop structures and cleaves them out of the primary transcript (Denli et al., 2004; Gregory et al., 2004; Landthaler et al., 2004; Lee et al., 2003). The double-stranded RNA binding protein, DGCR8, binds to the base of the stem-loop in order to guide Drosha, the catalytic RNase III enzyme, to the proper location for cleavage (Han et al., 2006). After Drosha cleavage, the hairpin, now 70-100bp long and called a pre-miRNA, exhibits a two nucleotide (nt) overhang at the 3' end (Gregory et al., 2004; Han et al., 2006). Pre-miRNAs are then exported into the cytosol by Exportin 5 (Bohnsack et al., 2004; Lund et al., 2004; Yi et al., 2003), where the RNase III enzyme, Dicer, binds to the 3' overhang of the pre-miRNA and cleaves the pre-miRNA into a double-stranded RNA 22nt long with 2nt overhangs on each 3' end (Bartel, 2009; Grishok et al., 2001). One of these strands, that which accumulates to a higher steady-state level, is considered the dominant miRNA of the hairpin and to be preferentially incorporated into Argonaute complexes, and the other miRNA is labeled as the (*) strand, which can also be functionally active. While Chapter II of this thesis was one of the first studies to attribute physiological relevance

to a miRNA*, regulatory activity of vertebrate miRNA* species was elegantly proven in a systematic fashion by Yang et al., 2011. This study identified transcriptome-wide miRNA* target regulation signatures and detected miRNA* seed conservation among vertebrate 3'UTRs. Furthermore, this study identified that small RNAs which immunoprecipitate with mammalian Argonaute proteins include substantial quantities of miRNA* species. Taken together with studies of individual miRNA* functions, this systematic study proves that miRNA* activity functionally contributes to the active miRNA target network.

The miRISC complex, containing Dicer, Argonaute (Ago), and TRBP, then interacts with the single-stranded mature miRNA and its target mRNA to mediate miRNA-mediated regulation (Chendrimada et al., 2005; Gregory et al., 2005; Haase et al., 2005). Human Argonaute binds preferentially to 5' U or A, likely contributing to the selective pressure for miRNA which are functionally loaded into the RISC complex to start at their 5' end with these nucleotides. miRNA* exhibit predominance for 5' A or C, which could account for a lesser predominance toward active RISC loading of these miRNA* molecules, whereas both miRNA and miRNA* exhibit an aversion to G at their 5' end (Yang et al., 2011). The miRNA selects its target by sequence complementarity of its nucleotides 2-8, the seed sequence, to its target mRNA usually within the 3'UTR region (Bartel, 2009). An A residue across from the start of the miRNA can strengthen the targeting, as can an A or U across from position 9, and loose complementarity of the 3' end of the miRNA functions to stabilize the targeting. In mammals, the miRNA will typically bind with partial complementarity to its targets and causes repression of translation or degradation of the mRNA target transcript (Krol et al., 2010).

1.4.2 miRNA in metabolism

miRNA have been implicated in essentially all physiological processes and a large range of diseases (Osman, 2012), including

metabolism and metabolic disorders (Rottiers and Naar, 2012). A key example is miR-122, which was shown to regulate hepatic cholesterol and lipid metabolism. Its expression in the liver allowed *in-vivo* targeting early on, and inhibition of endogenous miR-122 *in-vivo* was found to reduce plasma cholesterol levels (Krutzfeldt et al., 2005), circulating triglycerides, hepatic cholesterol, fatty acid biosynthesis, and high-fat diet-induced hepatosteatosis (Esau et al., 2006). The SREBP family of transcription factors are major regulators of cholesterol and fatty acid biosynthesis and uptake. SREBF1 regulates predominantly lipogenic genes, whereas SREBP2 more dominantly regulates genes implicated in cholesterol synthesis (Horton et al., 2002). Human SREBF1 encodes for mir-33b in intron 17, whereas SREBF2 contains mir-33a in intron 16, and both of these miRNAs are coexpressed with their host genes (Gerin et al., 2010b; Horie et al., 2010; Marquart et al., 2010; Najafi-Shoushtari et al., 2010; Rayner et al., 2010). These miRNAs work together and in concert with their host genes to regulate cholesterol and lipid homeostasis. Examples include direct targeting by miR-33 of *ABCA1* (Horie et al., 2010; Marquart et al., 2010; Najafi-Shoushtari et al., 2010; Rayner et al., 2010), the ATP-binding cassette transporter subfamily A member 1 which regulates cholesterol transport from the cell and is required for HDL formation (Tang and Oram, 2009). miR-33 was also implicated in the direct control of genes necessary for fatty acid oxidation, including *CROT*, *CPT1A*, and *HADHB* (Davalos et al., 2011; Gerin et al., 2010b; Rottiers et al., 2011). Other metabolic regulatory factors targeted by miR-33 include AMPKα1 (Davalos et al., 2011; Rottiers et al., 2011). Together, miR-33 acts in concert with its host genes, extensive yet precise modulators of the cholesterol and lipid homeostasis network. Regulation of adipose tissue has also been attributed to miRNA function, as a list of miRNA implicated in adipocyte differentiation and white adipocyte function have been identified (Romao et al., 2011). This includes miR-143, miR-204, miR-141, miR-200a, miR-200b, miR-200c, miR-429, miR-17-92 cluster, miR-130,

miR-27a, miR-27b, miR-378 and miR-378*. Brown adipose tissue also has implicated miRNA function, including the miR-193b-365 cluster (Sun et al., 2011). Throughout the course of this thesis work, the mir-378 hairpin has been shown to be implicated in a range of metabolic settings including adipogenesis (Gerin et al., 2010a), cardiac function (Knezevic et al., 2012; Tranter et al., 2011), muscle function (Davidsen et al., 2011) and liver regeneration (Song et al., 2010b), indicating an expansive range of diverse functions possible for one miRNA depending on the physiological context. mir-378 is located within the first intron of its host gene *Ppargc1b*, which encodes for the metabolic co-activator, PGC-1β, and should, therefore, be co-expressed together with this gene.[1] The co-expression of mir-378 with the well-established metabolic gene PGC-1β, by extension, further strengthens the connection between mir-378 and metabolic contexts and functions. Altogether, it is evident that miRNA are integrated components of metabolic homeostasis across varied physiological contexts.

There are also examples of miRNA misregulation in metabolic diseases. For example, adipose miRNA were linked to obesity (Xie et al., 2009). Another example is hepatic miR-34a, which is elevated in non-alcoholic fatty liver disease (Cheung et al., 2008) and patients with type 2 diabetes (Kong et al., 2011). Considering their roles in metabolic homeostasis, it follows that disease states in metabolic tissues would induce misregulation of miRNA expression and their downstream pathways.

1.4.3 miRNA in cancer

[1] It should be noted that, recently, after the bulk of this thesis work was completed, other mammalian miRNA with nearly identical sequences to mir-378, differing by one or two nucleotides, were identified in different locations throughout mammalian genomes. These miRNA were also named mir-378, and are distinguishing from each other by a lower case letter; “a” through “j” in human and “a” through “d” in mouse. The work throughout this thesis studies the originally-identified mir-378, now named mir-378a. This is the only mir-378 hairpin which encodes for miR-378*. This thesis uses the nomenclature “miR-378” to refer to the molecule currently renamed miR-378a-3P, and “miR-378*” to refer to the molecule currently renamed miR-378a-5P.

miRNA are now considered essential regulators of development and physiological processes (Ma and Weinberg, 2008), and extensive studies have demonstrated a correlation between aberrant miRNA expression with tumor formation, progression, and metastasis (Garzon et al., 2009). About 50% of the known miRNAs are located in fragile regions of the genome, which are often found to be deleted or multiplied in cancer (Calin et al., 2004). The first example of miRNA in human cancer came from B-cell chronic lymphocytic leukemia (CCL), where the chromosomal region 13q14 which is often deleted was found to contain miR-15a and miR-16-1 (Calin et al., 2002). These miRNA were later shown to repress the expression of the pro-apoptotic factor, Bcl-27. Since then, miRNA expression profiling using miRNA microarrays and sequencing approaches have identified aberrant miRNA expression in a multitude of different cancers, clearly implicating miRNA misregulation in this disease and, furthermore, suggesting the potential for these molecules to serve as diagnostic tools (Calin and Croce, 2006). The first study of miRNA in breast cancer identified 29 miRNAs significantly deregulated in breast cancer tumors as compared to normal mammary tissues, including the downregulation of miR-10b, miR-125b, and miR-145 and the upregulation of miR-155 and miR-21, implicating miRNA as both oncogenes and tumor suppressors in the same cancer context (Iorio et al., 2005). Subsequent study of these miRNA demonstrated involvement in breast tumor formation, progression, and metastasis (Iorio et al., 2011).

Breast cancer is a leading cause of death of women worldwide (Iorio et al., 2005). Hyperproliferation is often caused by mutations, either inherited or acquired. Common genomic aberrations include mutation of the TP53 tumor suppressor gene, loss of heterozygosity from chromosomes 8p, 13q, 16q, 17p and 17q, mutation of the *BRCA1* and *BRCA2* genes, and amplification of oncogenes, such as *MYC15*. Notably, in ~30% of breast cancer cases, the oncogene *ERBB2*, encoding the human epidermal growth factor receptor 2 (HER2), is amplified (Revillion

et al., 1998). miRNA expression profiling of different breast cancer subtypes, including estrogen receptor (ER), progesterone receptor (PR) and HER2 status, has extended the understanding of the molecular differences between these types of breast cancer (Iorio et al., 2005). Blenkiron *et al*. identified unique sets of miRNA associated with five specific subtypes of breast cancer, each group corresponding to a different prognosis (Blenkiron et al., 2007). It has become clear that miRNA expression provides valuable information about breast cancer (Lu et al., 2005).

miRNA implicated in breast cancer classify by function as either oncogenes or tumor suppressors. Oncogenic miRNA, or oncomirs, promote cell proliferation and/or inhibit apoptosis, often by repressing the expression of tumor suppressor genes. miR-21, a well-studied oncomiR, was shown to induce tumor growth in a variety of cancers including breast cancer. Knockdown of miR-21 in MCF-7 cells decreased cell growth *in vitro* and in a xenograft mouse model, and increased apoptosis (Si et al., 2007). Programmed cell death 4 (*PDCD4*), phosphatase and tensin homolog (*PTEN*), tropomyosin 1 (*TPM1*), and maspin were identified as miR-21 targets (Zhu et al., 2008). miR-27a was found to down-regulate Myt-1, a component of the G2M checkpoint and an inhibitor of cdc2/cyclin B, in order to regulate cell cycle progression (Mertens-Talcott et al., 2007). miR-27a, miR-96, and miR-182 were found to inhibit the transcription factor, FOXO1, which is also a putative tumor suppressor, in MCF-7 breast cancer cells (Guttilla and White, 2009). Oncogenic miR-155 inhibits the suppressor of cytokine signaling 1, SOCS1, itself an inhibitor of oncogenic STAT3. Correspondingly, expression of miR-155 was found to increase cellular proliferation *in vitro* and in a xenograft model (Jiang et al., 2010). Expression of the miR-378*/miR-378 hairpin was reported to enhance cell survival and promote tumor growth and angiogenesis in a pooled cell line through targeting the transcription factor SuFu and Fus-1, suggesting that miR-378* and/or miR-378 possesses oncogenic potential

(Lee et al., 2007). After the publication of Chapter II of this thesis, this hairpin was shown to be downstream of oncogenic Myc (Feng et al., 2011). However, little else is known about the molecular mechanisms underlying miR-378* or miR-378 function in cancer cells.

miRNA with functions as tumor suppressors have also been identified in breast cancer. One example is miR-125a/b, which was found to be downregulated in breast tumors. miR-125a/b expression in SKBR3 cells decreased anchorage-dependent growth, likely mediated through the ERK1/2 and AKT pathways. ERBB2 and ERBB3 were identified as direct targets of miR-125a/b (Scott et al., 2007). Interestingly, genetic variants of bone morphogenic receptor type 1 B (BMPR1B) were found to functionally interact with miR-125b. The T allele disrupts miR-125b regulation, leading to increased BMPR1B expression which is associated with proliferation and poor prognosis, whereas the C allele is functionally targeted by miR-125b (Saetrom et al., 2009), demonstrating a correlation between breast cancer risk and miRNA target binding site variation. Other tumor suppressor miRNA have been shown to regulate the cell cycle. miR-126 represses progression form G1/G0 to S phase, decreasing cell proliferation, through targeting the insulin receptor substrate 1 (IRS-1). IRS-1 is constitutively active in many tumors, including breast cancer, and exerts its proliferative effects though the PI3K/AKT pathway (Zhang et al., 2008). miR-17-5p/miR-20a expression was found to suppress cell proliferation through down-regulation of cyclin-D1, a regulator of the G1/S transition. Interestingly, cyclin-D1 is also required for induction of miR-17/20 expression, suggesting a mechanistic regulatory feedback loop (Yu et al., 2008b). Furthermore, the chromosomal region 13q31, which contains miR-17-5p, is often lost in breast cancer cells (Hossain et al., 2006). miR-17-5p was found to directly target AIB1, a gene amplified in beast cancer.

miRNA implicated in estrogen receptor-regulated pathways include miR-206 and miR-145. Mir-206 represses ERα protein levels (Adams et

al., 2007; Kondo et al., 2008), in a manner involving the steroid receptor co-activators, SRC-1 and SRC-3, as well as the GATA-4 transcription factor (Adams et al., 2009). miR-145 also represses ERα at the post-transcriptional level and indirectly activates the TP53 tumor suppressor gene. TP53, in turn, induces miR-145 expression, resulting to an overall increase in apoptosis (Spizzo et al., 2010).

Several miRNA have been implicated in the self-renewal of cancer cells. Differential expression of let-7 was identified from a screen of self-renewing breast tumor initiating cells (BT-IC). Let-7 expression was reduced in BT-IC, and its levels were found to increase with differentiation. Repression of H-RAS and HMGA2, known targets of let-7, led to decreased self-renewal and increased differentiation, respectively (Bussing et al., 2008). miR-30 expression is also reduced in BT-IC cells. The reduction in miR-30 results in reduced apoptosis and contributes to self-renewal, perhaps in part through its regulation of ubiquitin-conjugating enzyme 9 (Ubc9) and integrin β3 (ITGB3). Furthermore, let-7 and miR-30 function synergistically in the regulation of cancer cell renewal (Yu et al., 2010a).

Cancer metastasis is a complex, multi-step process that usually begins with a small fraction of cells undergoing the epithelial-mesenchymal transition (EMT), a process characterized by the loss of E-cadherin and the acquisition of mesenchymal characteristics. Subsequent cell invasion occurs, then intravasion and survival in circulation, extravasion into the distant site and, finally, colonization into a secondary tumor. In breast cancer, metastasis patterns typically involve migration to local lymph nodes, liver, or lung (Shi et al., 2010). Roles for miRNA in these processes have also recently begun to be elucidated. Oncogenic miR-21 was found to promote cell metastasis by repressing several invasion-related tumor suppressor genes, including tropomyosin 1 (TPM1), PDCD4, and maspin. Inhibition of miR-21 expression in metastatic MDA-MB-231 cells decreased invasion and lung metastasis

(Zhu et al., 2008). Other evidence expanded the known miR-21 targets to include metalloproteinase-3 (TIMP3), a peptidase involved in ECM degradation (Song et al., 2010a). Expression of miR-10b in the non-metastatic human breast cancer cell line, SUM159, induced lung metastasis when orthotopically transplanted into mice (Ma et al., 2007). Evidence of direct regulation of EMT by miRNAs has also been uncovered. One example of this is miR-9, which directly inhibits CDH1, the gene encoding E-cadherin, inducing the activation of the β-catenin pathway. Expression of miR-9 was found to promote metastatic potential of cells *in vivo*, whereas inhibition of miR-9 induced the opposite effect (Ma et al., 2010). Another example is miR-103/107, whose expression in breast cancer is associated with metastasis and poor outcome. Tumor cells expressing miR-107 exhibit decreased Ecadherin levels and an increase in mesenchymal markers including vimentin and fibronectin (Martello et al., 2010). The miR-200 family also suppresses metastasis by targeting ZEB1 and ZEB2, transcriptional repressors of E-cadherin (Korpal et al., 2008). The miR-200 family, along with miR-205, was also found to regulate transforming growth factor β (TGF-β)-induced EMT, and re-expression of miR-200 was sufficient to prevent this transition (Gregory et al., 2008). miR-335 is capable of inhibiting breast cancer metastasis through SOX4, a transcription factor implicated in regulating progenitor cell development and migration (Tavazoie et al., 2008). miR-7 suppresses metastasis by targeting directly Pak1, a p21-activated kinase which is involved in cell mobility and invasion (Reddy et al., 2008). Finally, miR-31 regulates several downstream targets involved in cell invasion and mobility. Inhibition of miR-31 in non-metastatic MCF-Ras cells, when orthotopically implanted into mice, induced lung metastasis. It has been suggested that miR-31 functions through predicted targets including RhoA and, in fact, the re-introduction of RhoA partially reversed miR-31-induced metastasis suppression (Valastyan et al., 2009). This body of evidence clearly identifies miRNA as functional components of metastasis.

Finally, miRNA function in cancer metabolism has yet to be thoroughly explored. One of the first examples of miRNA in cancer metabolism came from the identification that miR-23a and b target glutaminase (GLS), the enzyme which converts glutamine to glutamate, thereby contributing to the catabolic reactions necessary for proliferation. In fact, the oncogenic transcription factor, Myc, represses miR-23a and miR-23b, such that a miRNA is the molecular signal connecting oncogenic signaling to the regulation of glutamine metabolism (Gao et al., 2009). After the publication of Chapter 2 of this thesis, another study expanded the function of miR-23 regulation by myc. Liu et al. uncovered that miR-23 targets proline dehydrogenase (POX/PRODH), which is the first enzyme in proline catabolism and functions as a tumor suppressor (Liu et al., 2012). Glutamine is converted to glutamate by GLS, and this glutamate can be further processed to proline. Therefore, Myc repression of miR-23 functions to regulate glutamine metabolism via GLS but also via control of downstream proline catabolism. The combination of these two studies indicates the complexity and relevance of metabolic control in cancer cells, and the level of integration of miRNA in those pathways. However, much remains to be learned about the role of miRNA in cancer cell metabolism. While the relevance of miRNA in breast cancer is clear, the molecular understanding of how these small molecules integrate into breast cancer signaling pathways such that they could be manipulated for clinical and therapeutic applications remains to be fully elucidated.

1.5 Rationale and objectives of the research

ERRs have been identified as master regulators of metabolic gene expression programs. The expression of the ERRs is relevant in breast cancer, yet their function within that disease context is largely unknown. Furthermore, the contribution of miRNA to the function of the PGC-1/ERR pathway was entirely unexplored. The general goal of this thesis was to

elucidate the role of the PGC-1/ERR pathway in breast cancer cell metabolism.

In Chapter II, we identified a direct molecular link between PGC-1β and ERRγ, miR-378/378*, which allowed us to uncover a relevance to the metabolic function of both ERR and miR-378* in breast cancer cells. Chapter III is the extension of the study of the metabolic function of the mir-378 hairpin in breast cancer cells which allowed us to further expand our understanding of the metabolic molecular network under the control of this miRNA. As mouse models of mammary tumorigenesis are a powerful tool for the study of breast cancer, we turned to such a model in Chapter IV in order to study the metabolic function of ERRα in breast cancer *in-vivo*. The absence of mouse models available for the parallel study of miR-378/378* *in-vivo* drove us to generate the necessary conditional and total knockout mouse models. The generation and subsequent study of these models are the focus of Chapter V.

REFERENCES

Adams, B.D., Cowee, D.M., and White, B.A. (2009). The role of miR-206 in the epidermal growth factor (EGF) induced repression of estrogen receptor-alpha (ERalpha) signaling and a luminal phenotype in MCF-7 breast cancer cells. Molecular endocrinology *23*, 1215-1230.

Adams, B.D., Furneaux, H., and White, B.A. (2007). The micro-ribonucleic acid (miRNA) miR-206 targets the human estrogen receptor-alpha (ERalpha) and represses ERalpha messenger RNA and protein expression in breast cancer cell lines. Molecular endocrinology *21*, 1132-1147.

Alaynick, W.A., Kondo, R.P., Xie, W., He, W., Dufour, C.R., Downes, M., Jonker, J.W., Giles, W., Naviaux, R.K., Giguere, V.*, et al.* (2007). ERRgamma directs and maintains the transition to oxidative metabolism in the postnatal heart. Cell metabolism *6*, 13-24.

Alaynick, W.A., Way, J.M., Wilson, S.A., Benson, W.G., Pei, L., Downes, M., Yu, R., Jonker, J.W., Holt, J.A., Rajpal, D.K.*, et al.* (2010). ERRgamma regulates cardiac, gastric, and renal potassium homeostasis. Molecular endocrinology *24*, 299-309.

Andrulionyte, L., Zacharova, J., Chiasson, J.L., and Laakso, M. (2004). Common polymorphisms of the PPAR-gamma2 (Pro12Ala) and PGC-1alpha (Gly482Ser) genes are associated with the conversion from impaired glucose tolerance to type 2 diabetes in the STOP-NIDDM trial. Diabetologia *47*, 2176-2184.

Araki, M., and Motojima, K. (2006). Identification of ERRalpha as a specific partner of PGC-1alpha for the activation of PDK4 gene expression in muscle. The FEBS journal *273*, 1669-1680.

Arany, Z., He, H., Lin, J., Hoyer, K., Handschin, C., Toka, O., Ahmad, F., Matsui, T., Chin, S., Wu, P.H.*, et al.* (2005). Transcriptional coactivator PGC-1 alpha controls the energy state and contractile function of cardiac muscle. Cell metabolism *1*, 259-271.

Ariazi, E.A., Clark, G.M., and Mertz, J.E. (2002). Estrogen-related receptor alpha and estrogen-related receptor gamma associate with unfavorable and favorable biomarkers, respectively, in human breast cancer. Cancer research *62*, 6510-6518.

Ariazi, E.A., Kraus, R.J., Farrell, M.L., Jordan, V.C., and Mertz, J.E. (2007). Estrogen-related receptor alpha1 transcriptional activities are regulated in part via the ErbB2/HER2 signaling pathway. Mol Cancer Res *5*, 71-85.

Augereau, P., Badia, E., Carascossa, S., Castet, A., Fritsch, S., Harmand, P.O., Jalaguier, S., and Cavailles, V. (2006). The nuclear receptor transcriptional coregulator RIP140. Nucl Recept Signal *4*, e024.

Baar, K., Wende, A.R., Jones, T.E., Marison, M., Nolte, L.A., Chen, M., Kelly, D.P., and Holloszy, J.O. (2002). Adaptations of skeletal muscle to exercise: rapid increase in the transcriptional coactivator PGC-1. Faseb J *16*, 1879-1886.

Barry, J.B., and Giguere, V. (2005). Epidermal growth factor-induced signaling in breast cancer cells results in selective target gene activation by orphan nuclear receptor estrogen-related receptor alpha. Cancer research *65*, 6120-6129.

Bartel, D.P. (2009). MicroRNAs: target recognition and regulatory functions. Cell *136*, 215-233.

Belleannee, C., Calvo, E., Thimon, V., Cyr, D.G., Legare, C., Garneau, L., and Sullivan, R. (2012). Role of microRNAs in controlling gene expression in different segments of the human epididymis. PLoS One *7*, e34996.

Blenkiron, C., Goldstein, L.D., Thorne, N.P., Spiteri, I., Chin, S.F., Dunning, M.J., Barbosa-Morais, N.L., Teschendorff, A.E., Green, A.R., Ellis, I.O.*, et al.* (2007). MicroRNA expression profiling of human breast cancer identifies new markers of tumor subtype. Genome Biol *8*, R214.

Bohnsack, M.T., Czaplinski, K., and Gorlich, D. (2004). Exportin 5 is a RanGTP-dependent dsRNA-binding protein that mediates nuclear export of pre-miRNAs. Rna *10*, 185-191.

Bookout, A.L., Jeong, Y., Downes, M., Yu, R.T., Evans, R.M., and Mangelsdorf, D.J. (2006). Anatomical profiling of nuclear receptor expression reveals a hierarchical transcriptional network. Cell *126*, 789-799.

Busch, B.B., Stevens, W.C., Jr., Martin, R., Ordentlich, P., Zhou, S., Sapp, D.W., Horlick, R.A., and Mohan, R. (2004). Identification of a selective inverse agonist for the orphan nuclear receptor estrogen-related receptor alpha. J Med Chem *47*, 5593-5596.

Bussing, I., Slack, F.J., and Grosshans, H. (2008). let-7 microRNAs in development, stem cells and cancer. Trends Mol Med *14*, 400-409.

Buzzai, M., Bauer, D.E., Jones, R.G., Deberardinis, R.J., Hatzivassiliou, G., Elstrom, R.L., and Thompson, C.B. (2005). The glucose dependence of Akt-transformed cells can be reversed by pharmacologic activation of fatty acid beta-oxidation. Oncogene *24*, 4165-4173.

Cai, X., Hagedorn, C.H., and Cullen, B.R. (2004). Human microRNAs are processed from capped, polyadenylated transcripts that can also function as mRNAs. Rna *10*, 1957-1966.

Calin, G.A., and Croce, C.M. (2006). MicroRNA signatures in human cancers. Nat Rev Cancer *6*, 857-866.

Calin, G.A., Dumitru, C.D., Shimizu, M., Bichi, R., Zupo, S., Noch, E., Aldler, H., Rattan, S., Keating, M., Rai, K.*, et al.* (2002). Frequent deletions and down-regulation of micro- RNA genes miR15 and miR16 at 13q14 in chronic lymphocytic leukemia. Proceedings of the National Academy of Sciences of the United States of America *99*, 15524-15529.

Calin, G.A., Sevignani, C., Dumitru, C.D., Hyslop, T., Noch, E., Yendamuri, S., Shimizu, M., Rattan, S., Bullrich, F., Negrini, M.*, et al.* (2004). Human microRNA genes are frequently located at fragile sites and genomic regions involved in cancers. Proceedings of the National Academy of Sciences of the United States of America *101*, 2999-3004.

Carrier, J.C., Deblois, G., Champigny, C., Levy, E., and Giguere, V. (2004). Estrogen-related receptor alpha (ERRalpha) is a transcriptional regulator of apolipoprotein A-IV and controls lipid handling in the intestine. The Journal of biological chemistry *279*, 52052-52058.

Cartoni, R., Leger, B., Hock, M.B., Praz, M., Crettenand, A., Pich, S., Ziltener, J.L., Luthi, F., Deriaz, O., Zorzano, A.*, et al.* (2005). Mitofusins 1/2 and ERRalpha expression are increased in human skeletal muscle after physical exercise. The Journal of physiology *567*, 349-358.

Castet, A., Herledan, A., Bonnet, S., Jalaguier, S., Vanacker, J.M., and Cavailles, V. (2006). Receptor-interacting protein 140 differentially regulates estrogen receptor-related receptor transactivation depending on target genes. Molecular endocrinology *20*, 1035-1047.

Cervera, A.M., Apostolova, N., Crespo, F.L., Mata, M., and McCreath, K.J. (2008). Cells silenced for SDHB expression display characteristic features of the tumor phenotype. Cancer Res *68*, 4058-4067.

Chao, E.Y., Collins, J.L., Gaillard, S., Miller, A.B., Wang, L., Orband-Miller, L.A., Nolte, R.T., McDonnell, D.P., Willson, T.M., and Zuercher, W.J. (2006). Structure-guided synthesis of tamoxifen analogs with improved selectivity for the orphan ERRgamma. Bioorg Med Chem Lett *16*, 821-824.

Charest-Marcotte, A., Dufour, C.R., Wilson, B.J., Tremblay, A.M., Eichner, L.J., Arlow, D.H., Mootha, V.K., and Giguere, V. (2010). The homeobox protein Prox1 is a negative modulator of ERR{alpha}/PGC-1{alpha} bioenergetic functions. Genes & development *24*, 537-542.

Chen, J., and Nathans, J. (2007). Estrogen-related receptor beta/NR3B2 controls epithelial cell fate and endolymph production by the stria vascularis. Dev Cell *13*, 325-337.

Chen, L., and Wong, C. (2009). Estrogen-related receptor alpha inverse agonist enhances basal glucose uptake in myotubes through reactive oxygen species. Biological & pharmaceutical bulletin *32*, 1199-1203.

Chen, X., Xu, H., Yuan, P., Fang, F., Huss, M., Vega, V.B., Wong, E., Orlov, Y.L., Zhang, W., Jiang, J.*, et al.* (2008). Integration of external signaling pathways with the core transcriptional network in embryonic stem cells. Cell *133*, 1106-1117.

Chendrimada, T.P., Gregory, R.I., Kumaraswamy, E., Norman, J., Cooch, N., Nishikura, K., and Shiekhattar, R. (2005). TRBP recruits the Dicer complex to Ago2 for microRNA processing and gene silencing. Nature *436*, 740-744.

Christian, M., White, R., and Parker, M.G. (2006). Metabolic regulation by the nuclear receptor corepressor RIP140. Trends in endocrinology and metabolism: TEM *17*, 243-250.

Coward, P., Lee, D., Hull, M.V., and Lehmann, J.M. (2001). 4-Hydroxytamoxifen binds to and deactivates the estrogen-related receptor gamma. Proceedings of the National Academy of Sciences of the United States of America *98*, 8880-8884.

Cresci, S., Huss, J.M., Beitelshees, A.L., Jones, P.G., Minton, M.R., Dorn, G.W., Kelly, D.P., Spertus, J.A., and McLeod, H.L. (2010). A PPARalpha promoter variant impairs ERR-dependent transactivation and decreases mortality after acute coronary ischemia in patients with diabetes. PLoS One *5*, e12584.

Dang, L., White, D.W., Gross, S., Bennett, B.D., Bittinger, M.A., Driggers, E.M., Fantin, V.R., Jang, H.G., Jin, S., Keenan, M.C.*, et al.* (2009). Cancer-associated IDH1 mutations produce 2-hydroxyglutarate. Nature *462*, 739-744.

Davalos, A., Goedeke, L., Smibert, P., Ramirez, C.M., Warrier, N.P., Andreo, U., Cirera-Salinas, D., Rayner, K., Suresh, U., Pastor-Pareja, J.C.*, et al.* (2011). miR-33a/b contribute to the regulation of fatty acid metabolism and insulin signaling. Proceedings of the National Academy of Sciences of the United States of America *108*, 9232-9237.

Davidsen, P.K., Gallagher, I.J., Hartman, J.W., Tarnopolsky, M.A., Dela, F., Helge, J.W., Timmons, J.A., and Phillips, S.M. (2011). High responders to resistance exercise training demonstrate differential regulation of skeletal muscle microRNA expression. J Appl Physiol *110*, 309-317.

DeBerardinis, R.J., Mancuso, A., Daikhin, E., Nissim, I., Yudkoff, M., Wehrli, S., and Thompson, C.B. (2007). Beyond aerobic glycolysis: transformed cells can engage in glutamine metabolism that exceeds the requirement for protein and nucleotide synthesis. Proceedings of the National Academy of Sciences of the United States of America *104*, 19345-19350.

Debevec, D., Christian, M., Morganstein, D., Seth, A., Herzog, B., Parker, M., and White, R. (2007). Receptor interacting protein 140 regulates expression of uncoupling protein 1 in adipocytes through specific peroxisome proliferator activated receptor isoforms and estrogen-related receptor alpha. Molecular endocrinology *21*, 1581-1592.

Deblois, G., Chahrour, G., Perry, M.C., Sylvain-Drolet, G., Muller, W.J., and Giguere, V. (2010). Transcriptional control of the ERBB2 amplicon by ERRalpha and PGC-1beta promotes mammary gland tumorigenesis. Cancer research *70*, 10277-10287.

Deblois, G., and Giguere, V. (2008). Nuclear receptor location analyses in mammalian genomes: from gene regulation to regulatory networks. Molecular endocrinology *22*, 1999-2011.

Deblois, G., and Giguere, V. (2011). Functional and physiological genomics of estrogen-related receptors (ERRs) in health and disease. Biochimica et biophysica acta *1812*, 1032-1040.

Deblois, G., Hall, J.A., Perry, M.C., Laganiere, J., Ghahremani, M., Park, M., Hallett, M., and Giguere, V. (2009). Genome-wide identification of direct target genes implicates estrogen-related receptor alpha as a determinant of breast cancer heterogeneity. Cancer research *69*, 6149-6157.

Denli, A.M., Tops, B.B., Plasterk, R.H., Ketting, R.F., and Hannon, G.J. (2004). Processing of primary microRNAs by the Microprocessor complex. Nature *432*, 231-235.

Duellman, S.J., Calaoagan, J.M., Sato, B.G., Fine, R., Klebansky, B., Chao, W.R., Hobbs, P., Collins, N., Sambucetti, L., and Laderoute, K.R. (2010). A novel steroidal inhibitor of estrogen-related receptor alpha (ERR alpha). Biochem Pharmacol *80*, 819-826.

Dufour, C.R., Wilson, B.J., Huss, J.M., Kelly, D.P., Alaynick, W.A., Downes, M., Evans, R.M., Blanchette, M., and Giguere, V. (2007). Genome-wide orchestration of cardiac functions by the orphan nuclear receptors ERRalpha and gamma. Cell metabolism *5*, 345-356.

Dupuis, J., Langenberg, C., Prokopenko, I., Saxena, R., Soranzo, N., Jackson, A.U., Wheeler, E., Glazer, N.L., Bouatia-Naji, N., Gloyn, A.L., *et*

al. (2010). New genetic loci implicated in fasting glucose homeostasis and their impact on type 2 diabetes risk. Nature genetics *42*, 105-116.

Ek, J., Andersen, G., Urhammer, S.A., Gaede, P.H., Drivsholm, T., Borch-Johnsen, K., Hansen, T., and Pedersen, O. (2001). Mutation analysis of peroxisome proliferator-activated receptor-gamma coactivator-1 (PGC-1) and relationships of identified amino acid polymorphisms to Type II diabetes mellitus. Diabetologia *44*, 2220-2226.

Elstrom, R.L., Bauer, D.E., Buzzai, M., Karnauskas, R., Harris, M.H., Plas, D.R., Zhuang, H., Cinalli, R.M., Alavi, A., Rudin, C.M.*, et al.* (2004). Akt stimulates aerobic glycolysis in cancer cells. Cancer research *64*, 3892-3899.

Esau, C., Davis, S., Murray, S.F., Yu, X.X., Pandey, S.K., Pear, M., Watts, L., Booten, S.L., Graham, M., McKay, R.*, et al.* (2006). miR-122 regulation of lipid metabolism revealed by in vivo antisense targeting. Cell metabolism *3*, 87-98.

Evans, R.M. (1988). The steroid and thyroid hormone receptor superfamily. Science *240*, 889-895.

Fabian, M.R., and Sonenberg, N. (2012). The mechanics of miRNA-mediated gene silencing: a look under the hood of miRISC. Nat Struct Mol Biol *19*, 586-593.

Fan, Y., Dickman, K.G., and Zong, W.X. (2010). Akt and c-Myc differentially activate cellular metabolic programs and prime cells to bioenergetic inhibition. The Journal of biological chemistry *285*, 7324-7333.

Fantin, V.R., St-Pierre, J., and Leder, P. (2006). Attenuation of LDH-A expression uncovers a link between glycolysis, mitochondrial physiology, and tumor maintenance. Cancer Cell *9*, 425-434.

Feige, J.N., and Auwerx, J. (2007). Transcriptional coregulators in the control of energy homeostasis. Trends in cell biology *17*, 292-301.

Feng, B., Jiang, J., Kraus, P., Ng, J.H., Heng, J.C., Chan, Y.S., Yaw, L.P., Zhang, W., Loh, Y.H., Han, J.*, et al.* (2009). Reprogramming of fibroblasts into induced pluripotent stem cells with orphan nuclear receptor Esrrb. Nat Cell Biol *11*, 197-203.

Feng, M., Li, Z., Aau, M., Wong, C.H., Yang, X., and Yu, Q. (2011). Myc/miR-378/TOB2/cyclin D1 functional module regulates oncogenic transformation. Oncogene *30*, 2242-2251.

Figueroa, M.E., Abdel-Wahab, O., Lu, C., Ward, P.S., Patel, J., Shih, A., Li, Y., Bhagwat, N., Vasanthakumar, A., Fernandez, H.F*., et al.* (2010). Leukemic IDH1 and IDH2 mutations result in a hypermethylation phenotype, disrupt TET2 function, and impair hematopoietic differentiation. Cancer Cell *18*, 553-567.

Fradet, A., Sorel, H., Bouazza, L., Goehrig, D., Depalle, B., Bellahcene, A., Castronovo, V., Follet, H., Descotes, F., Aubin, J.E*., et al.* (2011). Dual function of ERRalpha in breast cancer and bone metastasis formation: implication of VEGF and osteoprotegerin. Cancer research *71*, 5728-5738.

Fujimoto, J., Alam, S.M., Jahan, I., Sato, E., Sakaguchi, H., and Tamaya, T. (2007). Clinical implication of estrogen-related receptor (ERR) expression in ovarian cancers. The Journal of steroid biochemistry and molecular biology *104*, 301-304.

Fujimoto, J., and Sato, E. (2009). Clinical implication of estrogen-related receptor (ERR) expression in uterine endometrial cancers. The Journal of steroid biochemistry and molecular biology *116*, 71-75.

Fujimura, T., Takahashi, S., Urano, T., Ijichi, N., Ikeda, K., Kumagai, J., Murata, T., Takayama, K., Horie-Inoue, K., Ouchi, Y*., et al.* (2010). Differential expression of estrogen-related receptors beta and gamma (ERRbeta and ERRgamma) and their clinical significance in human prostate cancer. Cancer Sci *101*, 646-651.

Fujimura, T., Takahashi, S., Urano, T., Kumagai, J., Ogushi, T., Horie-Inoue, K., Ouchi, Y., Kitamura, T., Muramatsu, M., and Inoue, S. (2007). Increased expression of estrogen-related receptor alpha (ERRalpha) is a negative prognostic predictor in human prostate cancer. International journal of cancer Journal international du cancer *120*, 2325-2330.

Gaillard, S., Grasfeder, L.L., Haeffele, C.L., Lobenhofer, E.K., Chu, T.M., Wolfinger, R., Kazmin, D., Koves, T.R., Muoio, D.M., Chang, C.Y*., et al.* (2006). Receptor-selective coactivators as tools to define the biology of specific receptor-coactivator pairs. Molecular cell *24*, 797-803.

Gao, M., Sun, P., Wang, J., Zhao, D., and Wei, L. (2006). Expression of estrogen receptor-related receptor isoforms and clinical significance in endometrial adenocarcinoma. Int J Gynecol Cancer *16*, 827-833.

Gao, P., Tchernyshyov, I., Chang, T.C., Lee, Y.S., Kita, K., Ochi, T., Zeller, K.I., De Marzo, A.M., Van Eyk, J.E., Mendell, J.T*., et al.* (2009). c-Myc suppression of miR-23a/b enhances mitochondrial glutaminase expression and glutamine metabolism. Nature *458*, 762-765.

Garzon, R., Calin, G.A., and Croce, C.M. (2009). MicroRNAs in Cancer. Annu Rev Med *60*, 167-179.

Gerin, I., Bommer, G.T., McCoin, C.S., Sousa, K.M., Krishnan, V., and MacDougald, O.A. (2010a). Roles for miRNA-378/378* in adipocyte gene expression and lipogenesis. Am J Physiol Endocrinol Metab *299*, E198-206.

Gerin, I., Clerbaux, L.A., Haumont, O., Lanthier, N., Das, A.K., Burant, C.F., Leclercq, I.A., MacDougald, O.A., and Bommer, G.T. (2010b). Expression of miR-33 from an SREBP2 intron inhibits cholesterol export and fatty acid oxidation. The Journal of biological chemistry *285*, 33652-33661.

Giguere, V. (2002). To ERR in the estrogen pathway. Trends in endocrinology and metabolism: TEM *13*, 220-225.

Giguere, V. (2008). Transcriptional control of energy homeostasis by the estrogen-related receptors. Endocrine reviews *29*, 677-696.

Giguere, V., Yang, N., Segui, P., and Evans, R.M. (1988). Identification of a new class of steroid hormone receptors. Nature *331*, 91-94.

Goto, M., Terada, S., Kato, M., Katoh, M., Yokozeki, T., Tabata, I., and Shimokawa, T. (2000). cDNA Cloning and mRNA analysis of PGC-1 in epitrochlearis muscle in swimming-exercised rats. Biochemical and biophysical research communications *274*, 350-354.

Gregory, P.A., Bert, A.G., Paterson, E.L., Barry, S.C., Tsykin, A., Farshid, G., Vadas, M.A., Khew-Goodall, Y., and Goodall, G.J. (2008). The miR-200 family and miR-205 regulate epithelial to mesenchymal transition by targeting ZEB1 and SIP1. Nat Cell Biol *10*, 593-601.

Gregory, R.I., Chendrimada, T.P., Cooch, N., and Shiekhattar, R. (2005). Human RISC couples microRNA biogenesis and posttranscriptional gene silencing. Cell *123*, 631-640.

Gregory, R.I., Yan, K.P., Amuthan, G., Chendrimada, T., Doratotaj, B., Cooch, N., and Shiekhattar, R. (2004). The Microprocessor complex mediates the genesis of microRNAs. Nature *432*, 235-240.

Grishok, A., Pasquinelli, A.E., Conte, D., Li, N., Parrish, S., Ha, I., Baillie, D.L., Fire, A., Ruvkun, G., and Mello, C.C. (2001). Genes and mechanisms related to RNA interference regulate expression of the small temporal RNAs that control C. elegans developmental timing. Cell *106*, 23-34.

Gross, S., Cairns, R.A., Minden, M.D., Driggers, E.M., Bittinger, M.A., Jang, H.G., Sasaki, M., Jin, S., Schenkein, D.P., Su, S.M.*, et al.* (2010). Cancer-associated metabolite 2-hydroxyglutarate accumulates in acute

myelogenous leukemia with isocitrate dehydrogenase 1 and 2 mutations. J Exp Med *207*, 339-344.

Guttilla, I.K., and White, B.A. (2009). Coordinate regulation of FOXO1 by miR-27a, miR-96, and miR-182 in breast cancer cells. The Journal of biological chemistry *284*, 23204-23216.

Haase, A.D., Jaskiewicz, L., Zhang, H., Laine, S., Sack, R., Gatignol, A., and Filipowicz, W. (2005). TRBP, a regulator of cellular PKR and HIV-1 virus expression, interacts with Dicer and functions in RNA silencing. EMBO Rep *6*, 961-967.

Hallberg, M., Morganstein, D.L., Kiskinis, E., Shah, K., Kralli, A., Dilworth, S.M., White, R., Parker, M.G., and Christian, M. (2008). A functional interaction between RIP140 and PGC-1alpha regulates the expression of the lipid droplet protein CIDEA. Molecular and cellular biology *28*, 6785-6795.

Han, J., Lee, Y., Yeom, K.H., Nam, J.W., Heo, I., Rhee, J.K., Sohn, S.Y., Cho, Y., Zhang, B.T., and Kim, V.N. (2006). Molecular basis for the recognition of primary microRNAs by the Drosha-DGCR8 complex. Cell *125*, 887-901.

Hara, K., Tobe, K., Okada, T., Kadowaki, H., Akanuma, Y., Ito, C., Kimura, S., and Kadowaki, T. (2002). A genetic variation in the PGC-1 gene could confer insulin resistance and susceptibility to Type II diabetes. Diabetologia *45*, 740-743.

Hawley, S.A., Pan, D.A., Mustard, K.J., Ross, L., Bain, J., Edelman, A.M., Frenguelli, B.G., and Hardie, D.G. (2005). Calmodulin-dependent protein kinase kinase-beta is an alternative upstream kinase for AMP-activated protein kinase. Cell metabolism *2*, 9-19.

He, L., and Hannon, G.J. (2004). MicroRNAs: small RNAs with a big role in gene regulation. Nat Rev Genet *5*, 522-531.

Heck, S., Rom, J., Thewes, V., Becker, N., Blume, B., Sinn, H.P., Deuschle, U., Sohn, C., Schneeweiss, A., and Lichter, P. (2009). Estrogen-related receptor alpha expression and function is associated with the transcriptional coregulator AIB1 in breast carcinoma. Cancer research *69*, 5186-5193.

Herzog, B., Cardenas, J., Hall, R.K., Villena, J.A., Budge, P.J., Giguere, V., Granner, D.K., and Kralli, A. (2006). Estrogen-related receptor alpha is a repressor of phosphoenolpyruvate carboxykinase gene transcription. The Journal of biological chemistry *281*, 99-106.

Hock, M.B., and Kralli, A. (2009). Transcriptional control of mitochondrial biogenesis and function. Annu Rev Physiol *71*, 177-203.

Hong, H., Darimont, B.D., Ma, H., Yang, L., Yamamoto, K.R., and Stallcup, M.R. (1999). An additional region of coactivator GRIP1 required for interaction with the hormone-binding domains of a subset of nuclear receptors. The Journal of biological chemistry *274*, 3496-3502.

Horie, T., Ono, K., Horiguchi, M., Nishi, H., Nakamura, T., Nagao, K., Kinoshita, M., Kuwabara, Y., Marusawa, H., Iwanaga, Y.*, et al.* (2010). MicroRNA-33 encoded by an intron of sterol regulatory element-binding protein 2 (Srebp2) regulates HDL in vivo. Proceedings of the National Academy of Sciences of the United States of America *107*, 17321-17326.

Horton, J.D., Goldstein, J.L., and Brown, M.S. (2002). SREBPs: activators of the complete program of cholesterol and fatty acid synthesis in the liver. The Journal of clinical investigation *109*, 1125-1131.

Hossain, A., Kuo, M.T., and Saunders, G.F. (2006). Mir-17-5p regulates breast cancer cell proliferation by inhibiting translation of AIB1 mRNA. Molecular and cellular biology *26*, 8191-8201.

Huss, J.M., Imahashi, K., Dufour, C.R., Weinheimer, C.J., Courtois, M., Kovacs, A., Giguere, V., Murphy, E., and Kelly, D.P. (2007). The nuclear receptor ERRalpha is required for the bioenergetic and functional adaptation to cardiac pressure overload. Cell metabolism *6*, 25-37.

Huss, J.M., and Kelly, D.P. (2005). Mitochondrial energy metabolism in heart failure: a question of balance. The Journal of clinical investigation *115*, 547-555.

Huss, J.M., Torra, I.P., Staels, B., Giguere, V., and Kelly, D.P. (2004). Estrogen-related receptor alpha directs peroxisome proliferator-activated receptor alpha signaling in the transcriptional control of energy metabolism in cardiac and skeletal muscle. Molecular and cellular biology *24*, 9079-9091.

Ichida, M., Nemoto, S., and Finkel, T. (2002). Identification of a specific molecular repressor of the peroxisome proliferator-activated receptor gamma Coactivator-1 alpha (PGC-1alpha). The Journal of biological chemistry *277*, 50991-50995.

Iorio, M.V., Casalini, P., Piovan, C., Braccioli, L., and Tagliabue, E. (2011). Breast cancer and microRNAs: therapeutic impact. Breast *20 Suppl 3*, S63-70.

Iorio, M.V., Ferracin, M., Liu, C.G., Veronese, A., Spizzo, R., Sabbioni, S., Magri, E., Pedriali, M., Fabbri, M., Campiglio, M.*, et al.* (2005). MicroRNA

gene expression deregulation in human breast cancer. Cancer research *65*, 7065-7070.

Jeong, J.W., Kwak, I., Lee, K.Y., White, L.D., Wang, X.P., Brunicardi, F.C., O'Malley, B.W., and DeMayo, F.J. (2006). The genomic analysis of the impact of steroid receptor coactivators ablation on hepatic metabolism. Molecular endocrinology *20*, 1138-1152.

Jiang, S., Zhang, H.W., Lu, M.H., He, X.H., Li, Y., Gu, H., Liu, M.F., and Wang, E.D. (2010). MicroRNA-155 functions as an OncomiR in breast cancer by targeting the suppressor of cytokine signaling 1 gene. Cancer research *70*, 3119-3127.

Jiang, W.G., Douglas-Jones, A., and Mansel, R.E. (2003). Expression of peroxisome-proliferator activated receptor-gamma (PPARgamma) and the PPARgamma co-activator, PGC-1, in human breast cancer correlates with clinical outcomes. International journal of cancer Journal international du cancer *106*, 752-757.

King, A., Selak, M.A., and Gottlieb, E. (2006). Succinate dehydrogenase and fumarate hydratase: linking mitochondrial dysfunction and cancer. Oncogene *25*, 4675-4682.

Klimcakova, E., Chenard, V., McGuirk, S., Germain, D., Avizonis, D., Muller, W.J., and St-Pierre, J. (2012). PGC-1alpha promotes the growth of ErbB2/Neu-induced mammary tumors by regulating nutrient supply. Cancer research *72*, 1538-1546.

Knezevic, I., Patel, A., Sundaresan, N.R., Gupta, M.P., Solaro, R.J., Nagalingam, R.S., and Gupta, M. (2012). A novel cardiomyocyte-enriched microRNA, miR-378, targets insulin-like growth factor 1 receptor: implications in postnatal cardiac remodeling and cell survival. The Journal of biological chemistry *287*, 12913-12926.

Knutti, D., Kressler, D., and Kralli, A. (2001). Regulation of the transcriptional coactivator PGC-1 via MAPK-sensitive interaction with a repressor. Proceedings of the National Academy of Sciences of the United States of America *98*, 9713-9718.

Kondo, N., Toyama, T., Sugiura, H., Fujii, Y., and Yamashita, H. (2008). miR-206 Expression is down-regulated in estrogen receptor alpha-positive human breast cancer. Cancer research *68*, 5004-5008.

Kong, L., Zhu, J., Han, W., Jiang, X., Xu, M., Zhao, Y., Dong, Q., Pang, Z., Guan, Q., Gao, L.*, et al.* (2011). Significance of serum microRNAs in pre-diabetes and newly diagnosed type 2 diabetes: a clinical study. Acta Diabetol *48*, 61-69.

Korpal, M., Lee, E.S., Hu, G., and Kang, Y. (2008). The miR-200 family inhibits epithelial-mesenchymal transition and cancer cell migration by direct targeting of E-cadherin transcriptional repressors ZEB1 and ZEB2. The Journal of biological chemistry *283*, 14910-14914.

Kressler, D., Schreiber, S.N., Knutti, D., and Kralli, A. (2002). The PGC-1-related protein PERC is a selective coactivator of estrogen receptor alpha. The Journal of biological chemistry *277*, 13918-13925.

Krol, J., Loedige, I., and Filipowicz, W. (2010). The widespread regulation of microRNA biogenesis, function and decay. Nat Rev Genet *11*, 597-610.

Krutzfeldt, J., Rajewsky, N., Braich, R., Rajeev, K.G., Tuschl, T., Manoharan, M., and Stoffel, M. (2005). Silencing of microRNAs in vivo with 'antagomirs'. Nature *438*, 685-689.

Landthaler, M., Yalcin, A., and Tuschl, T. (2004). The human DiGeorge syndrome critical region gene 8 and Its D. melanogaster homolog are required for miRNA biogenesis. Curr Biol *14*, 2162-2167.

Lee, D.Y., Deng, Z., Wang, C.H., and Yang, B.B. (2007). MicroRNA-378 promotes cell survival, tumor growth, and angiogenesis by targeting SuFu and Fus-1 expression. Proceedings of the National Academy of Sciences of the United States of America *104*, 20350-20355.

Lee, Y., Ahn, C., Han, J., Choi, H., Kim, J., Yim, J., Lee, J., Provost, P., Radmark, O., Kim, S.*, et al.* (2003). The nuclear RNase III Drosha initiates microRNA processing. Nature *425*, 415-419.

Lee, Y., Kim, M., Han, J., Yeom, K.H., Lee, S., Baek, S.H., and Kim, V.N. (2004). MicroRNA genes are transcribed by RNA polymerase II. The EMBO journal *23*, 4051-4060.

Lehman, J.J., Barger, P.M., Kovacs, A., Saffitz, J.E., Medeiros, D.M., and Kelly, D.P. (2000). Peroxisome proliferator-activated receptor gamma coactivator-1 promotes cardiac mitochondrial biogenesis. The Journal of clinical investigation *106*, 847-856.

Leonardsson, G., Steel, J.H., Christian, M., Pocock, V., Milligan, S., Bell, J., So, P.W., Medina-Gomez, G., Vidal-Puig, A., White, R.*, et al.* (2004). Nuclear receptor corepressor RIP140 regulates fat accumulation. Proceedings of the National Academy of Sciences of the United States of America *101*, 8437-8442.

Leone, T.C., Lehman, J.J., Finck, B.N., Schaeffer, P.J., Wende, A.R., Boudina, S., Courtois, M., Wozniak, D.F., Sambandam, N., Bernal-Mizrachi, C.*, et al.* (2005). PGC-1alpha deficiency causes multi-system

energy metabolic derangements: muscle dysfunction, abnormal weight control and hepatic steatosis. PLoS biology *3*, e101.

Li, F., Wang, Y., Zeller, K.I., Potter, J.J., Wonsey, D.R., O'Donnell, K.A., Kim, J.W., Yustein, J.T., Lee, L.A., and Dang, C.V. (2005). Myc stimulates nuclearly encoded mitochondrial genes and mitochondrial biogenesis. Molecular and cellular biology *25*, 6225-6234.

Lin, J., Handschin, C., and Spiegelman, B.M. (2005). Metabolic control through the PGC-1 family of transcription coactivators. Cell Metab *1*, 361-370.

Lin, J., Puigserver, P., Donovan, J., Tarr, P., and Spiegelman, B.M. (2002). Peroxisome proliferator-activated receptor gamma coactivator 1beta (PGC-1beta), a novel PGC-1-related transcription coactivator associated with host cell factor. The Journal of biological chemistry *277*, 1645-1648.

Lin, J., Wu, P.H., Tarr, P.T., Lindenberg, K.S., St-Pierre, J., Zhang, C.Y., Mootha, V.K., Jager, S., Vianna, C.R., Reznick, R.M.*, et al.* (2004). Defects in adaptive energy metabolism with CNS-linked hyperactivity in PGC-1alpha null mice. Cell *119*, 121-135.

Liu, W., Le, A., Hancock, C., Lane, A.N., Dang, C.V., Fan, T.W., and Phang, J.M. (2012). Reprogramming of proline and glutamine metabolism contributes to the proliferative and metabolic responses regulated by oncogenic transcription factor c-MYC. Proceedings of the National Academy of Sciences of the United States of America *109*, 8983-8988.

Locasale, J.W., Grassian, A.R., Melman, T., Lyssiotis, C.A., Mattaini, K.R., Bass, A.J., Heffron, G., Metallo, C.M., Muranen, T., Sharfi, H.*, et al.* (2011). Phosphoglycerate dehydrogenase diverts glycolytic flux and contributes to oncogenesis. Nature genetics *43*, 869-874.

Louet, J.F., Coste, A., Amazit, L., Tannour-Louet, M., Wu, R.C., Tsai, S.Y., Tsai, M.J., Auwerx, J., and O'Malley, B.W. (2006). Oncogenic steroid receptor coactivator-3 is a key regulator of the white adipogenic program. Proc Natl Acad Sci U S A *103*, 17868-17873.

Lu, J., Getz, G., Miska, E.A., Alvarez-Saavedra, E., Lamb, J., Peck, D., Sweet-Cordero, A., Ebert, B.L., Mak, R.H., Ferrando, A.A.*, et al.* (2005). MicroRNA expression profiles classify human cancers. Nature *435*, 834-838.

Lund, E., Guttinger, S., Calado, A., Dahlberg, J.E., and Kutay, U. (2004). Nuclear export of microRNA precursors. Science *303*, 95-98.

Luo, J., Sladek, R., Bader, J.A., Matthyssen, A., Rossant, J., and Giguere, V. (1997). Placental abnormalities in mouse embryos lacking the orphan nuclear receptor ERR-beta. Nature *388*, 778-782.

Luo, J., Sladek, R., Carrier, J., Bader, J.A., Richard, D., and Giguere, V. (2003). Reduced fat mass in mice lacking orphan nuclear receptor estrogen-related receptor alpha. Molecular and cellular biology *23*, 7947-7956.

Luo, Z., Saha, A.K., Xiang, X., and Ruderman, N.B. (2005). AMPK, the metabolic syndrome and cancer. Trends Pharmacol Sci *26*, 69-76.

Ma, L., Teruya-Feldstein, J., and Weinberg, R.A. (2007). Tumour invasion and metastasis initiated by microRNA-10b in breast cancer. Nature *449*, 682-688.

Ma, L., and Weinberg, R.A. (2008). MicroRNAs in malignant progression. Cell Cycle *7*, 570-572.

Ma, L., Young, J., Prabhala, H., Pan, E., Mestdagh, P., Muth, D., Teruya-Feldstein, J., Reinhardt, F., Onder, T.T., Valastyan, S.*, et al.* (2010). miR-9, a MYC/MYCN-activated microRNA, regulates E-cadherin and cancer metastasis. Nat Cell Biol *12*, 247-256.

Mangelsdorf, D.J., Thummel, C., Beato, M., Herrlich, P., Schutz, G., Umesono, K., Blumberg, B., Kastner, P., Mark, M., Chambon, P.*, et al.* (1995). The nuclear receptor superfamily: the second decade. Cell *83*, 835-839.

Mardis, E.R., Ding, L., Dooling, D.J., Larson, D.E., McLellan, M.D., Chen, K., Koboldt, D.C., Fulton, R.S., Delehaunty, K.D., McGrath, S.D.*, et al.* (2009). Recurring mutations found by sequencing an acute myeloid leukemia genome. N Engl J Med *361*, 1058-1066.

Marquart, T.J., Allen, R.M., Ory, D.S., and Baldan, A. (2010). miR-33 links SREBP-2 induction to repression of sterol transporters. Proceedings of the National Academy of Sciences of the United States of America *107*, 12228-12232.

Martello, G., Rosato, A., Ferrari, F., Manfrin, A., Cordenonsi, M., Dupont, S., Enzo, E., Guzzardo, V., Rondina, M., Spruce, T.*, et al.* (2010). A MicroRNA targeting dicer for metastasis control. Cell *141*, 1195-1207.

Mazurek, S. (2011). Pyruvate kinase type M2: a key regulator of the metabolic budget system in tumor cells. Int J Biochem Cell Biol *43*, 969-980.

Mertens-Talcott, S.U., Chintharlapalli, S., Li, X., and Safe, S. (2007). The oncogenic microRNA-27a targets genes that regulate specificity protein transcription factors and the G2-M checkpoint in MDA-MB-231 breast cancer cells. Cancer research *67*, 11001-11011.

Mirebeau-Prunier, D., Le Pennec, S., Jacques, C., Gueguen, N., Poirier, J., Malthiery, Y., and Savagner, F. (2010). Estrogen-related receptor alpha and PGC-1-related coactivator constitute a novel complex mediating the biogenesis of functional mitochondria. The FEBS journal *277*, 713-725.

Mitsunaga, K., Araki, K., Mizusaki, H., Morohashi, K., Haruna, K., Nakagata, N., Giguere, V., Yamamura, K., and Abe, K. (2004). Loss of PGC-specific expression of the orphan nuclear receptor ERR-beta results in reduction of germ cell number in mouse embryos. Mechanisms of development *121*, 237-246.

Mootha, V.K., Handschin, C., Arlow, D., Xie, X., St Pierre, J., Sihag, S., Yang, W., Altshuler, D., Puigserver, P., Patterson, N.*, et al.* (2004). Erralpha and Gabpa/b specify PGC-1alpha-dependent oxidative phosphorylation gene expression that is altered in diabetic muscle. Proceedings of the National Academy of Sciences of the United States of America *101*, 6570-6575.

Mootha, V.K., Lindgren, C.M., Eriksson, K.F., Subramanian, A., Sihag, S., Lehar, J., Puigserver, P., Carlsson, E., Ridderstrale, M., Laurila, E.*, et al.* (2003). PGC-1alpha-responsive genes involved in oxidative phosphorylation are coordinately downregulated in human diabetes. Nature genetics *34*, 267-273.

Mori, T., Sawada, M., Kuroboshi, H., Tatsumi, H., Katsuyama, M., Iwasaku, K., and Kitawaki, J. (2011). Estrogen-related receptor alpha expression and function are associated with vascular endothelial growth factor in human cervical cancer. Int J Gynecol Cancer *21*, 609-615.

Morita, H., Seidman, J., and Seidman, C.E. (2005). Genetic causes of human heart failure. The Journal of clinical investigation *115*, 518-526.

Mortensen, O.H., Frandsen, L., Schjerling, P., Nishimura, E., and Grunnet, N. (2006). PGC-1alpha and PGC-1beta have both similar and distinct effects on myofiber switching toward an oxidative phenotype. Am J Physiol Endocrinol Metab *291*, E807-816.

Mortensen, O.H., Plomgaard, P., Fischer, C.P., Hansen, A.K., Pilegaard, H., and Pedersen, B.K. (2007). PGC-1beta is downregulated by training in human skeletal muscle: no effect of training twice every second day vs. once daily on expression of the PGC-1 family. J Appl Physiol *103*, 1536-1542.

Motoshima, H., Goldstein, B.J., Igata, M., and Araki, E. (2006). AMPK and cell proliferation--AMPK as a therapeutic target for atherosclerosis and cancer. The Journal of physiology *574*, 63-71.

Najafi-Shoushtari, S.H., Kristo, F., Li, Y., Shioda, T., Cohen, D.E., Gerszten, R.E., and Naar, A.M. (2010). MicroRNA-33 and the SREBP host genes cooperate to control cholesterol homeostasis. Science *328*, 1566-1569.

Norrbom, J., Sundberg, C.J., Ameln, H., Kraus, W.E., Jansson, E., and Gustafsson, T. (2004). PGC-1alpha mRNA expression is influenced by metabolic perturbation in exercising human skeletal muscle. J Appl Physiol *96*, 189-194.

Oberkofler, H., Linnemayr, V., Weitgasser, R., Klein, K., Xie, M., Iglseder, B., Krempler, F., Paulweber, B., and Patsch, W. (2004). Complex haplotypes of the PGC-1alpha gene are associated with carbohydrate metabolism and type 2 diabetes. Diabetes *53*, 1385-1393.

Ollila, S., and Makela, T.P. (2011). The tumor suppressor kinase LKB1: lessons from mouse models. J Mol Cell Biol *3*, 330-340.

Onishi, A., Peng, G.H., Poth, E.M., Lee, D.A., Chen, J., Alexis, U., de Melo, J., Chen, S., and Blackshaw, S. (2010). The orphan nuclear hormone receptor ERRbeta controls rod photoreceptor survival. Proceedings of the National Academy of Sciences of the United States of America *107*, 11579-11584.

Osman, A. (2012). MicroRNAs in health and disease--basic science and clinical applications. Clin Lab *58*, 393-402.

Palomer, X., Alvarez-Guardia, D., Rodriguez-Calvo, R., Coll, T., Laguna, J.C., Davidson, M.M., Chan, T.O., Feldman, A.M., and Vazquez-Carrera, M. (2009). TNF-alpha reduces PGC-1alpha expression through NF-kappaB and p38 MAPK leading to increased glucose oxidation in a human cardiac cell model. Cardiovascular research *81*, 703-712.

Parsons, D.W., Jones, S., Zhang, X., Lin, J.C., Leary, R.J., Angenendt, P., Mankoo, P., Carter, H., Siu, I.M., Gallia, G.L.*, et al.* (2008). An integrated genomic analysis of human glioblastoma multiforme. Science *321*, 1807-1812.

Permuth-Wey, J., Chen, Y.A., Tsai, Y.Y., Chen, Z., Qu, X., Lancaster, J.M., Stockwell, H., Dagne, G., Iversen, E., Risch, H.*, et al.* (2011). Inherited variants in mitochondrial biogenesis genes may influence epithelial ovarian cancer risk. Cancer Epidemiol Biomarkers Prev *20*, 1131-1145.

Pettersson, K., Svensson, K., Mattsson, R., Carlsson, B., Ohlsson, R., and Berkenstam, A. (1996). Expression of a novel member of estrogen response element-binding nuclear receptors is restricted to the early stages of chorion formation during mouse embryogenesis. Mechanisms of development *54*, 211-223.

Picard, F., Gehin, M., Annicotte, J., Rocchi, S., Champy, M.F., O'Malley, B.W., Chambon, P., and Auwerx, J. (2002). SRC-1 and TIF2 control energy balance between white and brown adipose tissues. Cell *111*, 931-941.

Possemato, R., Marks, K.M., Shaul, Y.D., Pacold, M.E., Kim, D., Birsoy, K., Sethumadhavan, S., Woo, H.K., Jang, H.G., Jha, A.K.*, et al.* (2011). Functional genomics reveal that the serine synthesis pathway is essential in breast cancer. Nature *476*, 346-350.

Puigserver, P., Wu, Z., Park, C.W., Graves, R., Wright, M., and Spiegelman, B.M. (1998). A cold-inducible coactivator of nuclear receptors linked to adaptive thermogenesis. Cell *92*, 829-839.

Rayner, K.J., Suarez, Y., Davalos, A., Parathath, S., Fitzgerald, M.L., Tamehiro, N., Fisher, E.A., Moore, K.J., and Fernandez-Hernando, C. (2010). MiR-33 contributes to the regulation of cholesterol homeostasis. Science *328*, 1570-1573.

Reddy, S.D., Ohshiro, K., Rayala, S.K., and Kumar, R. (2008). MicroRNA-7, a homeobox D10 target, inhibits p21-activated kinase 1 and regulates its functions. Cancer research *68*, 8195-8200.

Revillion, F., Bonneterre, J., and Peyrat, J.P. (1998). ERBB2 oncogene in human breast cancer and its clinical significance. Eur J Cancer *34*, 791-808.

Rodriguez-Calvo, R., Jove, M., Coll, T., Camins, A., Sanchez, R.M., Alegret, M., Merlos, M., Pallas, M., Laguna, J.C., and Vazquez-Carrera, M. (2006). PGC-1beta down-regulation is associated with reduced ERRalpha activity and MCAD expression in skeletal muscle of senescence-accelerated mice. J Gerontol A Biol Sci Med Sci *61*, 773-780.

Rohas, L.M., St-Pierre, J., Uldry, M., Jager, S., Handschin, C., and Spiegelman, B.M. (2007). A fundamental system of cellular energy homeostasis regulated by PGC-1alpha. Proc Natl Acad Sci U S A *104*, 7933-7938.

Romao, J.M., Jin, W., Dodson, M.V., Hausman, G.J., Moore, S.S., and Guan le, L. (2011). MicroRNA regulation in mammalian adipogenesis. Exp Biol Med (Maywood) *236*, 997-1004.

Rottiers, V., and Naar, A.M. (2012). MicroRNAs in metabolism and metabolic disorders. Nat Rev Mol Cell Biol *13*, 239-250.

Rottiers, V., Najafi-Shoushtari, S.H., Kristo, F., Gurumurthy, S., Zhong, L., Li, Y., Cohen, D.E., Gerszten, R.E., Bardeesy, N., Mostoslavsky, R.*, et al.* (2011). MicroRNAs in metabolism and metabolic diseases. Cold Spring Harbor symposia on quantitative biology *76*, 225-233.

Rutanen, J., Yaluri, N., Modi, S., Pihlajamaki, J., Vanttinen, M., Itkonen, P., Kainulainen, S., Yamamoto, H., Lagouge, M., Sinclair, D.A.*, et al.* (2010). SIRT1 mRNA expression may be associated with energy expenditure and insulin sensitivity. Diabetes *59*, 829-835.

Saetrom, P., Biesinger, J., Li, S.M., Smith, D., Thomas, L.F., Majzoub, K., Rivas, G.E., Alluin, J., Rossi, J.J., Krontiris, T.G.*, et al.* (2009). A risk variant in an miR-125b binding site in BMPR1B is associated with breast cancer pathogenesis. Cancer research *69*, 7459-7465.

Salzman, J., Marinelli, R.J., Wang, P.L., Green, A.E., Nielsen, J.S., Nelson, B.H., Drescher, C.W., and Brown, P.O. (2011). ESRRA-C11orf20 is a recurrent gene fusion in serous ovarian carcinoma. PLoS biology *9*, e1001156.

Sanyal, S., Matthews, J., Bouton, D., Kim, H.J., Choi, H.S., Treuter, E., and Gustafsson, J.A. (2004). Deoxyribonucleic acid response element-dependent regulation of transcription by orphan nuclear receptor estrogen receptor-related receptor gamma. Molecular endocrinology *18*, 312-325.

Schreiber, S.N., Emter, R., Hock, M.B., Knutti, D., Cardenas, J., Podvinec, M., Oakeley, E.J., and Kralli, A. (2004). The estrogen-related receptor alpha (ERRalpha) functions in PPARgamma coactivator 1alpha (PGC-1alpha)-induced mitochondrial biogenesis. Proceedings of the National Academy of Sciences of the United States of America *101*, 6472-6477.

Scott, G.K., Goga, A., Bhaumik, D., Berger, C.E., Sullivan, C.S., and Benz, C.C. (2007). Coordinate suppression of ERBB2 and ERBB3 by enforced expression of micro-RNA miR-125a or miR-125b. The Journal of biological chemistry *282*, 1479-1486.

Seth, A., Steel, J.H., Nichol, D., Pocock, V., Kumaran, M.K., Fritah, A., Mobberley, M., Ryder, T.A., Rowlerson, A., Scott, J.*, et al.* (2007). The transcriptional corepressor RIP140 regulates oxidative metabolism in skeletal muscle. Cell metabolism *6*, 236-245.

Shackelford, D.B., and Shaw, R.J. (2009). The LKB1-AMPK pathway: metabolism and growth control in tumour suppression. Nat Rev Cancer *9*, 563-575.

Shaw, R.J. (2009). LKB1 and AMP-activated protein kinase control of mTOR signalling and growth. Acta Physiol (Oxf) *196*, 65-80.

Shi, M., Liu, D., Duan, H., Shen, B., and Guo, N. (2010). Metastasis-related miRNAs, active players in breast cancer invasion, and metastasis. Cancer Metastasis Rev *29*, 785-799.

Si, M.L., Zhu, S., Wu, H., Lu, Z., Wu, F., and Mo, Y.Y. (2007). miR-21-mediated tumor growth. Oncogene *26*, 2799-2803.

Sihag, S., Cresci, S., Li, A.Y., Sucharov, C.C., and Lehman, J.J. (2009). PGC-1alpha and ERRalpha target gene downregulation is a signature of the failing human heart. Journal of molecular and cellular cardiology *46*, 201-212.

Sladek, R., Bader, J.A., and Giguere, V. (1997). The orphan nuclear receptor estrogen-related receptor alpha is a transcriptional regulator of the human medium-chain acyl coenzyme A dehydrogenase gene. Molecular and cellular biology *17*, 5400-5409.

Slamon, D.J., Godolphin, W., Jones, L.A., Holt, J.A., Wong, S.G., Keith, D.E., Levin, W.J., Stuart, S.G., Udove, J., Ullrich, A*., et al.* (1989). Studies of the HER-2/neu proto-oncogene in human breast and ovarian cancer. Science *244*, 707-712.

Song, B., Wang, C., Liu, J., Wang, X., Lv, L., Wei, L., Xie, L., Zheng, Y., and Song, X. (2010a). MicroRNA-21 regulates breast cancer invasion partly by targeting tissue inhibitor of metalloproteinase 3 expression. J Exp Clin Cancer Res *29*, 29.

Song, G., Sharma, A.D., Roll, G.R., Ng, R., Lee, A.Y., Blelloch, R.H., Frandsen, N.M., and Willenbring, H. (2010b). MicroRNAs control hepatocyte proliferation during liver regeneration. Hepatology *51*, 1735-1743.

Song, G., and Wang, L. (2008). Transcriptional mechanism for the paired miR-433 and miR-127 genes by nuclear receptors SHP and ERRgamma. Nucleic acids research *36*, 5727-5735.

Song, G., and Wang, L. (2009). A conserved gene structure and expression regulation of miR-433 and miR-127 in mammals. PLoS One *4*, e7829.

Sonoda, J., Laganiere, J., Mehl, I.R., Barish, G.D., Chong, L.W., Li, X., Scheffler, I.E., Mock, D.C., Bataille, A.R., Robert, F*., et al.* (2007a). Nuclear receptor ERR alpha and coactivator PGC-1 beta are effectors of IFN-gamma-induced host defense. Genes & development *21*, 1909-1920.

Sonoda, J., Mehl, I.R., Chong, L.W., Nofsinger, R.R., and Evans, R.M. (2007b). PGC-1beta controls mitochondrial metabolism to modulate circadian activity, adaptive thermogenesis, and hepatic steatosis. Proc Natl Acad Sci U S A *104*, 5223-5228.

Soriano, F.X., Liesa, M., Bach, D., Chan, D.C., Palacin, M., and Zorzano, A. (2006). Evidence for a mitochondrial regulatory pathway defined by peroxisome proliferator-activated receptor-gamma coactivator-1 alpha, estrogen-related receptor-alpha, and mitofusin 2. Diabetes *55*, 1783-1791.

Sorlie, T., Tibshirani, R., Parker, J., Hastie, T., Marron, J.S., Nobel, A., Deng, S., Johnsen, H., Pesich, R., Geisler, S.*, et al.* (2003). Repeated observation of breast tumor subtypes in independent gene expression data sets. Proceedings of the National Academy of Sciences of the United States of America *100*, 8418-8423.

Spizzo, R., Nicoloso, M.S., Lupini, L., Lu, Y., Fogarty, J., Rossi, S., Zagatti, B., Fabbri, M., Veronese, A., Liu, X.*, et al.* (2010). miR-145 participates with TP53 in a death-promoting regulatory loop and targets estrogen receptor-alpha in human breast cancer cells. Cell Death Differ *17*, 246-254.

St-Pierre, J., Lin, J., Krauss, S., Tarr, P.T., Yang, R., Newgard, C.B., and Spiegelman, B.M. (2003). Bioenergetic analysis of peroxisome proliferator-activated receptor gamma coactivators 1alpha and 1beta (PGC-1alpha and PGC-1beta) in muscle cells. The Journal of biological chemistry *278*, 26597-26603.

Stein, R.A., Chang, C.Y., Kazmin, D.A., Way, J., Schroeder, T., Wergin, M., Dewhirst, M.W., and McDonnell, D.P. (2008). Estrogen-related receptor alpha is critical for the growth of estrogen receptor-negative breast cancer. Cancer research *68*, 8805-8812.

Sun, L., Xie, H., Mori, M.A., Alexander, R., Yuan, B., Hattangadi, S.M., Liu, Q., Kahn, C.R., and Lodish, H.F. (2011). Mir193b-365 is essential for brown fat differentiation. Nat Cell Biol *13*, 958-965.

Sun, P., Sehouli, J., Denkert, C., Mustea, A., Konsgen, D., Koch, I., Wei, L., and Lichtenegger, W. (2005). Expression of estrogen receptor-related receptors, a subfamily of orphan nuclear receptors, as new tumor biomarkers in ovarian cancer cells. J Mol Med (Berl) *83*, 457-467.

Suzuki, T., Miki, Y., Moriya, T., Shimada, N., Ishida, T., Hirakawa, H., Ohuchi, N., and Sasano, H. (2004). Estrogen-related receptor alpha in human breast carcinoma as a potent prognostic factor. Cancer research *64*, 4670-4676.

Swinnen, J.V., Brusselmans, K., and Verhoeven, G. (2006). Increased lipogenesis in cancer cells: new players, novel targets. Curr Opin Clin Nutr Metab Care *9*, 358-365.

Takayanagi, S., Tokunaga, T., Liu, X., Okada, H., Matsushima, A., and Shimohigashi, Y. (2006). Endocrine disruptor bisphenol A strongly binds to human estrogen-related receptor gamma (ERRgamma) with high constitutive activity. Toxicol Lett *167*, 95-105.

Tang, C., and Oram, J.F. (2009). The cell cholesterol exporter ABCA1 as a protector from cardiovascular disease and diabetes. Biochimica et biophysica acta *1791*, 563-572.

Tavazoie, S.F., Alarcon, C., Oskarsson, T., Padua, D., Wang, Q., Bos, P.D., Gerald, W.L., and Massague, J. (2008). Endogenous human microRNAs that suppress breast cancer metastasis. Nature *451*, 147-152.

Teyssier, C., Gallet, M., Rabier, B., Monfoulet, L., Dine, J., Macari, C., Espallergues, J., Horard, B., Giguere, V., Cohen-Solal, M.*, et al.* (2009). Absence of ERRalpha in female mice confers resistance to bone loss induced by age or estrogen-deficiency. PLoS One *4*, e7942.

Tranter, M., Helsley, R.N., Paulding, W.R., McGuinness, M., Brokamp, C., Haar, L., Liu, Y., Ren, X., and Jones, W.K. (2011). Coordinated post-transcriptional regulation of Hsp70.3 gene expression by microRNA and alternative polyadenylation. J Biol Chem *286*, 29828-29837.

Tremblay, A.M., Dufour, C.R., Ghahremani, M., Reudelhuber, T.L., and Giguere, V. (2010). Physiological genomics identifies estrogen-related receptor alpha as a regulator of renal sodium and potassium homeostasis and the renin-angiotensin pathway. Molecular endocrinology *24*, 22-32.

Tremblay, A.M., and Giguere, V. (2007). The NR3B subgroup: an ovERRview. Nuclear receptor signaling *5*, e009.

Tremblay, A.M., Wilson, B.J., Yang, X.J., and Giguere, V. (2008). Phosphorylation-dependent sumoylation regulates estrogen-related receptor-alpha and -gamma transcriptional activity through a synergy control motif. Molecular endocrinology *22*, 570-584.

Tremblay, G.B., Bergeron, D., and Giguere, V. (2001a). 4-Hydroxytamoxifen is an isoform-specific inhibitor of orphan estrogen-receptor-related (ERR) nuclear receptors beta and gamma. Endocrinology *142*, 4572-4575.

Tremblay, G.B., Kunath, T., Bergeron, D., Lapointe, L., Champigny, C., Bader, J.A., Rossant, J., and Giguere, V. (2001b). Diethylstilbestrol

regulates trophoblast stem cell differentiation as a ligand of orphan nuclear receptor ERR beta. Genes & development *15*, 833-838.

Turcan, S., Rohle, D., Goenka, A., Walsh, L.A., Fang, F., Yilmaz, E., Campos, C., Fabius, A.W., Lu, C., Ward, P.S.*, et al.* (2012). IDH1 mutation is sufficient to establish the glioma hypermethylator phenotype. Nature *483*, 479-483.

Uldry, M., Yang, W., St-Pierre, J., Lin, J., Seale, P., and Spiegelman, B.M. (2006). Complementary action of the PGC-1 coactivators in mitochondrial biogenesis and brown fat differentiation. Cell Metab *3*, 333-341.

Valastyan, S., Reinhardt, F., Benaich, N., Calogrias, D., Szasz, A.M., Wang, Z.C., Brock, J.E., Richardson, A.L., and Weinberg, R.A. (2009). A pleiotropically acting microRNA, miR-31, inhibits breast cancer metastasis. Cell *137*, 1032-1046.

Villena, J.A., Hock, M.B., Chang, W.Y., Barcas, J.E., Giguere, V., and Kralli, A. (2007). Orphan nuclear receptor estrogen-related receptor alpha is essential for adaptive thermogenesis. Proceedings of the National Academy of Sciences of the United States of America *104*, 1418-1423.

Vu, E.H., Kraus, R.J., and Mertz, J.E. (2007). Phosphorylation-dependent sumoylation of estrogen-related receptor alpha1. Biochemistry *46*, 9795-9804.

Wang, J., Wang, Y., and Wong, C. (2010). Oestrogen-related receptor alpha inverse agonist XCT-790 arrests A549 lung cancer cell population growth by inducing mitochondrial reactive oxygen species production. Cell Prolif *43*, 103-113.

Wang, Z., Qi, C., Krones, A., Woodring, P., Zhu, X., Reddy, J.K., Evans, R.M., Rosenfeld, M.G., and Hunter, T. (2006). Critical roles of the p160 transcriptional coactivators p/CIP and SRC-1 in energy balance. Cell metabolism *3*, 111-122.

Warburg, O. (1956). On respiratory impairment in cancer cells. Science *124*, 269-270.

Ward, P.S., Patel, J., Wise, D.R., Abdel-Wahab, O., Bennett, B.D., Coller, H.A., Cross, J.R., Fantin, V.R., Hedvat, C.V., Perl, A.E.*, et al.* (2010). The common feature of leukemia-associated IDH1 and IDH2 mutations is a neomorphic enzyme activity converting alpha-ketoglutarate to 2-hydroxyglutarate. Cancer Cell *17*, 225-234.

Ward, P.S., and Thompson, C.B. (2012). Metabolic reprogramming: a cancer hallmark even warburg did not anticipate. Cancer Cell *21*, 297-308.

Watanabe, A., Kinoshita, Y., Hosokawa, K., Mori, T., Yamaguchi, T., and Honjo, H. (2006). Function of estrogen-related receptor alpha in human endometrial cancer. J Clin Endocrinol Metab *91*, 1573-1577.

Watkins, G., Douglas-Jones, A., Mansel, R.E., and Jiang, W.G. (2004). The localisation and reduction of nuclear staining of PPARgamma and PGC-1 in human breast cancer. Oncol Rep *12*, 483-488.

Wei, W., Wang, X., Yang, M., Smith, L.C., Dechow, P.C., Sonoda, J., Evans, R.M., and Wan, Y. (2010). PGC1beta mediates PPARgamma activation of osteoclastogenesis and rosiglitazone-induced bone loss. Cell metabolism *11*, 503-516.

Wende, A.R., Huss, J.M., Schaeffer, P.J., Giguere, V., and Kelly, D.P. (2005). PGC-1alpha coactivates PDK4 gene expression via the orphan nuclear receptor ERRalpha: a mechanism for transcriptional control of muscle glucose metabolism. Molecular and cellular biology *25*, 10684-10694.

Wilson, B.J., Tremblay, A.M., Deblois, G., Sylvain-Drolet, G., and Giguere, V. (2010). An acetylation switch modulates the transcriptional activity of estrogen-related receptor alpha. Molecular endocrinology *24*, 1349-1358.

Wise, D.R., DeBerardinis, R.J., Mancuso, A., Sayed, N., Zhang, X.Y., Pfeiffer, H.K., Nissim, I., Daikhin, E., Yudkoff, M., McMahon, S.B.*, et al.* (2008). Myc regulates a transcriptional program that stimulates mitochondrial glutaminolysis and leads to glutamine addiction. Proceedings of the National Academy of Sciences of the United States of America *105*, 18782-18787.

Woods, A., Dickerson, K., Heath, R., Hong, S.P., Momcilovic, M., Johnstone, S.R., Carlson, M., and Carling, D. (2005). Ca2+/calmodulin-dependent protein kinase kinase-beta acts upstream of AMP-activated protein kinase in mammalian cells. Cell metabolism *2*, 21-33.

Xiao, M., Yang, H., Xu, W., Ma, S., Lin, H., Zhu, H., Liu, L., Liu, Y., Yang, C., Xu, Y.*, et al.* (2012). Inhibition of alpha-KG-dependent histone and DNA demethylases by fumarate and succinate that are accumulated in mutations of FH and SDH tumor suppressors. Genes & development *26*, 1326-1338.

Xie, C.Q., Jeong, Y., Fu, M., Bookout, A.L., Garcia-Barrio, M.T., Sun, T., Kim, B.H., Xie, Y., Root, S., Zhang, J.*, et al.* (2009). Expression profiling of nuclear receptors in human and mouse embryonic stem cells. Molecular endocrinology *23*, 724-733.

Xie, W., Hong, H., Yang, N.N., Lin, R.J., Simon, C.M., Stallcup, M.R., and Evans, R.M. (1999). Constitutive activation of transcription and binding of

coactivator by estrogen-related receptors 1 and 2. Molecular endocrinology *13*, 2151-2162.

Xu, W., Yang, H., Liu, Y., Yang, Y., Wang, P., Kim, S.H., Ito, S., Yang, C., Xiao, M.T., Liu, L.X.*, et al.* (2011). Oncometabolite 2-hydroxyglutarate is a competitive inhibitor of alpha-ketoglutarate-dependent dioxygenases. Cancer Cell *19*, 17-30.

Yang, J., Williams, R.S., and Kelly, D.P. (2009). Bcl3 interacts cooperatively with peroxisome proliferator-activated receptor gamma (PPARgamma) coactivator 1alpha to coactivate nuclear receptors estrogen-related receptor alpha and PPARalpha. Molecular and cellular biology *29*, 4091-4102.

Yang, J.S., Phillips, M.D., Betel, D., Mu, P., Ventura, A., Siepel, A.C., Chen, K.C., and Lai, E.C. (2011). Widespread regulatory activity of vertebrate microRNA* species. Rna *17*, 312-326.

Yi, R., Qin, Y., Macara, I.G., and Cullen, B.R. (2003). Exportin-5 mediates the nuclear export of pre-microRNAs and short hairpin RNAs. Genes & development *17*, 3011-3016.

Yu, D.D., and Forman, B.M. (2005). Identification of an agonist ligand for estrogen-related receptors ERRbeta/gamma. Bioorg Med Chem Lett *15*, 1311-1313.

Yu, F., Deng, H., Yao, H., Liu, Q., Su, F., and Song, E. (2010). Mir-30 reduction maintains self-renewal and inhibits apoptosis in breast tumor-initiating cells. Oncogene *29*, 4194-4204.

Yu, S., Wong, Y.C., Wang, X.H., Ling, M.T., Ng, C.F., Chen, S., and Chan, F.L. (2008a). Orphan nuclear receptor estrogen-related receptor-beta suppresses in vitro and in vivo growth of prostate cancer cells via p21(WAF1/CIP1) induction and as a potential therapeutic target in prostate cancer. Oncogene *27*, 3313-3328.

Yu, Z., Wang, C., Wang, M., Li, Z., Casimiro, M.C., Liu, M., Wu, K., Whittle, J., Ju, X., Hyslop, T.*, et al.* (2008b). A cyclin D1/microRNA 17/20 regulatory feedback loop in control of breast cancer cell proliferation. J Cell Biol *182*, 509-517.

Yuneva, M., Zamboni, N., Oefner, P., Sachidanandam, R., and Lazebnik, Y. (2007). Deficiency in glutamine but not glucose induces MYC-dependent apoptosis in human cells. J Cell Biol *178*, 93-105.

Zhang, H., Gao, P., Fukuda, R., Kumar, G., Krishnamachary, B., Zeller, K.I., Dang, C.V., and Semenza, G.L. (2007). HIF-1 inhibits mitochondrial

biogenesis and cellular respiration in VHL-deficient renal cell carcinoma by repression of C-MYC activity. Cancer Cell *11*, 407-420.

Zhang, J., Du, Y.Y., Lin, Y.F., Chen, Y.T., Yang, L., Wang, H.J., and Ma, D. (2008). The cell growth suppressor, mir-126, targets IRS-1. Biochemical and biophysical research communications *377*, 136-140.

Zhang, Y., Ma, K., Sadana, P., Chowdhury, F., Gaillard, S., Wang, F., McDonnell, D.P., Unterman, T.G., Elam, M.B., and Park, E.A. (2006). Estrogen-related receptors stimulate pyruvate dehydrogenase kinase isoform 4 gene expression. The Journal of biological chemistry *281*, 39897-39906.

Zhao, Y., Li, Y., Lou, G., Zhao, L., Xu, Z., Zhang, Y., and He, F. (2012). MiR-137 targets estrogen-related receptor alpha and impairs the proliferative and migratory capacity of breast cancer cells. PLoS One *7*, e39102.

Zhu, S., Wu, H., Wu, F., Nie, D., Sheng, S., and Mo, Y.Y. (2008). MicroRNA-21 targets tumor suppressor genes in invasion and metastasis. Cell Res *18*, 350-359.

Zuercher, W.J., Gaillard, S., Orband-Miller, L.A., Chao, E.Y., Shearer, B.G., Jones, D.G., Miller, A.B., Collins, J.L., McDonnell, D.P., and Willson, T.M. (2005). Identification and structure-activity relationship of phenolic acyl hydrazones as selective agonists for the estrogen-related orphan nuclear receptors ERRbeta and ERRgamma. J Med Chem *48*, 3107-3109.

CHAPTER II: miR-378* Mediates Metabolic Shift in Breast Cancer Cells via the PGC-1β/ERRγ Transcriptional Pathway

PREFACE

As I undertook this study, miRNA regulation of ERR had not been established, nor had miRNA or ERR involvement in cancer cell metabolism. This chapter describes the identification of the molecular network connecting PGC-1β, miR-378* and ERRγ. We identify that this pathway is downstream of oncogenic ERBB2 signaling in breast cancer cells, and functions to induce the metabolic shift inherent to cancer cells known as the Warburg effect. In such, we revealed important functional differences between the ERR isoforms. Furthermore, we establish that miR-378* expression correlates with breast cancer progression in the human disease.

This chapter is a manuscript that has been published in the journal *Cell Metabolism*.

ABSTRACT

Cancer cell metabolism is often characterized by a shift from an oxidative to a glycolytic bioenergetic pathway, a phenomenon known as the Warburg effect. miR-378* is embedded within *PPARGC1b* which encodes PGC-1β, a transcriptional regulator of oxidative energy metabolism. Here we show that miR-378* expression is regulated by ERBB2 and induces a metabolic shift in breast cancer cells. miR-378* performs this function by inhibiting the expression of two PGC-1β partners, ERRγ and GABPA, leading to a reduction in tricarboxylic acid cycle gene expression and oxygen consumption as well as an increase in lactate production and in cell proliferation. *In situ* hybridization experiments show that miR-378* expression correlates with progression of human breast cancer. These results identify miR-378* as a molecular switch involved in the orchestration of the Warburg effect in breast cancer cells via interference with a well-integrated bioenergetics transcriptional pathway.

INTRODUCTION

The shift from aerobic, oxidative metabolism to anaerobic, glycolytic metabolism is a characteristic feature of cancer cells. To utilize glucose for energy, cells metabolize glucose to pyruvate which, under normal oxygen conditions, is processed by the tricarboxylic acid (TCA) cycle to reducing equivalents. Oxidative phosphorylation (OXPHOS) then produces ATP from the reducing equivalents, resulting in the production of cellular energy. In hypoxic conditions, pyruvate does not enter the TCA cycle, but instead is converted to lactic acid. This process of anaerobic glucose metabolism produces much less energy per molecule of glucose consumed, but occurs more rapidly than OXPHOS. Warburg observed that even under normal oxygen conditions, cancer cells rely more on glycolysis than OXPHOS, a now well recognized hallmark of cancer cell metabolism (Warburg, 1956a).

Recent work indicates that targeting metabolic pathways could be a powerful method to inhibit cancer growth and progression. Inhibiting lactate dehydrogenase A (LDH-A), the enzyme which mediates the processing of pyruvate to lactate, the final step of glycolysis, enhanced oxidative phosphorylation and respiration while it suppressed cell growth and tumorigenicity in *ERBB2*-initiated mammary epithelial tumor cell lines (Fantin et al., 2006). This directly links cellular proliferative ability to the switch between oxidative and anaerobic metabolism, and indicates the significance of the regulation of glucose metabolism for cancer cell maintenance and progression. Other studies have identified specific genes within the TCA cycle whose expression is important for inhibiting cancer cell proliferation. Succinate dehydrogenase (SDH) and fumarate hydratase (FH) were reported not only to be necessary for normal OXPHOS but also to possess tumor suppressor activity (Cervera et al., 2008; King et al., 2006), thus providing evidence that the oxidative metabolic switch is not only correlated with rates of cell proliferation but that these pathways are linked at a molecular level.

Members of the peroxisome proliferator activated receptor (PPAR) γ coactivator-1 (PGC-1) family (PGC-1α, PGC-1β and PPRC1) of transcriptional coactivator proteins are essential regulators of cellular energy metabolism (Lin et al., 2005). The PGC-1s work in concert with different transcription factors involved in regulating cellular energy metabolism, most notably the estrogen related receptors (ERRα, β and γ), a family of orphan nuclear receptors, and GA-binding protein α (GABPA), which have been shown to orchestrate cellular programs of oxidative phosphorylation (OXPHOS) and mitochondrial biogenesis (Dufour et al., 2007b; Giguere, 2008a; Mootha et al., 2004b; Schreiber et al., 2004b).

miRNAs are short, endogenous, non-coding RNAs known to inhibit the translation of their target transcripts. miRNAs are now considered essential regulators of development and physiological processes (Ma and Weinberg, 2008) and, by modulating oncogenic and tumor suppressor pathways, miRNAs might also play significant roles in cancer (Ventura and Jacks, 2009). Recently, expression of the miR-378*/miR-378 hairpin was reported to enhance cell survival and promote tumor growth and angiogenesis in a pooled cell line through targeting the transcription factor SuFu and Fus-1, suggesting that miR-378* and/or miR-378 possesses oncogenic potential (Lee et al., 2007). However, little else is known about the molecular mechanisms underlying miR-378* or miR-378 function in cancer cells. Herein, we report that miR-378*, a miRNA embedded within the *PPARGC1b* locus whose expression is under the control of the oncogene ERBB2 and increases during breast cancer progression, targets mRNAs encoding two important regulators of energy metabolism, ERRγ and GABPA, and induces the Warburg effect in breast cancer cells.

RESULTS

miR-378* is co-expressed with *PPARGC1b* in human breast cancer cells

The PGC-1-driven transcriptional network is subject to significant amounts of regulation, including at the transcriptional and post-translational levels, but a role for miRNAs in controlling this network has yet to be described (Lin et al., 2005). Scanning the genomic locations of known miRNAs revealed that the first intron of *PPARGC1b* (PGC-1β) contains a miRNA hairpin with the potential of generating two miRNAs, miR-378* and miR-378 (Fig. 2.1A). We also noticed that the Pictar miRNA prediction algorithm (http://pictar.mdc-berlin.de/) predicts miR-378* to target *ESRRG* (ERRγ), one of the nuclear receptors co-activated by PGC-1β. *GABPA*, a transcription factor directly downstream of the ERRs in the PGC-1 pathway, was also a predicted target of miR-378* according to both Pictar and Targetscan (http://www.targetscan.org/) algorithms. Because of miR-378*'s functional relationship to its host gene, *PPARGC1b*, and the observation that miRNAs located within introns are commonly co-transcribed with their host genes (Kim and Kim, 2007a), we hypothesized that miR-378* could be implicated in the regulation of a transcriptional network with PGC-1β at its nexus.

We first sought to determine whether the predicted miRNA genomic hairpin is processed into mature miRNAs in breast cancer cells. BT-474 cells, an ERBB2 positive cell line of human origin that also expresses PGC-1β, ERRα, ERRγ and GABPA, were chosen for further study. BT-474 cells were infected with an adenovirus containing the miR-378*/miR-378 genomic sequence, and qRT-PCR was used to detect the mature forms of the miRNAs. The expression data show that both mature miR-378* and miR-378 were produced from the genomic sequence (Fig. 2.1B). These results indicate that the genomic sequence does not promote the processing of one miRNA over the other, and that both mature miRNAs are formed in the context of breast cancer cells.

In contrast to PGC-1α, little is known about factors and pathways regulating the expression of PGC-1β. However, it has recently been shown that PGC-1β expression is up-regulated by c-Myc in renal carcinoma cells (Zhang et al., 2007), demonstrating that PGC-1β expression can be regulated by oncogenic signals. We next investigated whether PGC-1β expression could be influenced by manipulating the oncogenic ERBB2 pathway that plays a preeminent role in tumors of the breast. Indeed, siRNA knockdown of *ERBB2* expression in SkBr3 human breast cancer cells led to a parallel decrease (~50%) in *PPARGC1b* and mature miR-378* and miR-378 expression (Fig. 2.1C). This regulatory pathway is also operational in the BT-474 breast cancer cell line (Fig. 2.1D). These results show that *PPARGC1b* and its intronic miRNAs are co-regulated, in addition to linking the expression of these genes to changes in *ERBB2* levels.

miR-378* targets endogenous *ESRRG* and *GABPA*

Human *ESRRG* is predicted to be targeted by miR-378* at two regions within its 3'UTR (Fig. 2.2A) while a single sequence within the *GABPA* 3'UTR is predicted to be recognized by the miRNA (Fig. 2.2B). Target site locations are numbered relative to the start of the 3'UTR. To validate *ESRRG* and *GABPA* as *bona fide* targets of miR-378*, we cloned the miR-378* predicted target regions within each gene's 3'UTR downstream of a Renilla luciferase reporter gene. These reporter plasmids were then co-transfected with either control miRNA or miR-378* and cell extracts monitored for luciferase activity. Repression of luciferase activity, as compared to control, was observed for all predicted target sites (Fig. 2.2, C and D) and completely abolished for all targeted regions by the mutation of one base at position 4 of the seed sequence within the *ESRRG* target sequence and at position 3-6 of the *GABPA* target sequence, indicating the specificity of the interaction between miR-378* and its target regions. The same result was obtained for the mouse genes indicating that the

targeting functions of miR-378* are conserved between species (Fig. 2.3). To determine if miR-378* could target endogenous *ESRRG* and *GABPA*, we measured RNA levels of *ESRRA*, *ESRRB*, *ESRRG* and *GABPA* in BT-474 cells transfected either with control miRNA or miR-378*. We found that introduction of miR-378* decreases the levels of *ESRRG* and *GABPA* transcripts at 2, 4, and 6 days post-transfection, but that the levels of *ESRRA*, which is not a target of miR-378*, were unaffected (Fig. 2.2E). *ESRRB* transcripts were not detected. We confirmed this result at the protein level by testing BT-474 cells transfected with control miRNA or miR-378* either 2 days or 7 days after transfection by Western blotting. Again there was no noticeable change of ERRα levels, while both ERRγ and GABPA levels were decreased upon miR-378* expression (Fig. 2.2F). To further verify the specificity of interactions between miR-378* and its targets, we used a miRNA inhibitor to specifically block miR-378* action. Upon transfection of BT-474 cells with the miR-378* inhibitor, we detected a statistically significant increase (~30%, $p \leq 0.01$) in endogenous transcript levels of both *ESRRG* and *GABPA*, indicating that inhibiting endogenous miR-378* alleviates the repressive effect on its targets (Fig. 2.2G). Similarly, the reduction in endogenous transcript levels of *ESRRG* and *GABPA* in response to miR-378* expression is rescued when miR-378* is co-transfected with the miR-378* inhibitor (Fig. 2.2G). Inhibition of endogenous miR-378* also causes an increase in endogenous ERRγ and GABPA proteins (Fig. 2.2H). Finally, knock-down of *ERBB2* leads to an increase in mRNA levels of both *ESRRG* and *GABPA* (Fig. 2.2I). Taken together, these results indicate that *ESRRG* and *GABPA* are genuine endogenous ERBB2 and miR-378* targets in breast cancer cells and that, notably, the regulatory effect of miR-378* upon ERR family members is specific to *ESRRG*.

miR-378* regulates metabolic genes via its target, ERRγ

We next asked what role miR-378* would have in regulating the PGC-1β/ERR pathway in cancer cells. Recent genome-wide location analyses by ChIP-on-chip have identified ERRα and γ as direct regulators of TCA cycle genes (Alaynick et al., 2007b; Charest-Marcotte et al., 2010b; Deblois et al., 2009a; Dufour et al., 2007b; Sonoda et al., 2007; Tremblay et al., 2010b), suggesting that changes in ERRγ levels could have a direct impact on the expression of metabolic genes in breast cancer cells and thereby inducing a push toward the anaerobic, glycolytic pathway by affecting OXPHOS. Using a ChIP-based assay, we first established that ERRγ binds to regulatory regions located in the vicinity of TCA cycle genes in BT-474 cells. ERRγ binds to promoters or proximal enhancers of genes encoding enzymes participating in nearly all steps of the TCA cycle (Fig. 2.4A). Table 2.1 outlines the conservation between human and mouse of the ERR response elements (ERREs) found within the ERRγ-bound regions. The expression of most of these target genes is down-regulated via knock-down of ERRγ by a specific siRNA, further validating a major role for ERRγ in the control of TCA cycle gene expression (Fig. 2.4, B and D). ERRγ also controls the expression of a subset of glycolytic genes as *LDHA* levels are increased in response to si*ESRRG* treatment whereas *LDHB* expression is decreased (Fig. 2.4C). Since the *LDHA* isoform has been shown to play a major role in *neu*-initiated mammary tumorigenesis (Fantin et al., 2006) and considering that its expression is the highest of the *LDH* isoforms in BT-474 cells, it is possible that repression of *LDHA* by ERRγ mediates an inhibition of glycolysis.

We next tested the hypothesis that the expression of these metabolic genes could be affected by the presence of miR-378*. qRT-PCR data indeed shows that miR-378* expression causes a decrease in transcript levels of key TCA cycle genes while inhibition of endogenous miR-378* using a specific inhibitor causes an increase in the expression of many TCA cycle genes (Fig. 2.4D). Of the glycolytic genes, miR-378* decreases *HK2* levels and increases *LDHD* levels (Fig. 2.4C).

Interestingly, not all of the known TCA cycle ERR target genes were downregulated in response to miR-378*. It should be noted that ERRα is present in abundance in these cells, and ERR isoforms are known to compensate for each others' absence (Dufour et al., 2007b). This indicates that the direct ERRγ target genes which are downregulated in response to miR-378*, *CS*, *SDHB* and *FH*, could be specific genes for which ERRα cannot compensate in response to downregulation of ERRγ. We validated this hypothesis by using a siRNA specific for ERRα (Fig. 2.4B and D) and found that, while some ERR target genes respond in the same way to depletion of either ERRα or γ, ERRα is not capable of compensating for the loss of control of *CS*, *SDHB* or *FH* by ERRγ. Of note, *SDHB* and *FH* have recently been reported to act as tumor suppressors (King et al., 2006), further implicating the function of this pathway simultaneously in regulation of both metabolism and cancer. Of the glycolytic genes tested in these conditions, *LDHA* responded in an opposite manner to ERRα and γ depletion, while *LDHB* levels decreased in response to depletion of both ERRs (Fig. 2.4C). Furthermore, these experiments suggest that *GABPA* is downstream of ERRγ, as it is down-regulated in response to miR-378* and similarly so in response to ERRγ knock-down (Fig. 2.4D). Notably, *GABPA* increases slightly in expression in response to ERRα knock-down, indicating that it could be regulated by the ERRs in an isoform-specific fashion. Taken together, these results suggest that miR-378* regulates gene expression in a manner that represses oxidative metabolism and, in so doing, favors glycolysis.

miR-378* induces a metabolic shift in cancer cells

We next sought to determine if miR-378* was capable of inducing a metabolic shift in cancer cells. First, short term exposure to miR-378* by transient transfection slightly but significantly increases cell proliferation of BT-474 breast cancer cells (Fig. 2.5A). Furthermore, induction of miR-378* caused an increase of cellular lactate (Fig. 2.5B) and a reduction of total

cellular respiration (Fig. 2.5C). Knock-down of ERRγ expression using a siRNA generated a similar reduction in total cellular respiration (Fig. 2.5D). Cellular respiration is composed of non-mitochondrial and mitochondrial components. In BT-474 cells, we did not detect any non-mitochondrial respiration. Mitochondrial respiration is comprised of coupled and uncoupled respiration. Coupled respiration is linked to ATP turnover while uncoupled respiration is linked to proton leak. Introduction of miR-378* decreased coupled respiration by approximately a third (Fig. 2.5E). ATP levels were stable in cancer cells expressing miR-378* (Fig. 2.5F), indicating that the overall energy homeostasis was maintained.

We then confirmed that miR-378* induces a metabolic shift by measuring cellular bioenergetic outputs in response to inhibition of endogenous miR-378* in BT-474 cells using a miRNA inhibitor. Inhibition of miR-378* caused a decrease in cell number (Fig. 2.5G), a reduction in lactate production (Fig. 2.5H), and an increase in cellular respiration (Fig. 2.5I). Mitochondrial content of BT-474 cells treated with either miR-378* or the miRNA inhibitor was not significantly different from control cells (Fig. A.2.1). Taken together, both gain and loss of function studies validate that miR-378* regulates the Warburg effect. These data indicate that miR-378* displays the oncogenic characteristic of promoting cell proliferation while simultaneously inducing a metabolic shift away from oxidative metabolism.

In order to validate our model of miR-378* function in a different model of breast cancer, we used parental mouse mammary epithelial cells, NMuMG, as a control cell line and the NT2196 cell line as an *ex-vivo* model of ERBB2-induced mammary tumorigenesis (Ursini-Siegel et al., 2007a). Endogenous miR-378*, miR-378 and *Ppargc1b* expression was upregulated in the NT2196 cells expressing high levels of ERBB2 as compared to the parental NMuMG mammary cells (Fig. 2.5J). We next measured the endogenous levels of the miR-378* downstream targets in both cells lines (Fig. 2.5K and L). Interestingly, *Gabpa* mRNA levels were unchanged between the two cell lines (Fig. 2.5K) but GABPA protein was

remarkably decreased in the NT2196 cells as compared to NMuMG cells (Fig. 2.5L). *Esrrg* mRNA expression was too low to quantify accurately but ERRγ protein was decreased in NT2196 cells as compared to NMuMG cells (Fig. 2.5L). These results show that ERRγ and GABPA are direct targets of endogenous miR-378* across different cell lines of mouse and human origin. In addition, two of the three miR-378*- and ERRγ-controlled TCA cycle genes, *Fh1* and *Sdhb*, were significantly downregulated in NT2196 cells as compared to NMuMG cells (Fig. 2.5K), thereby recapitulating much of the effect of miR-378* on TCA cycle genes identified in human breast cancer cells. Correspondingly, NT2196 cells display the Warburg effect in comparison to NMuMG cells, in that NT2196 cells produce more lactate (Fig. 2.5M) and have a decreased rate of respiration (Fig. 2.5N). Importantly, while both miR-378* and *Ppargc1b* expression is increased by similar amounts in NT2196 cells compared to NMuMG cells, the ERBB2 expressing cells display a shift toward the Warburg effect, thereby overriding the ability of *Ppargc1b* to promote oxidative metabolism.

miR-378* expression and breast cancer progression

To determine the physiological relevance of miR-378* in breast cancer, we performed *in situ* hybridization on sections of normal breast tissue, tumors and lymph node metastases with a probe directed against miR-378*. Representative miR-378* staining on a tissue microarray (TMA) containing 160 cores of tissue classified as normal, ductal carcinoma *in situ* (DCIS), tumor or metastatic lymph node is shown on Fig. 2.6A. We scored miR-378* expression in each core on a scale from 0 (no expression) to 3 (high expression) based on colorimetric signal intensity (Fig. 2.6B). The mean score of normal tissue was significantly lower than that of DCIS, tumor or lymph node tissue, indicating that miR-378* expression increases as tissue progresses from a normal to a cancerous state. Indeed, ~60% of the normal tissue cores scored 0, suggesting that in most cases miR-378*

is only expressed after the onset of cancerous progression. In addition, the mean score of metastatic lymph node tissue was significantly higher than that of both DCIS and tumor tissue. To analyze the data by matched samples, cores from the same patient but with different pathologies were grouped and the corresponding scores were compared (Table 2.2). A similar trend was recapitulated as with the unmatched samples; the mean score of normal cores was significantly lower than that of any other type of core. The mean score of tumor cores was significantly higher than that of matched DCIS cores, indicating that within a patient, as a cancer progresses from DCIS to tumor, miR-378* expression increases. The means of matched DCIS and tumor cores are smaller than that of the corresponding lymph node cores, but the differences are not significant due to the small sample size of these groups.

DISCUSSION

The molecular mechanisms that govern a shift in energy metabolism to the advantage of cancer cells are complex and only partially understood. In this study, we demonstrate that a specific miRNA, miR-378*, plays an important role in reprogramming breast cancer cells such that TCA cycle activity is reduced and the cells are less dependent on OXPHOS to fulfill their energy demands. miR-378*, whose expression is regulated by the ERBB2 signaling pathway, achieves this metabolic shift by suppressing the expression of two key regulators of energy metabolism, ERRγ and GABPA. This study shows that a miRNA can be both a component and a regulator of a well integrated transcriptional pathway, and that cancer cells can specifically exploit the PGC-1β/ERR/GABPA bioenergetics pathway for growth and proliferation (Fig. 2.7A).

Since miR-378* affects cellular respiration in an opposite manner from PGC-1β, it can appear that these two co-transcribed molecules function in a contradictory manner. However, when taken together with knowledge regarding the function of these two molecules and recent literature on transcriptional feedback loops, the miR-378*/PGC-1β relationship can be integrated in a cohesive mechanism. First, miR-378* causes a decrease in cellular respiration and an increase in lactate production in breast cancer cells. Overexpression of PGC-1β has been shown to induce cellular respiration (St-Pierre et al., 2003a), yet its effect on lactate production has not been shown. Studies based on PGC-1β knockout mice are limited in terms of their contribution to what we understand about the relationship between miR-378* and PGC-1β as miR-378* is still expressed in these mice (Fig. 2.8). To shed light on the role of PGC-1β in breast cancer cells, we knocked down its expression in breast cancer cells using siRNA. We observed a decrease in genes required for cellular respiration and glycolysis (Fig. 2.9), indicating that PGC-1β is required for both metabolic processes. Thus, the function of PGC-1β is not

to inhibit the Warburg effect but to maintain overall metabolic gene expression. This would make miR-378* the 'decision maker' in terms of which metabolic pathway is used most dominantly, while not diminishing the importance of PGC-1β for allowing cellular metabolic function. Second, since miR-378* is able to modulate the relative levels of PGC-1β partners, it can directly influence the metabolic function of PGC-1β. In essence, the role of PGC-1β as a co-activator only allows it to dictate cellular programs that its available transcriptional binding partners are capable of mediating. By targeting and regulating specific partners of PGC-1β, miR-378* amplifies its ability to choose which metabolic pathways dominate under specific physiological cues. This hypothesis is supported by our data from the NMuMG/NT2196 *ex-vivo* cell system (Fig. 2.5J-N) in which the Warburg effect is induced in a context where both miR-378* and *PPARGC1B* expression levels are endogenously elevated in response to *Neu* expression. Third, feedforward loops are the most common network motifs in transcription networks (Alon, 2007). In particular, the incoherent type-1 feedforward loop motif (Fig. 2.7B), which describes the miR-378*/PGC-1β/ERRγ relationship (Fig. 2.7C), functions as a pulse generator and response accelerator in biological systems. It has been demonstrated that the incoherent type-1 feedforward loop motif network response can be dependent on the fold-change in the input signal, and not on its absolute level, a trait important for cellular signaling (Goentoro et al., 2009). Taken together, the type of feedback loop in which miR-378* and PGC-1β participate in is not only very common in biology but the seemingly contradictory functions of two molecules within this same loop actually allows for a specific type of network response.

The observation that decreased cell respiration in response to miR-378* is accompanied by increased cell number suggests that other biochemical pathways could be activated to allow for sufficient anapleurosis. For example, miR-378* could promote aerobic glycolysis and simultaneously increase glutaminolytic flux (Jones and Thompson,

2009). However, we did not observe any major changes in the expression of key enzymes involved in glutamine metabolism in response to modulation of miR-378* levels (Fig. A2.2). These results indicate that the remaining mitochondrial function may be adequate to support the anapleurotic reactions necessary for enhanced cell proliferation.

It had previously been shown that a genomic construct co-expressing the miR-378*/miR-378 sequence causes an increase in cell survival and a decrease in Caspase 3 activity in U87 cells, and injection of these cells into nude mice induces tumor formation, indicating the ability of this hairpin to promote oncogenesis (Lee et al., 2007). Our TMA data quantifies miR-378* expression in breast cancer, and shows that miR-378* expression increases with tumor progression in a statistically significant manner (Fig. 2.6B). In addition, ERBB2 positivity status of the DCIS samples showed a trend (p = 0.0996) of increased miR-378* expression. The mean miR-378* expression within the ERBB2 positive samples is also higher in normal and tumor tissue of patients whose cancer recurred compared to those whose cancer did not recur. Small sample size limits statistical significance as matched samples are rare, but these results indicate another interesting trend of miR-378* expression in breast cancer.

The observation that miR-378* specifically targets ERRγ provides a possible mechanism to account for the correlative opposing roles that ERRα and γ play as negative and positive breast cancer biomarkers, respectively (Ariazi et al., 2002a; Suzuki et al., 2004a). ERR regulation of target genes can depend on many factors including tissue context and the presence of cofactors. In this respect, our results suggest that ERRα/PGC-1β favors activation of the glycolytic pathway while ERRγ/PGC-1β promotes oxidative metabolism in cancer cells, and that modulation of ERR isoform levels by miR-378* allows it to promote one pairing over the other. Less well studied are the differences between the ERR isoforms with respect to regulation of target gene levels. While Dufour et al. (2007) have shown that ERRα and ERRγ can regulate the

same direct target genes, the *SHP* promoter is activated by ERRγ but not ERRα or ERRβ (Sanyal et al., 2002). In breast cancer cells, we also observed different responses of specific metabolic genes to ERRα and ERRγ. This suggests that the transcriptional output of each ERR is not equivalent, thus adding to the complexity of their function. Taken together with their opposing roles in breast cancer, it will be important to further elucidate the functional differences between these two isoforms in breast cancer and metabolic diseases.

MATERIALS AND METHODS

Cell Culture

In general, cells were maintained in 5% CO_2 at 37°C. Unless stated otherwise, BT-474, SkBr3 and COS-1 cells were grown in DMEM supplemented with 10% fetal bovine serum (Sigma), 1 mM sodium pyruvate (GIBCO), 200 Units/mL penicillin (GIBCO), 200 μg/mL streptomycin (GIBCO) and 4 mM l-glutamine (GIBCO). NMuMG and NMuMG NT2196 cells were grown in DMEM supplemented as above but instead with half the antibiotics, plus the addition of 20 mM Hepes and 10 μg/mL insulin. 1 mg/mL puromycin was added to media used for NT2196 cells.

To harvest, cells were washed with 1X PBS and centrifuged at 5,000 rpm for 15min. The cell pellets were flash-frozen and stored at -80°C.

Adenovirus Generation and Infection

The human miR-378* genomic sequence with ~150 bp on either side of the miRNA hairpin was cloned into an adenovirus vector. The human miR-378* genomic sequence was obtained from the UCSC genome browser database, and cloned from human genomic DNA (Roche) using PCR with primers forward:

5'-TGGAACTAAGCTTATGAGCTTTGAGCCGC-CCCTAGAAGG

and reverse:

5'-GAACTTGATATCATCTCACATGCAAACACTGCTCACCC (underlined bases were added for restriction enzyme recognition and cleavage) into the *Hind*III and *Eco*RV sites of the Dual-CCM plasmid. Clones were sequenced by Genome Quebec. Qbiogene generated and amplified adenovirus expressing this miR-378* genomic sequence. Cells were infected at MOI=25.

BT-474 cells were plated at 100,000 cells/mL 24hrs before infection. Cells were infected with either control adenovirus expressing GFP (Qbiogene) or miR-378*-expressing adenovirus. Media was replaced

24hrs after infection, and cells were harvested 48hrs post-infection. RNA was isolated and Taqman miRNA qRT-PCR was performed as described below. The experiment was independently repeated twice.

siRNA experiments:

Cells were transfected using HiPerFect according to the reverse-transfection protocol. For optimal protein knockdown, cells were harvested 48 h post-transfection for siERBB2 and siESRRA, 60 h post-transfection for siPPARGC1b experiments, and 6 d post-transfection for siESRRG experiments.

siERBB2 experiment

Cells (supplemented with 25U/mL penicillin and streptomycin) were transfected with SMARTpool ERBB2 siRNA or scramble siRNA (Dharmacon) using HiPerFect transfection reagent (Qiagen). Typically, transfections were performed in a 24-well format using 4.5 μL of HiPerFect reagent at 0.5 X 10^5 cells per well. The concentration of siRNA was 50 nM in a final volume of 600 μL. The same RNA sample was used for reverse transcription using polyA primers (to make standard cDNA) and Taqman miRNA qRT-PCR. cDNA was tested by Real-Time PCR in triplicate, and the entire experiment was repeated at least twice.

siESRRA experiment

Cells were transfected with ERRα siRNA or scramble siRNA (IDT) at 50nM in a final volume of 600 μL. Typically, transfections were performed in a 24-well format using 4.5 μL of HiPerFect reagent at 1.5 X 10^5 cells per well. Transfection was otherwise carried out as for the siErbB2 experiment (see above).

Duplex sequences of siRNA against human ERRα:

5'-/5Phos/rArGrArGrGrArGrUrArUrGrUrUrCrUrArCrUrArArArGrGCC-3'

and

5'-rGrGrCrCrUrUrUrArGrUrArGrArArCrArUrArCrUrCrCrUrCrUrCrG-3'

Duplex sequences of siRNA human scramble:

5’-/5Phos/rCrUrUrCrCrUrCrUrCrUrUrUrCrUrCrUrCrCrCrUrUrGrUGA-3’
and
5’-rUrCrArCrArArGrGrGrArGrArGrArArArGrArGrArGrGrArArGrGrA-3’

<u>siESRRG and siPPARGC1b experiments</u>

Unless stated otherwise, cells were transfected with SMARTpool ESRRG siRNA, siPPARGC1b or scramble siRNA (Dharmacon) at 100 nM in a final volume of 5 mL. Typically, transfections were performed in 6cm plates using 37.5 μL of HiPerFect reagent and 800,000 cells per plate. For siESRRG, media was changed 2 days after transfection. The experiments were otherwise carried out as for the siErbB2 experiment (see above).

Reporter Construct Cloning and Transfection

Regions of the human *ESRRG* and *GABPA* 3’UTRs (sequences from http://genome.ucsc.edu database, human March 2006 assembly) predicted to be targeted by miR-378* (by Pictar, http://pictar.bio.nyu.edu/) were cloned into the phRL-TK(Int-) vector (Promega) at the 3’UTR position relative to the Renilla luciferase gene. Mutants were generated the same way. Primers are listed in Appendix Table A.2.1. Data shown is based on cloning done by annealing oligos containing miR-378* target regions ± 16 nucleotides of endogenous flanking region sequence on either side of the miR-378* binding site. The same experiment was performed with the mouse miR-378* target regions in the *Gabpa* and *Esrrg* 3’UTRs (Figure 2.3). Human miR-378* target regions of these genes were also cloned with ± 150 nucleotides of endogenous flanking region sequence on either side of the miR-378* binding site (selected by PCR), and the same result was achieved (data not shown). Point mutations of these constructs also abolished the repressive effect of miR-378* (data not shown).

Reporter constructs were co-transfected with miR-378* Mimic or control miRNA Mimic into COS-1 cells using Lipofectamine 2000. COS-1 cells were transfected with Lipofectamine 2000 (Invitrogen) according to the manufacturer’s protocol (using 2 μL Lipofectamine 2000 and 100μL

Opti-Mem Reduced Serum Medium 1X (GIBCO) per well) in 12-well plates with 200ng luciferase reporter, 10pmol RNA (hsa-miR-378* miRIDIAN Mimic (Dharmacon, catalog #C-300685-03) or miRIDIAN microRNA Mimic Negative Control #2 (Dharmacon, catalog #CN-002000-01)) and 1 µL β-galactosidase protein (Sigma) per well. Cells were harvested and assayed for luciferase activity using the Renilla Luciferase Assay System (Promega) and β-galactosidase activity 24 h post-transfection. Luciferase data was normalized to the β-galactosidase transfection efficiency control levels. Experiments were performed in quadruplicate and each experiment was repeated multiple times.

miRNA Transfection

Unless stated otherwise, all miRNA transfection experiments were carried out as follows. Cells were plated at 150,000 cells/mL (usually in 6cm plates) and transfected after 24hrs with 100nM (final concentration) of either miR-378* Mimic (Dharmacon, currently named hsa-miR-378* Mimic) or Negative Control #2 (see above for product details) with Lipofectamine 2000 (Invitrogen). Following the standard protocol, Lipofectamine 2000 was complexed with Opti-mem 1 Reduced Serum Medium 1X (GIBCO) at a ratio of 1:30, and a 2:3 ratio of Lipofectamine 2000 to 20 µM RNA was followed. Cells were harvested 48 hrs after transfection. The experiment was always independently repeated at least three times.

miRNA Inhibitor Transfection

For Fig. 2.2G experiments, BT-474 cells were plated at 200,000 cells/mL in 6-well plates 24 hrs before transfection. Cells were transfected simultaneously with final concentrations of either 75nM miRIDIAN miRNA Mimic Negative Control #2 or hsa-miR-378* miRIDIAN Mimic and either 100nM miRIDIAN miRNA Inhibitor Negative Control #2 (Dharmacon, IN-002000) or miRIDIAN miR-378* Inhibitor (Dharmacon, I-300175). Following the standard protocol, Lipofectamine 2000 was complexed with

Opti-mem 1 Reduced Serum Medium 1X (GIBCO) at a ratio of 3:100, and a 1:2.3 ratio of Lipofectamine 2000 to 20 μM RNA. Cells were harvested two days after transfection. The experiment was independently repeated three times.

For other miR-378* inhibitor experiments, BT-474 cells were plated at 150,000 cells/mL typically in 6 cm plates 24 hrs before transfection. Transfection for respiration experiments was carried out in 10 cm plates, and materials and reagents were scaled up accordingly. Cells were transfected with a 90 nM final concentration of either control or miR-378* inhibitors (Dharmacon, as above). Transfection was carried out as above, typically using 10uL Lipofectamine and 600 μL Optimem 1 per 6 cm plate. Cells were harvested 4 days after transfection for all experiments except samples for ERRγ detection in Fig. 2.2H which were harvested 6 days after transfection.

RNA Isolation, Reverse Transcription and Real Time quantitative PCR

All RNA was isolated using the miRNeasy Mini Kit (Qiagen) except for RNA used in Fig. 2.4C which was isolated using the RNeasy Mini Kit (Qiagen). DNase treatment was always performed during RNA isolation. cDNA was made from either 1 or 2 μg of total RNA by reverse transcription with Oligo(dT) primer, dNTPs, 5X 1st strand buffer, DTT, RNase inhibitor, and Superscript II RNase H Reverse Transcriptase (Invitrogen). cDNA was amplified by qRT-PCR using specific primers (Appendix Tables A.2.3 and A.2.4) and the QuantiTect SYBR Green PCR Kit (Qiagen) following the Qiagen software protocol. Real-Time qRT-PCR was carried out in a LightCycler instrument (Roche). All primers were designed using Oligo 4.04 Primer Analysis Software with sequence data from the http://genome.ucsc.edu database human March 2006 assembly. Primers to detect cDNA were designed so that either the product included at least one intron and/or one primer was located on both an exon and an intron in order to avoid detecting genomic DNA contamination. All

experiments were repeated at least twice (see figure legends for specific details).

miRNA levels were detected using Taqman miRNA qRT-PCR following the manufacturer's instructions (Applied Biosystems). Taqman miRNA qRT-PCR was performed using 0.01 μg total RNA isolated using the Qiagen miRNeasy Kit. All primers used were from the Taqman miRNA Assay Kits (Applied Biosystems), and the corresponding Real-Time qRT-PCR reactions were carried out in a Corbett Research Rotor-Gene instrument. All experiments were repeated at least twice.

Primer sets were tested on cDNA dilutions, and the REST spreadsheet was used to determine the primer efficiency (Nucleic Acids Research 2001 Vol 29 (9) e45 and 2002 Vol 29 (9) e36). Only primers with good efficiencies were used, and only data produced using primers with similar efficiencies was compared. Care was taken to test multiple control primers in order to ensure control gene stability between treatments and to ensure that normalization to different control primers gave the same result. Each qRT-PCR reaction was performed in triplicate, and the Ct values were averaged before normalization. A Student's t-test was applied to determine significance.

Western Blots

Briefly, protein was harvested with RIPA buffer and quantified, and then resolved on an SDS-PAGE gel. Protein was then transferred onto a membrane, blocked, and then incubated with primary antibody. After three washes, membranes were incubated with secondary antibody. After three more washes, proteins were detected using chemiluminescence. The loading control protein was either detected on the same membrane simultaneously with the target proteins if size differences allowed, or the membranes were stripped and re-probed to detect the loading control. Precise details and antibody conditions follow.

Immunoblotting to detect ERRα, ERRγ and GABPA in cells transfected

with miRNA was performed by isolating protein from harvested cell pellets using RIPA protein lysis buffer containing a mini protease inhibitor cocktail tablet (Roche). Protein was quantified using the Bradford method (Bio-Rad Protein Assay), and 75 µg of protein was resolved on a 10% SDS-PAGE gel, transferred onto a PVDF membrane (Amersham Biosciences) and blocked overnight at 4°C in PBS-T containing 5% milk. Membranes were incubated for 1hr with either anti-ERRα antibody (see protocol to verify siRNA knock-down, below), purified specific anti-ERRγ polyclonal antibody (gift from Dr. Ronald M. Evans) (1:2000), or anti-GABP-α (G-1) (1:500, sc-28312, lot F1804) diluted in PBS-T containing 5% milk. Following three washes in PBS-T containing 5% milk, the membranes were incubated for 1hr with secondary antibody diluted in PBS-T containing 5% milk: anti-rabbit (NA9340V, GE Healthcare, 1:5000) was used for membranes probed for ERRα and ERRγ, and anti-mouse (NA931V, GE Healthcare, 1:5000) was used for those probed for GABPA. After washing three times with PBS-T, proteins were detected using Lumi-Light Plus Western Blotting Substrate (Roche). Blots were stripped, detected to assure no remaining antibody, and re-probed with anti-α-Tubulin (see protocol to verify siRNA knock-down, below) for 1hr, washed three times with PBS-T and milk, and incubated with anti-mouse (NA931V, GE Healthcare, 1:10000) secondary antibody for 1hr before the final wash and detection with Lumi-Light Substrate. This was done to confirm equal protein loading and transfer.

Immunoblotting to verify *ESRRG*, *ESRRA* and *ERBB2* siRNA knockdown was carried out as follows. Treated cells were washed twice with PBS and solubilized on ice (as above). Protein was quantified using the MicroBCA Protein Assay (Themoscientific) and 25 µg of protein was resolved on a 7.5% SDS-PAGE gel for ErbB2 or a 12% SDS-PAGE gel for ERRα. Gels were subjected to SDS-PAGE and electroblotted onto PVDF membranes. Blots were blocked overnight in TBS-T containing 5% dry milk, followed by a 1 hr incubation with primary antibody (anti-ErbB2 used

at 1:500 (sc-31153, SantaCruz,), anti-ERRα used at 1:500 (07-662, Millipore), anti-ERRγ used at 1:2000 (same as above), and anti-Tubulin (CLT9002, Cedarlane)). Blots were washed three times with TBS-T followed by a 1 h incubation with horseradish peroxidase-conjugated secondary antibodies directed against goat for anti-ERBB2 blots (sc-2020, SantaCruz, 1:2000) or rabbit for anti-ERRα and anti-ERRγ (NA9340V, GE Healthcare, 1:5000) or mouse for anti-Tubulin (same as above). Blots were again washed three times with TBS-T, and detection was performed using enhanced chemiluminescent reagents (Roche) according to the manufacturer's instructions.

Immunoblotting to detect ERRγ, GABPA and RPLP0 in BT-474 cells transfected with miRNA inhibitor or in NMuMG cells and to detect PGC-1β in SkBR3 cells was performed as above for cells transfected with miRNA except for the following differences. Protein was quantified using the MicroBCA Protein Assay (Themoscientific). For PGC-1β, 37.5 μg of protein were used per lane. Membranes were blocked either overnight at 4°C or at room temperature for an hour. The primary polyclonal antibody used to detect PGC-1β was used at 1:500 (Novus Biologicals, H00133522-A01), and the corresponding secondary antibody used was anti-mouse (1:5000). The primary polyclonal antibody used to detect RPLP0 was used at 1:2000 (ProteinTech Group, Inc., 11290-2-AP), and the corresponding secondary antibody used was anti-rabbit (NA9340V, GE Healthcare, 1:5000). RPLP0 was detected with Lumi-Light Western Blotting Substrate (Roche), PGC-1β with Lumi-Light Plus (Roche). Blots were not stripped and re-probed because the loading control, RPLP0, could be detected on the same membrane simultaneously with detection of ERRγ, GABPA and PGC-1β.

Chromatin Immunoprecipitation

In brief, cells were crosslinked with formaldehyde and sonicated. The material was pre-cleared before being immunoprecipitated with antibody

(or without, as control). After addition of beads, and a subsequent series of washes, samples were decrosslinked and purified, and tested for enrichment of DNA segments by Real-Time qRT-PCR. Protocol details follow.

ChIP assays were performed on BT-474 cells. Cells were crosslinked with 1% formaldehyde for 10min, washed with cold 1X PBS, scraped on ice, and centrifuged for 10min at 1600 rpm at 4°C. Pelleted cells were incubated 10min on ice in 100 µL lysis buffer (50 mM Tris-HCl, pH 8.1, 10 mM EDTA, 1% SDS supplemented with protease inhibitor cocktail (Roche)) per 140 cm-diameter cell culture plate. Samples were sonicated on ice at power 10 using a VirSonic 100 (Virtis) sonicator for 6X 8sec pulses. Sonicated material was centrifuged at 13000 rpm for 10 min at 4°C, and the supernatant was used for ChIP experiments.

Sonicated chromatin was diluted 2.5X in buffer (0.5% Triton X-100, 2 mM EDTA, 100 mM NaCl, 20 mM Tris-HCl, pH 8.1 with 1 protease inhibitor cocktail (Roche) per 5mL buffer). 10% input sample was prepared by incubating $1/10^{th}$ the volume of sonicated material used in the immunoprecipitations diluted with 200 µL of decrosslink buffer (1% SDS, 0.1 M $NaHCO_3$) at 65°C overnight. Thereafter, the 10% input was purified using the QIAquick Spin Kit (Qiagen). For antibody-enriched and no-antibody control samples, aliquots of chromatin corresponding to 1.92 cell culture plates were pre-cleared using 75 µl of salmon sperm DNA/protein A beads (Upstate) for 1½ h at 4°C. Samples were briefly centrifuged at 1500 rpm and precleared chromatin was either immunoprecipitated (target enriched material) or not (no antibody control) overnight with 10 µL of a purified specific anti-ERRγ polyclonal antibody (gift from Dr. Ronald Evans) with subsequent addition of 75 µl of salmon sperm DNA/protein A beads for 3h at 4°C. The beads were washed sequentially for 10 min at 4°C with three different buffers requiring centrifugation at 1200 rpm at 4°C after each wash. Initially, buffer I (1% Triton X-100, 0.1% SDS, 150 mM NaCl, 2 mM EDTA, pH 8.0, 20 mM Tris-HCl, pH 8.1) was used, then buffer

II (1% Triton X 100, 0.1% SDS, 500 mM NaCl, 2 mM EDTA, pH 8.0, 20 mM Tris-HCl, pH 8.1) and finally buffer III (1% NP-40, 0.25 mM LiCl, 1% Na-deoxycholate, 1 mM EDTA, pH 8.0, 10 mM Tris HCl, pH 8.1). The beads were next washed briefly with TE buffer (10 mM Tris-HCl, pH 7.5, 1 mM EDTA, pH 8.0) and decrosslinked (1% SDS, 0.1 M $NaHCO_3$) at 65°C overnight. Decrosslinked samples were purified using the QIAquick Spin Kit (Qiagen). DNA was tested for ERRγ enrichment with specific primers (Appendix Table A.2.2) by qRT-PCR.

Lactate Detection Assay

For lactate assays in BT-474 cells, 500,000 cells were plated per 6 cm plate. 24 hrs after plating, cells were washed with 1X PBS and then fed 3 mL media without antibiotics. Cells were then transfected with 100nM (final concentration) of control miRNA Mimic #2 or miR-378* Mimic using Lipofectamine 2000 following the manufacturer's protocol (see above for transfection and product details). Generally, 10 µL Lipofectamine 2000 (Invitrogen) and 600 µL total Opti-mem 1 1X Reduced Serum Medium (GIBCO) were used per 6 cm plate. 4-6 hrs after transfection, media was removed and replaced with fresh media with antibiotics. 48 hrs post-transfection, lactate was assayed using the Lactate Assay Kit II (BioVision) according to the manufacturer's protocol. The experiment was independently repeated three times.

For lactate assays with the miR-378* inhibitor, cells were transfected as described above with a final concentration of 90 nM of miRNA inhibitor. Four days after transfection, media was harvested and assayed using the Lactate Assay Kit (Eton Bioscience Inc.) according to the manufacturer's protocol, and the cells were used for respiration assays. The experiment was independently repeated 9 times and significance was calculated using paired Student's *t* test.

For lactate assays in NMuMG or NT2196 cells, the Lactate Assay Kit (Eton Bioscience Inc.) was used and the standard protocol was followed.

Media from cells was harvested 48hrs after plating and assayed for lactate levels. The experiment was independently repeated 9 times, the average across all replicates is reported, and significance was calculated with paired Student's *t* tests.

Measurement of ATP

Cellular ATP levels were determined using the luciferase-based ATP Bioluminescence Assay Kit HS (Roche) following the manufacturer's protocol. 24hrs after plating, cells were transfected with miR-378* Mimic or Negative Control miRNA mimic #2 as described above. 48hrs post-transfection cells were harvested and counted, and aliquots of equal numbers of cells were processed. An unpaired Student's t-test was applied to determine significance.

Respiration Assay and Cell Proliferation Assay

In brief, cells were trypsinized, washed and resuspended in supplemented PBS. Cell viability was determined and cells were counted. One million cells were placed into the chamber of a Clark-type electrode and cellular respiration was measured. Oligomycin and myxothiazol were used to identify rates of ATP turnover and non-mitochondrial respiration, respectively. Protocol details follow.

For BT-474 cells, $1.5X10^6$ cells were plated per 10 cm plate 24 hrs before being washed with 1X PBS and then fed 10mL media without antibiotics. Cells were then transfected with 90 nM (final concentration) of control miRNA Mimic #2 or control miRNA Inhibitor or miR-378* Mimic or miR-378* Inhibitor using Lipofectamine 2000 following the manufacturer's protocol (see above for transfection and product details). Generally, 30 µL Lipofectamine 2000 (Invitrogen) and 1800 µL total Opti-mem 1 1X Reduced Serum Medium (GIBCO) were used per 10 cm plate. Four-6 hrs after transfection, media was removed and replaced with fresh media with antibiotics. This experiment was independently repeated 6 times for

miRNA Mimic experiments and 9 times for miRNA Inhibitor experiments, and the average across all replicates is reported. Significance was calculated with paired Student's *t* tests.

For respiration assays done with NMuMG or NMuMG NT2196 cells, cells were grown in 10cm cell culture dishes and assayed when 85-95% confluent. The experiment was independently repeated 4 times, the average across all replicates is reported, and significance was calculated with paired Student's *t* tests.

48 hrs post-transfection for BT-474 cells for miRNA Mimic experiments or 4 d post-transfection for miRNA Inhibitor or when proper confluency was reached for NMuMG cells, the cells were isolated by washing with phosphate-buffered saline (PBS) and trypsinized. Complete medium was added to stop the reaction, and the cells were resuspended and spun twice at 1200 rpm for 5 min at room temperature. Finally, the cells were resuspended in 800 µL PBS supplemented with 25 mM glucose, 1 mM pyruvate, and 2% bovine serum albumin. Cell viability was determined using trypan blue. In all experiments, viability was over 95%. Cells were counted with a hemocytometer. The mean difference in cell number between control- and miR-378*- or miR-378* Inhibitor-transfected cells was reported.

Cellular respiration rates were measured using a Rank Brothers Ltd Digital Model 10 Clark type electrode with a Kipp & Zonen flatbed recorder. 10^6 cells were assayed in a total volume of 500 µL. After measuring the total rate of cellular respiration, 2.5 µL oligomycin was added to the cells (for a final concentration of 5µg/mL) in order to determine ATP turnover. ATP turnover represents the fraction of mitochondrial respiration sensitive to oligomycin, while proton leak represents the fraction of mitochondrial respiration that is insensitive to oligomycin. One µL myxothiazol (final concentration of $5X10^{-6}$ µmol/µL) was then added to ascertain nonmitochondrial respiration. No non-mitochondrial respiration was detected.

siESRRG Cellular Respiration Assay

800,000 BT-474 cells were plated in 10 cm plates and transfected with 100 nM SMARTpool ESRRG siRNA or scramble siRNA (Dharmacon) in a final volume of 10 mL. 40 μL of HiPerfect reagent (Qiagen) were used per transfection according to the Manufacturer's Reverse Transfection Protocol. Media was changed after three days, and cells harvested for respiration experiments 5 days after transfection. Respiration experiments were otherwise carried out as indicated in the Respiration Assay methods section.

Patient information and tissue microarray (TMA)

The study cohort consisted of 63 patients who underwent breast surgery between 2000 and 2004 at the McGill University Health Centre (MUHC), both for diagnosed breast cancer (n=57) and non-malignant conditions (n=6). Paraffin blocks and corresponding slides were retrieved from the clinical pathology archive and assessed by a clinical pathologist for inclusion in a TMA. Fifty areas containing invasive carcinoma, 28 areas containing ductal carcinoma *in situ* (DCIS), 12 areas of lymph nodes with evidence of metastatic disease, and 62 areas of normal/benign breast tissue were identified under microscopic investigation, and 1 x 1.0 mm core was extracted from each of the corresponding areas of the paraffin blocks and used to construct a TMA block.

Data for pathological variables reported as per the clinical criteria in use at time of examination (pathological stage, histological grade, tumor size, ER, PR and ERBB2 receptor status) was collected from the original pathology reports. In cases where ERBB2 status was equivocal, fluorescence *in situ* hybridization (FISH) was performed to derive a definitive assignment. Clinical data was collected from initial interviews with patients as well as examination of medical records housed at the MUHC. Clinical follow-up for patients was conducted through annual

review of medical records between the surgery date and November 2009. In this period, we documented death from breast cancer or from other causes unrelated to cancer, as well as distant metastasis and/or local recurrence of disease. These studies were approved by the Research Ethics Board of the MUHC (studies SDR-99-780, SDR-00-966 and SDR-04-022).

In-situ hybridization on FFPE sections

In brief, tissue sections were hybridized with double-DIG labeled probe, which was recognized by an anti-DIG-HRP antibody. The TSA Plus DNP AP System (PerkinElmer) was used to amplify the signal, the NBT/BCIP reagent (Roche) produced the colorimetric reaction, and Nuclear Fast Red was used as a counter stain. Protocol details follow.

Four μm paraffin-embedded sections were obtained and subjected to *in-situ* hybridization as follows. Sections were de-paraffinized in histoclear and rehydrated in an ethanol dilution series from 100% to 75%. Endogenous peroxidase activity was quenched with 0.3% H_2O_2 treatment for 10min before pepsin (8 mg/mL) treatment was carried out at 37°C for 20 min. 0.2% glycine treatment was performed before sections were refixed in 4% paraformaldehyde. Sections were submerged in acetylation solution (66 mmol/L HCl, 1.5% (v/v) Triethanolamine, 0.66% acetic anhydride) 10 min and then prehybridized with *in situ* hybridization buffer (Enzo Life Sciences, ENZ-33808) 30 min at 50°C in a humidified chamber. 10 pmol of double-DIG (5' and 3') labeled LNA-modified probe (Exiqon) recognizing miR-378*, U6 or a scramble sequence was hybridized to the sections in 150 μL *in situ* hybridization buffer in a humidified chamber for 2h at T_m - 20°C to 23°C for each probe. Coverslips were used to avoid evaporation. Stringency washes of 10min each from 2X to 0.2X SSC were carried out at 55°C. After a 30min incubation with TNB buffer (from Perkin Elmer TSA kit) in a humidified chamber, slides were incubated in a humidified chamber with anti-digoxigenin-HRP (POD) (Roche) for 30 min

at room temperature. Signal amplification was then carried out using the TSA Plus DNP (AP) System (Perkin Elmer, NEL746A001KT) according to the manufacturer's instructions. Sections were incubated with DNP reagent for 3min if hybridized with probe recognizing U6, and 6min if hybridized with probe recognizing scramble or miR-378*. Slides were incubated with NBT/BCIP for 30min to produce the chromogenic reaction, counterstained with Nuclear Fast Red for 1min, and dehydrated in an ethanol dilution series (75% to 100%). After histoclear treatment, sections were mounted with Permount.

Once the conditions were worked out such that the scramble negative control probe produced no background and the positive control probe, U6, produced a strong and consistent signal, we hybridized a tissue microarray (TMA, see above details) containing 160 cores of tissue classified as normal, DCIS, tumor or lymph node with the probe recognizing miR-378*. miR-378* expression in each core was scored independently by three trained observers on a scale from 0 (no expression) to 3 (high expression) based on colorimetric signal intensity. The Pearson correlations between observers were between 0.89 and 0.92. The median score for each core was used in further analysis.

Animals

Ppargc1b knockout mice (gift from Dr. Ronald M. Evans, Salk Institute for Biological Studies) and wild-type littermate female mice bred in the FVB genetic background were housed and fed standard chow in the animal facility at the Rosalind and Morris Goodman Cancer Centre. Mice were sacrificed and mammary glands were isolated at seven weeks of age.

Mitotracker Experiments

Ten cm plates of BT-474 cells were transfected with miRNA mimic, miRNA inhibitor or siRNA or the corresponding controls according to the conditions outlined for miRNA Transfection, miRNA Inhibitor Transfection,

and siESRRG experiments. Cells were trypsinized, resuspended in media, and aliquoted into eppendorf tubes. Cell pellets were spun down 5minutes at 4,000 rpm and then resuspended in 700 μL media alone, with 100 nM MitoTracker Red CMX Ros (Invitrogen Molecular Probes M7512), with 40 nM MitoTracker Green FM (Invitrogen Molecular Probes M7514), or with both MitoTracker dyes together, as indicated. After 35 min of incubation with the dyes, cells were spun down and resuspended in 400 μL 1XPBS before being run through a BD FACSCalibur machine until 10,000 cells were counted per sample; cell staining with MitoTracker Red dye was recognized by the FL2 channel, and staining with MitoTracker Green dye was recognized by the FL1 channel. FACS analysis was carried out using FlowJo Software.

ACKNOWLEDGEMENTS

We thank T. Duchaine for helpful discussion and critical reading of the manuscript, W. Muller for the NMuMG and NT2196 cell lines, A. Dydensborg for guidance with the MitoTracker experiments and V. Chenard, J.A. Bader and M. Souleimanova for technical assistance. We thank R.M. Evans (Salk Institute) for the *Ppargc1b* knock-out mice. L.J.E. is a recipient of studentships from the McGill University Health Centre Research Institute and the Fonds de la Recherche en Santé du Québec (FRSQ). M.C.P. is a recipient of a studentship from the National Science and Engineering Research Council of Canada. V.G. and J.St-P. are supported by the Canadian Institutes for Health Research (grants MOP-64275, MOP-77763, MOP-84227 and IC10102947). M.P., J.St-P. and V.G. are supported by an institutional grant from the FRSQ to the Morris and Rosalind Goodman Cancer Research Centre. This work was also supported by grants from the Québec Breast Cancer Foundation (QBCF) and the Banque de tissu et de données of the Réseau de la recherche sur le cancer (RRCancer) of the FRSQ (to M.P.), and a Program Project grant from the Canadian Cancer Society Research Institute/Terry Fox Foundation (to M.P. and V.G.). M.P. holds the Diane and Sal Guerrera Chair in Cancer Genetics at McGill University.

REFERENCES

Alaynick, W.A., Kondo, R.P., Xie, W., He, W., Dufour, C.R., Downes, M., Jonker, J.W., Giles, W., Naviaux, R.K., Giguère, V.*, et al.* (2007). ERRγ directs and maintains the transition to oxidative metabolism in the post-natal heart. Cell Metab *6*, 16-24.

Alon, U. (2007). Network motifs: theory and experimental approaches. Nat Rev Genet *8*, 450-461.

Ariazi, E.A., Clark, G.M., and Mertz, J.E. (2002). Estrogen-related receptor a and estrogen-related receptor g associate with unfavorable and favorable biomarkers, respectively, in human breast cancer. Cancer Res *62*, 6510-6518.

Cervera, A.M., Apostolova, N., Crespo, F.L., Mata, M., and McCreath, K.J. (2008). Cells silenced for SDHB expression display characteristic features of the tumor phenotype. Cancer Res *68*, 4058-4067.

Charest-Marcotte, A., Dufour, C.R., Wilson, B.J., Tremblay, A.M., Eichner, L.J., Arlow, D.H., Mootha, V.K., and Giguère, V. (2010). The homeobox protein Prox1 is a negative modulator of ERRα/PGC-1α bioenergetic functions. Genes Dev *24*, 537-542.

Deblois, G., Hall, J.A., Perry, M.-C., Laganière, J., Ghahremani, M., Park, M., Hallett, M., and Giguère, V. (2009). Genome-wide identification of direct target genes implicates estrogen-related receptor α as a determinant of breast cancer heterogeneity. Cancer Res *69*, 6149-6157.

Dufour, C.R., Wilson, B.J., Huss, J.M., Kelly, D.P., Alaynick, W.A., Downes, M., Evans, R.M., Blanchette, M., and Giguère, V. (2007). Genome-wide orchestration of cardiac functions by orphan nucler receptors ERRα and γ. Cell Metab *5*, 345-356.

Fantin, V.R., St-Pierre, J., and Leder, P. (2006). Attenuation of LDH-A expression uncovers a link between glycolysis, mitochondrial physiology, and tumor maintenance. Cancer Cell *9*, 425-434.

Giguère, V. (2008). Transcriptional control of energy homeostasis by the estrogen-related receptors. Endocr Rev *29*, 677-696.

Goentoro, L., Shoval, O., Kirschner, M.W., and Alon, U. (2009). The incoherent feedforward loop can provide fold-change detection in gene regulation. Mol Cell *36*, 894-899.

Jones, R.G., and Thompson, C.B. (2009). Tumor suppressors and cell metabolism: a recipe for cancer growth. Genes Dev *23*, 537-548.

Kim, Y., and Kim, V. (2007). Intronic miRNA. EMBO J *26*, 775.

King, A., Selak, M.A., and Gottlieb, E. (2006). Succinate dehydrogenase and fumarate hydratase: linking mitochondrial dysfunction and cancer. Oncogene *25*, 4675-4682.

Lee, D.Y., Deng, Z., Wang, C.H., and Yang, B.B. (2007). MicroRNA-378 promotes cell survival, tumor growth, and angiogenesis by targeting SuFu and Fus-1 expression. Proc Natl Acad Sci U S A *104*, 20350-20355.

Lin, J., Handschin, C., and Spiegelman, B.M. (2005). Metabolic control through the PGC-1 family of transcription coactivators. Cell Metab *1*, 361-370.

Ma, L., and Weinberg, R.A. (2008). MicroRNAs in malignant progression. Cell Cycle *7*, 570-572.

Mootha, V.K., Handschin, C., Arlow, D., Xie, X., St Pierre, J., Sihag, S., Yang, W., Altshuler, D., Puigserver, P., Patterson, N.*, et al.* (2004). ERRα and GABPAα/β specify PGC-1α-dependent oxidative phosphorylation gene expression that is altered in diabetic muscle. Proc Natl Acad Sci U S A *101*, 6570-6575.

Sanyal, S., Kim, J.Y., Kim, H.J., Takeda, J., Lee, Y.K., Moore, D.D., and Choi, H.S. (2002). Differential regulation of the orphan nuclear receptor SHP gene promoter by orphan nuclear receptor ERR isoforms. J Biol Chem *277*, 1739-1748.

Schreiber, S.N., Emter, R., Hock, M.B., Knutti, D., Cardenas, J., Podvinec, M., Oakeley, E.J., and Kralli, A. (2004). The estrogen-related receptor alpha (ERRα) functions in PPARγ coactivator 1α (PGC-1α)-induced mitochondrial biogenesis. Proc Natl Acad Sci U S A *101*, 6472-6477.

Sonoda, J., Laganière, J., Mehl, I.R., Barish, G.D., Chong, L.W., Li, X., Scheffler, I.E., Mock, D.C., Bataille, A.R., Robert, F*., et al.* (2007). Nuclear receptor ERRα and coactivator PGC-1β are effectors of IFN-γ induced host defense. Genes Dev *21*, 1909-1920.

St-Pierre, J., Lin, J., Krauss, S., Tarr, P.T., Yang, R., Newgard, C.B., and Spiegelman, B.M. (2003). Bioenergetic analysis of peroxisome proliferator-activated receptor gamma coactivators 1alpha and 1beta (PGC-1alpha and PGC-1beta) in muscle cells. J Biol Chem *278*, 26597-26603.

Suzuki, T., Miki, Y., Moriya, T., Shimada, N., Ishida, T., Hirakawa, H., Ohuchi, N., and Sasano, H. (2004). Estrogen-related receptor a in human breast carcinoma as a potent prognostic factor. Cancer Res *64*, 4670-4676.

Tremblay, A.M., Dufour, C.R., Ghahremani, M., Reudelhuber, T.L., and Giguère, V. (2010). Physiological genomics identifies estrogen-related receptor α as a regulator of renal sodium and potassium homeostasis and the renin-angiotensin pathway. Mol Endocrinol *24*, 22-32.

Ursini-Siegel, J., Rajput, A.B., Lu, H., Sanguin-Gendreau, V., Zuo, D., Papavasiliou, V., Lavoie, C., Turpin, J., Cianflone, K., Huntsman, D.G.*, et al.* (2007). Elevated expression of DecR1 impairs ErbB2/Neu-induced mammary tumor development. Mol Cell Biol *27*, 6361-6371.

Ventura, A., and Jacks, T. (2009). MicroRNAs and cancer: short RNAs go a long way. Cell *136*, 586-591.

Warburg, O. (1956). On respiratory impairment in cancer cells. Science *124*, 269-270.

Zhang, H., Gao, P., Fukuda, R., Kumar, G., Krishnamachary, B., Zeller, K.I., Dang, C.V., and Semenza, G.L. (2007). HIF-1 inhibits mitochondrial biogenesis and cellular respiration in VHL-deficient renal cell carcinoma by repression of C-MYC activity. Cancer Cell *11*, 407-420.

TABLES AND FIGURES

Figure 2.1. Expression of miR-378* in human breast cancer cells.

(**A**) Schematic representation of the *PPARGC1B* locus indicating the location of miR-378* in the first intron. (**B**) Expression of miR-378* and miR-378 from an intronic *PPARGC1B* genomic sequence. BT-474 human breast cancer cells were infected with adenovirus containing the sequence of green fluorescent protein (GFP) as control or that of the miR-378*/miR-378 genomic sequence flanked by approximately 200 bp on either side of the hairpin, and quantitative polymerase chain reaction (qRT-PCR) was used to detect the mature forms of the two miRNAs. Results are presented as relative expression in cells expressing the intronic *PPARGC1B* genomic sequence versus GFP as normalized to *U6* (set at 1). (**C**) Decreased expression of *PPARGC1B*, miR-378* and miR-378 upon depletion of ERBB2 in SkBr3 cells. siRNA against ERBB2 (siE) results in parallel down-regulation of *PPARGC1B* mRNA levels, miR-378* and miR-378 as determined via relative quantitation by qRT-PCR. Results are expressed as relative expression from values obtained in response to the presence of siE normalized to values obtained with siC (scramble siRNA). Expression of control gene products 18S and U6 is set at 1. Knockdown of ERBB2 was quantified by Western blotting and tubulin was used as a control (inset). (**D**) Decreased expression of *PPARGC1B* and miR-378* upon depletion of ERBB2 in BT-474 cells. Experiment was conducted as in (**C**). Data from a representative experiment is shown. Data are represented as mean ± SEM. Unpaired student's *t* test was used for evaluation of statistical significance in **B**, **C** and **D**. *P<0.05, **P< 0.01, ***P< 0.001.

Figure 2.1

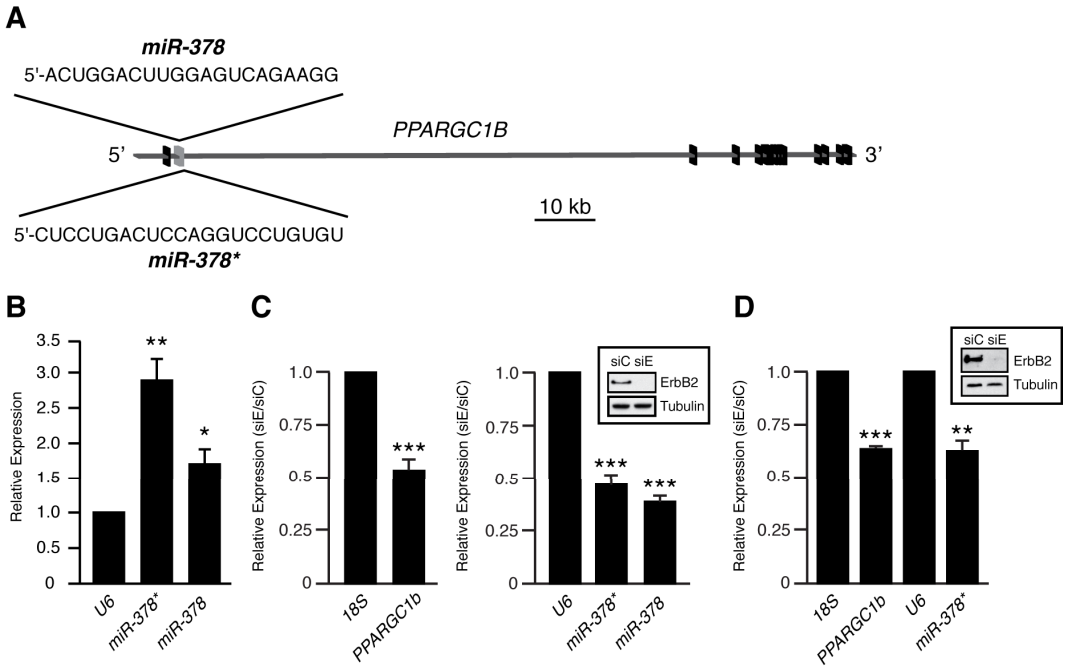
A
miR-378
5'-ACUGGACUUGGAGUCAGAAGG
PPARGC1B
5'
3'
10 kb
5'-CUCCUGACUCCAGGUCCUGUGU
miR-378*
B
Relative Expression
U6
miR-378*
miR-378
C
Relative Expression (siE/siC)
18S
PPARGC1b
siC siE
ErbB2
Tubulin
D
Relative Expression (siE/siC)
18S
PPARGC1b
U6
miR-378*

Figure 2.2. miR-378* targets endogenous *ESRRG* and *GABPA* and reduces their expression in human breast cancer cells.

(**A**) Sequences present in the 3'UTR of *ESRRG* targeted by miR-378* and conservation across species. The boxed sequences are complementary to the seed sequence of miR-378*. (**B**) Sequences present in the 3'UTR of *GABPA* targeted by miR-378* and conserved across species. The boxed sequences are complementary to the seed sequence of miR-378*. (**C**) Expression of miR-378* decreases luciferase reporter gene activity in Cos-1 cells when linked to the targeted segment of the 3'UTR of *ESRRG*. Mutation of the seed sequence within the target sequence at position 4 (m4) abolishes the miR-378*-dependent repression. Control miR is a control miRNA mimic and the control is empty vector. (**D**) Expression of miR-378* decreases luciferase reporter gene activity in Cos-1 cells when linked to the targeted segment of the 3'UTR of *GABPA*. Mutation of the seed sequence within the target sequence at position 3 to 6 (m3-6) abolishes the miR-378*-dependent repression. (**E**) mRNA levels of *ESRRA*, *ESRRG* and *GABPA* in BT-474 cells upon expression of miR-378* as compared to cells expressing control miRNA (measured by qRT-PCR and normalized to *RPLP0* (dashed line)). (**F**) Protein levels of ERRα, ERRγ and GABPA in BT-474 cells upon expression of miR-378* or control miRNA as measured by Western blotting. (**G**) A miRNA inhibitor (miR-378*-I) blocks the action of endogenous miR-378* in BT-474 cells. mRNA levels of *ESRRG* and *GABPA* were measured by qRT-PCR and normalized to *TUBA1A*. Control-I, control hairpin inhibitor. (**H**) miR-378*-I blocks the action of endogenous miR-378* in BT-474 cells. Protein levels of ERRγ and GABPA were measured by Western blotting. (**I**) ERBB2 knock-down leads to elevated expression of *ESRRG* and *GABPA* in SKBr3 cells. siRNA against ERBB2 (siE) results in up-regulation of *ESRRG* and *GABPA* mRNA levels as determined via relative quantitation by qRT-PCR. Results are expressed as relative expression from values obtained in response to the presence of siE normalized to values obtained

with siC. Expression of control gene 18S is set at 1. For all bar graphs, data are represented as the mean ± SEM. Unpaired student's *t* test was used for evaluation of statistical significance. *P< 0.05, **P< 0.01, ***P< 0.001.

Figure 2.2

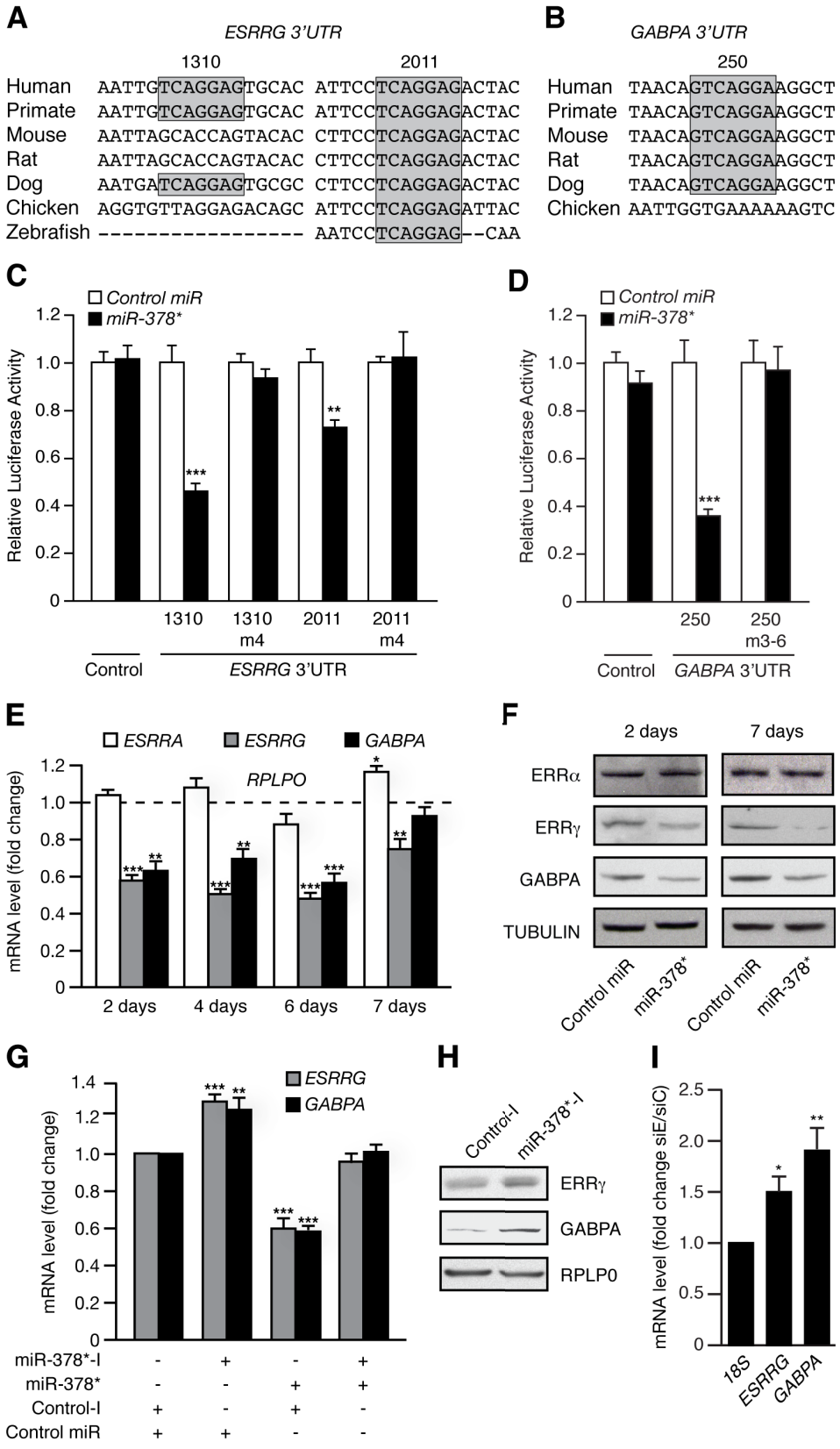
A
ESRRG 3'UTR
1310
2011
Human AATTGTCAGGAGTGCAC ATTCCTCAGGAGACTAC
Primate AATTGTCAGGAGTGCAC ATTCCTCAGGAGACTAC
Mouse AATTAGCACCAGTACAC CTTCCTCAGGAGACTAC
Rat AATTAGCACCAGTACAC CTTCCTCAGGAGACTAC
Dog AATGATCAGGAGTGCGC CTTCCTCAGGAGACTAC
Chicken AGGTGTTAGGAGACAGC ATTCCTCAGGAGATTAC
Zebrafish ---------- AATCCTCAGGAG--CAA
B
GABPA 3'UTR
250
Human TAACAGTCAGGAAGGCT
Primate TAACAGTCAGGAAGGCT
Mouse TAACAGTCAGGAAGGCT
Rat TAACAGTCAGGAAGGCT
Dog TAACAGTCAGGAAGGCT
Chicken AATTGGTGAAAAAAGTC
C
Control miR
miR-378*
Relative Luciferase Activity
1.2
1.0
0.8
0.6
0.4
0.2
0
1310
1310 m4
2011
2011 m4
Control
ESRRG 3'UTR
D
Control miR
miR-378*
Relative Luciferase Activity
250
250 m3-6
Control
GABPA 3'UTR
E
ESRRA
ESRRG
GABPA
RPLPO
mRNA level (fold change)
2 days
4 days
6 days
7 days
F
2 days
7 days
ERRα
ERRγ
GABPA
TUBULIN
Control miR
miR-378*
Control miR
miR-378*
G
ESRRG
GABPA
mRNA level (fold change)
1.4
1.2
1.0
0.8
0.6
0.4
0.2
0
miR-378*-I - + - +
miR-378* - - + +
Control-I + - + -
Control miR + + - -
H
Control-I
miR-378*-I
ERRγ
GABPA
RPLP0
I
mRNA level (fold change siE/siC)
2.5
2.0
1.5
1.0
0.5
0
18S
ESRRG
GABPA

Figure 2.3. miR-378* targets regions of the mouse *Esrrg* and *Gabpa* 3'UTR.

(**A**) Sequence present in the 3'UTR of *Esrrg* targeted by miR-378* and conserved across species. The boxed sequences are complementary to the seed sequence of miR-378*. (**B**) Expression of miR-378* decreases luciferase reporter gene activity when linked to the 3'UTR regions of *Esrrg*. Mutation of the seed sequence within the target sequence at position 4 (m4) abolishes the miR-378*-dependent repression. (**C**) Sequence present in the 3'UTR of *Gabpa* targeted by miR-378* and conserved across species. The boxed sequences are complementary to the seed sequence of miR-378*. (**D**) Expression of miR-378* decreases luciferase reporter gene activity when linked to the 3'UTR region of *Gabpa*. Mutation of the seed sequence within the target sequence at position 4 (m4) abolishes the miR-378*-dependent repression. All data are represented as the mean ± SEM. Unpaired student's *t* test was used for evaluation of statistical significance. *P< 0.05, **P< 0.01, ***P< 0.001.

Figure 2.3

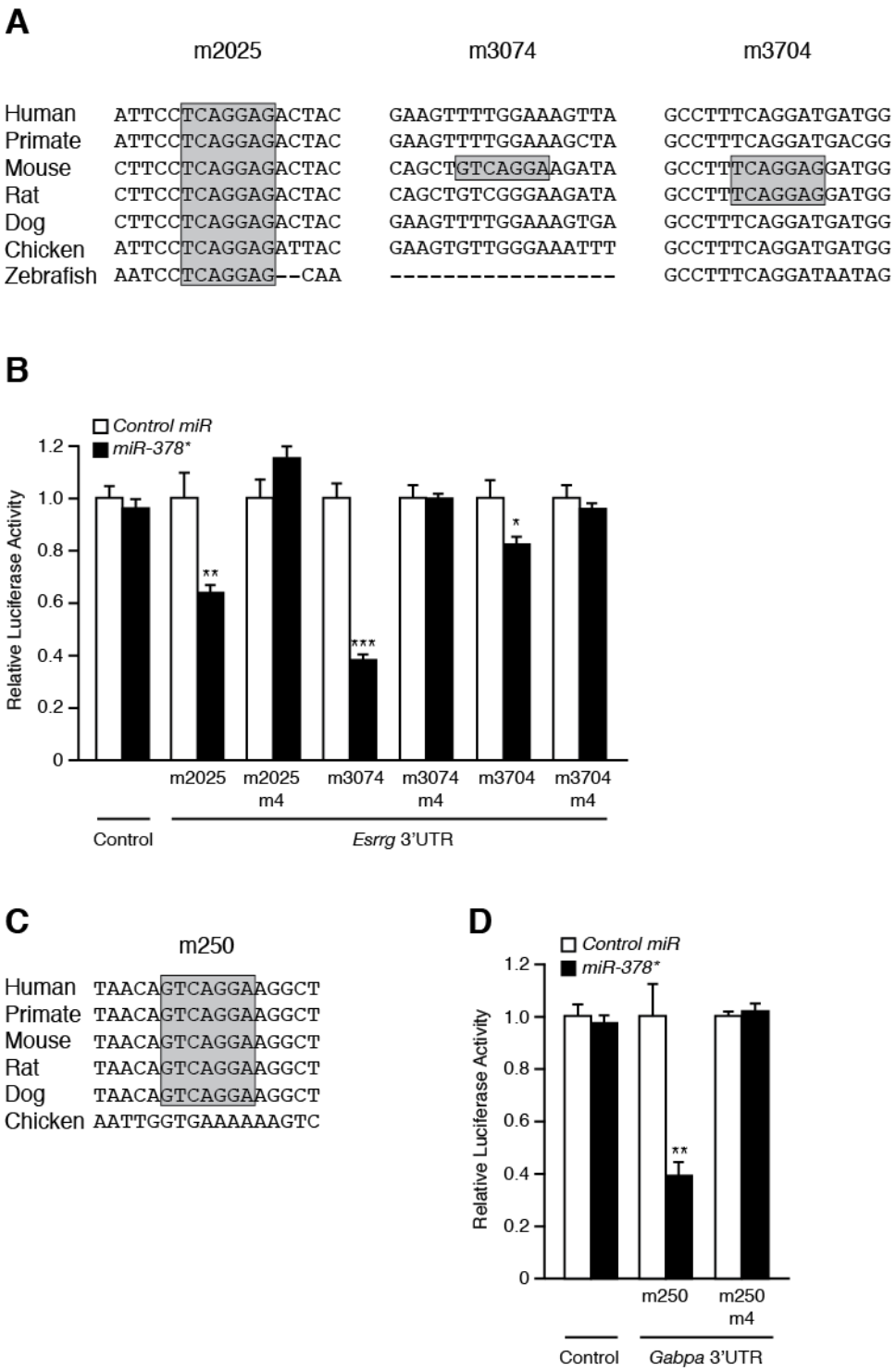
A
m2025
m3074
m3704
Human ATTCCTCAGGAGACTAC GAAGTTTTGGAAAGTTA GCCTTTCAGGATGATGG
Primate ATTCCTCAGGAGACTAC GAAGTTTTGGAAAGCTA GCCTTTCAGGATGACGG
Mouse CTTCCTCAGGAGACTAC CAGCTGTCAGGAAGATA GCCTTTTCAGGAGGATGG
Rat CTTCCTCAGGAGACTAC CAGCTGTCGGGAAGATA GCCTTTTCAGGAGGATGG
Dog CTTCCTCAGGAGACTAC GAAGTTTTGGAAAGTGA GCCTTTCAGGATGATGG
Chicken ATTCCTCAGGAGATTAC GAAGTGTTGGGAAATTT GCCTTTCAGGATGATGG
Zebrafish AATCCTCAGGAG--CAA ---------- GCCTTTCAGGATAATAG
B
Control miR
miR-378*
Relative Luciferase Activity
1.2
1.0
0.8
0.6
0.4
0.2
0
**
***
*
m2025
m2025 m4
m3074
m3074 m4
m3704
m3704 m4
Control
Esrrg 3'UTR
C
m250
Human TAACAGTCAGGAAGGCT
Primate TAACAGTCAGGAAGGCT
Mouse TAACAGTCAGGAAGGCT
Rat TAACAGTCAGGAAGGCT
Dog TAACAGTCAGGAAGGCT
Chicken AATTGGTGAAAAAAGTC
D
Control miR
miR-378*
Relative Luciferase Activity
1.2
1.0
0.8
0.6
0.4
0.2
0
**
m250
m250 m4
Control
Gabpa 3'UTR

Figure 2.4. Regulation of metabolic genes by miR-378* and its target, ERRγ, in breast cancer cells.

(**A**) Standard ChIP of promoter and enhancer elements confirmed direct regulation of metabolic genes by ERRγ in human breast cancer cells. Location relative to the transcriptional start site and sequences of ERR response elements (ERREs) are also indicated. (**B**) Introduction of siRNAs targeting *ESRRA* and *ESRRG* results in specific down-regulation of ERRα and ERRγ, respectively, in BT-474 cells. (**C**) Introduction of miR-378* or a miR-378* inhibitor as well as siRNAs against *ESRRA* and *ESRRG* results in specific regulation of glycolytic gene mRNA levels in BT-474 cells as determined by qRT-PCR and normalized to *18S* and *TUBA1A* as internal controls and compared to corresponding control miR, miR inhibitor or scramble siRNA treatments. (**D**) Same as in (**C**) for *GABPA* and TCA cycle genes. Unpaired student's *t* test was used for evaluation of statistical significance in **C** and **D**, in which data from one representative experiment is shown. For all bar graphs, data are represented as the mean ± SEM. *P< 0.05, **P< 0.01, ***P< 0.001.

Figure 2.4

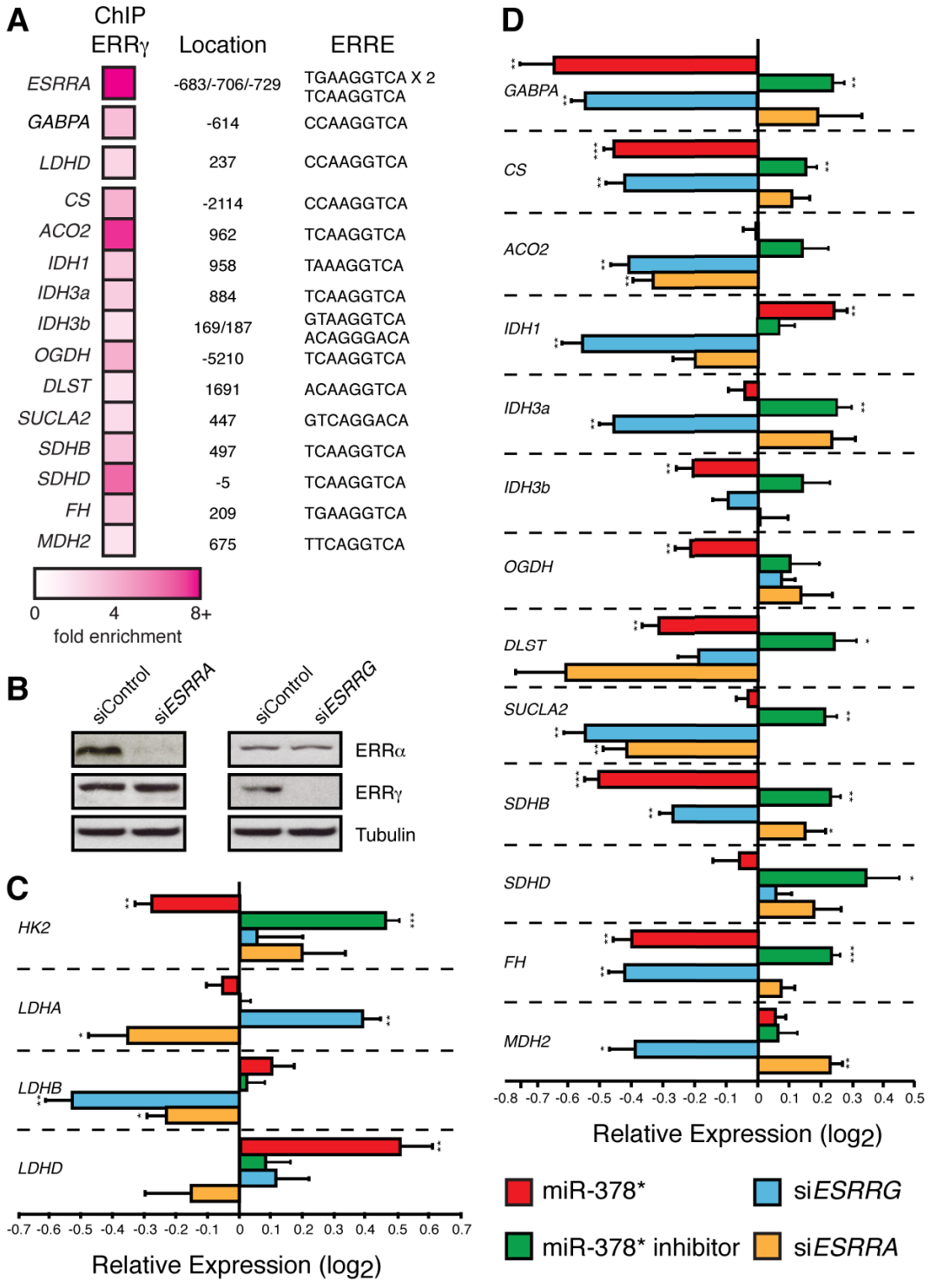
A
ChIP ERRγ
Location
ERRE
ESRRA
-683/-706/-729
TGAAGGTCA X 2
TCAAGGTCA
GABPA
-614
CCAAGGTCA
LDHD
237
CCAAGGTCA
CS
-2114
CCAAGGTCA
ACO2
962
TCAAGGTCA
IDH1
958
TAAAGGTCA
IDH3a
884
TCAAGGTCA
IDH3b
169/187
GTAAGGTCA
ACAGGGACA
OGDH
-5210
TCAAGGTCA
DLST
1691
ACAAGGTCA
SUCLA2
447
GTCAGGACA
SDHB
497
TCAAGGTCA
SDHD
-5
TCAAGGTCA
FH
209
TGAAGGTCA
MDH2
675
TTCAGGTCA
0
4
8+
fold enrichment
B
siControl
siESRRA
siControl
siESRRG
ERRα
ERRγ
Tubulin
C
HK2
LDHA
LDHB
LDHD
-0.7 -0.6 -0.5 -0.4 -0.3 -0.2 -0.1 0 0.1 0.2 0.3 0.4 0.5 0.6 0.7
Relative Expression (log2)
D
GABPA
CS
ACO2
IDH1
IDH3a
IDH3b
OGDH
DLST
SUCLA2
SDHB
SDHD
FH
MDH2
-0.8 -0.7 -0.6 -0.5 -0.4 -0.3 -0.2 -0.1 0 0.1 0.2 0.3 0.4 0.5
Relative Expression (log2)
miR-378*
siESRRG
miR-378* inhibitor
siESRRA

Table 2.1. TCA cycle gene ERRE conservation between human and mouse

Site locations listed relative to the Transcriptional Start Site (TSS).

Gene name	human ERRE location	human ERRE sequence	mouse ERRE location	mouse ERRE sequence
CS	-2114	cCAAGGTCA	-2003	cCAAGGTCA
ACO2	962	TCAAGGTCA	-233	TCAAGGTCA
IDH1	958	TAAAGGTCA	977	TAAAGGTCA
IDH3A	884	TCAAGGTCA	751	TCAAGGTCA
IDH3B	169/187	gTAAGGTCA/ aCAGGGaCA	120/161	gCAAGGTCA/ aCAAGGTCA
OGDH	-5224/5218 from short isoform	TCAAGGTCA/ TCAGGGTCA	-5053	cCAAGGTCA
DLST	1697	aCAAGGTCA	1881	TCAAGGTCA
SUCLA 2	447	GTCAGGACA	373	gCAAGGaCA
SDHB	497	TCAAGGTCA	458	TCAAGGTCA
SDHD	-5	TCAAGGTCA	5	TCAAGGTCA
FH	209	TGAAGGTCA	164	TGAAGGTCA
MDH2	675	TTcAGGTCA	507	TCAGGGTCA
LDHD	237	cCAAGGTCA		
ESRRA	-682	TCAAGGTCA	-528	TCAAGGTCA
GABPA	-614	cCAAGGTCA	-614	cCAAGGTCA

Figure 2.5. miR-378* induces a metabolic shift in breast cancer cells of human and mouse origin.

(**A**) Expression of miR-378* increases BT-474 cell proliferation. (**B**) Increase in lactate levels upon expression of miR-378*. (**C**) Total cellular respiration of BT-474 cells is reduced by expression of miR-378*. (**D**) Total cellular respiration of BT-474 cells is reduced by expression of siESRRG. (**E**) Introduction of miR-378* decreases mitochondrial coupled respiration. Total respiration is broken down into coupled (black) and uncoupled (white) components. (**F**) Effect of expression of miR-378* on ATP levels. (**G**) Expression of a miR-378* inhibitor (miR-378*-I) decreases BT-474 cell proliferation. (**H**) Decrease in lactate levels upon expression of miR-378*-I. (**I**) Total cellular respiration of BT-474 cells is increased by expression of miR-378*-I. (**J**) The murine mammary epithelial cell line (NMuMG) and an *ex-vivo* NMuMG tumor cell line overexpressing the *Neu* receptor (NT2196) were assayed for miR-378*, miR-378 and *Ppargc1b* expression levels by qRT-PCR and normalized to U6 or *Arbp.* (**K**) Some key genes downstream of miR-378*, as detected by qRT-PCR, are downregulated at the mRNA level in NT2196 cells as compared to NMuMG cells. *Esrrg* mRNA levels were detectable but too low to accurately quantitate. *Arbp* was used as an internal control. (**L**) ERRγ and GABPA protein levels are decreased in NT2196 cells as compared to NMuMG cells as measured by Western blotting. RPLP0 was used as a loading control. Arrow indicates band corresponding to ERRγ. (**M**) Increase in lactate levels in NT2196 cells as compared to NMuMG. (**N**) Total cellular respiration is reduced in NT2196 cells as compared to NMuMG. Unpaired student's *t* test was used for evaluation of statistical significance in **B**, **F**, **J**, and **K** in which data from one representative experiment is shown. Paired student's *t* test was used for evaluation of significance in **A, C**, **D**, **G**, **H**, **I, M** and **N** in which data from at least 4 independent experiments is shown. Lactate and ATP data is normalized to cell number. For all bar graphs, data are represented as the mean ± SEM. *P< 0.05, **P< 0.01, ***P< 0.001.

Figure 2.5

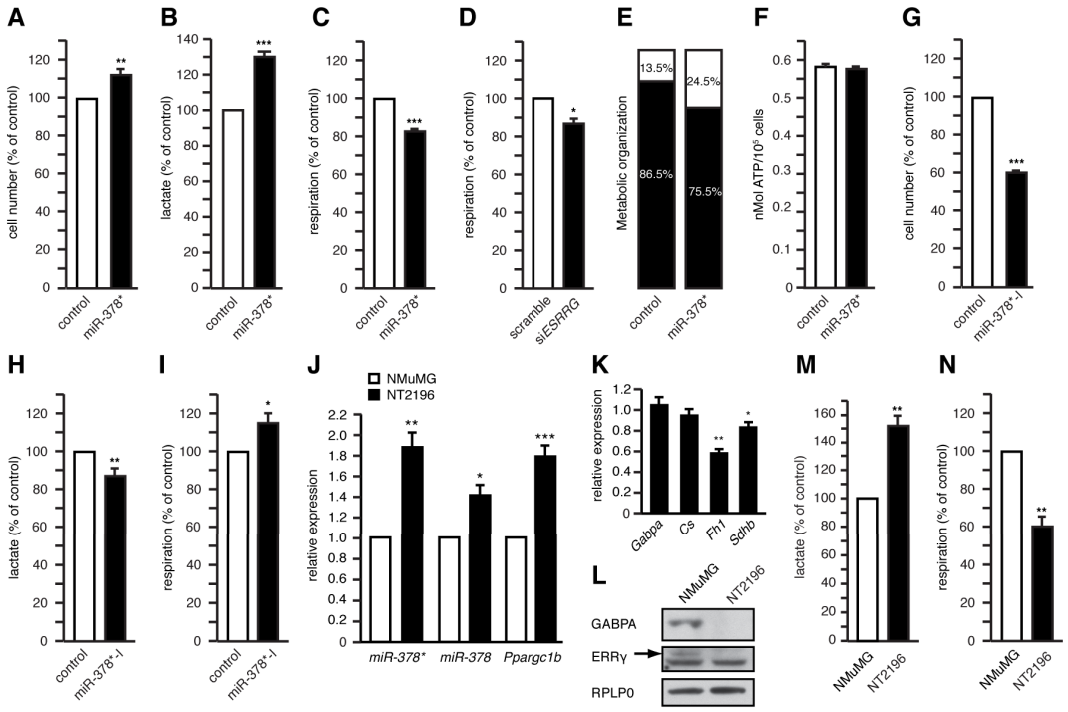
A
cell number (% of control)
control
miR-378*
B
lactate (% of control)
C
respiration (% of control)
D
scramble
siESRRG
E
Metabolic organization
13.5%
24.5%
86.5%
75.5%
F
nMol ATP/10^5 cells
G
miR-378*-I
H
I
J
NMuMG
NT2196
relative expression
miR-378*
miR-378
Ppargc1b
K
Gabpa
Cs
Fh1
Sdhb
L
GABPA
ERRγ
RPLP0
M
N

Figure 2.6. Expression of miR-378* in normal and cancerous breast tissue.

(**A**) Representative images of normal and cancerous breast tissue subjected to *in situ* hybridization with a probe directed against miR-378*. DCIS; ductal carcinoma *in situ*. Nuclear staining was performed using Nuclear Fast Red and visualization of miR-378* expression was generated by a colorimetric reaction resulting in purple coloring. Images are at 20X magnification. (**B**) Quantification of miR-378* expression as assessed by *in situ* hybridization of a tissue microarray containing 160 cores of distinct normal and cancerous breast samples. Levels of miR-378* expression were scored from 0 (absent, blue) to 3 (highly expressed, red). Number (n) of samples for each type of breast tissue is indicated on top of each column. Significance was determined using the Mann-Whitney test.

Figure 2.6

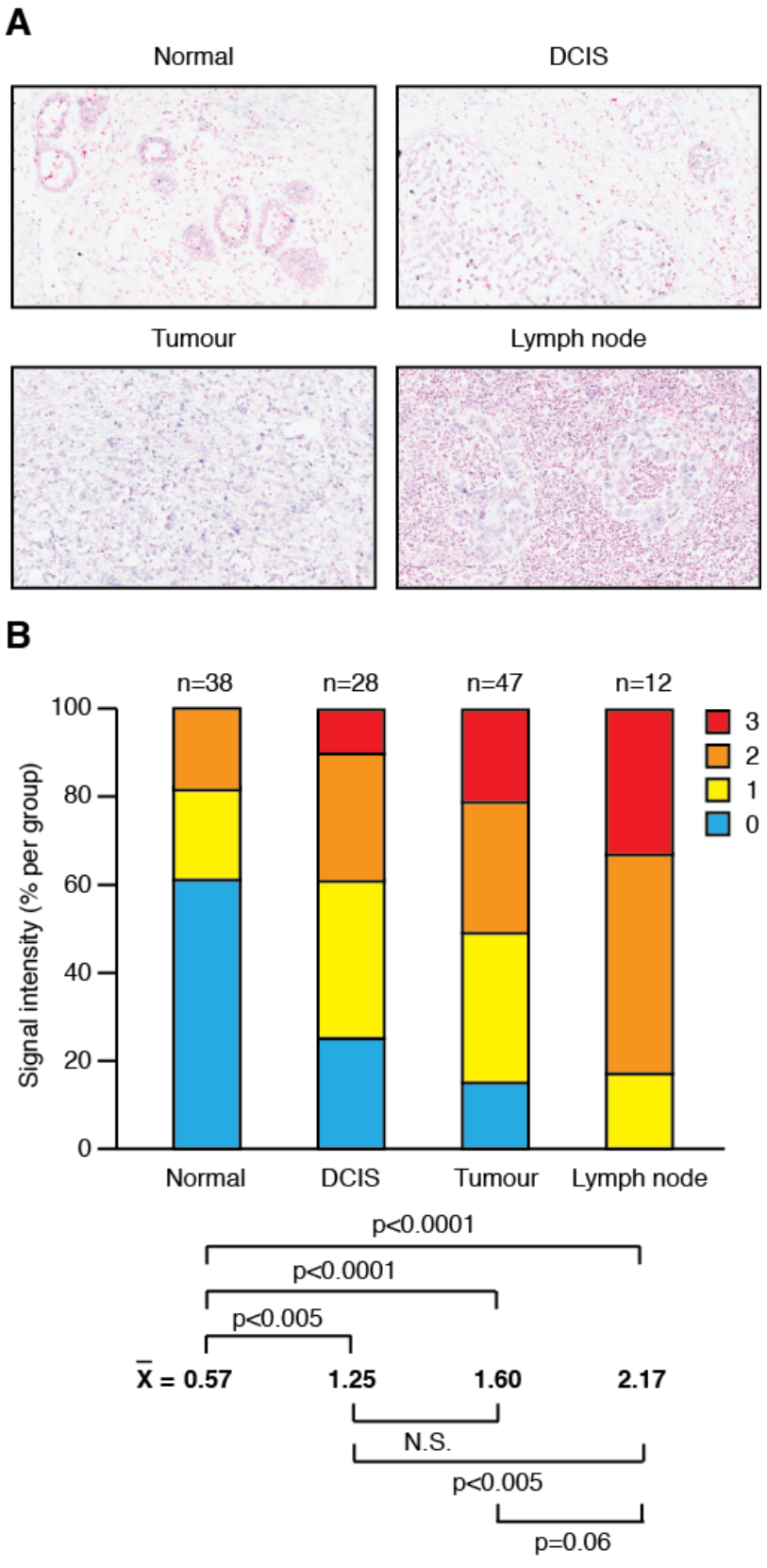
A
Normal
DCIS
Tumour
Lymph node
B
n=38
n=28
n=47
n=12
100
80
60
40
20
0
Signal intensity (% per group)
3
2
1
0
Normal
DCIS
Tumour
Lymph node
p<0.0001
p<0.0001
p<0.005
X̄ = 0.57
1.25
1.60
2.17
N.S.
p<0.005
p=0.06

Table 2.2. Expression of miR-378* in matched breast samples

	Normal	DCIS	Tumor	Lymph node	≠	p-value	#
DCIS vs normal	0.65	1.29			0.65	0.061	17
Tumor vs normal	0.63		1.63		1.00	<0.0001	30
Lymph node vs normal	0.83			2.33	1.50	0.021	6
Tumor vs DCIS		1.13	1.67		0.54	0.046	24
Lymph node vs DCIS		2.25		2.50	0.25	NS	4
Lymph node vs tumor			1.75	2.38	0.63	NS	8

Values represent mean score for miR-378* expression signal. ≠, difference between matched groups; #, number of patients.

Figure 2.7. Schematic representations of the metabolic pathways influenced by miR-378* and the PGC-1β/miR-378*/ERRγ transcriptional network motif.

(**A**) Presence of the oncogene ERBB2 leads to co-expression of *PPARGC1B* and miR-378*. Loss of expression of ERRγ and GABPA through the action of miR-378* is accompanied by a reduction in the expression of genes in the TCA cycle. PGC-1β remains present to co-activate ERRα and/or other transcription factors (TFs) to promote other functions, including glycolysis. Overall, miR-378* expression results in a shift from aerobic, oxidative metabolism (OXPHOS) to glycolytic metabolism in the presence of available oxygen (Warburg effect) as represented by an increase in lactate levels and a reduction in oxygen consumption. (**B**) Incoherent feedforward loop type-1 displaying opposite regulation of Z by factors X and Y. Wavy arrow indicates input regulatory signal for factor X. (**C**) Incoherent feedforward loop type-1 illustrating the functional relationship between ERBB2 (regulatory signal), PGC-1β and miR-378* as transcription modulators influencing the activity of ERRγ.

Figure 2.7

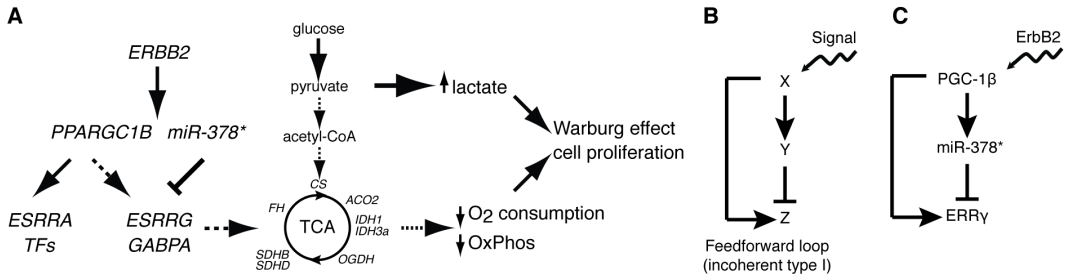
A
ERBB2
PPARGC1B
miR-378*
ESRRA
TFs
ESRRG
GABPA
glucose
pyruvate
acetyl-CoA
lactate
Warburg effect
cell proliferation
CS
ACO2
FH
TCA
IDH1
IDH3a
SDHB
SDHD
OGDH
O2 consumption
OxPhos
B
Signal
X
Y
Z
Feedforward loop
(incoherent type I)
C
ErbB2
PGC-1β
miR-378*
ERRγ

Figure 2.8. Expression of miR-378* in the mammary gland of *Ppargc1b* knock-out mice.

(**A**) Schematic representation of the *Ppargc1b* genomic region and locations of amplicons tested for expression. Exons 4 and 5 are deleted in the *Ppargc1b* knock-out mice (shown in red). (**B**) Validation of continued expression of the modified locus in *Ppargc1b* knock-out mice mammary glands as compared to wild-type and detected by qRT-PCR. As expected, the amplicon covering exons 4 and 5 cannot be detected in the *Ppargc1b* knock-out mice. 18S serves as a control. (**C**) Expression of miR-378* and miR-378 in the mammary gland of *Ppargc1b* knock-out mice as compared to wild-type mice and detected by qRT-PCR. U6 serves as a control.

Figure 2.8

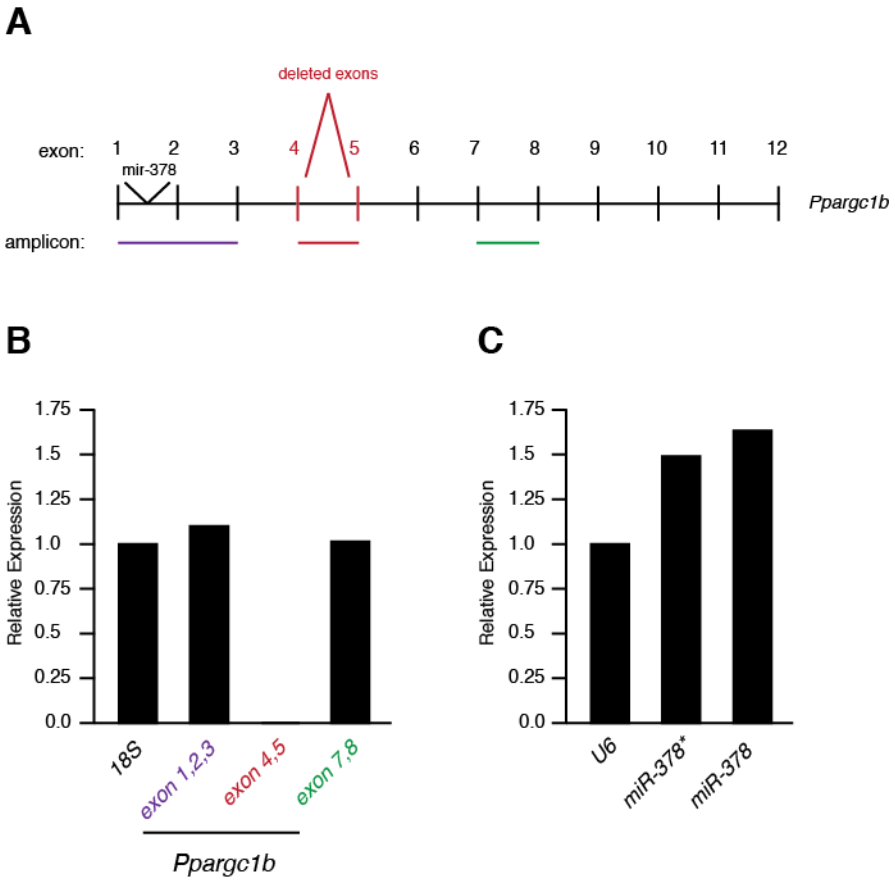
A
deleted exons
exon:
1
2
3
4
5
6
7
8
9
10
11
12
mir-378
Ppargc1b
amplicon:
B
Relative Expression
1.75
1.5
1.25
1.0
0.75
0.5
0.25
0.0
18S
exon 1,2,3
exon 4,5
exon 7,8
Ppargc1b
C
Relative Expression
1.75
1.5
1.25
1.0
0.75
0.5
0.25
0.0
U6
miR-378*
miR-378

Figure 2.9. Ablation of PGC-1β in human SKBr3 breast cancer cells results in a decrease in the expression of oxidative and glycolytic genes.

(**A**) Western blot showing reduction of PGC-1β in response to treatment of SKBr3 cells with si-*PPARGC1b*. RPLP0 is a loading control. (**B**) Relative expression of oxidative and glycolytic genes in response to treatment of SKBr3 cells with si-*PPARGC1b* as compared to scramble and measured by qRT-PCR using 18S as an internal control. *P< 0.05, **P< 0.01, ***P< 0.001.

Figure 2.9

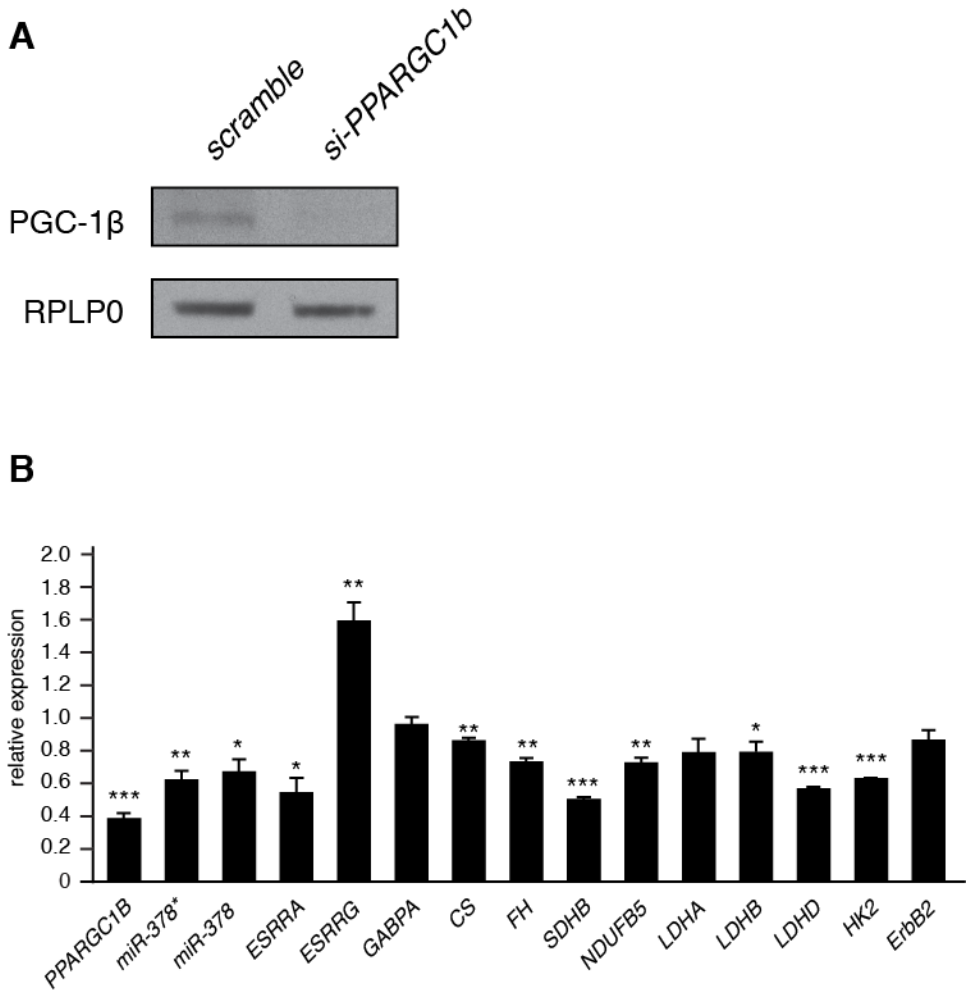
A
scramble
si-PPARGC1b
PGC-1β
RPLP0
B
relative expression
2.0
1.8
1.6
1.4
1.2
1.0
0.8
0.6
0.4
0.2
0
PPARGC1B
miR-378*
miR-378
ESRRA
ESRRG
GABPA
CS
FH
SDHB
NDUFB5
LDHA
LDHB
LDHD
HK2
ErbB2

CHAPTER III: miR-378* Regulates the AMPK Pathway in Breast Cancer Cells Through Direct Control of CAMKK2

PREFACE

Having established a role for miR-378* in breast cancer cell metabolism in Chapter II, this chapter extends the investigation of that topic. Applying a stable cell system to identify long-term effects of mir-378 hairpin expression, we identify a novel direct target of miR-378*, *CAMKK2*. Further elucidation of this molecular pathway identified that miR-378*-induced repression of *CAMKK2* results in reduced pAMPKα and pACC levels, implicating miR-378* in the regulation of AMPK pathway activity. Furthermore, metabolomics revealed interesting unexpected consequences of mir-378 hairpin expression in breast cancer cells.

ABSTRACT

The AMPK pathway is a key energy sensing pathway known to have an important role in cancer metabolism. The mir-378 miRNA hairpin, encoding for mature miR-378 and miR-378*, is an oncogenic miRNA that is known to contribute to the metabolic shift central to cancer progression, the Warburg effect. In this study, we further investigate the metabolic function of mir-378 in breast cancer cells, and uncover a link between miR-378* and AMPK pathway activity. Using stable cells and transient transfection assays to modulate mir-378 levels for gain- and loss-of-function experiments, we uncover that the upstream kinase of AMPK, CAMKK2, is in fact a functional direct target of miR-378* in breast cancer cells. We identify further that the mir-378 hairpin represses AMPK activity, as measured by pAMPKα and pACC levels, and that miR-378* alone is sufficient to induce these effects. Using metabolomics to identify the metabolic output of long-term mir-378 hairpin expression, we have uncovered mir-378 hairpin-mediated regulation of the hexosamine pathway, which is responsible for O-GlcNAc post-translational modification. Taken together, our results implicate oncogenic miR-378* as an upstream regulator of the AMPK pathway in breast cancer cells, and identify a specific underlying molecular explanation.

INTRODUCTION

The importance of metabolism in cancer has recently regained prominence, and an increasing body of evidence is linking metabolic dysregulation to cancer development (Kroemer and Pouyssegur, 2008). A prominent example of the fundamental link between metabolic function and cancer is the Warburg effect (Warburg, 1956b), which is described as a shift in intracellular metabolism that accompanies the onset of cancer. In this metabolic reprogramming, cancer cells exhibit a predominant dependence on aerobic glycolysis to fulfill cellular energy demands, and this is accompanied by a decreased reliance on oxidative metabolism pathways. Furthermore, the complexity of metabolic dysregulation in cancer is becoming increasingly apparent, as recent studies continue to identify new nodes of metabolic misregulation in cancer cells, including accelerated glucose intake and truncated TCA cycling (Deberardinis et al., 2008). Further examples include HIF-1, a transcription factor overexpressed in human cancer in response to hypoxia or as a result of genetic alterations (Semenza, 2003). Its upregulation induces the expression of a cohort of metabolic enzymes themselves linked to facilitating oncogenesis, notably, LDHA, PDK, BNIP3, and the glucose transporter GLUT1 (Semenza, 2008). Interestingly, certain TCA cycle genes, FH and SDH, which are silenced by mutation in cancer, serve as tumor suppressors themselves (King et al., 2006). As the regulation of metabolic modulation in cancer is mediated by a network of factors that respond to intracellular and extracellular signals including genetic mutations, and nutrient and oxidative stress (Cairns et al., 2011), the study of cancer cell metabolism will, thus, help elucidate molecular links between oncogenic stimuli and the acquisition of cancer phenotypes.

The AMPK pathway is one of the well-recognized junctions between metabolism and cancer cell development. A Ser/Thr kinase, AMPK is a heterotrimer comprised of subunits α, β, and γ. There exist at least 2 isoforms of each subunit. AMPK acts as a cellular energy sensor to

regulate glucose and lipid metabolism in response to nutrient availability and metabolic stress. When the AMP:ATP ratio is high, AMPK undergoes a conformational change that enables its activation by phosphorylation on the α subunit (Thr-172) by an AMPK kinase (reviewed in (Luo et al., 2005)). The activity of AMPK is largely considered to be conferred by Liver Kinase B (LKB1) (Shackelford and Shaw, 2009), however the Calmodulin-Dependent Protein Kinase Kinase 2 (CAMKK2) also functions as an important upstream AMPK kinase (Hawley et al., 2005; Woods et al., 2005). The role of LKB1 as a tumor suppressor, which is inactivated in some cancers, functionally links AMPK activity to cancer (Ollila and Makela, 2011). Repression of AMPK activation leads to a series of effects on downstream networks, including stimulation of the mTOR pathway (Shaw, 2009) and reduced cell cycle regulation by p53 and p21, thus promoting cell proliferation and survival (Motoshima et al., 2006). Reduced AMPK activity also induces upregulation of fatty acid and lipid synthesis through Acetyl-Coenzyme A Carboxylase Alpha (ACC) and Fatty Acid Synthase (FAS) activity, a metabolic change increasingly associated with cancer development (Swinnen et al., 2006).

microRNAs (miRNAs) are a new class of molecules which have been implicated in the regulation of cancer metabolism. miRNAs are short, endogenous RNAs of ~22nt in length which regulate gene expression networks at the post-transcriptional level. Through imperfect sequence base-pairing, miRNAs suppress their specific mRNA targets by inhibiting translation initiation or promoting mRNA degradation (He and Hannon, 2004). Extensive studies have demonstrated a correlation between aberrant miRNA expression with tumor formation, progression, and metastasis (Garzon et al., 2009). One such example is the mir-378 hairpin, which encodes for both mature miR-378 and miR-378*, and is embedded in intron 1 of *PPARGC1b*, a gene encoding the metabolic co-activator Peroxisome Proliferator Activated Receptor γ Coactivator-1 β (PGC1-β). The mir-378 hairpin has been shown to promote cell survival and

tumorigenesis (Lee et al., 2007). Furthermore, at least one component of this hairpin has been identified to be upregulated in breast cancer (Eichner et al., 2010) and, more precisely, was determined to be downstream of important oncogenic signaling including ErbB2 (Eichner et al., 2010) and Myc (Feng et al., 2011). Furthermore, in breast cancer cells, miR-378* was found to induce the metabolic shift away from oxidative metabolism and towards glycolysis, at least in part by suppressing the expression of Estrogen-Related Receptor γ (ERRγ), a nuclear receptor important for the regulation of oxidative metabolic gene expression (Eichner et al., 2010). In such, miR-378* directly links oncogenic function to metabolic regulation.

In this study, we use BT-474 cells stably expressing the mir-378 hairpin to investigate the long-term metabolic regulation imparted by miR-378/miR-378* in human breast cancer cells. Of the two major kinases known to phosphorylate AMPK, LKB1 and CAMKK2, we uncover that only CAMKK2 is affected by the mir-378 hairpin and that, furthermore, CAMKK2 is a direct target of miR-378*. We then show that the mir-378 hairpin represses AMPK activity, as measured by pAMPKα and pACC levels, and we further identify that miR-378* alone is sufficient to induce these effects. Metabolomics analysis of the mir-378 hairpin-expressing clones indicates miR-378*-mediated regulation of the hexosamine pathway both in parallel to and downstream of its control of AMPK activity, thereby broadening the known functions of this miRNA to include regulation of O-GlcNAc-mediated post-translational modification. Taken together, our results implicate miR-378* as an upstream repressor of the AMPK pathway, thereby expanding the understanding of miR-378*'s simultaneous function as both an oncomiR and metabolic regulator.

RESULTS

Validation of mir-378 hairpin expression in BT-474 stable cell clones

To investigate the long-term metabolic effects of mir-378 in breast cancer cells, we chose to study the BT-474 cell context, in which miR-378* was previously shown to regulate breast cancer cell metabolism (Eichner et al., 2010). BT-474 stable cell clones were generated by transfection of either a vector construct containing the mir-378 hairpin (Fig. 3.1A) or empty vector for control, and subsequent antibiotic selection for stable construct expression. Initial screening for mir-378 overexpression was performed by qRT-PCR on 16 mir-378 hairpin-expressing and 16 control clonally-derived cell lines. A subset of stable cell lines exhibiting elevated expression of both mature miR-378* and miR-378 were then assayed for downregulation of ERRγ, a known target of miR-378* (Eichner et al., 2010). Of the clones further validated, three mir-378 hairpin-expressing (mir-378 hairpin) and three control clones were chosen for further study. An average increase of 1.5 and 1.8 fold in miR-378* and miR-378 levels (Fig. 3.1B), respectively, and a pronounced downregulation of ERRγ protein levels (Fig. 3.1D) were observed in the mir-378 hairpin stable clones as compared to controls. The mRNA levels of established miR-378* direct target, *ESRRG,* and mir-378 host gene, *PPARGC1b*, exhibited no significant differences between the two clone types (Fig. 3.1C), suggesting that, in this long-term expression system, the cellular transcriptional machinery can compensatorily recover from the effects of miR-378* expression on the *ESRRG* mRNA transcript, while the effect on ERRγ protein levels remain robust. Notably, PGC-1β levels were unaffected at either the RNA or protein levels, suggesting that, in our system, an increase in mir-378 expression does not induce a regulatory feedback response of its host gene. To validate the functional biological activity of mir-378 hairpin overexpression in our system, we verified that our mir-378 hairpin stable clones exhibit accelerated cell proliferation (45% greater than control) (Fig. 3.1E), corresponding to the published effect of

this miRNA hairpin (Eichner et al., 2010; Lee et al., 2007). Thus, we have generated a stable cell system in BT-474 breast cancer cells which exhibits moderate but significant upregulation of mir-378 hairpin levels in a manner that robustly recapitulates the known mir-378 effects on both protein targets and biological function. This system allows for the study of mir-378 induction that may more closely correspond to the more modest changes in expression likely to occur in homeostatic biological systems.

CAMKK2 is a direct target of miR-378*

We screened miRNA target prediction algorithms for predicted direct targets of miR-378* and miR-378 which are related to metabolic regulation. Both the TargetScan and Pictar algorithms predict that *CAMKK2*, a kinase known to regulate the activitiy of the energy sensor AMPK, is a direct target of miR-378*. We validated the predicted target site (Fig. 3.2A), located at nucleotide 597 of the human *CAMKK2* 3'UTR, using a luciferase-based assay. The target site location is numbered relative to the start of the 3'UTR. A reporter plasmid containing the predicted target region downstream (in the 3'UTR region) of a Renilla luciferase reporter gene was cotransfected with either control miRNA or miR-378*, and cell extracts were monitored for luciferase activity (Fig. 3.2B). 50% repression of luciferase, as compared to control, was observed for the predicted target site, and mutation of one base in the seed target region at position 4 was sufficient to completely abolish this repression, proving the specificity of action of miR-378* on this region of *CAMKK2*. Of note, the miR-378 predicted target site in *CAMKK2* did not validate by luciferase assay (data not shown).

We next investigated the capacity for miR-378* to modulate endogenous CAMKK2. In naïve BT-474 cells, transient inhibition of endogenous miR-378* was able to derepress *CAMKK2* mRNA levels 30% (Fig. 3.2C, left panel), whereas inhibition of miR-378 had no effect (Figure A.3.1). Furthermore, in a similar transient transfection experiment, specific

inhibition of miR-378* was sufficient to rescue *CAMKK2* mRNA repression induced by a miR-378* mimic (Fig. 3.2C, right panel). Together, these experiments indicate that miR-378*, in short-term experiments, represses endogenous *CAMKK2* mRNA levels. We next probed for the protein levels of two major AMPK kinases, LKB1 and CAMKK2, and identified that CAMKK2 protein levels are derepressed in response to a miR-378* inhibitor, while LKB1 levels remained unchanged (Fig. 3.2D). Short-term inhibition of endogenous miR-378* alone was sufficient to rescue the protein level of CAMKK2 but LKB1 protein levels were unaffected by miR-378* inhibition (Fig. 3.2D), indicating that miR-378* affects only CAMKK2 but not the other known AMPK kinase. Moreover, miR-378 inhibition did not affect CAMKK2 or LKB1 protein levels (data not shown), suggesting that miR-378* is the mature miRNA responsible for the mir-378 hairpin-induced CAMKK2 response. Moreover, mir-378 hairpin stable cells exhibited a robust depletion of CAMKK2 protein, while LKB1 levels were relatively uniform across control and mir-378 hairpin stable cells (Fig. 3.2E). Altogether, the mir-378 hairpin, through the action of miR-378*, directly targets and induces the repression of the AMPK kinase, CAMKK2, in BT-474 breast cancer cells, suggesting that miR-378* regulates AMPK pathway activity in breast cancer cells through regulation of an upstream AMPK kinase.

AMPK pathway activity is repressed by mir-378

Considering that miR-378* regulates CAMKK2, which functions to regulate AMPK activity, we next investigated the response of the AMPK pathway to mir-378. We found that, in our stable cell system, mir-378 hairpin expression causes significant reduction in protein levels of total AMPKα as well as the active (phosphorylated) form of AMPKα, pAMPKα (Fig. 3.3A). We further confirmed that the mir-378 hairpin reduces AMPK pathway activity by blotting for protein levels of phosphorylated ACC (pACC), an established direct kinase target of AMPK, which is implicated

in fatty acid synthesis (Winder and Hardie, 1996). pACC levels were also reduced in mir-378 hairpin-expressing cells (Fig. 3.3A), confirming that mir-378 hairpin-induced reduction in pAMPKα translates to a parallel reduction in target substrate phosphorylation and, consequently, activity. Data from the 6 selected clonal lines is shown for all afore mentioned proteins, including three different lines of each type, control and mir-378 hairpin. While expression variation between different clonal populations can be attributed to clonal variation, this variation does not diminish the clarity of the overall trend for negative regulation of AMPK activity by the mir-378 hairpin.

We next set out to establish which of the mature mir-378 hairpin products, miR-378 or miR-378*, are responsible for the effect on the AMPK pathway. To this aim, we transiently transfected the mir-378 hairpin clones with either a control miRNA inhibitor or a specific inhibitor directed against either miR-378 or miR-378*. While total AMPKα levels were not affected by inhibition of either miR-378 or miR-378*, pAMPKα and pACC levels increased in response to inhibition of endogenous miR-378* (Fig. 3.3B). Notably, miR-378 inhibition did not generate this response (data not shown), suggesting that miR-378* is the mature miRNA from the mir-378 hairpin responsible for the observed AMPK pathway response. We proceeded to further validate this result in naïve BT-474 cells (not passaged through antibiotic clonal selection), where transient inhibition of endogenous miR-378* alone was sufficient to induce AMPK pathway activity (Fig. 3.3C), thus eliminating concerns about artifactual molecular relationships generated by the clonal selection process. Taken together, we have identified that the mir-378 hairpin, and specifically mature miR-378*, represses AMPK pathway activity in breast cancer cells, at least in part through its direct regulation of CAMKK2.

Metabolic profiling of mir-378 hairpin stable cells implicates the hexosamine biosynthesis pathway

Considering that miR-378* is known to regulate breast cancer cell metabolism, and that we have, herein, identified another key metabolic pathway under the control of mir-378, we applied non-targeted NMR-based metabolomics to investigate the metabolome modulated in our mir-378 hairpin stable cell lines. In this manner, we identified a number of metabolites present at significantly different levels in the mir-378 hairpin-expressing cells as compared to control cells (Fig. 3.4). Metabolite levels were normalized to cell number at the time of harvest, and all results were replicated when data was normalized instead to protein concentration (data not shown). Metabolites present at significantly different levels between mir-378 hairpin-expressing and control cells include amino acids, sugars and those implicated in the TCA cycle. Interestingly, levels of the TCA cycle intermediate fumarate were depleted in response to the mir-378 hairpin, corresponding to the known effect of mir-378 on Succinate Dehydrogenase B (*SDHB*) levels, which is attributed to its direct regulation of ERRγ (Eichner et al., 2010). Moreover, one of the metabolites whose levels are most dramatically modulated by mir-378 hairpin expression is UDP-*N*-acetylglucosamine, as the mir-378 hairpin clones exhibit only 30% of the UDP-*N*-acetylglucosamine levels present in the control cells.

UDP-*N*-acetylglucosamine, or UDP-GlcNAc, is the end product of the hexosamine biosynthesis pathway, which functions to convert cellular glucose to UDP-GlcNAc. UDP-GlcNAc is a substrate for *O*-linked *N*-acetylglucosamine transferase (OGT), which transfers *N*-acetylglucosamine residues to serine or threonine residues, functioning to modify its target proteins with a glucose-moiety-containing post-translational modification in order to impart functional regulation (Wells et al., 2001). Interestingly, while *O*-GlcNAc signaling regulates the response to nutrients such as glucose and stress (Butkinaree et al., 2010), we found no significant difference in cellular glucose levels between mir-378 hairpin and control cells (data not shown), suggesting that the mir-378 hairpin control of UDP-GlcNAc levels occurs further downstream than cellular

glucose uptake. Indeed, UDP-GlcNAc levels are dependent on not only glucose flux, but also on nitrogen, fatty acid, and nucleic acid metabolism (Slawson et al., 2010). Furthermore, we noticed that OGT itself is a predicted target of miR-378*, providing a potential direct link between hexosamine pathway regulation and mir-378. CAMK itself was found to activate OGT, and OGT was determined to have an essential role in mediating downstream signaling (Song et al., 2008), providing further evidence that AMPK pathway activity is an upstream component of GlcNAc signaling, and suggesting that CAMKK-specific regulation of AMPK pathway activity is particularly linked to the OGT pathway. Furthermore, glucose deprivation was found to activate OGT expression in an AMPK-dependent manner (Cheung and Hart, 2008), suggesting that AMPK pathway regulation by miR-378* could extend as far downstream as the OGT/GlcNAc pathway. Having identified that, in breast cancer cells, miR-378* negatively regulates AMPK pathway activity by directly targeting and inhibiting CAMKK2 and that, in addition, mir-378 hairpin expression results in reduced cellular levels of UDP-GlcNAc, mir-378 appears to regulate the availability of GlcNAc post-translational signaling through its control of the AMPK pathway, and perhaps also by directly targeting the key enzyme OGT (Fig. 3.5).

DISCUSSION

In this study, we have identified that mir-378 functions as an upstream regulator of AMPK pathway activity in a breast cancer cell context, thus extending the metabolic role of this oncogenic miRNA to control of a central metabolic network. By directly targeting the upstream AMPK kinase, CAMKK2, miR-378* is able to repress pAMPKα and pACC levels. Furthermore, mir-378 reduces cellular levels of the metabolite UDP-GlcNAc, a key component in GlcNAcylation post-translational modification, suggesting that this miRNA is capable of controlling a whole new level of regulation of cellular activity both through and perhaps independently of the AMPK pathway.

As the mir-378 hairpin encodes for two mature miRNAs, it is interesting to note that AMPK pathway regulation in BT-474 cells appears to occur only through mature miR-378*. Classically, the (*) isoform of a miRNA hairpin is considered the less prevalent molecule, but there is clear indication from both this study and previous studies (Eichner et al., 2010; Lee et al., 2007) that miR-378* is an active, mature miRNA in the contexts studied. In fact, all of these studies have identified that miR-378* is concomitantly expressed from the endogenous mir-378 hairpin along with mature miR-378, and that the fold induction is similar for both mature miRNAs. In this study, the mir-378 hairpin clearly induces long-term effects on CAMKK2 and pAMPKα, which are only reproducible by modulation of mature miR-378*, indicating that miR-378* is a functionally active component of endogenous mir-378 hairpin expression. Furthermore, all systems studied in this thesis in which the expression of miR-378* is induced long-term, including the stable cell clones in this chapter as well as the NMuMG cell system in Chapter 2, exhibited no modulation of mRNA levels but robust effects on the protein levels of all direct targets identified in this thesis, ERRγ, GABPA, and CAMKK2. This effect, which is consistent for all three direct targets studied, suggests that the cellular transcriptional machinery can compensatorily recover from the

effects of long-term miR-378* expression on target mRNA levels, but that the effect on target protein levels, and the resulting physiological consequence of such regulation, remain robust.

Also interesting is the relationship of this miRNA hairpin to its metabolic host gene, *PPARGC1B* (PGC-1β), as these molecules are endogenously co-expressed. Already shown to be functionally and biologically relevant in contexts and pathways where PGC-1β plays important roles (Eichner et al., 2010) it is reasonable to consider that there may exist some regulatory feedback loops between the mir-378 hairpin and PGC-1β. Perhaps surprisingly, modulation of mir-378 hairpin levels did not affect PGC-1β mRNA or protein levels in our systems.

The first link of AMPK function to cancer came from the discovery that mice lacking the AMPK kinase LKB1 develop spontaneous tumors (Ollila and Makela, 2011). This work identified that AMPK activity may have a tumor suppressive role, and it follows that oncogenic miR-378*, whose levels increase with breast cancer progression (Eichner et al., 2010) would act on this pathway as a negative regulator. Furthermore, it is noteworthy that mir-378 functions to regulate AMPK specifically through CAMKK2 and not LKB1. This molecular specificity parallels the precise ERR isoform targeting we previously identified for miR-378* (Eichner et al., 2010) and, taken together with the underlying biological function corresponding to miR-induced specific ERR isoform modulation, raises questions about the functional differences imparted by CAMKK2 and LKB1 in cancer. It would be interesting to uncover the biological purpose in cancer of miR-378* targeting specifically CAMKK2 but not LKB1.

By searching for the long-term metabolic impact of mir-378 hairpin expression using an untargeted approach, we identified an unexpected component of mir-378 function; its control of cellular UDP-GlcNAc levels and, by extension, GlcNAcylation regulation. It is interesting to consider the extent of post-transcriptional regulation imparted by the mir-378 hairpin, as it not only directly affects a multitude of targets, many with their

own extensive regulatory pathways, but also appears to control a form of post-translational modification. Like any other biological networks, GlcNAcylation, produced through the hexosamine biosynthesis pathway works, not in isolation, but in coordination with other nutrient-sensing metabolic regulators including mTOR and AMPK (Slawson et al., 2010). Because the mir-378 hairpin appears to regulate the *O*-GlcNAcylation pathway from multiple avenues – through the AMPK pathway, perhaps independently of AMPK, and predicted direct targeting of the key enzyme, OGT – the importance of this molecular relationship is apparent. Taken together, the more the nexus controlled by the fine-tuning molecule mir-378 is expanded, the more it begs the question as to how all of the targets and target pathways integrate to produce a biologically coherent outcome.

The role of miRNAs in cancer metabolism is only beginning to be explored. A few examples include miR-23a/b, which regulates glutamine metabolism by targeting mitochondrial glutaminase (Gao et al., 2009) and miR-451, which was shown to regulate the LKB1/AMPK pathway as an adaptive mechanism to metabolic stress (Godlewski et al., 2010). It is evident that the mir-378 hairpin is one of the founding members of this group, and that its metabolic regulatory function in cancer – known now to include two major metabolic nodes: the PGC-1/ERR and AMPK pathways – is multifaceted and complex. If the other published metabolic mir-378 targets, such as *IGF1R* (Knezevic et al., 2012), which were originally identified for their functional roles in different biological contexts, are validated in cancer settings, the role of the mir-378 hairpin as a master regulator of cancer metabolism will be quickly expanded even further.

MATERIALS AND METHODS

Stable Cell Clones Generation

BT-474 breast cancer cells were stably transfected with either empty pcDNA3.1 vectors for control, or a pcDNA3.1 construct with the genomic region including that encoding the human mir-378 hairpin subcloned (from construct used for adenovirus generation in (Eichner et al., 2010)) downstream of the CMV promoter. G418 antibiotic was used for selection of cells stably expressing the vector construct. Individual clones were isolated for further studies.

RNA Isolation, Reverse Transcription, and Real-Time Quantitative PCR

RNA was isolated using QIAGEN miRNeasy Kit with DNAse treatment and quantified with RNA NanoDrop. Relative levels of miR-378*/378 levels were determined using Taqman miRNA qRT-PCR, according to instructions of the manufacturer (Applied Biosystems), followed by real-time qRT-PCR using the Corbett Research Rotor-Gene. Primers were obtained from the Taqman miRNA Assay Kits (miR-378*: 000567, miR-378: 002243, U18: 001204). Each reaction was carried out with 0.01 μg of total isolated RNA.

Relative mRNA levels were determined by reverse transcription into cDNA, followed by real-time qRT-PCR using LightCycler 480. Reverse transcription reactions were carried out with 1 μg of RNA using Oligo(dT) primer, dNTPs, 5X 1st strand buffer, DTT, RNase inhibitor, and Superscript II RNase H Reverse Transcriptase (Invitrogen). Primers used are described in the Supplementary Table A.3.1. All real-time qRT-PCR reactions for miRNA and mRNA were performed in duplicates.

Western Blots

Proteins were harvested from cells with modified RIPA buffer and quantified by the Bradford method. For detection of each target protein, 25 μg of total protein was resolved on 10% SDS-PAGE gel. Proteins were transferred onto nitrocellulose membrane and blocked with 5% milk in

TBS-T. Membranes were incubated with either anti-ERRγ (1:2000, from Dr. Ronald Evans) antibodies at room temperature for 1 h; or with anti-PGC1-β (sc-67285, lot#A0610, 1:1000), anti-ACC (cs#3662, lot 2, 1:1000), anti-P-ACC (sc#36618, lot 4, 1:1000), anti-AMPKα (cs#2532L, lot 19, 1:1000), anti-P-APMPKα (cs#2535s, lot 14, 1:1000), anti-LKB1 (sc-3245 lot#B0309, 1:1000), anti-CAMKK2 (ab96531 lot: GR6688-9, 1:1000), or anti-actin (sc-1616, lot#D2105, 1:200) at 4°C, overnight. After three washes with TBS-T and 5% milk, blots were incubated at room temperature for 1 h with secondary antibodies. Anti-rabbit antibodies (NA9340V, GE Healthcare, 1:5000) were used to detect ERRγ, ACC, P-ACC, AMPKα, P-AMPKα, and CAMKK2; anti-mouse antibodies were used to detect PGC1-β and LKB1 (NA931V, GE Healthcare, 1:5000); and anti-goat antibodies were used to detect actin (sc-2020, lot#E2710, 1:5000). After four washes with TBS-T, enhanced chemiluminescent reagents (Roche) were used for visualization of target proteins, according to the manufacturer's instructions.

Cell Culture

BT-474 stable cell clones were cultured at 37°C in 5%CO_2 using high glucose Dulbecco's modified Eagle's medium (DMEM, 11965), with added 10% fetal bovine serum (Sigma), 1 mM sodium pyruvate (GIBCO), 200 Units/mL penicillin (GIBCO), and 200 μg/mL streptomycin (GIBCO). For metabolomics, the media was changed 1 day before harvest.

Cell Extraction and Metabolomic Analysis

Each of the selected stable clones was cultured in eight (8) replicates of 15 cm plates, according to the conditions previous described. Cells were washed with 0.9% NaCl (isotonic saline) before harvesting. Five replicates were collected for non-targeted NMR analyses. Pellets were suspended in 80% methanol and disrupted using the TissueLyser (Qiagen) for 2 min at maximum speed. After removing cell debris, the remaining supernatant containing metabolites was frozen in liquid nitrogen and stored at -80°C. The other three replicates were used for cell counting

at the time of harvest, and later, protein quantification by the Bradford Assay, as two means of normalization for the spectral data generated by each clone.

Proliferation Assay

One control and two mir-378 hairpin stable clones were each plated onto a set of three 5cm plates, at 200,000 cells per plate. Cells were counted at four days after initial plating. Experiment was repeated three times. Results were confirmed with a separate mir-378 hairpin stable clone.

miRNA Inhibitor Transfection

Non-transfected BT-474 cells, two control and three mir-378 hairpin stable cell clones were plated at 400,000 cells/plate for 6 cm plates, and 2 x 10^6 cells/plate for 10 cm plates 24 h before transfection. Cells were transfected with 100 nM miRIDIAN miRNA Inhibitor Negative Control #2 (Dharmacon, IN-002000) or with combined 100 nM miRIDIAN miR-378* Inhibitor (Dharmacon, I-300175). Lipofectamine 2000 was complexed with Opti-mem 1 Reduced Serum Medium 1X (GIBCO) at a ratio of 3:100; Lipofectamine 2000 to 20 μM RNA was combined at a ratio of 1:2.3 ratio. The media was changed the following day, and cells were harvested four days after initial transfection.

For Figure 3B, BT-474 cells were plated at 400,000 cells per 6 cm plate 24 h before co-transfection with either 75nM miRIDIAN miRNA Mimic Negative Control #2 or hsa-miR-378* miRIDIAN Mimic and either 100 nM miRIDIAN miRNA Inhibitor Negative Control #2 or miRIDIAN miR-378* Inhibitor. Lipofectamine 2000 was complexed with Opti-mem 1 Reduced Serum Medium 1X (GIBCO) at a ratio of 3:100, and to RNA at a ratio of 1:2.3 Lipofectamine 2000 to 20 μM RNA. Cells were harvested four days after transfection. The experiment was independently repeated two times.

Reporter Construct Cloning and Transfection

Regions of the human *CAMKK2* 3'UTRs (sequences from www.genome.ucsc.edu, human genome assembly Feb. 2009) predicted to

be targeted by miR-378* (by Pictar, http://pictar.bio.nyu.edu/ and TargetScan, http://www.targetscan.org) were cloned into the phRL-TK(Int-) vector (Promega). Mutants were generated the same way. Primers are listed in Supplementary Table A.3.2. Data shown is based on cloning done by annealing oligos containing miR-378* target regions ± 16 nucleotides of endogenous flanking region sequence on either side of the miR-378* binding site.

COS-1 cells were transfected with Lipofectamine 2000 (Invitrogen) according to the manufacturer's protocol (using 2 µL Lipofectamine 2000 and 100 µL Opti-Mem Reduced Serum Medium 1X (GIBCO) per well) in 12-well plates with 200 ng luciferase reporter, 10 pmol RNA (hsa-miR-378* miRIDIAN Mimic (Dharmacon, catalog #C-300685-03) or miRIDIAN microRNA Mimic Negative Control #2 (Dharmacon, catalog #CN-002000-01)) and 1 µL β-galactosidase protein (Sigma) per well. Cells were harvested and assayed for luciferase activity using the Renilla Luciferase Assay System (Promega) and β-galactosidase activity 24 h post-transfection. Luciferase data was normalized to the β-galactosidase transfection efficiency control levels. Experiments were performed in quadruplicate and each experiment was repeated multiple times.

ACKNOWLEDGEMENTS

We thank M.C. Perry, M. Ghahremani and C.R. Dufour for helpful discussions and technical assistance. We thank R.M. Evans for the ERRγ antibody. NMR experiments were recorded at the Québec/Eastern Canada High Field NMR Facility, supported by the Natural Sciences and Engineering Research Council of Canada, the Canada Foundation for Innovation (CFI), the Québec ministère de la recherche en science et technologie and McGill University. Measurements of metabolites were conducted by Dr. Daina Avizonis at the Metabolomics core facility of the GCRC which is funded by the CFI. L.J.E. is a recipient of a studentship from the Fonds de la Recherche en Santé du Québec (FRSQ). This work was supported by grants from the Canadian Institutes for Health Research.

REFERENCES

Butkinaree, C., Park, K., and Hart, G.W. (2010). O-linked beta-N-acetylglucosamine (O-GlcNAc): Extensive crosstalk with phosphorylation to regulate signaling and transcription in response to nutrients and stress. Biochimica et biophysica acta *1800*, 96-106.

Cairns, R.A., Harris, I.S., and Mak, T.W. (2011). Regulation of cancer cell metabolism. Nat Rev Cancer *11*, 85-95.

Cheung, W.D., and Hart, G.W. (2008). AMP-activated protein kinase and p38 MAPK activate O-GlcNAcylation of neuronal proteins during glucose deprivation. The Journal of biological chemistry *283*, 13009-13020.

Deberardinis, R.J., Sayed, N., Ditsworth, D., and Thompson, C.B. (2008). Brick by brick: metabolism and tumor cell growth. Curr Opin Genet Dev *18*, 54-61.

Eichner, L.J., Perry, M.C., Dufour, C.R., Bertos, N., Park, M., St-Pierre, J., and Giguere, V. (2010). miR-378(*) mediates metabolic shift in breast cancer cells via the PGC-1beta/ERRgamma transcriptional pathway. Cell metabolism *12*, 352-361.

Feng, M., Li, Z., Aau, M., Wong, C.H., Yang, X., and Yu, Q. (2011). Myc/miR-378/TOB2/cyclin D1 functional module regulates oncogenic transformation. Oncogene *30*, 2242-2251.

Gao, P., Tchernyshyov, I., Chang, T.C., Lee, Y.S., Kita, K., Ochi, T., Zeller, K.I., De Marzo, A.M., Van Eyk, J.E., Mendell, J.T.*, et al.* (2009). c-Myc suppression of miR-23a/b enhances mitochondrial glutaminase expression and glutamine metabolism. Nature *458*, 762-765.

Garzon, R., Calin, G.A., and Croce, C.M. (2009). MicroRNAs in Cancer. Annu Rev Med *60*, 167-179.

Giguere, V. (2008). Transcriptional control of energy homeostasis by the estrogen-related receptors. Endocrine reviews *29*, 677-696.

Godlewski, J., Nowicki, M.O., Bronisz, A., Nuovo, G., Palatini, J., De Lay, M., Van Brocklyn, J., Ostrowski, M.C., Chiocca, E.A., and Lawler, S.E. (2010). MicroRNA-451 regulates LKB1/AMPK signaling and allows adaptation to metabolic stress in glioma cells. Molecular cell *37*, 620-632.

Hawley, S.A., Pan, D.A., Mustard, K.J., Ross, L., Bain, J., Edelman, A.M., Frenguelli, B.G., and Hardie, D.G. (2005). Calmodulin-dependent protein kinase kinase-beta is an alternative upstream kinase for AMP-activated protein kinase. Cell metabolism *2*, 9-19.

He, L., and Hannon, G.J. (2004). MicroRNAs: small RNAs with a big role in gene regulation. Nat Rev Genet *5*, 522-531.

King, A., Selak, M.A., and Gottlieb, E. (2006). Succinate dehydrogenase and fumarate hydratase: linking mitochondrial dysfunction and cancer. Oncogene *25*, 4675-4682.

Knezevic, I., Patel, A., Sundaresan, N.R., Gupta, M.P., Solaro, R.J., Nagalingam, R.S., and Gupta, M. (2012). A novel cardiomyocyte-enriched microRNA, miR-378, targets insulin-like growth factor 1 receptor: implications in postnatal cardiac remodeling and cell survival. The Journal of biological chemistry *287*, 12913-12926.

Kroemer, G., and Pouyssegur, J. (2008). Tumor cell metabolism: cancer's Achilles' heel. Cancer Cell *13*, 472-482.

Lee, D.Y., Deng, Z., Wang, C.H., and Yang, B.B. (2007). MicroRNA-378 promotes cell survival, tumor growth, and angiogenesis by targeting SuFu and Fus-1 expression. Proceedings of the National Academy of Sciences of the United States of America *104*, 20350-20355.

Luo, Z., Saha, A.K., Xiang, X., and Ruderman, N.B. (2005). AMPK, the metabolic syndrome and cancer. Trends Pharmacol Sci *26*, 69-76.

Motoshima, H., Goldstein, B.J., Igata, M., and Araki, E. (2006). AMPK and cell proliferation--AMPK as a therapeutic target for atherosclerosis and cancer. The Journal of physiology *574*, 63-71.

Ollila, S., and Makela, T.P. (2011). The tumor suppressor kinase LKB1: lessons from mouse models. J Mol Cell Biol *3*, 330-340.

Semenza, G.L. (2003). Targeting HIF-1 for cancer therapy. Nat Rev Cancer *3*, 721-732.

Semenza, G.L. (2008). Tumor metabolism: cancer cells give and take lactate. The Journal of clinical investigation *118*, 3835-3837.

Shackelford, D.B., and Shaw, R.J. (2009). The LKB1-AMPK pathway: metabolism and growth control in tumour suppression. Nat Rev Cancer *9*, 563-575.

Shaw, R.J. (2009). LKB1 and AMP-activated protein kinase control of mTOR signalling and growth. Acta Physiol (Oxf) *196*, 65-80.

Slawson, C., Copeland, R.J., and Hart, G.W. (2010). O-GlcNAc signaling: a metabolic link between diabetes and cancer? Trends Biochem Sci *35*, 547-555.

Song, M., Kim, H.S., Park, J.M., Kim, S.H., Kim, I.H., Ryu, S.H., and Suh, P.G. (2008). o-GlcNAc transferase is activated by CaMKIV-dependent phosphorylation under potassium chloride-induced depolarization in NG-108-15 cells. Cellular signalling *20*, 94-104.

Swinnen, J.V., Brusselmans, K., and Verhoeven, G. (2006). Increased lipogenesis in cancer cells: new players, novel targets. Curr Opin Clin Nutr Metab Care *9*, 358-365.

Warburg, O. (1956). On the origin of cancer cells. Science *123*, 309-314.

Wells, L., Vosseller, K., and Hart, G.W. (2001). Glycosylation of nucleocytoplasmic proteins: signal transduction and O-GlcNAc. Science *291*, 2376-2378.

Winder, W.W., and Hardie, D.G. (1996). Inactivation of acetyl-CoA carboxylase and activation of AMP-activated protein kinase in muscle during exercise. Am J Physiol *270*, E299-304.

Woods, A., Dickerson, K., Heath, R., Hong, S.P., Momcilovic, M., Johnstone, S.R., Carlson, M., and Carling, D. (2005). Ca2+/calmodulin-dependent protein kinase kinase-beta acts upstream of AMP-activated protein kinase in mammalian cells. Cell metabolism *2*, 21-33.

TABLES AND FIGURES

Figure 3.1. Validation and selection of mir-378 hairpin-expressing BT-474 stable cell clones

(**A**) mir-378 hairpin. (**B** and **C**) Validation of the six stable cell clones selected for further study. (**B**) Expression of mature miR-378* and miR-378 is elevated in the three selected mir-378 hairpin stable clones (mir-378 hairpin) compared to the three selected control clones (control), as determined by qRT-PCR and normalized to U18. (**C**) Expression of *ESRRG* and *PPARGC1b* mRNA in these clones, as detected by qRT-PCR and normalized to 18S. (**D**) ERRγ is downregulated at the protein level in the selected mir-378 hairpin stable cell clones, as determined by western blotting. No change observed in PGC1-β protein levels. Actin serves as the loading control. N indicates non-transfected BT-474 cells. (**E**) mir-378 hairpin stable cell clones exhibit increased cell proliferation as compared to control clone. * indicates $p<0.05$, *** $p<0.001$.

Figure 3.1

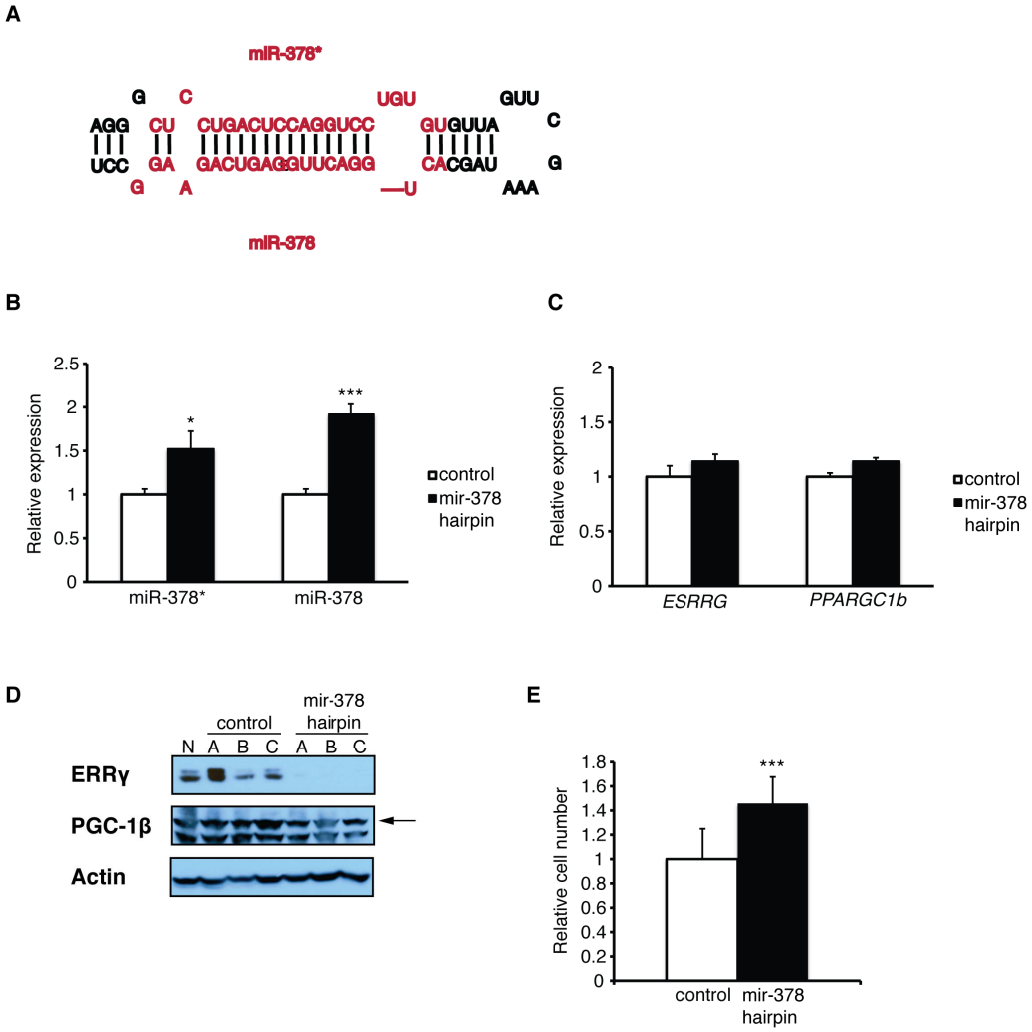
A
miR-378*
miR-378
B
Relative expression
control
mir-378 hairpin
miR-378*
miR-378
C
Relative expression
control
mir-378 hairpin
ESRRG
PPARGC1b
D
control
mir-378 hairpin
N A B C A B C
ERRγ
PGC-1β
Actin
E
Relative cell number
control
mir-378 hairpin

Figure 3.2. *CAMKK2* is a direct target of miR-378*

(**A**) The *CAMKK2* 3'UTR region predicted to be targeted by miR-378*. Sequence conservation across species is indicated. Yellow designates the seed region. (**B**) Expression of miR-378* decreases luciferase reporter gene activity in COS-1 cells when linked to the targeted segment of the 3'UTR of *CAMKK2* (597). Mutation of the seed sequence at position 4 (597m) abolishes the miR-378*-dependent repression. Control mimic is a control miRNA mimic, and the control is empty vector. * indicates $p<0.01$. (**C**) Left Panel: Transient transfection of naïve BT-474 cells with miR-378* inhibitor (miR-378*-i) derepresses *CAMKK2* mRNA transcript level as compared to control inhibitor (ctrl-i). Right Panel: Transient co-transfection of naïve BT-474 cells with either control miRNA mimic (ctrl miR) or miR-378* mimic (miR-378*), and either control (ctrl-i) or miR-378* inhibitor (miR-378*-i), as determined by qRT-PCR and normalized to 18S. (**D**) Naïve BT-474 cells transiently transfected with miR-378* inhibitor (miR-378*-i) exhibit an increase in CAMKK2 but not LKB1 levels as compared to cells transfected with control inhibitor (ctrl-i), as determined by western blotting. Actin serves as a loading control. (**E**) CAMKK2 and LKB1 levels in stable clones, as determined by western blotting.

Figure 3.2

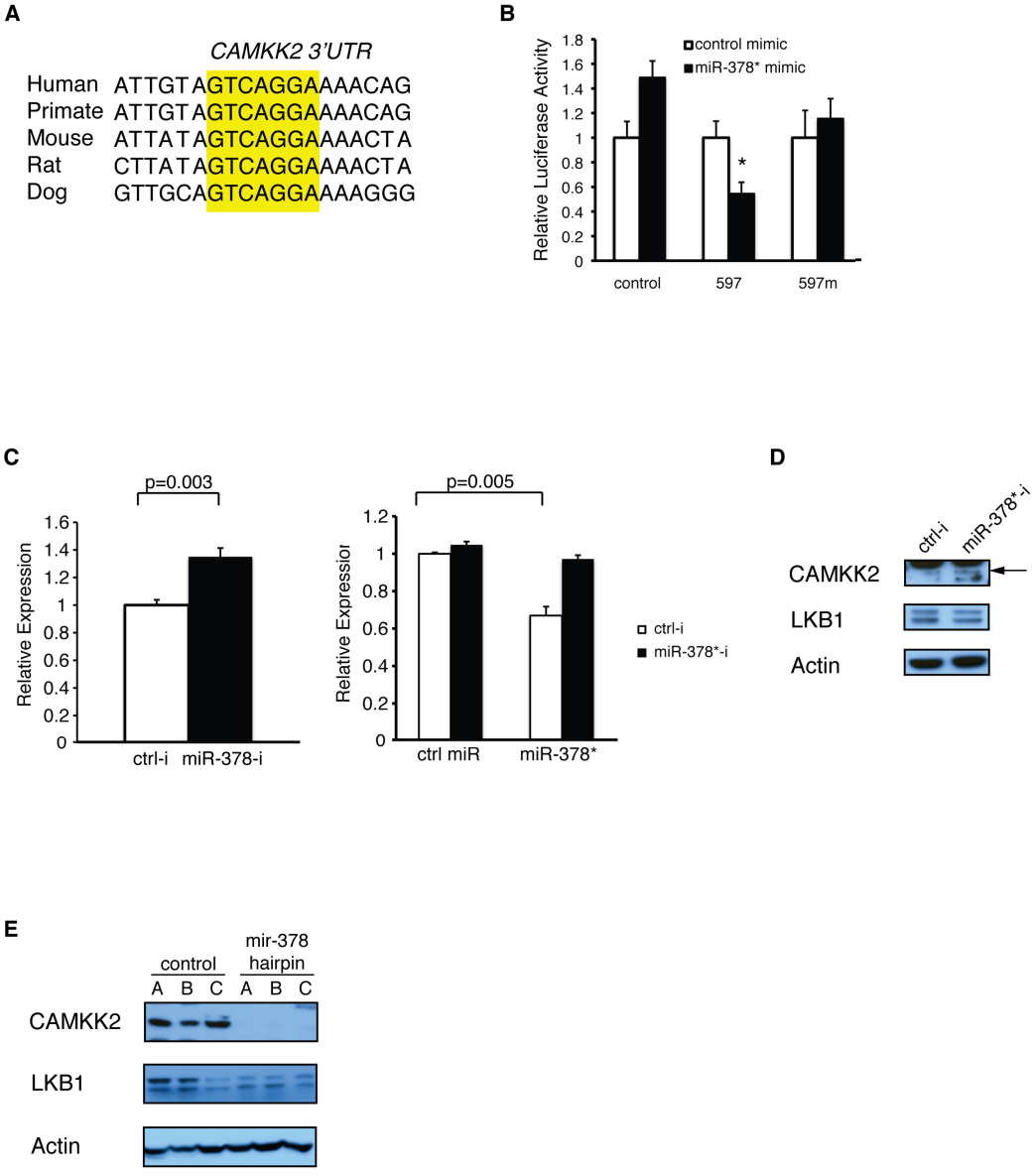
A
CAMKK2 3'UTR
Human ATTGTAGTCAGGAAAACAG
Primate ATTGTAGTCAGGAAAACAG
Mouse ATTATAGTCAGGAAAACTA
Rat CTTATAGTCAGGAAAACTA
Dog GTTGCAGTCAGGAAAAGGG
B
Relative Luciferase Activity
control mimic
miR-378* mimic
control
597
597m
C
p=0.003
Relative Expression
ctrl-i
miR-378-i
p=0.005
ctrl miR
miR-378*
ctrl-i
miR-378*-i
D
ctrl-i
miR-378*-i
CAMKK2
LKB1
Actin
E
control
mir-378 hairpin
A B C A B C
CAMKK2
LKB1
Actin

Figure 3.3. miR-378* represses AMPK pathway activity in BT-474 cells

(**A**) pAMPKα, AMPKα, and pACC protein levels are reduced in mir-378 hairpin-expressing stable cell clones (mir-378 hairpin) as compared to control stable clones (control), as determined by western blotting. Actin serves as a loading control. (**B**) Transient transfection of mir-378 hairpin clones with miR-378* inhibitor (miR-378*-i) alleviates repression of AMPK activity as compared to transfection with control miRNA inhibitor (control-i), as determined by western blotting. Actin serves as a loading control. (**C**) Naïve BT-474 cells transiently transfected with miR-378* inhibitor (miR-378*-i) exhibit reactivation of AMPK pathway activity as compared to cells transfected with control inhibitor (ctrl-i), as determined by western blotting. Actin serves as a loading control.

Figure 3.3

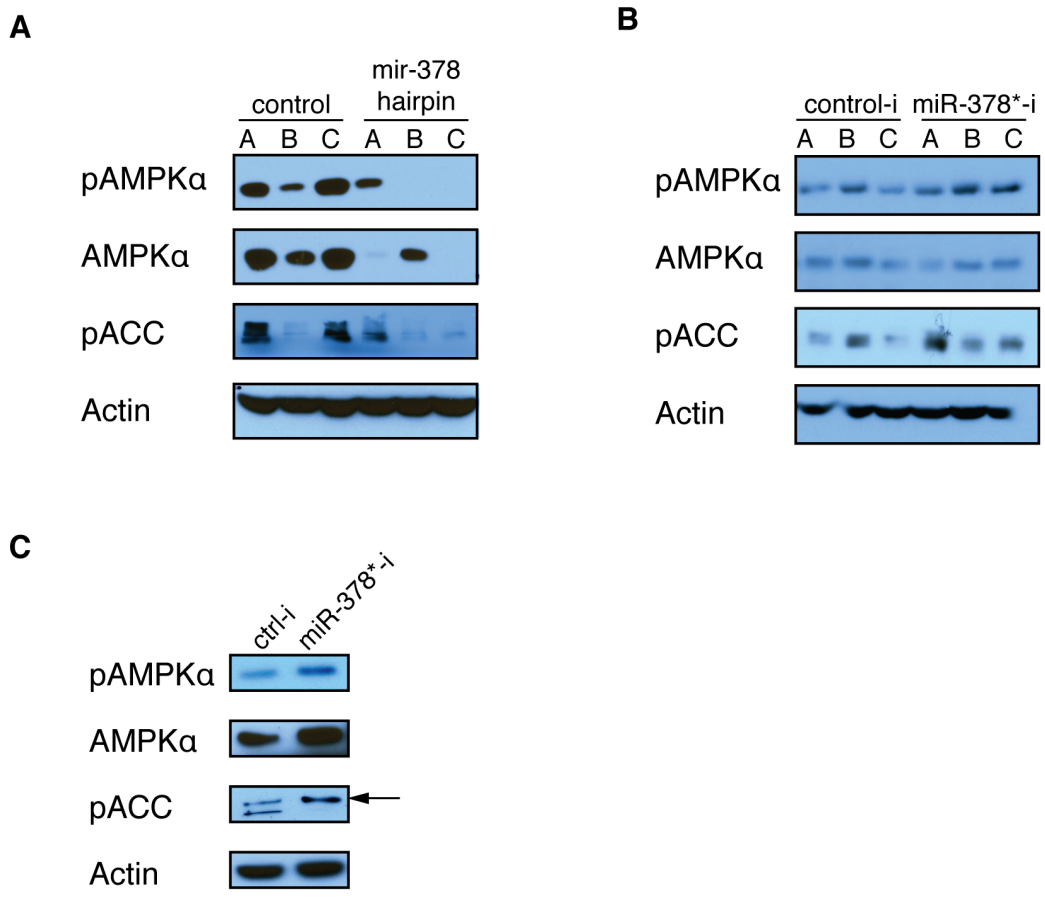
A
control
mir-378 hairpin
A B C A B C
pAMPKα
AMPKα
pACC
Actin
B
control-i
miR-378*-i
A B C A B C
pAMPKα
AMPKα
pACC
Actin
C
ctrl-i
miR-378*-i
pAMPKα
AMPKα
pACC
Actin

Figure 3.4. Metabolomics analysis of mir-378 hairpin stable cell lines implicates the hexosamine biosynthesis pathway

Non-targeted NMR-based metabolomics was performed. Data represent the average value (in nmol) from three independent mir-378 hairpin stable cell clones normalized to the average obtained from three independent control clones (shown as fold). 5 replicates of each stable cell clone line were assayed. Data is shown for all metabolites that exhibit significantly different levels in the mir-378 hairpin-expressing cells compared to control cells ($p < 0.05$). Metabolite amounts were normalized to cell number at the time of harvest, and data is ordered according to metabolite type. Statistical significance was determined by Student's *t*-test.

Figure 3.4

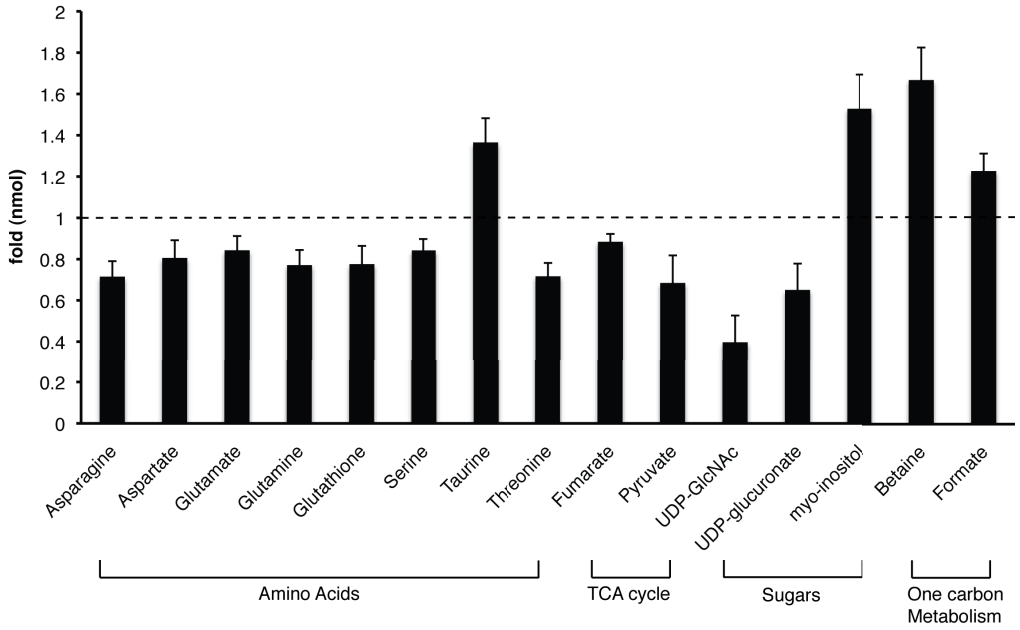
fold (nmol)
2
1.8
1.6
1.4
1.2
1
0.8
0.6
0.4
0.2
0
Asparagine
Aspartate
Glutamate
Glutamine
Glutathione
Serine
Taurine
Threonine
Fumarate
Pyruvate
UDP-GlcNAc
UDP-glucuronate
myo-inositol
Betaine
Formate
Amino Acids
TCA cycle
Sugars
One carbon Metabolism

Figure 3.5. Schematic representation of AMPK and GlcNAcylation pathway regulation by miR-378*

miR-378* directly targets *CAMKK2*, resulting in a downstream reduction of pAMPKα and pACC levels. Simultaneously, miR-378* induces a reduction in UDP-GlcNAc levels. The prediction that *OGT* is a direct target of miR-378* and the published link between AMPK activity and OGT expression further expand this miR-378* network. Arrows indicate activation, and inhibition is designated with red bars. Dashed-line arrows; downregulation of an activation event. Multiple arrows between two pathway components indicate indirect pathway relationships.

Figure 3.5

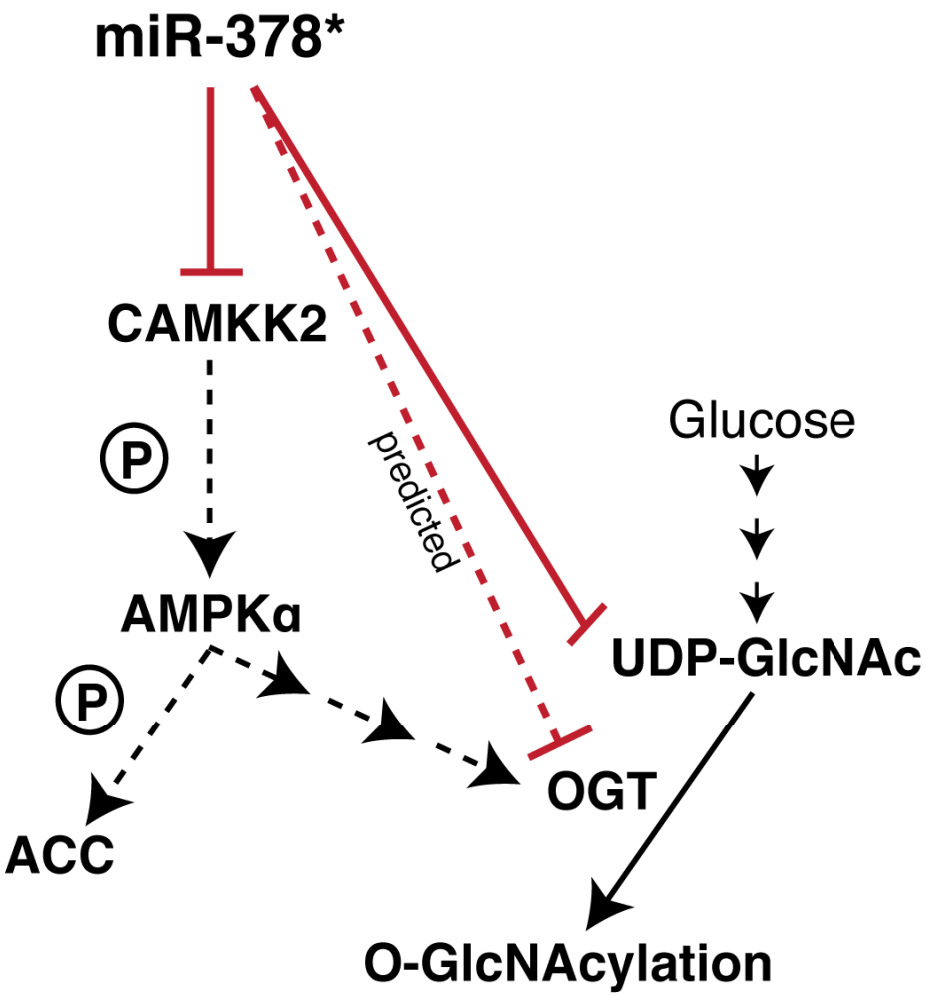
miR-378*
CAMKK2
P
AMPKα
P
ACC
predicted
Glucose
UDP-GlcNAc
OGT
O-GlcNAcylation

CHAPTER IV: Systemic Ablation of ERRα Predisposes the Host to Cancer Cachexia

PREFACE

Having established in Chapter II that ERRα and ERRγ exhibit divergent functions in breast cancer cell metabolism, we determined to further investigate the metabolic contribution of ERR in breast cancer *in-vivo*. Considering that ERRα expression correlates with that of the breast cancer oncogene ERBB2, we used an ERBB2-driven model of mammary tumorigenesis to investigate the contribution of ERRα to the onset and progression of this disease. We found that the absence of ERRα delays ERBB2-induced mammary tumor onset but, contrastingly, accelerates disease progression after onset. We identified that ERRα-/- tumors exhibit elevated levels of inflammation, while the systemic ablation of ERRα affects the metabolic status of these animals, such that the progression of mammary tumorigenesis induces these mice to exhibit cachexia. These results identify a novel metabolic disease in which ERRα participates, raising important considerations for therapeutic targeting of ERRα in breast cancer.

ABSTRACT

Cellular metabolic capacity has an established importance in cancer, yet the underlying regulatory mechanisms remain unclear. I have previously identified that, in breast cancer cells, modulation of the relative availabilities of the Estrogen-Related Receptor (ERR) isoforms ERRα and γ is capable of inducing the metabolic shift away from oxidative metabolism known as the Warburg effect. In order to further investigate the role of ERR in breast cancer, including its metabolic function in this context, I turned to an *in-vivo* model of ERBB2-initiated mammary tumorigenesis. The choice of mouse model was motivated by the fact that the expression of ERRα in breast cancer correlates with that of the poor prognostic marker ERBB2.

We followed the onset and progression of mammary tumorigenesis in wildtype (WT) and ERRα-/- mice harboring mammary-specific expression of the NeuNDL2-5 oncogene imparted by the MMTV promoter (MMTV-Neu-NDL). We found that the absence of ERRα delays ERBB2-induced mammary tumor onset but, contrastingly, accelerates disease progression after onset. Moreover, we identified that ERRα-/- mice fail to maintain the progression of body weight observed in WT animals after tumor onset, suggesting that inhibition of ERRα activity may predispose to a cachectic state. Genome-wide gene expression profiling identified increased inflammatory signaling in the ERRα-/- tumors. Metabolomics identified amino acid differerences in the serum and skeletal muscle which point toward accelerated systemic protein turnover. When combined with molecular studies of cachexia markers in the skeletal muscle and adipose tissue of pre-onset and tumor-bearing mice, as well as data from a short-term, *in-vivo* model of ERRα inhibition, our data suggests that systemic ablation of ERRα may render the host more succeptible to cancer cachexia, a disease characterized by heightened inflammation, metabolic derangements and tissue atrophy.

INTRODUCTION

While the Estrogen-Related Receptors (ERRs) are predominantly known for their role in regulating metabolic function and related gene expression programs (Eichner and Giguere, 2011; Giguere, 2008b), important roles for the ERRs in cancer have become increasingly apparent. In fact, the ERRs have been linked to many cancers including endometrial (Gao et al., 2006; Watanabe et al., 2006), lung (Wang et al., 2010), cervical (Mori et al., 2011), ovarian (Fujimoto et al., 2007; Permuth-Wey et al., 2011; Salzman et al., 2011; Sun et al., 2005), prostate (Fujimura et al., 2010; Fujimura et al., 2007; Yu et al., 2008a), uterine (Fujimoto and Sato, 2009) cancers. However, a large body of research linking ERR to cancer has come from breast cancer research (Deblois and Giguere, 2011).

Breast cancer has been established to be a heterogeneous disease which can be subdivided into at least four different sub-types based on gene expression profiles, including two luminal-like, one basal-like and one ERBB2-overexpressing subtype (Sorlie et al., 2003). Mouse models of breast cancer have proven to be key tools for advancing the understanding of this complex disease, allowing for the study of onset and progression *in-vivo* in a controlled, genetically-driven system. Mouse models of the ERBB2-overexpressing sub-type, which describes 20-30% of primary human breast cancer cases, have been particularly successful, as this disease is defined by one precise genetic event, the overexpression or amplification of ERBB2, which has a causal role in breast cancer development (Ursini-Siegel et al., 2007b).

These mouse models allow not only for the dissection of the underlying molecular components of breast cancer, but also for the study of this disease *in-vivo*, including systemic aspects which affect disease progression and aggressivity. Inflammation is one such systemic component that originates from the host, yet profoundly affects tumor progression (Wu and Zhou, 2009). It has been clearly established that the

tumor microenvironment, which includes innate and adaptive immune cells in addition to the cancer cells and their surrounding stroma, very often exhibits protumor inflammation (Grivennikov et al., 2010).

In fact, inflammation does not only accelerate tumor development, but elevated systemic inflammatory levels are also known to induce cachexia. This disease, which causes up to 20% of all cancer deaths, is characterized by weight loss which cannot be reversed with food intake, metabolic derangements including predominantly depletion of both lean and fat mass, and elevated systemic inflammation (Tisdale, 2002). In cancer cachexia, the tumor produces excreted inflammatory cytokines which induce skeletal muscle and adipose tissue breakdown (Argiles et al., 1992; Pajak et al., 2008; Tisdale, 2002). Skeletal muscle is broken down by proteolysis into individual amino acids which are released into the serum, while adipose tissue breakdown stems from increased lipolysis (Argiles et al., 1992; Bing, 2011; Tisdale, 2002).

Cellular metabolic capacity has an established importance in cancer, yet the underlying regulatory mechanisms remain unclear. I have identified in Chapter 2 that, in breast cancer cells, modulation of the relative availabilities of the Estrogen-Related Receptor (ERR) isoforms ERRα and γ is capable of inducing the metabolic shift away from oxidative metabolism known as the Warburg effect. In order to further investigate the role of ERR in breast cancer, including its metabolic function in this context, I turned to an *in-vivo* model of ERBB2-initiated mammary tumorigenesis.

RESULTS

We followed the onset and progression of ERBB2-driven mammary tumorigenesis in littermate wildtype (WT) and ERRα-/- mice harboring mammary-specific expression of the NeuNDL2-5 oncogene imparted by the MMTV promoter (MMTV-Neu-NDL). The choice of mouse model was motivated by the fact that the expression of ERRα in breast cancer correlates with that of the poor prognostic marker ERBB2. We found that the absence of ERRα (Neu ERRα-/-) delays ERBB2-induced mammary tumor onset as compared to that observed in Neu WT mice (Fig. 4.1A). This recapitulates the trend observed in a different ERBB2-driven model of mammary tumorigenesis (Deblois et al., 2010), where ERRα functions as an oncogene at disease onset.

In contrast, our Neu ERRα-/- mice exhibit accelerated disease progression after onset, as quantified by total tumor burden (total tumor volume; Fig. 4.1B) and focality (# tumors per mouse; Fig. 4.1C). Surprisingly, after disease onset, the absence of ERRα allows mammary tumorigenesis to progress more aggressively than was observed for the Neu WT animals, as indicated by results in Fig 4.1B and 4.1C.

Moreover, we also tracked total body weight before and after tumor onset. Before disease onset, Neu ERRα-/- mice displayed ~10% less body weight than Neu WT animals (Fig. 4.2A, left), corresponding to the published weight difference between ERRα-/- and WT animals (Luo et al., 2003c). Furthermore, the lines plotted to the data corresponding to each genotype are both flat with slopes not statistically different from zero or from each other (Fig. 4.2A, plotted lines on left, slopes and corresponding statistics in table on right). Therefore, before onset of mammary tumorigenesis, mice of both genotypes exhibit body weights that do not change over time, indicating that both groups of mice are comprised of mature, adult mice with stable body weight. Disease onset corresponds to the accumulation of tumors that, by extension, add mass to the total body weight of each mouse. By multiplying the measured total tumor volume at

each measurement by the pre-calculated average tumor density, we were able to determine the weight of each mouse at each time interval which was due to increased tumor burden. After subtracting this tumor weight from total body weight, we were able to plot the remaining body weight of each mouse (labelled Non-Tumor Body Weight) throughout disease progression starting at the day of tumor onset (Fig. 4.2B, left). Regression analysis was used to plot lines through this data for both genotypes (Fig. 4.2B, left). Interestingly, the slope corresponding to the Neu ERRα-/- mouse data is significantly flatter than that based on the Neu WT data (Fig. 4.2B, table on right). This indicates that Neu ERRα-/- mice fail to maintain the progression of body weight observed in Neu WT animals after tumor onset. As the failure to maintain body weight is a hallmark of cancer cachexia (Tisdale, 2002), this data suggests that the absence of ERRα may predispose tumor-bearing animals to a cachectic state.

Next, we used genome-wide gene expression profiling to investigate the molecular differences between Neu ERRα-/- tumors and Neu WT tumors (Fig. 4.3A). After careful consideration, we chose to study tumors of similar size from mice sacrificed at endpoints ~70 days after tumor onset. Microarray analysis identified elevated levels of inflammatory signalling in the Neu ERRα-/- tumors that may contribute to the explanation of the accelerated tumor growth in these mice. More precisely, the three most significantly modulated gene function categories, as identified by Ingenuity Pathway Analysis (IPA) software, include two pathways directly linked to immunity and inflammation, Role of Pattern Recognition Receptors in Recognition of Bacteria/Viruses and Interferon Signaling (Fig. 4.3B). The majority of the modulated genes belonging to these pathways are upregulated in the Neu ERRα-/- tumors, indicating an activation of inflammatory signalling. Furthermore, based on the gene expression data, several inflammatory transcription factors were predicted to be activated in the Neu ERRα-/- tumors, including Irf7, Irf1, Stat1, Irf3 and Stat2 (Fig. 4.3C). Two of these genes, *Irf7* and *Stat2*, were

themselves upregulated at the mRNA level in the Neu ERRα-/- tumors. Figure 4.3D outlines the molecular relationships of several of these inflammatory genes upregulated (shown in red) in the Neu ERRα-/- tumors, including where they fit in the Interferon (IFN) Signaling Pathway. IFNs are cytokines with established roles in cachexia, which recruit and promote the activating dimerization of Signal Transducer and Activator of Transcription (Stat) proteins, allowing them to interact with IFN-regulatory factors (IRFs) to regulate target gene transcription networks (Pajak et al., 2008).

We then investigated the protein levels of Stat1, Stat2, and Stat3, as well as their active, phosphorylated forms (Fig. 4.3E). We found that Stat1, pStat1, Stat2, and pStat2 levels were all clearly elevated in the Neu ERRα-/- tumors as compared to the Neu WT tumors. Interestingly, Stat3 and pStat3 were not modulated in a genotype-specific manner, as protein levels were highly variable across different mice in a seemingly random fashion. In the absence of a genotype-specific relationship regulating the Stat3 levels, this variation likely reflects the extensive *in-vivo* heterogeneity commonly observed between different tumors, highlighting, by contrast, the strength and reproducibility of the Stat1/Stat2 findings despite the inevitable biological variation between tumors. ERRα ablation was also verified at the protein level. Finally, the gene expression levels of several genes identified to be differentially modulated by the microarray were successfully validated by qRT-PCR (Fig. 4.3F). Taken together, the Neu ERRα-/- tumors display elevated levels of inflammation, and this appears to occur through from the Stat1/Stat2 but not the Stat3 pathways.

Considering that cachexia is defined by increased systemic inflammation that affects other organ systems including adipose tissue and skeletal muscle to induce their breakdown (Fig. 4.4A), and we have identified that the Neu ERRα-/- tumor environment is a source of elevated inflammatory signalling, we next turned to metabolomics as a tool to investigate systemic indicators of cachexia. We first measured metabolites

in small tumors from mice at endpoint. The only metabolites at significantly different levels were NADH, O-Phosphoethanolamine, and Glutamine (Fig. 4.4B). Interestingly, Glutamine is known to be more actively absorbed and consumed by rapidly growing tumors (Wise and Thompson, 2010), so its elevated levels in the Neu ERRα-/- tumors may be an indicator of increased flux into the more aggressive tumors.

We also investigated the levels of serum metabolites, both in tumor-free mice and tumor-bearing mice. We observed an overall trend for elevated amino acid levels in the tumor-bearing Neu ERRα-/- mouse serum as compared to tumor-bearing Neu WT animals, and this genotype-related difference was not observed in tumor-free mice (Fig. 4.4C) (Differentially regulated non-amino acid metabolites shown in Fig. A.4.1A). More precisely, with an *n* of only 4, only Asparagine and Glutamine levels reached statistical significance of $p<0.05$, but the overall trend appears likely to extend beyond those two amino acids. In the absence of a larger cohort of mice, based on this data, we can conclude only that tumor accumulation in the Neu ERRα-/- mice correlates with increases in certain serum amino acid levels. Skeletal muscle breakdown due to cancer cachexia is accompanied by a release of the resulting free amino acids into the serum (Fig. 4.4A) (Tisdale, 2002). Therefore, the elevated levels of certain free amino acids observed in the Neu ERRα-/- serum may indicate the possibility of the presence of cancer cachexia in the Neu ERRα-/- mice, and could suggest the involvement of the skeletal muscle. However, obtaining and testing serum from a larger cohort of mice would provide crucial additional statistical power necessary for drawing extensive conclusions from this data.

Metabolomics analysis of skeletal muscle from tumor-bearing mice suggests a mild general trend of reduced amino acid levels in Neu ERRα-/- mice (Fig. 4.4D), which may be a preliminary indication of accelerated protein turnover (differentially regulated non-amino acid metabolites shown in Fig. A.4.1B). Again, as with the serum data above, small sample

size limits the statistical power of this data and, correspondingly, of the amino acids quantified, only Alanine and Aspartate levels reached statistical significance. However, as 9 of the 18 amino acids quantified (50%) in this limited set of samples display reduced levels in the Neu ERRα-/- skeletal muscle, whereas only one amino acid exhibited increased levels, this preliminary data may suggests a generalized trend toward reduced amino acid levels in the skeletal muscle of tumor-bearing ERRα-/- animals. Considering this, it would be worthwhile to expand the analysis across a larger cohort of mice, as it would allow us to verify if this is a real trend.

As cachexia induces a breakdown of adipose and skeletal muscle tissues, we examined these two tissues in tumor-bearing mice at endpoint. Representative hind limb skeletal muscle and abdominal adipose depot are shown in Fig. 4.5A. Neu ERRα-/- mice exhibit markedly less inguinal fat (90%) than Neu WT animals at endpoint, whereas skeletal muscle quantity was not different between the genotype groups (Fig. 4.5B). ERRα-/- mice are known to have less fat than WT mice (40% less inguinal adipose mass) (Luo et al., 2003c), however, this basal difference is far from the 90% difference we observe here in the tumor-bearing Neu ERRα-/- mice at endpoint, suggesting that accumulating tumor burden exacerbates the adipose phenotype.

We then screened for molecular markers of cachexia in both the skeletal muscle and adipose tissue. In the skeletal muscle, several genes involved in authophagy, *Agt10*, *Becn1*, *Bnip3*, were downregulated in the ERRα-/- mice (Fig. 4.5C), whereas activation of autophagy is one major mechanism used to explain cachexia-induced skeletal muscle breakdown. These effects were dependent on genotype regardless of tumor burden, indicating that these are ERRα-related molecular relationships that may not play into the phenotype observed in response to accumulating tumor burden. A downregulation of genes implicated in autophagy such as those observed here could suggest a mechanism through which these animals

could be resistant to cachectic skeletal muscle breakdown. However, western blotting for autophagy proteins including the protein product of *Becn1*, Beclin-1, revealed no differences in protein levels (Fig. 4.5D), suggesting that these genotype-specific gene expression differences do not translate into a functional regulatory output which is likely to contribute to the explanation of the observed phenotypes. Notably, a cathepsin, *Ctsf*, exhibits a gene expression pattern which could implicate it in the cachectic response induced by accumulating tumor burden, as tumor-bearing Neu ERRα-/- mice exhibit significantly elevated levels of this gene as compared to Neu WT animals, but this pattern is not observed in mice before tumor onset. As cathepsins are major components of the lysosomal proteolytic system that is also implicated in the cachectic induction of skeletal muscle breakdown, this gene could contribute to a molecular explanation underlying skeletal muscle breakdown in our system if the preliminary metabolomics data is confirmed across a larger set of samples. Western blotting would be necessary to determine if this mRNA result translates into a functional tumor-induced response at the protein level. In contrast, the marker of the ubiquitin-proteasome pathway, *Fbxo32*, does not exhibit a genotype-related pattern of expression, decreasing the likelihood that this system of protein degradation is the major explanation for our phenotype. The expression of *Mstn*, known as myostatin and implicated in negatively regulating skeletal muscle growth, is induced in the Neu ERRα-/- mice only under the stress of tumor burden. While the limited sample size (n) kept this result from reaching statistical significance at the $p<0.05$ level, it is likely that this molecular pathway is also involved in the skeletal muscle phenotype in this system. Taken together, there is indication that the cathepsin-based lysosomal pathway and perhaps the myostatin pathway may be implicated in the Neu ERRα-/- skeletal muscle response to accumulating tumor burden.

We also screened the skeletal muscle at the protein level. While the proteins we probed for in the ubiquitin (total Ubiquitin) and autophagy

(Beclin-1, ATG5, ATG12) pathways showed no indication of genotype or tumor-related involvement, the energy sensor AMPK provided a surprising and interesting result (Fig. 4.5D). Total AMPKα levels were completely stable regardless of genotype or tumor status. In contrast, pAMPKα levels, while variable regardless of genotype in early muscle before tumor onset, were robustly depleted in the Neu ERRα-/- muscle from tumor-bearing mice at endpoint compared to levels in tumor-bearing Neu WT mice. Thus, accumulation of tumor burden induces a genotype-specific response in AMPKα activity in the skeletal muscle, implicating the deregulation of a major energy-sensing pathway in the tumor-induced phenotype. Taken together, while the total skeletal muscle mass of tumor-bearing Neu ERRα-/- mice does not exhibit observable differences in mass from Neu WT mice (Fig. 4.5B), the metabolomics data from the serum together with the modulated mRNA and protein markers in this context suggest the possibility of tumor-related involvement of the skeletal muscle.

We also screened the adipose tissue for the levels of molecular markers linked to cachexia-induced lipolysis (Fig. 4.5E). We identified several genes whose expression corresponds to ERRα status, in either a tumor-dependent or tumor-independent fashion. *Lep* and *Lpl*, both involved in the maintenance of adipose mass and function, are downregulated only in the adipose tissue of diseased Neu ERRα-/- mice, indicating that the effect of tumor burden on these genes may contribute to the molecular explanation for the observed adipose tissue loss with disease progression. In contrast, a separate set of genes, *Fabp4*, *Lepr*, and *Nrip1*, whose reduced expression in adipose tissue are markers of cachectic effects acting on this tissue, are downregulated in the ERRα-/- context regardless of whether or not the mice are burdened with tumors. This basal downregulation of adipose maintenance genes may predispose ERRα-/- adipose tissue to the effects of circulating inflammatory signals and could, thereby, contribute to the explanation for why ERRα-/- mice are more susceptible to the onset of cachexia.

We next turned to a different *in-vivo* system in order to study the effects of short-term inhibition of ERRα activity independently of the tumorigenic and resulting inflammatory context. To do this, we treated WT mice for 10 days with Compound 29, an ERRα inhibitor (Patch et al., 2011a). In this short period, neither total body weight, skeletal muscle content, nor adipose tissue content was affected by ERRα inhibition (Fig. 4.6A). However, at the molecular level, we observed important changes in the adipose tissue (Fig. 4.6B). *Fabp4*, the marker of adipose maintenance that was reduced in ERRα-/- mice regardless of tumor state in the Neu model, exhibited reduced expression in response to Compound 29, confirming that inhibition of ERRα via both genetic and pharmacological targeting and across short- and long-term time scales affects this gene's expression in a consistent fashion. Other markers of adipose function and maintenance including *Plin1*, *Cebpa*, and *CD36*, were also downregulated in response to Compound 29 treatment, providing more evidence that systemic inhibition of ERRα affects the adipose tissue. Most strikingly, *Gr*, encoding the glucocorticoid receptor (GR), is robustly upregulated in response to Compound 29. Considering that GR upregulation is an early event in the onset of cachexia (Tanaka et al., 1990) which induces adipose tissue loss (Russell and Tisdale, 2005), it is possible that early induction of *Gr* may be one manner in which the lipolysis gene expression programs are instigated at the start of the cachectic response in the adipose context. Finally, we confirmed that many of these genes are in fact direct targets of ERRα (Fig. 4.6C), as identified by ERRα binding near the transcriptional start site of each gene according to an ERRα ChIP-sequencing dataset available from our laboratory. This suggests a direct mechanism through which ERRα could impart its regulatory effect on these target genes.

When combined with molecular studies of cachexia markers in the skeletal muscle and adipose tissue of pre-onset and tumor-bearing mice, our data suggests that systemic ablation of ERRα may render the host

more susceptible to cancer cachexia, a disease characterized by heightened inflammation, metabolic derangements and tissue atrophy.

DISCUSSION

We have identified that systemic ERRα ablation delays tumor onset but accelerates disease progression after onset. Furthermore, disease progression corresponds with a concomitant inability to maintain normal total body weight. We identified underlying molecular explanations including elevated inflammation in the ERRα-/- tumors and dysregulation of skeletal muscle and adipose tissue maintenance markers. Taken together with the metabolomics data from the serum and skeletal muscle, the ERRα null mice display systemic signs of the onset of cachexia, thereby identifying a systemic role for ERRα in the host during cancer progression.

We have also verified that short-term inhibition of ERRα in non-tumor-bearing WT mice induces a gene expression response in the adipose tissue, bringing to the forefront the importance of ERRα levels in host tissues distant from the tumor site for the maintenance of those tissues and, ultimately, the ability to resist cachexia. As our tumor model also exhibits elevated inflammatory signalling stemming from the tumor site, it will be important to dissect whether the predisposition for developing cachexia comes from the elevated levels of inflammation present in the ERRα-/- tumors, or from the absence of ERRα in other tissues affected by cachexia such as the skeletal muscle and adipose contexts. One interesting experiment which could contribute elegantly to this discussion would be to inject equal quantities of cachexia-inducing cancer cells into WT and ERRα-/- mice and observe if the host genotype causes differential development and progression of the cachectic state. The Lewis Lung Carcinoma model of cachexia could be a good model for this type of experiment.

In fact, this type of animal model, which is based on implanted tumor cells, comprises the majority of animal models used to study this complex disease *in-vivo* (Deboer, 2009). As cachexia is by definition a systemic disease, it is paramount that it be studied *in-vivo*, yet relevant

mouse models remain limited. Our ERRα-/- model is fundamentally different from the implanted tumor cell models, in that it is a genetics-based system that develops cachexia when crossed into a genetically-driven cancer context. This allows for a slower and milder onset of cachexia which could most likely be titrated by the choice of cancer model, allows for the study of early-onset markers and changes, and avoids the sudden insult of foreign material injection, perhaps more naturally mimicking the type of slow, long-term insult a cancer patient experiences who will exhibit the onset of cachexia. As such, this new genre of model may prove to be a powerful tool to expand our resources for studying cancer cachexia.

As ERRα is considered a marker of poor prognosis in breast cancer, and the idea of ERRα inhibitors as therapeutics is becoming a hot topic, this study adds important insights relevant for proper predictions about targeting ERRα in ERBB2-positive breast cancer. As our study has uncovered a major undesired consequence of long-term inhibition of ERRα, temporal treatment conditions will be very important when considering ERRα inhibitors for systemic therapeutic application.

MATERIALS AND METHODS

Ethics statement

Animal use followed the guidelines of the Canadian Council on Animal Care. The animal use protocol was approved by the local Facility Animal Care Committee (FACC) at McGill University.

Animals

All mice were housed and fed standard chow in the animal facility at the McGill University Rosalind and Morris Goodman Cancer Research Centre. Mouse strains used in this study have been previously described: female wild-type and ERRα-null mice (Luo et al., 2003b) carrying the MMTV-NeuNDL2-5 (Guy et al., 1992) oncogene in an FVB genetic background. Animals were sacrificed by cervical dislocation during the day at ZT (Zeitgeber time) 4. At necropsy, mammary glands, mammary tumours, hindlimb skeletal muscle and epididymal or inguinal adipose tissue were frozen in liquid nitrogen, ground using a mortar and pestle and kept frozen until further processing. Tissue weights, when measured, were taken immediately after dissection and before further tissue processing or storage. Blood was let to clot for >30min at room temperature, spun for 30min at 5,000rpm at room temperature, and the serum (top) layer selected before being frozen at -80^{o}C.

Animals carrying the MMTV-NeuNDL2-5 (NeuNDL2-5 OR Neu) transgene were monitored for tumor onset by bi-weekly physical palpation, at which time they were also weighed, and necropsied at endpoint (determined and approved by the FACC as 2.5 cm^3 for an individual tumor or 6 cm^3 total tumor burden for one mouse). Tumor volume measurements were taken weekly. Endpoint data was generated from material from mice sacrificed within one week of the ideal endpoint, defined as 70days after tumor onset.

For Compound 29, the drug was diluted directly into the injection buffer (5.2% PEG400 and 5.2% Tween 80 Ringer's saline solution) for a

final concentration of 10 mg/kg. Adult male C57BL/6J mice were administered daily intraperitioneal injections of 10mg/kg compound 29 or the drug vehicle for 10 days. Mice were then sacrified as described above and tissues were collected.

Regression Analysis of Weight Data

The values of the slopes and the corresponding statistical analysis were obtained by performing OLS (ordinary least squares) regression analysis using Stata software. For before tumor onset analysis, Weight was set as the dependent variable, and Age and a Constant Term were the independent variables. A separate regression for each genotype was performed. For after tumor onset analysis, Non-Tumor Body Weight was set as the dependent variable, and Days After Onset, Genotype, Genotype interacted with Days after Onset, and a Constant Term were the independent variables. Tumor burden weight was subtracted from the total body weight of each animal at each timepoint to obtain the Non-Tumor Body Weight used in the regressions. To compute tumor burden weight, measured tumor volume was multiplied by tumor density. To compute tumor density, 5 tumors from different mice at endpoint were weighed and their volume measured, and the corresponding average density calculated (0.90).

RNA Isolation, Reverse Transcription and quantitative Real-Time PCR

Tumor RNA was isolated using the RNeasy Mini Kit (Qiagen), Skeletal muscle RNA was isolated with the RNeasy Fibrous Tissue Mini Kit (Qiagen), and Adipose RNA was isolated with the RNeasy Lipid Tissue Mini Kit (Qiagen). DNase treatment was always performed during RNA isolation. cDNA was made from either 1 or 2 µg of total RNA by reverse transcription with Oligo(dT) primer, dNTPs, 5X 1st strand buffer, DTT, RNase inhibitor, and Superscript II RNase H Reverse Transcriptase

(Invitrogen). cDNA was amplified by qRT-PCR using specific primers (Appendix Table A.4.1) qRT-PCR was carried out in a LightCycler 480 instrument using the QuantiTect SYBR Green PCR Kit (Qiagen) following the Qiagen software protocol. All primers were designed using Oligo 6.8 Primer Analysis Software with sequence data from the http://genome.ucsc.edu database mouse July 2007 or December 2011 assemblies. Primers to detect cDNA were designed so that either the product included at least one intron and/or one primer was located on both an exon and an intron in order to avoid recognition of genomic DNA. Primer sets were tested on cDNA dilutions to determine primer efficiency. qRT-PCR reactions were performed in duplicate, and the Ct values were averaged before normalization.

Microarray

Microarray analysis of was performed on four tumors of each genotype. RNA was extracted as described above, and RNA quality control was determined by Bioanalyzer. Microarray sample preparation and chip hybridization was performed by the Génome Québec Innovation Centre at McGill University using 5 µg of total RNA per sample and a mouse 60k Agilent expression array chip. FlexArray software (http://genomequebec.mcgill.ca/FlexArray/) was used to analyze resulting data. A p-value threshold of 0.05 and a relative fold change cutoff of ±1.5 were used The Ingenuity Pathway systems Analysis program was used for analysis of pathways, gene functions and transcription factor binding sites in modulated genes.

Western Blots

Briefly, protein was harvested with modified RIPA buffer containing protease and phosphatase inhibitors and quantified using MicroBCA or Bradford methods, and then resolved on an SDS-PAGE gel (40 µg protein per well tumor extracts, 60 µg per well for muscle extracts). Protein was

then transferred onto a membrane, blocked for one hour, and then incubated with primary antibody overnight. After three washes, membranes were incubated with secondary antibody for one hour at a dilution of 1:5000. After three more washes, proteins were detected using chemiluminescence. The loading control protein was either detected on the same membrane simultaneously with the target proteins if size differences allowed, or the membranes were stripped and re-probed to detect the loading control. See Chapter 2 for more Western blotting protocol details. The following antibodies and conditions were used:
pStat1 (Cell Signaling cs-9171s, 1:200), Stat1 (Upstate 06-501, 1:1000), pStat2 (Abcam ab53132, 1:200), Stat2 (ProteinTech 16674-1-AP, 1:200), pStat3 (Cell Signaling cs-9134s+cs-9131s, 1:400+1:400), Stat3 (Cell Signaling cs-9132s, 1:400), ERRα (Epitomics 2131-1, 1:5000), Actin (SantaCruz sc-1616-R, 1:200), LC3A, Beclin-1, ATG5, ATG12 (Cell Signaling Autophagy Antibody Sampler Kit, 4445), Ubiquitin (Cell Siganling cs-3933s, 1:1000), AMPKα (Cell Signaling cs-2532L, lot 19, 1:1000), P-APMPKα (Cell Signaling, cs-2535s, lot 14, 1:1000)

Metabolomics

Targeted quantitative metabolite profiling was accomplished using NMR. Tissue extractions were prepared according to a modified Folch extraction (Wu et al., 2008). Crushed tissues were weighed precisely, and 36-101 mg per tumor sample or ~70 mg (63-92 mg) per skeletal muscle sample were used. Samples were kept on ice at all times during the extractions. 4 ml/g tissue cold methanol was added to each sample. Then 0.85 ml/g cold water was added. Samples were homogenized for 2 min at 20Hz using a TissueLyser (Qiagen) in combination with the corresponding steel beads. 4 mg/g cold $CHCl_3$ was added, then 2 ml/g cold water. Samples were vortexed for 60sec, then set on ice for 10min. After centrifugation at 2000 g for 15 min at 4°C, the polar (top) layer was carefully selected and frozen at -80°C until further processing.

The aqueous layer was dried in a pre-cooled vacuum centrifuge (Labconco Corp. Kansas City, MO, USA) operating at -4 ^{o}C. The dried samples were stored at -80 ^{o}C until the day of NMR data collection. Extracted tissue samples were re-suspended in 220 ml water containing 10% deuterated water, 0.01 mM sodium azide, 0.2mM DSS (4,4-dimethyl-4-silapentane-1-sulfonic acid), the chemical shift and concentration standard and, 0.1mM DFTMP (difluorotrimethylsilanylphosphonic acid) an internal pH standard (Reily et al., 2006). The pH of each sample was manually adjusted to pH of 6.8 +/- 0.1.

Serum samples were ultra-filtered for >2 hrs at 4000 g at 4°C using pre-washed Nanosep 3 kd molecular weight cut-off spin filters (Pall Corporation, Ann Arbor Michigan, USA). Filters were prepared beforehand by washing in MilliQ water for several hours (water was exchanged regularly). Water was then centrifuged through the filters twice at 8000 g for 15 min. Excess water was removed with a clean Kimwipe before serum was filtered. A volume of 30-70 ml serum was recovered and diluted to 120 ml water containing 10% deuterium oxide, 0.2 mM DSS, 0.1 mM DFTMP and 0.01mM sodium azide. Samples were transferred to 3 mm susceptibility matched Shigemi tubes (Shigemi Inc, Allison Park, PA, USA) for NMR data acquisition.

NMR data were acquired on a 500MHz Inova NMR system (Agilent Technologies, Palo Alto, CA, USA) equipped with a HCN cryogenically cooled probe operating at 25 K. One-dimensional NMR spectra of samples were collected using the first increment of the standard NOESY experiment supplied with the instrument. All spectra were recorded at 25^{o}C with a mixing time of 100 ms, 256 transients with 8 equilibration pre-scans, a spectral window of 12 ppm centered on the residual water which was suppressed by a low power pre-saturation pulse during both the mixing time and 2 sec relaxation delay. The acquisition time was 3 sec for a total scan recycle time of 5 sec. The same pre-saturation and gain were used for all data acquisitions while 90^{o} pulses were calibrated for each

sample. Metabolite identification and chemical shift assignments were confirmed by two-dimensional 75 ms mixing time total correlation spectra (Z-filtered dipsi-Tocsy) and through the use of the Human Metabolome Database and Madison Metabolomics Consortium database (Cui et al., 2008; Wishart et al., 2009).

NMR data were Fourier transformed after zero-filling to 128k data points and exponential weighting of 0.333 Hz. Fifty-five serum metabolites, fifty-seven muscle tissue metabolites and Sixty-five mammary tissue metabolites were quantitatively profiled using Chenomx NMR Suite 7.0 and the 500MHz library (Chenomx, Inc, Edmonton, AB, Canada). The amount of each metabolite was then normalized to the weight of the extracted tissue. Serum metabolite concentrations were corrected by the sample's dilution factor.

ChIP-Sequencing Dataset

See Appendix II:

Chaveroux et al. Molecular Crosstalk Between mTOR and ERRα is a Key Determinant of Rapamycin-induced Non-Alcoholic Fatty Liver.

ACKNOWLEDGEMENTS

We thank William Muller for the MMTV-Neu-NDL2-5 mouse model, and his lab members Babette Schade, Harvey Smith and Cynthia Lavoie for guidance on how to properly use and study this model. NMR experiments were recorded at the Québec/Eastern Canada High Field NMR Facility, supported by the Natural Sciences and Engineering Research Council of Canada, the Canada Foundation for Innovation (CFI), the Québec ministère de la recherche en science et technologie and McGill University. Measurements of metabolites were conducted by Dr. Daina Avizonis at the Metabolomics core facility of the GCRC which is funded by the CFI. We acknowledge Carlo Ouellet for mouse husbandry, and we thank M. Ghahremani for technical assistance.

REFERENCES

Argiles, J.M., Garcia-Martinez, C., Llovera, M., and Lopez-Soriano, F.J. (1992). The role of cytokines in muscle wasting: its relation with cancer cachexia. Med Res Rev *12*, 637-652.

Bing, C. (2011). Lipid mobilization in cachexia: mechanisms and mediators. Curr Opin Support Palliat Care *5*, 356-360.

Cui, Q., Lewis, I.A., Hegeman, A.D., Anderson, M.E., Li, J., Schulte, C.F., Westler, W.M., Eghbalnia, H.R., Sussman, M.R., and Markley, J.L. (2008). Metabolite identification via the Madison Metabolomics Consortium Database. Nat Biotechnol *26*, 162-164.

Deblois, G., Chahrour, G., Perry, M.C., Sylvain-Drolet, G., Muller, W.J., and Giguere, V. (2010). Transcriptional control of the ERBB2 amplicon by ERRalpha and PGC-1beta promotes mammary gland tumorigenesis. Cancer research *70*, 10277-10287.

Deblois, G., and Giguere, V. (2011). Functional and physiological genomics of estrogen-related receptors (ERRs) in health and disease. Biochimica et biophysica acta *1812*, 1032-1040.

Deboer, M.D. (2009). Animal models of anorexia and cachexia. Expert Opin Drug Discov *4*, 1145-1155.

Eichner, L.J., and Giguere, V. (2011). Estrogen related receptors (ERRs): a new dawn in transcriptional control of mitochondrial gene networks. Mitochondrion *11*, 544-552.

Guy, C.T., Webster, M.A., Schaller, M., Parsons, T.J., Cardiff, R.D., and Muller, W.J. (1992). Expression of the neu protooncogene in the mammary epithelium of transgenic mice induces metastatic disease. Proceedings of the National Academy of Sciences of the United States of America *89*, 10578-10582.

Fujimoto, J., Alam, S.M., Jahan, I., Sato, E., Sakaguchi, H., and Tamaya, T. (2007). Clinical implication of estrogen-related receptor (ERR) expression in ovarian cancers. The Journal of steroid biochemistry and molecular biology *104*, 301-304.

Fujimoto, J., and Sato, E. (2009). Clinical implication of estrogen-related receptor (ERR) expression in uterine endometrial cancers. The Journal of steroid biochemistry and molecular biology *116*, 71-75.

Fujimura, T., Takahashi, S., Urano, T., Ijichi, N., Ikeda, K., Kumagai, J., Murata, T., Takayama, K., Horie-Inoue, K., Ouchi, Y.*, et al.* (2010).

Differential expression of estrogen-related receptors beta and gamma (ERRbeta and ERRgamma) and their clinical significance in human prostate cancer. Cancer Sci *101*, 646-651.

Fujimura, T., Takahashi, S., Urano, T., Kumagai, J., Ogushi, T., Horie-Inoue, K., Ouchi, Y., Kitamura, T., Muramatsu, M., and Inoue, S. (2007). Increased expression of estrogen-related receptor alpha (ERRalpha) is a negative prognostic predictor in human prostate cancer. International journal of cancer Journal international du cancer *120*, 2325-2330.

Gao, M., Sun, P., Wang, J., Zhao, D., and Wei, L. (2006). Expression of estrogen receptor-related receptor isoforms and clinical significance in endometrial adenocarcinoma. Int J Gynecol Cancer *16*, 827-833.

Giguere, V. (2008). Transcriptional control of energy homeostasis by the estrogen-related receptors. Endocr Rev *29*, 677-696.

Grivennikov, S.I., Greten, F.R., and Karin, M. (2010). Immunity, inflammation, and cancer. Cell *140*, 883-899.

Luo, J., Sladek, R., Carrier, J., Bader, J.A., Richard, D., and Giguere, V. (2003). Reduced fat mass in mice lacking orphan nuclear receptor estrogen-related receptor alpha. Mol Cell Biol *23*, 7947-7956.

Mori, T., Sawada, M., Kuroboshi, H., Tatsumi, H., Katsuyama, M., Iwasaku, K., and Kitawaki, J. (2011). Estrogen-related receptor alpha expression and function are associated with vascular endothelial growth factor in human cervical cancer. Int J Gynecol Cancer *21*, 609-615.

Pajak, B., Orzechowska, S., Pijet, B., Pijet, M., Pogorzelska, A., Gajkowska, B., and Orzechowski, A. (2008). Crossroads of cytokine signaling--the chase to stop muscle cachexia. J Physiol Pharmacol *59 Suppl 9*, 251-264.

Patch, R.J., Searle, L.L., Kim, A.J., De, D., Zhu, X., Askari, H.B., O'Neill, J.C., Abad, M.C., Rentzeperis, D., Liu, J.*, et al.* (2011). Identification of Diaryl Ether-Based Ligands for Estrogen-Related Receptor alpha as Potential Antidiabetic Agents. J Med Chem *54*, 788-808.

Permuth-Wey, J., Chen, Y.A., Tsai, Y.Y., Chen, Z., Qu, X., Lancaster, J.M., Stockwell, H., Dagne, G., Iversen, E., Risch, H.*, et al.* (2011). Inherited variants in mitochondrial biogenesis genes may influence epithelial ovarian cancer risk. Cancer Epidemiol Biomarkers Prev *20*, 1131-1145.

Reily, M.D., Robosky, L.C., Manning, M.L., Butler, A., Baker, J.D., and Winters, R.T. (2006). DFTMP, an NMR reagent for assessing the near-neutral pH of biological samples. J Am Chem Soc *128*, 12360-12361.

Russell, S.T., and Tisdale, M.J. (2005). The role of glucocorticoids in the induction of zinc-alpha2-glycoprotein expression in adipose tissue in cancer cachexia. Br J Cancer *92*, 876-881.

Salzman, J., Marinelli, R.J., Wang, P.L., Green, A.E., Nielsen, J.S., Nelson, B.H., Drescher, C.W., and Brown, P.O. (2011). ESRRA-C11orf20 is a recurrent gene fusion in serous ovarian carcinoma. PLoS biology *9*, e1001156.

Sorlie, T., Tibshirani, R., Parker, J., Hastie, T., Marron, J.S., Nobel, A., Deng, S., Johnsen, H., Pesich, R., Geisler, S*., et al.* (2003). Repeated observation of breast tumor subtypes in independent gene expression data sets. Proceedings of the National Academy of Sciences of the United States of America *100*, 8418-8423.

Sun, P., Sehouli, J., Denkert, C., Mustea, A., Konsgen, D., Koch, I., Wei, L., and Lichtenegger, W. (2005). Expression of estrogen receptor-related receptors, a subfamily of orphan nuclear receptors, as new tumor biomarkers in ovarian cancer cells. J Mol Med (Berl) *83*, 457-467.

Tanaka, Y., Eda, H., Tanaka, T., Udagawa, T., Ishikawa, T., Horii, I., Ishitsuka, H., Kataoka, T., and Taguchi, T. (1990). Experimental cancer cachexia induced by transplantable colon 26 adenocarcinoma in mice. Cancer research *50*, 2290-2295.

Tisdale, M.J. (2002). Cachexia in cancer patients. Nat Rev Cancer *2*, 862-871.

Ursini-Siegel, J., Schade, B., Cardiff, R.D., and Muller, W.J. (2007). Insights from transgenic mouse models of ERBB2-induced breast cancer. Nat Rev Cancer *7*, 389-397.

Wang, J., Wang, Y., and Wong, C. (2010). Oestrogen-related receptor alpha inverse agonist XCT-790 arrests A549 lung cancer cell population growth by inducing mitochondrial reactive oxygen species production. Cell Prolif *43*, 103-113.

Watanabe, A., Kinoshita, Y., Hosokawa, K., Mori, T., Yamaguchi, T., and Honjo, H. (2006). Function of estrogen-related receptor alpha in human endometrial cancer. J Clin Endocrinol Metab *91*, 1573-1577.
Wise, D.R., and Thompson, C.B. (2010). Glutamine addiction: a new therapeutic target in cancer. Trends Biochem Sci *35*, 427-433.

Wishart, D.S., Knox, C., Guo, A.C., Eisner, R., Young, N., Gautam, B., Hau, D.D., Psychogios, N., Dong, E., Bouatra, S.*, et al.* (2009). HMDB: a knowledgebase for the human metabolome. Nucleic acids research *37*, D603-610.

Wu, H., Southam, A.D., Hines, A., and Viant, M.R. (2008). High-throughput tissue extraction protocol for NMR- and MS-based metabolomics. Anal Biochem *372*, 204-212.

Wu, Y., and Zhou, B.P. (2009). Inflammation: a driving force speeds cancer metastasis. Cell Cycle *8*, 3267-3273.

Yu, S., Wong, Y.C., Wang, X.H., Ling, M.T., Ng, C.F., Chen, S., and Chan, F.L. (2008). Orphan nuclear receptor estrogen-related receptor-beta suppresses in vitro and in vivo growth of prostate cancer cells via p21(WAF1/CIP1) induction and as a potential therapeutic target in prostate cancer. Oncogene *27*, 3313-3328.

TABLES AND FIGURES

Figure 4.1. Neu ERRα-/- mice exhibit delayed tumor onset but accelerated disease progression after onset.

(**A**) Neu ERRα-/- mice exhibit delayed tumor onset. Percentage of tumor-free mice over time for the indicated genotypes. (**B**) Neu ERRα-/- mice display accelerated accumulation of tumor burden after tumor onset. Total tumor volume (in cm^3) per mouse over time, from tumor onset until 13 weeks after onset, for the indicated genotypes. (**C**) Neu ERRα-/- mice exhibit increased tumor focality after tumor onset. Number of tumors per mouse over time, from tumor onset until 12.5 weeks after onset, for the indicated genotypes. Statistical significance was determined by Log-rank Mantel-Cox test and Gehan-Breslow-Wilcoxon test in **A** and by applying linear regressions in **B** and **C** using GraphPad Prism software.

Figure 4.1

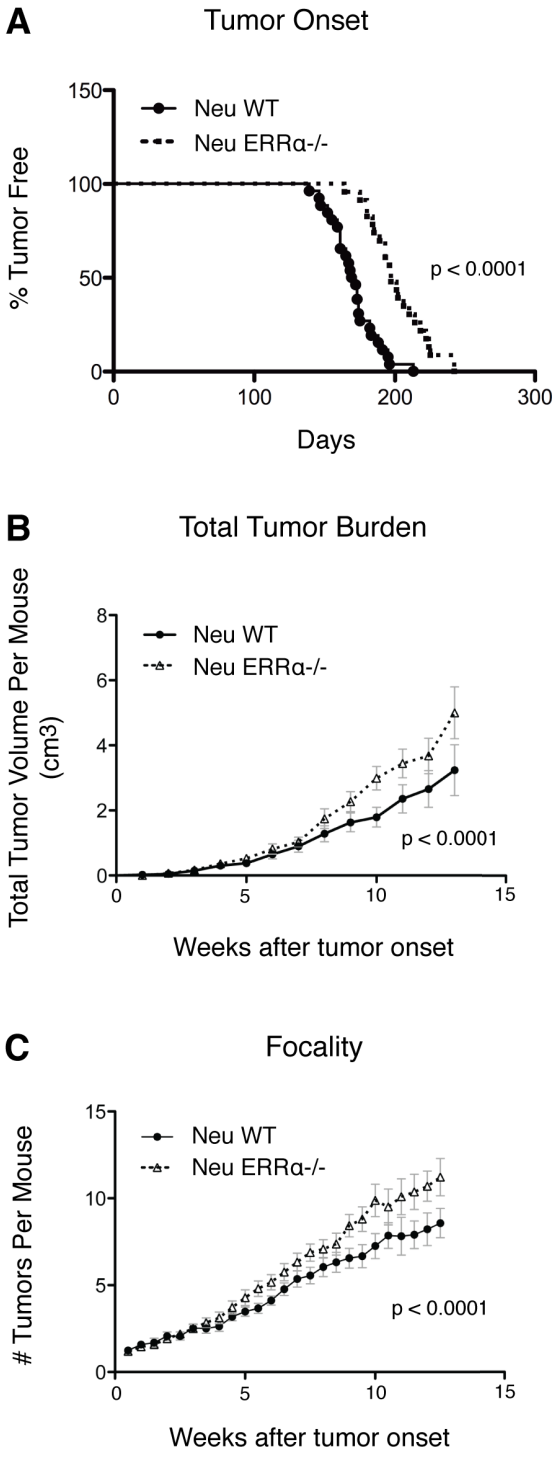
A
Tumor Onset
% Tumor Free
150
100
50
0
Neu WT
Neu ERRα-/-
p < 0.0001
0
100
200
300
Days
B
Total Tumor Burden
Total Tumor Volume Per Mouse (cm3)
8
6
4
2
0
Neu WT
Neu ERRα-/-
p < 0.0001
0
5
10
15
Weeks after tumor onset
C
Focality
Tumors Per Mouse
15
10
5
0
Neu WT
Neu ERRα-/-
p < 0.0001
0
5
10
15
Weeks after tumor onset

Figure 4.2. Absence of ERRα negates weight gain observed in WT animals after tumor onset, suggesting that inhibition of ERRα activity may predispose to a cachectic state.

(**A**) Total body weight of Neu WT (red circles) and Neu ERRα-/- (blue circles) mice is stable before tumor onset. Fitted regression lines represent the average change of total body weight with age for each group of mice. Red line represents Neu WT data, blue line Neu ERRα-/- data. Slopes of these lines are shown on table at right. The statistical significance of the difference between the two slopes is indicated. N.S. indicates Not Significant. (**B**) Non-tumor body weight of Neu ERRα-/- mice (green circles) fails to maintain trend of Neu WT mice non-tumor body weight (orange circles) after tumor onset. Fitted regression lines represent the average change of non-tumor body weight with time after tumor onset for each group of mice. Orange line represents Neu WT data, green line Neu ERRα-/- data. Slopes of these lines are shown on table at right. The statistical significance of the difference between the two slopes, as determined by regression analysis done with Stata software, is indicated. Non-tumor body weight was calculated by subtracting the weight of the tumors from the total body weight at each measurement.

Figure 4.2

A Total Body Weight Before Tumor Onset

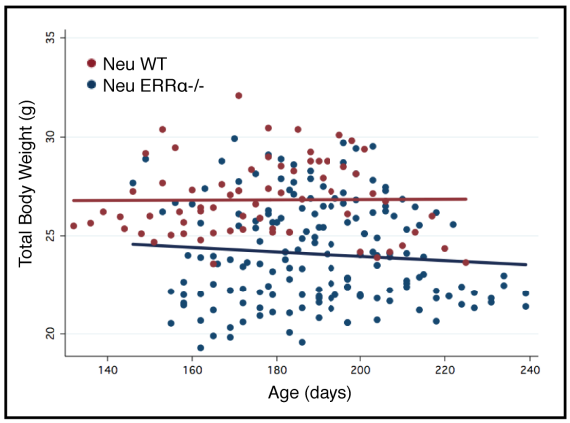

Before Tumor Onset			
	Neu WT	Neu ERRα-/-	Difference Between Slopes
Slope	0.001	-0.011	N.S.

B Non-Tumor Body Weight After Tumor Onset

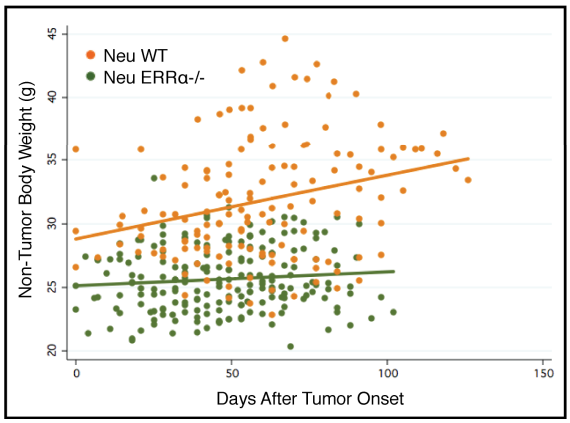

After Tumor Onset			
	Neu WT	Neu ERRα-/-	Difference Between Slopes
Slope	0.050	0.011	p-value < 0.014

Figure 4.3. Neu ERRα-/- tumors exhibit heightened levels of inflammatory signaling.

(**A**) Gene expression profiling of tumors similar in size obtained from Neu ERRα-/- versus Neu WT mice 70days after tumor onset identifies differentially-regulated genes. >1.5 fold expression change and p-value <0.05 cut-off parameters were applied. (**B**) Analysis of microarray data by gene function reveals an upregulation of genes involved in immune response in Neu ERRα-/- tumors. The three most significantly modulated (TOP 3) gene function categories identified by Ingenuity Pathway Analysis (IPA) software are shown. Red indicates genes upregulated in the Neu ERRα-/- tumors, green indicates genes downregulated in the Neu ERRα-/- tumors. Significance is shown as –log(p-value), where the greater the value, the more significant the p-value. (**C**) IPA Transcription Factor binding site Analysis of the genes modulated in the microarray predicts the activation of inflammatory transcription factors in the Neu ERRα-/- tumors. Transcription factor is identified as Factor. Z-score indicates the strength of the IPA prediction, while Prediction indicates if the transcription factor is predicted to be Activated or Inhibited based on the direction of modulation of its target genes in the microarray data. Red boxes indicate genes whose expression is upregulated in the microarray, and green boxes identify genes downregulated. (**D**) Many genes of the interferon signaling pathway are upregulated in Neu ERRα-/- tumors. Genes upregulated in the microarray are shaded red. (**E**) Stat1 and Stat2 activity is elevated in Neu ERRα-/- tumors. Protein levels of Stat1, Stat2, Stat3 and their corresponding phosphorylated forms, as well as total ERRα levels, in Neu WT and Neu ERRα-/- tumors as measured by Western blotting. Actin serves as a loading control. (**F**) Validation by qRT-PCR of the microarray data is shown for several modulated genes.

Figure 4.3

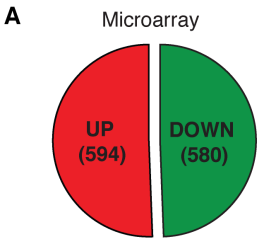

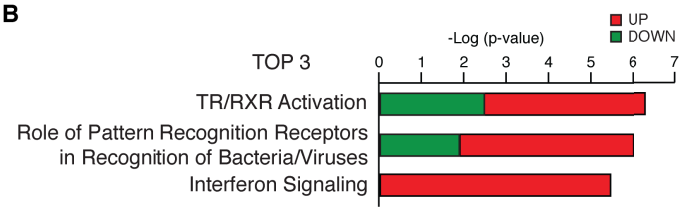

C

Factor	Z-score	Prediction
IRF7	4.884	Activated
IRF1	4.402	Activated
STAT1	4.104	Activated
SREBF1	4.100	Activated
SREBF2	4.039	Activated
IRF3	3.933	Activated
E2F1	3.916	Activated
TBX2	3.799	Activated
ATF4	3.406	Activated
E2F3	2.809	Activated
JUN	2.751	Activated
HIF1A	2.746	Activated
STAT2	2.668	Activated
SIRT2	2.629	Activated
E2f	2.625	Activated
ESR2	2.575	Activated
GLI1	2.520	Activated
MYC	2.514	Activated

Factor	Z-score	Prediction
TRIM24	-5.407	Inhibited
CDKN2A	-4.077	Inhibited
TP53	-2.986	Inhibited
RB1	-2.913	Inhibited
TCF3	-2.784	Inhibited
CLOCK	-2.758	Inhibited

D

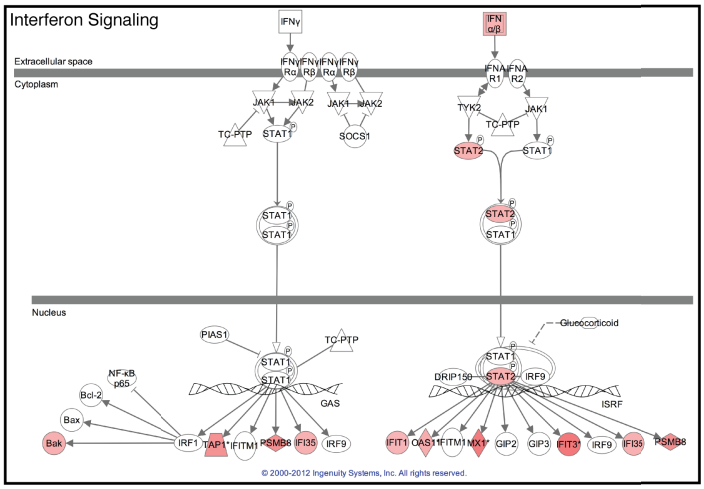

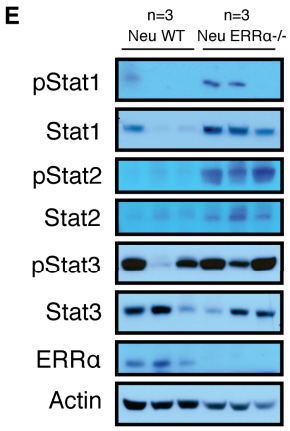

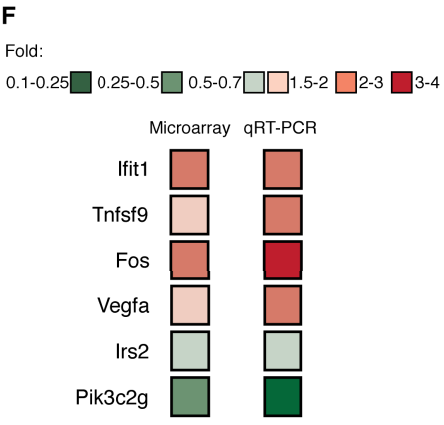

Figure 4.4. Metabolomics of mammary tumors, serum and skeletal muscle provides systemic indicators of an elevated cancer cachectic state in Neu ERRα-/- mice.

(**A**) Diagram from Tisdale M, *Nature Reviews*, 2002 outlining the interplay between different tissues in cancer cachexia. The tumor produces factors secreted into the blood stream, which induce the breakdown of adipose tissue into fatty acids and the protein degradation of skeletal muscle into amino acids, such as lipid-mobilizing factor (LMF), proteolysis-inducing factor (PIF) and inflammatory cytokines including TNF-α. The liver uses these gluconeogenic substrates for acute-phase protein synthesis (APP). (**B**) Metabolites identified by NMR-based metabolomics to exhibit significantly different levels in small tumors from Neu ERRα-/- mice than Neu WT mice. Results are expressed as fold from values obtained from Neu ERRα-/- tumors normalized to values obtained from Neu WT tumors. n=4. (**C**) Many amino acids exhibit a tendency toward upregulation in the serum of Neu ERRα-/- tumor-bearing mice. Serum amino acid levels identified by metabolomics are expressed as fold from values obtained from Neu ERRα-/- mice normalized to values obtained from Neu WT mice. White bars indicate measurements from tumor-free mice, black bars represent data from tumor-bearing mice. n=4. (**D**) Many amino acids exhibit a tendency toward downregulation in the skeletal muscle of tumor-bearing Neu ERRα-/- mice. Amino acid levels identified by metabolomics are expressed as fold from values obtained from Neu ERRα-/- mice normalized to values from Neu WT mice. n=5. Unpaired student's *t* test was used for evaluation of statistical significance. *P< 0.05, **P< 0.01.

Figure 4.4

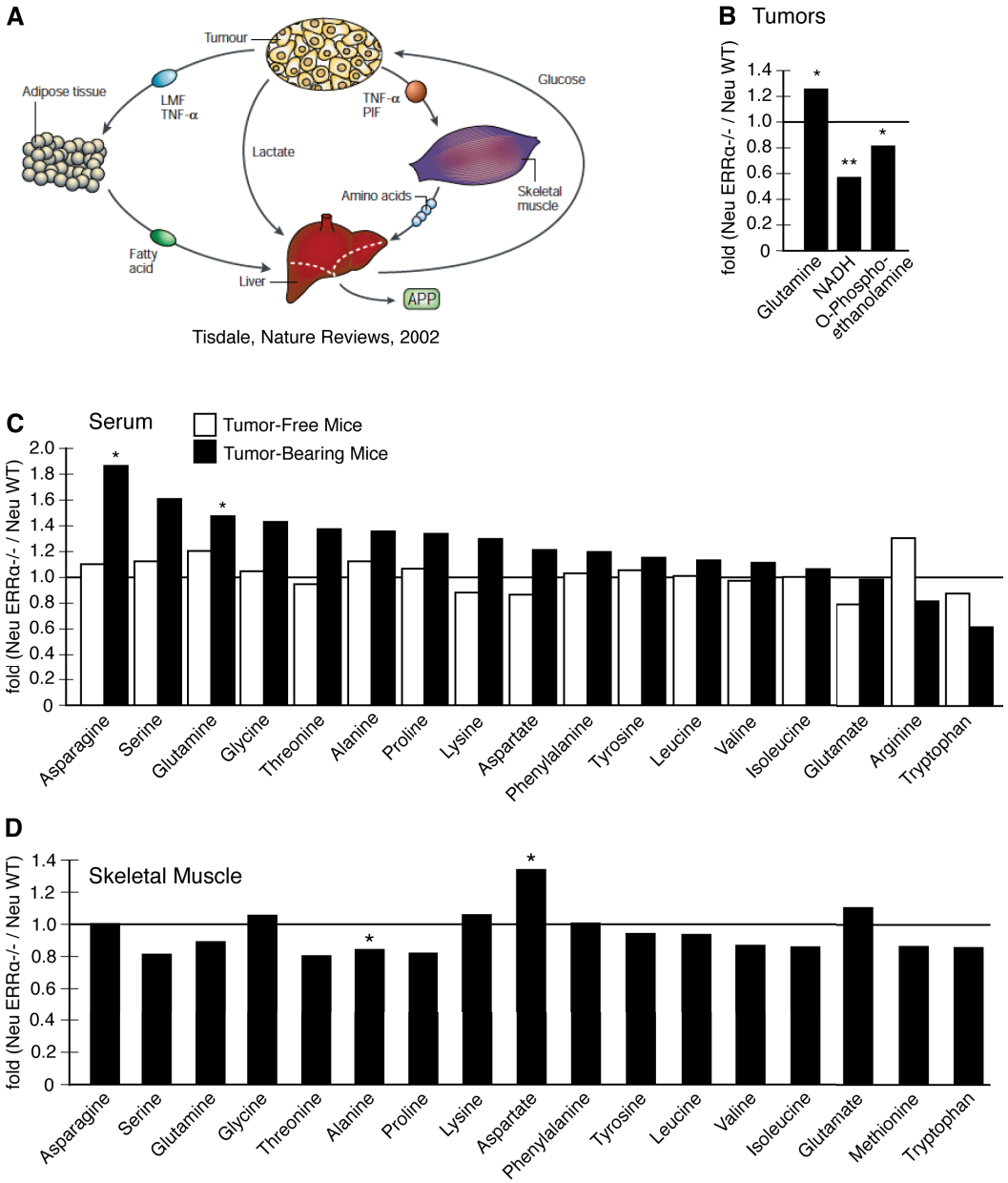
A
Tumour
Adipose tissue
LMF
TNF-α
TNF-α
PIF
Glucose
Lactate
Amino acids
Skeletal muscle
Fatty acid
Liver
APP
Tisdale, Nature Reviews, 2002
B Tumors
fold (Neu ERRα-/- / Neu WT)
Glutamine
NADH
O-Phospho-ethanolamine
C
Serum
Tumor-Free Mice
Tumor-Bearing Mice
fold (Neu ERRα-/- / Neu WT)
Asparagine
Serine
Glutamine
Glycine
Threonine
Alanine
Proline
Lysine
Aspartate
Phenylalanine
Tyrosine
Leucine
Valine
Isoleucine
Glutamate
Arginine
Tryptophan
D
Skeletal Muscle
fold (Neu ERRα-/- / Neu WT)
Asparagine
Serine
Glutamine
Glycine
Threonine
Alanine
Proline
Lysine
Aspartate
Phenylalanine
Tyrosine
Leucine
Valine
Isoleucine
Glutamate
Methionine
Tryptophan

Figure 4.5. Skeletal muscle and adipose tissue analysis reveals phenotypic and molecular indicators of cachexia in the tumor-bearing Neu ERRα-/- mice.

(**A**) Gross differences in adipose tissue quantity are seen by eye between tumor-bearing Neu ERRα-/- and Neu WT mice at endpoint. Hind limb skeletal muscle is also visible. (**B**) Quantification of hind limb skeletal muscle and inguinal adipose tissue weight. Tissue weights are normalized the total body weight of the mouse two weeks after tumor onset. (**C**) Skeletal muscle gene expression markers of cachexia are differentially expressed between Neu ERRα-/- and Neu WT mice, as determined by qRT-PCR. Black and grey bars represent Neu WT and Neu ERRα-/- mice before tumor onset, respectively. Purple and pink bars; tumor-bearing Neu WT and Neu ERRα-/- mice at disease endpoint, respectively. Gene levels in Neu WT mice before tumor onset are set to 1. Arbp was used as an internal control. (**D**) Protein levels of key energy homeostasis and autophagy proteins in skeletal muscle before tumor onset and at disease endpoint were measured by Western blotting. Actin was used as an internal control. (**E**) Adipose tissue gene expression markers of cachexia are differentially expressed between Neu ERRα-/- and Neu WT mice. Experiment was conducted as in (C). Unpaired student's *t* test was used for evaluation of statistical significance. *P< 0.05, **P< 0.01, ***P<0.001.

Figure 4.5

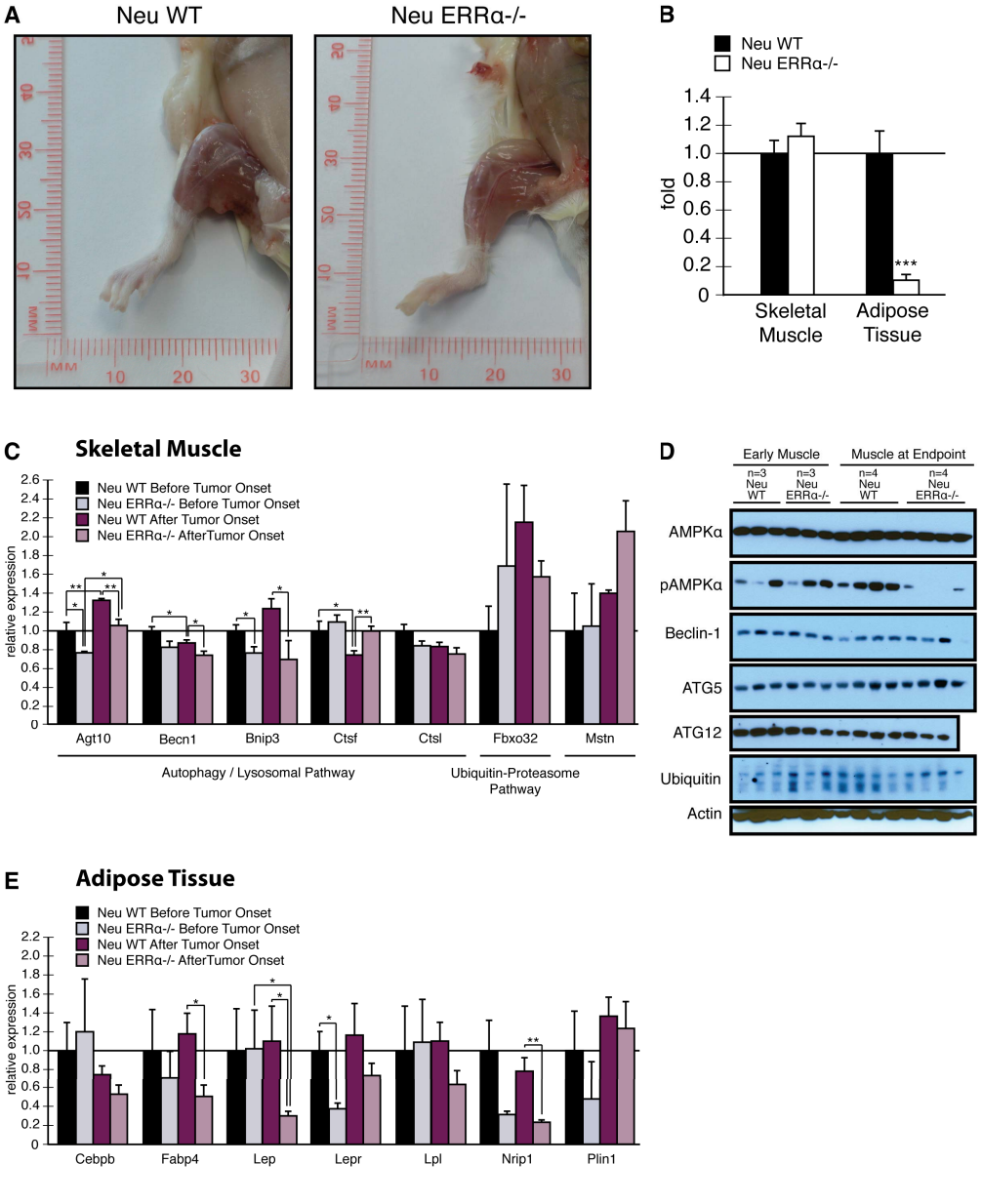
A
Neu WT
Neu ERRα-/-
B
Neu WT
Neu ERRα-/-
fold
1.4
1.2
1.0
0.8
0.6
0.4
0.2
0
***
Skeletal Muscle
Adipose Tissue
C
Skeletal Muscle
Neu WT Before Tumor Onset
Neu ERRα-/- Before Tumor Onset
Neu WT After Tumor Onset
Neu ERRα-/- AfterTumor Onset
relative expression
Agt10
Becn1
Bnip3
Ctsf
Ctsl
Fbxo32
Mstn
Autophagy / Lysosomal Pathway
Ubiquitin-Proteasome Pathway
D
Early Muscle
Muscle at Endpoint
n=3 Neu WT
n=3 Neu ERRα-/-
n=4 Neu WT
n=4 Neu ERRα-/-
AMPKα
pAMPKα
Beclin-1
ATG5
ATG12
Ubiquitin
Actin
E
Adipose Tissue
Neu WT Before Tumor Onset
Neu ERRα-/- Before Tumor Onset
Neu WT After Tumor Onset
Neu ERRα-/- AfterTumor Onset
relative expression
Cebpb
Fabp4
Lep
Lepr
Lpl
Nrip1
Plin1

Figure 4.6. Mice depleted for ERRα activity with Compound 29 exhibit molecular dysregulation of adipose tissue.

(**A**) Total body weight, hindlimb skeletal muscle, and inguinal adipose tissue quantity are not affected by treatment with Compound 29. Tissue weights are normalized to the total body weight of each mouse. Black bars represent control treated mice, white bars represent mice treated with Compound 29. (**B**) Adipose gene expression markers of tissue maintenance are differentially expressed between Control and Compound 29-treated mice, as determined by qRT-PCR. Gene levels in Control treated mice are set to 1. *Arbp* was used as an internal control. (**C**) Most of the genes modulated in the adipose tissue of mice treated with Compound 29 are ERRα direct targets. ERRα ChIP-sequencing profiles for genes modulated in (B). Red indicates ERRα binding. **P< 0.01, ***P< 0.001.

Figure 4.6

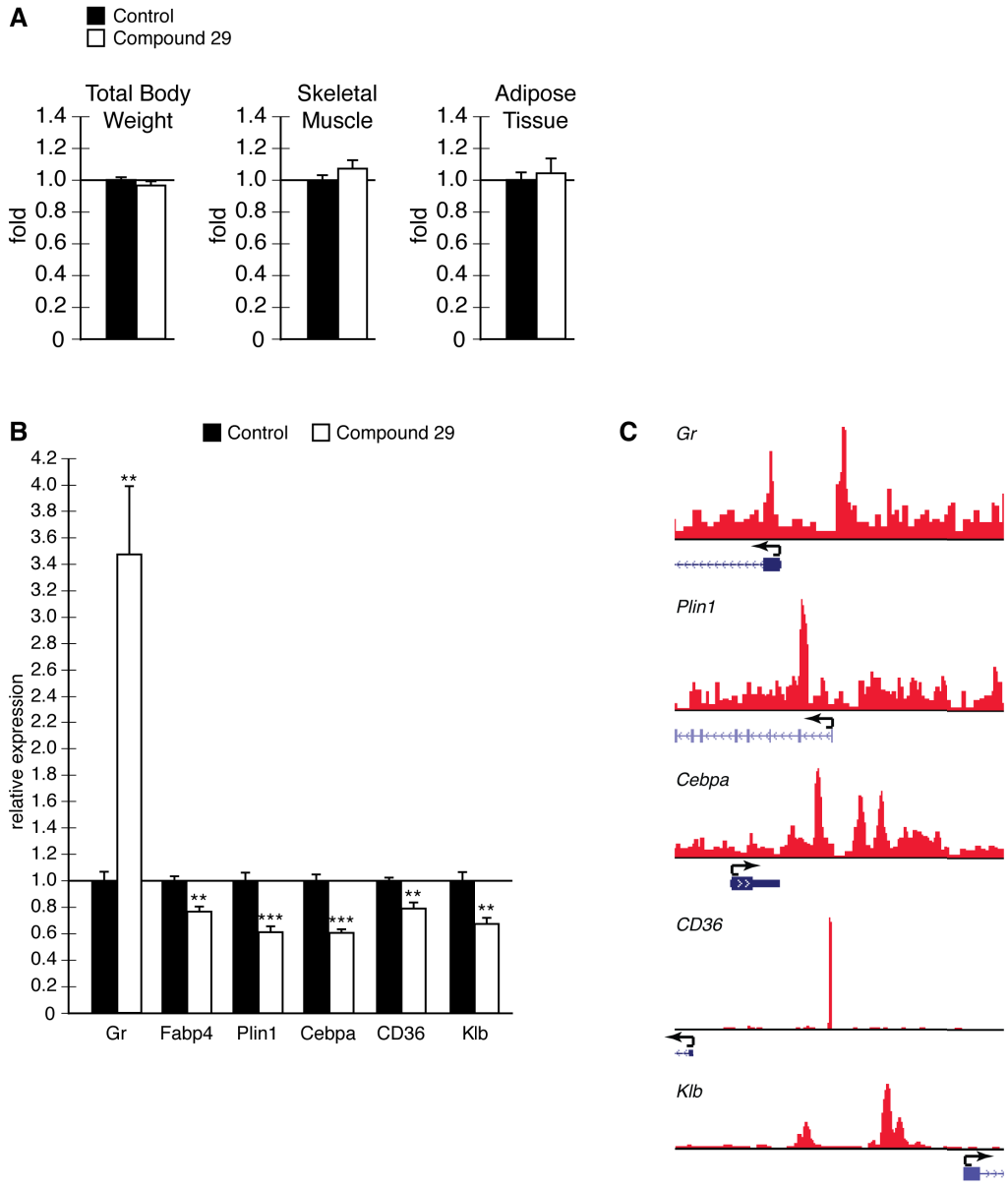
A
Control
Compound 29
Total Body Weight
Skeletal Muscle
Adipose Tissue
fold
1.4
1.2
1.0
0.8
0.6
0.4
0.2
0
B
Control
Compound 29
relative expression
4.2
4.0
3.8
3.6
3.4
3.2
3.0
2.8
2.6
2.4
2.2
2.0
1.8
1.6
1.4
1.2
1.0
0.8
0.6
0.4
0.2
0
**
**
***
***
**
**
Gr
Fabp4
Plin1
Cebpa
CD36
Klb
C
Gr
Plin1
Cebpa
CD36
Klb

CHAPTER V: A Knockout Mouse Model Reveals Essential Roles for miR-378/378* in Brown Adipose Tissue Function

PREFACE

The absence of mir-378 mouse models prevented the *in-vivo* study of this miRNA in breast cancer, and has limited the general understanding of the physiological role of this molecule. To overcome this obstacle, we generated both a conditional and a total knockout mouse model for this miRNA. To understand the physiological role of mir-378, we began by studying the basal phenotypes of the mir-378 total knockout mice. We uncovered phenotypes in the brown adipose tissue, suggesting a role for mir-378 in thermogenesis.

ABSTRACT

The mir-378 miRNA hairpin, encoding both mature miR-378 and miR-378*, has been implicated as a metabolic miRNA with functions in normal physiology and disease. To study the role of mir-378 *in-vivo*, we have generated both a mir-378 conditional and a mir-378 total knockout mouse model. The total knockout animals are produced at expected mendelian frequencies regardless of gender, have no reproductive difficulty, and exhibit no differences in body weight from wildtype or heterozygous mice throughout development to maturity. A screen of tissue weight combined with histological analyses revealed that the brown adipose tissue of mir-378 knockout mice exhibits the clearest basal phenotypic differences from wildtype mice of all eight tissues examined. Male mir-378 knockout mice have approximately 20% less interscapular brown adipose tissue than wildtype counterparts, and phenotypic differences are visible by histology and electron microscopy. Gene expression analysis identified significant downregulation of key genes involved in brown adipose tissue maintenance and function, *Dio2*, *Ucp1*, and *Ppargc1a*. Taken together with the knowledge that PGC-1β (the mir-378 host gene) and the closely related ERRs have established functions in brown adipose tissue function, our results suggest that mir-378 is an essential component of the thermogenesis program.

INTRODUCTION

MiRNA are short, endogenous RNAs which post-transcriptionally regulate their mRNA targets, with the functional output of controlling target protein levels (Fabian and Sonenberg, 2012). miRNA have been implicated in essentially all physiological processes and a large range of diseases (Osman, 2012), including metabolism and metabolic disorders (Rottiers and Naar, 2012). mir-378, which encodes for both mature miR-378 and miR-378*, has been shown to regulate a major metabolic nuclear receptor, ERRγ, and a transcription factor known for its regulation of mitochondrial gene expression, GABPA (Eichner et al., 2010). While this study explored these molecular relationships in a cancer context, mir-378 has been shown to be implicated in normal metabolic physiological settings as well, including adipogenesis (Gerin et al., 2010a), cardiac function (Knezevic et al., 2012; Tranter et al., 2011), muscle function (Davidsen et al., 2011) and liver regeneration (Song et al., 2010b). Furthermore, it is generally considered that miRNA, if intronically located within a host gene, are co-expressed with this host gene (Kim and Kim, 2007b). mir-378 is located within the first intron of its host gene *Ppargc1b*, which encode for the metabolic co-activator, PGC-1β, and has been proven to be co-expressed with this gene (Eichner et al., 2010). The co-expression of mir-378 with the well-established metabolic gene PGC-1β, by extension, further strengthens the connection between mir-378 and metabolic contexts and functions. While the current literature has clearly linked mir-378 to metabolic function, the absence of mir-378 mouse models has greatly limited the exploration of mir-378 function, both in metabolic tissues as well as tissue contexts with fundamentally different functions.

Therefore, to study the role of mir-378 (recently renamed mir-378a, as noted in Chapter I earlier) *in-vivo*, we have generated both a mir-378 conditional and a mir-378 total knockout mouse model. The total knockout mice exhibit no obvious developmental or reproductive defects, allowing

for the immediate study of mir-378 function in the adult mouse. We identified that the brown adipose tissue of mir-378 knockout mice, of all tissues examined, exhibits the clearest basal phenotypic differences from wildtype (WT) mice. In fact, mir-378 knockout mice have significantly less interscapular brown adipose tissue than WT counterparts, and phenotypic differences are visible by histology and electron microscopy. Gene expression analysis identified significant downregulation of key genes involved in brown adipose tissue maintenance and function, *Dio2*, *Ucp1*, and *Ppargc1a*. Taken together with the knowledge that PGC-1β (the mir-378 host gene) and the functionally-related ERRs have established roles in brown adipose tissue function, our results suggest that mir-378 is an essential component of the thermogenesis program.

RESULTS

Generation of the mir-378 conditional knockout mouse and the mir-378 total knockout mouse

To target the mir-378 hairpin for *in-vivo* modulation, we designed one targeting construct for the generation of both the mir-378 conditional knockout mouse, mir378CKO, and the mir-378 total knockout mouse, mir378TKO (Fig. 5.1A). The targeting construct, with homologous arms >3kb long, was designed to introduce a LoxP site-flanked neomycin cassette (Neo) downstream of mir-378, along with one LoxP site just upstream of mir-378. Care was taken to include as few base pairs as possible between the LoxP sites flanking mir-378 (265bp total) in order to minimize the chance of modifying *Ppargc1b* expression. This was key, as mir-378 is located within the first intron of its host gene *(Ppargc1b)*, a regulatory region known for its importance for gene expression. After electroporation of the targeting construct into embryonic stem (ES) cells and following antibiotic selection, we screened the 394 resulting clones by PCR for proper incorporation of the targeted allele (Fig. 5.1B). Our screen was designed to verify correct location of the construct in the genome, inclusion of the floxed miRNA, incorporation of the Neomycin cassette, and absence of undesired targeting construct incorporation beyond the homologous arms. We identified 6 such positive clones, and the two most ideal clones, as identified by karyotyping, were selected for blastocyst microinjection and subsequent chimera generation. One clone generated 5 chimeras with ≥95% agouti coat color, and the second clone produced 9 chimeras with ≥75% agouti coat color. Resulting chimeras were mated with female C57Bl/6 mice, and germline transmission of the modified allele to the F1 generation was determined by transmission of the ES cell-derived agouti coat color to the resulting pups.

Having established germline transmission of our genetic modification, we crossed these mice to MORE mice, which express Cre recombinase under the control of the germline-expressing Mox2 promoter

(Tallquist and Soriano, 2000). The resulting mice, in which our LoxP-containing modification had been exposed to Cre recombinase, exhibited the results of LoxP-mediated genetic recombination. Two types of disrupted alleles were identified by PCR-based genotyping; the mir-378 conditional knockout (mir378CKO), which retained the floxed mir-378 sequence after specific deletion of the neomycin cassette (Fig. 5.1C, left panel), and the mir-378 total knockout (mir378TKO), where both the neomycin cassette and the mir-378 region had been removed from the genome following LoxP collapse, leaving only one remaining LoxP site (Fig. 5.1C, right panel). To study the result of removing mir-378 entirely from the genome, we bred the mir378TKO mice (from hereon called mir378KO) to homozygosity.

Heterozygous mir378KO animals were mated to produce littermate WT and KO animals for study. Heterozygous mir378KO animals exhibited no reproductive difficulty, and total knockout animals of both genders were produced at expected mendelian frequencies (data not shown), indicating that this genetic modification is not detrimental to development.

In order to predict the tissue contexts where mir378KO mice are most likely to exhibit phenotypes, we screened the expression of mature miR-378 and miR-378* across different tissues of adult male wildtype (WT) mice (Fig. 5.1D). As expected, mir-378 is most highly expressed in metabolic tissues with high energy demands including the heart, skeletal muscle, brown adipose tissue (BAT) and white adipose tissue (WAT), less expressed in the liver, and expressed the least in the spleen and testes. Also as expected, mature forms of both miR-378 and miR-378* display extremely similar expression patterns. The high expression of mir-378 in metabolic tissues parallels the expression of its host gene, *Ppargc1b* (encoding PGC-1β) (Lin et al., 2002), contributing more proof that mir-378 is co-expressed with its host gene, and suggesting that mir-378 is biologically relevant in tissue contexts where *Ppargc1b* is expressed, further implicating mir-378 as a metabolic miRNA.

We next validated our knockout mouse model at the functional level by verifying that miR-378 and miR-378* are not expressed in the mir378KO mice (Fig. 5.1E). Importantly, *Ppargc1b* expression is retained in the mir378KO mice (Fig. 5.1E), indicating that we had succeeded in deleting mir-378 from the genome without affecting the expression of its host gene.

Screen for phenotypes in mir378KO animals

mir378KO mice develop normally, and exhibit no differences in body weight from WT or heterozygous mice throughout development to maturity (Fig. 5.2A and data not shown). Therefore, we set out to investigate the basal phenotypes of this mouse model by screening different tissue contexts in the adult mir378KO mouse. Weight measurements of interscapular brown (BAT) and white (WAT) adipose tissues, heart, skeletal muscle, spleen, testes, liver and lungs, after normalization to total body weight, revealed differences between WT and KO animals in BAT, WAT and Spleen weight (Fig. 5.2A). More precisely, two-month-old male mir378KO mice exhibit 20% less BAT, 57% less WAT, and a 30% heavier spleen. Histological analysis of these tissues revealed the most striking differences between the mir378KO and WT mice in the BAT (Fig. 5.2B). Of note, cardiac tissue from mir378KO mice exhibited defects in mitochondrial organization observed by electron microscopy (Fig. A.5.1). Considering, in addition to the tissue weight and histology data, that mir-378 is highly expressed in the BAT (Fig. 5.1D), that ERRγ is a direct target of miR-378* (Eichner et al., 2010), that ERRα and ERRγ are expressed at high levels in the BAT (Sladek et al., 1997b), and that ERR has been implicated in adaptive thermogenesis controlled by the BAT (Villena et al., 2007), we hypothesized that mir-378 could have a physiologically-relevant role in this tissue context. Therefore, we chose to focus our study on the BAT context, the major site of mammalian heat production (Cannon et al., 2004).

Basal adipose tissue defects in male mir378KO mice

Mir378KO mice exhibit gross differences in basal BAT quantity, as visible by eye (Fig. 5.3A), while structural defects of mir378KO BAT lipid droplets were identified by electron microscopy (Fig. 5.3B). These phenotypes were not accompanied by differences in mitochondrial content (Fig. 5.3C).

To understand how the deletion of mir-378 affects basal BAT, we screened the expression levels of genes with established roles in BAT function (Fig. 5.3D). We found that *Dio2*, the gene responsible for the uptake and mobilization of circulating T4 hormone into the T3 form active in the BAT (Christoffolete et al., 2004), is 57% downregulated in male mir378KO mice as compared to WT animals. *Ucp1*, the major gene responsible for heat production (Cannon and Nedergaard, 2004), is 40% downregulated in the mir378KO animals. And *Ppargc1a*, the gene responsible for co-activating the gene expression programs necessary for the thermogenic response (Lowell and Spiegelman, 2000), is downregulated 53%. Notably, *Thra*, thyroid hormone receptor alpha, exhibits a trend toward downregulation in the knockout mice which, however, does not reach statistical significance with this sample size. Of the transcription factors responsible for mitochondrial gene expression programs, *Nrf1, Gabpa* and *Tfam,* only *Nrf1* is significantly misregulated in the KOs. The brown fat marker, *Prdm16*, shows a slight trend toward downregulation in the KO BAT without reaching statistical significance, while other adipose tissue markers, *Adipoq* and *Fabp4*, are unmodulated. Nuclear receptors with established functions in adipose tissue, *Ppara* and *Pparg1*, exhibit trends toward downregulation in the mir378KO mice, while not reaching statistical significance within this sample size. *Esrrg*, the direct target of miR-378*, tends lightly toward downregulation in the KOs, while *Esrra* exhibits a trend in the opposite direction, but neither reach statistical significance. As both miR-378 and miR-378* are expressed in

the BAT (Fig. 5.1D), it is reasonable to expect miR-378* targets to be modulated in mir378KO tissues. Thus, it is possible that the mild *Esrrg* mRNA response observed is a reflection of a cellular attempt to compensate for long-term mir-378*-related modulation of ERRγ protein levels, a hypothesis which should be confirmed by western blotting for ERRγ protein levels. This hypothesis is the most likely explanation for these observed mRNA-level results, considering the mRNA/protein-level effects observed in all other models studied throughout the work of this thesis where mir-378 levels were modulated long-term, as discussed in Chapter 3 (p.126-127). If, however, western blotting does not confirm the expected modulation of ERRγ at the protein level, this would indicate that miR-378* targeting of ERRγ may instead be tissue context specific. Exploration of the underlying mechanism behind such tissue-specific targeting would itself be an interesting finding to investigate further. Taken together, there is clear indication that the mir378KO mouse BAT exhibits aberrations in the basal gene expression of key genes responsible for BAT function. Furthermore, many genes exhibit trends toward basal misregulation which would likely become exacerbated in conditions when the mice need to activate their adaptive thermogenesis program, such as if the mice were placed in the cold. Therefore, these trends in gene expression, while not conclusive if statistical significance is not reached, may still be indicative of mir-378 function in BAT that could prove to be functionally important when the thermogenic program is more drastically activated.

Adipose and cardiac analysis of female mir378KO mice

Interestingly, female mir378KO mice of the same age did not recapitulate the differences observed in the male mice. Unlike the males, histological analysis of female mice did not reveal clear differences in BAT (Fig. 5.4A), while WAT from females appears to exhibit a difference in cell size between the genotypes (Fig. 5.4B). Similarly to the males, there were

no major cardiac differences observed by histological analysis in the females (Fig. 5.4C). Interestingly, of the three genes most differentially regulated in the male mir378KO mice, *Ppargc1a*, *Ucp1*, and *Dio2*, only *Ppargc1a* exhibited a trend of downregulation similar to that which was observed in the males (Fig. 5.4D), although this trend does not reach statistical significance. In contrast to what was observed in the males, *Ucp1* levels were unchanged in the female KOs, and *Dio2* levels exhibited a trend in the opposite direction; toward upregulation, that also did not reach statistical significance. One caveat is that the failure of these gene expression differences observed in the females to reach statistical significance can be attributed to the smaller *n* available for gene expression analysis, rather than a biological rationale. Regardless of the smaller *n*, however, two genes do exhibit statistically significant differences between the genotypes in the female mice; *Pparg2* and *Esrrg*. Taken together, while mir378KO mice exhibit differences from WT animals in a gender-specific manner, it is clear that mice of both genders exhibit differences from their WT counterparts in the BAT that implicates mir-378 in adaptive thermogenesis.

DISCUSSION

We have generated both a conditional mir378KO mouse and a total mir378KO mouse. Our data show that mir-378, like its host gene, *Ppargc1b*, is most expressed in highly metabolic tissues including heart, skeletal muscle, white adipose and brown adipose tissues. Furthermore, it seems that mir-378 is not essential for development, as our total KO mice develop successfully to adulthood and have no reproductive difficulties. Of the 8 tissues screened, male mir378KO mice have differences in BAT, WAT and spleen weights. Histological and electron microscopy analyses revealed in more detail how the BAT from mir378KO mice differs from WT mice. Gene expression analyses identified misregulation of key genes in the BAT of mir378KO mice, suggesting a role for mir-378 in adaptive thermogenesis. An acute cold exposure experiment, where mice are placed at 4°C and their core body temperature monitored as they adjust to the cold by activating their adaptive thermogenesis program, is the next step with which we will verify and examine the functional role of mir-378 in this process.

Importantly, expression of the host gene, *Ppargc1b*, is not affected in our mir378KO mouse. Therefore, our models extend the available animal model tools available for studying this genomic locus in an important fashion. While, previously, all mouse models affecting the *Ppargc1b*/mir-378 genomic locus have inactivated the protein product of the *Ppargc1b* gene (Lelliott et al., 2006; Sonoda et al., 2007b; Vianna et al., 2006) without affecting mir-378 expression (discussed and proven in Chapter 2 earlier; page 70 and Figure 2.8), our models allow for the *in-vivo* study of the small but physiologically-relevant mir-378 region alone. These models should make a large contribution toward a more complete understanding of this genomic locus.

Of note, recently, after the bulk of this thesis work was completed, other mammalian miRNA with nearly identical sequences to mir-378, differing by one or two nucleotides, were identified in different locations

throughout mammalian genomes (as outlined in Chapter I footnote). These miRNA were also named mir-378, and are distinguishing from each other by a lower case letter; “a” through “j” in human and “a” through “d” in mouse. The mouse models generated in this chapter genetically alter solely the originally-identified mir-378, currently renamed mir-378a. (To maintain consistent nomenclature throughout this thesis, we continue to refer to the current “mir-378a” as “mir-378.”) This mir-378 hairpin is the only mir-378 that encodes for miR-378*. Interestingly, since the mouse models generated in this chapter disrupt only mir-378 (currently termed mir-378a), this suggests that the deletion of solely this mir-378 hairpin from the genome (Fig. 5.1E) is sufficient to generate the phenotypes observed, regardless of the potential presence of other mir-378s (mir-378b-d). Importantly, only miR-378c shares the same seed sequence as miR-378, whereas miR-378b is shorter than miR-378 at the 5’ end and the seed of miR-378d differs from that of miR-378 by one nucleotide. This suggests that, even if miR-378a-d were co-expressed in the same tissue, which itself remains to be determined, targeting would likely not be redundant between most of these different miR-378s, as the exact seed is crucial for determining miRNA targets. By extension, this logic suggests that only miR-378c could impart redundant function in the mouse to that of miR-378, begging the question about the tissue expression of particularly mir-378c. The tissue source of the sequencing reads in mirbase (mirbase.org) indicate that miR-378c was detected in embryo, newborn and brain, indicating that this miRNA may exhibit tissue expression that is limited predominantly to devopment. miR-378, too, was detected by sequencing in the developing embryo but also across a wide range of adult tissues. Considering that the mir-378KO mice developed in this chapter do not display developmental defects but do exhibit basal phenotypes in the adult, it would be interesting to test if miR-378c expression during development contributes to a biological redundancy that is lost as miR-378c expression diminishes in the adult while miR-378

expression remains. In general, determining the tissue distribution of miR-378b-d expression, and particularly their expression in the brown adipose tissue, would add to the understanding of the mir-378 family.

Our analysis of eight different tissues in the mir378KO mouse provides the first glimpse into the physiological function of the mir-378 hairpin. Notably, both the PGC-1β KO mice (Lelliott et al., 2006; Sonoda et al., 2007b) and our mir-378KO mice exhibit defects in thermogenesis, yet again reaffirming the close function relationship between these two molecules produced from the same genomic locus. While we have focused this investigation on the BAT, it is interesting to note that the WAT and spleen also exhibited significant differences in tissue weight between WT and mir378KO mice, suggesting that those tissues are also contexts which merit further study in this animal model. That the mir-378 hairpin has a role in both types of adipose tissue speaks to its relevance in general adipose function. In fact, it was recently shown that the expression of mir-378 in adipose tissue is responsive to high fat diet (Chartoumpekis et al., 2012) and that mir-378 expression in white adipose tissue correlates with bovine backfat thickness (Jin et al., 2010). Furthermore, studies using the 3T3-L1 and ST2 cell lines identified that mir-378 is induced during adipogenesis, and increases lipid droplet size and triacylglycerol accumulation (Gerin et al., 2010a). These affects were attributed at least in part to increased transcriptional activity of C/EBPα and C/EBPβ on adipocyte gene promoters. It would be interesting to investigate these processes of adipogenesis and adipocyte differentiation further and *in-vivo* using our mir378KO models.

Notably, we have not yet identified the miRNA targets responsible for the phenotypes observed in the BAT of the mir378KO mice. This is of course the natural next step in understanding this interesting miRNA if the short-term cold exposure experiment reveals the expected defect in thermogenesis. The direct miR-378* targets already identified in Chapter II, *ESRRG* and *GABPA*, are also likely to play a role in the BAT context

and may themselves contribute to the mir-378KO phenotype observed. As introduced above, ERR expression level is very high in the BAT, and ERRα KO mice have already been implicated in adaptive thermogenesis driven by the BAT (Villena et al., 2007). Based on tissue expression as well as the importance of mitochondrial metabolism in BAT function, it is likely that the metabolic regulator ERRγ also plays an important role in this process. If so, its regulation by miR-378* may, therefore, contribute to the mir378KO phenotype observed. Western blotting in the mir378KO BAT will identify if miR-378* targeting of ERRγ and GABPA could be involved in these KO mice in this context. It is also possible that other direct targets are implicated in the phenotypes observed, and this will be an interesting avenue for further investigation.

The increased spleen weight that we observed in our mir378KO mice suggests the interesting yet unexpected idea that this miRNA may have a role in immune system function. Only very recently is there any indication that mir-378 may be relevant in such contexts (Erdogan et al., 2011; Hasler et al., 2012; Wang et al., 2012), and the idea is not only enticing but speaks to the potential breadth of function of this small molecule.

Our data on the heart acts as an important reminder; while at the histological level we identified no major differences between WT and mir378KO hearts, electron microscopy of hearts from male mice revealed clear misregulation of mitochondrial organization in the mir378KO animals. In addition to suggesting a role for mir-378 in cardiac metabolic function, this serves as a reminder that negative results at one level of investigation does not necessarily indicate an absence of physiological function in that tissue context. It may very well be that careful investigation of many tissue contexts of our mouse models will reveal many different roles for mir-378 *in-vivo*.

It is interesting to note that the changes observed in the BAT are different between genders. Considering that the main function of BAT is to

generate heat, gender-related differences in BAT function bring to mind the differences in body temperature often observed between women and men. Also noteworthy is the fact that these experiments have all been carried out in mice with a mixed genetic background. The rationale for this was simply expediency, but the outcome is actually greater confidence that mir-378 has a significant role in BAT function, as we know that it is not a pure background artifact which allows for the phenotypes we observe. It should also be considered, that tissue contexts where we have not observed phenotypes in animals with a mixed background may yet reveal phenotypes as mice are bred further to pure genetic backgrounds.

Taken together, the mir378KO mouse model that we generated has allowed us to identify basal differences in the BAT of our mir378KO mice that suggest a role for mir-378 in adaptive thermogenesis. The underlying molecular relationships, including the miRNA targets responsible for the observed phenotypes, remain to be elucidated, but the recent identification of brown adipose tissue in humans (Ouellet et al., 2012) brings additional relevance to these research avenues.

MATERIALS AND METHODS

Ethics statement

Animal use followed the guidelines of the Canadian Council on Animal Care. The animal use protocol was approved by the local Facility Animal Care Committee (FACC) at McGill University.

Animals

All mice were housed and fed standard chow in the animal facility at the McGill University Rosalind and Morris Goodman Cancer Research Centre. ES cell electroporation, karyotyping, ES cell microinjection into blastocyst injection and chimera generation were carried out by the McGill Transgenic Facility. Animals studied were of mixed 129 X C57Bl/6 genetic background; originating from ES cells from a 129 genetic backgroung, crossed three times into the C57Bl/6 background. Animals were sacrificed during the day at ZT (Zeitgeber time) 4. Tissues were frozen in liquid nitrogen, ground using a mortar and pestle and kept frozen until further processing, or prepared for histology as outlined below. Tissue weights, when measured, were taken immediately after dissection and before further tissue processing or storage.

ES Cell PCR Screen

Sequences of primers used can be found in the Appendix Table A.5.1. Expand High Fidelity PCR System (Roche) was used to amplify long-range products.

Genotyping

Sequences of primers used can be found in the Appendix Table A.5.1.

RNA Isolation, Reverse Transcription and quantitative Real-Time PCR

RNA used in Fig. 4.1 was isolated using a miRNeasy Mini Kit (Qiagen). Adipose RNA was isolated with the RNeasy Lipid Tissue Mini Kit (Qiagen). DNase treatment was always performed during RNA isolation. RNA was quantified with a NanoDrop. cDNA was made from either 1 or 2 µg of total RNA by reverse transcription with Oligo(dT) primer, dNTPs, 5X 1st strand buffer, DTT, RNase inhibitor, and Superscript II RNase H Reverse Transcriptase (Invitrogen). cDNA was amplified by qRT-PCR using specific primers (Appendix Table A.5.1) qRT-PCR was carried out in a LightCycler 480 instrument using the QuantiTect SYBR Green PCR Kit (Qiagen) following the Qiagen software protocol. All primers were designed using Oligo 6.8 Primer Analysis Software with sequence data from the http://genome.ucsc.edu database mouse July 2007 or December 2011 assemblies. Primer sets were tested on cDNA dilutions to determine primer efficiency. qRT-PCR reactions were performed in duplicate, and the Ct values were averaged before normalization. For miRNA qRT-PCR, Applied Biosystems miRNA Taqman Assays were used as described in Chapter II.

Histology

All histological procedures were performed at the histology facility of the Goodman Cancer Research Centre (GCRC). Tissues were fixed in 10% buffered formalin for 48hrs and then blocked in paraffin. Paraffin-embedded tissues were sectioned at 4 µm and were hematoxylin and eosin stained.

Electron Microscopy

Tissues were fixed in 0.1M phosphate buffer containing 2.5% glutaraldehyde and 2% paraformaldehyde, post-fixed in 0.1M sodium cacodylate buffer containing 1% osmium teroxide, and embedded in epon. Sections were counterstained with uranyl acetate/lead citrate.

Mitochondrial Content Assay

The relative number of mitochondria in BAT isolated from adult WT and mir-378KO mice was determined by measuring the ratio of mtDNA to nuclear DNA. DNA was isolated using a Qiagen DNeasy Blood & Tissue kit. Relative levels of mtDNA and nuclear DNA were quantified using primers specific for mitochondrial cytochrome b (*CYTB*) and *Pgk2*, respectively. Error bars represent means +/- SEM (n = 5).

Primers:

m-cytochro b (mtDNA)-F	CTCCTCTTCCTCCACGAAACAG
m-cytochro b (mtDNA)-R	GTTTATTGGGGATTGAGCGTAG
Pgk2 RT-PCR-F	GAAGACAAGGTCAGCCATGTGAGC
Pgk2 RT-PCR-R	GGTTGAGTTGGTTCTGGTCCTGTG

ACKNOWLEDGEMENTS

We acknowledge Janice Penney of the McGill Transgenics Core and members of the histology core facility of the Goodman Cancer Research Centre (GCRC) at McGill University. We thank M. Ghahremani and D.W.K. Tsang for technical assistance.

REFERENCES

Cannon, B., and Nedergaard, J. (2004). Brown adipose tissue: function and physiological significance. Physiol Rev *84*, 277-359.

Chartoumpekis, D.V., Zaravinos, A., Ziros, P.G., Iskrenova, R.P., Psyrogiannis, A.I., Kyriazopoulou, V.E., and Habeos, I.G. (2012). Differential expression of microRNAs in adipose tissue after long-term high-fat diet-induced obesity in mice. PLoS One *7*, e34872.

Christoffolete, M.A., Linardi, C.C., de Jesus, L., Ebina, K.N., Carvalho, S.D., Ribeiro, M.O., Rabelo, R., Curcio, C., Martins, L., Kimura, E.T.*, et al.* (2004). Mice with targeted disruption of the Dio2 gene have cold-induced overexpression of the uncoupling protein 1 gene but fail to increase brown adipose tissue lipogenesis and adaptive thermogenesis. Diabetes *53*, 577-584.

Davidsen, P.K., Gallagher, I.J., Hartman, J.W., Tarnopolsky, M.A., Dela, F., Helge, J.W., Timmons, J.A., and Phillips, S.M. (2011). High responders to resistance exercise training demonstrate differential regulation of skeletal muscle microRNA expression. J Appl Physiol *110*, 309-317.

Eichner, L.J., Perry, M.C., Dufour, C.R., Bertos, N., Park, M., St-Pierre, J., and Giguere, V. (2010). miR-378(*) mediates metabolic shift in breast cancer cells via the PGC-1beta/ERRgamma transcriptional pathway. Cell Metab *12*, 352-361.

Erdogan, B., Facey, C., Qualtieri, J., Tedesco, J., Rinker, E., Isett, R.B., Tobias, J., Baldwin, D.A., Thompson, J.E., Carroll, M.*, et al.* (2011). Diagnostic microRNAs in myelodysplastic syndrome. Exp Hematol *39*, 915-926 e912.

Fabian, M.R., and Sonenberg, N. (2012). The mechanics of miRNA-mediated gene silencing: a look under the hood of miRISC. Nat Struct Mol Biol *19*, 586-593.

Gerin, I., Bommer, G.T., McCoin, C.S., Sousa, K.M., Krishnan, V., and MacDougald, O.A. (2010). Roles for miRNA-378/378* in adipocyte gene expression and lipogenesis. Am J Physiol Endocrinol Metab *299*, E198-206.

Hasler, R., Jacobs, G., Till, A., Grabe, N., Cordes, C., Nikolaus, S., Lao, K., Schreiber, S., and Rosenstiel, P. (2012). Microbial pattern recognition causes distinct functional micro-RNA signatures in primary human monocytes. PLoS One *7*, e31151.

Jin, W., Dodson, M.V., Moore, S.S., Basarab, J.A., and Guan, L.L. (2010). Characterization of microRNA expression in bovine adipose tissues: a potential regulatory mechanism of subcutaneous adipose tissue development. BMC Mol Biol *11*, 29.

Kim, Y.K., and Kim, V.N. (2007). Processing of intronic microRNAs. Embo J *26*, 775-783.

Knezevic, I., Patel, A., Sundaresan, N.R., Gupta, M.P., Solaro, R.J., Nagalingam, R.S., and Gupta, M. (2012). A novel cardiomyocyte-enriched microRNA, miR-378, targets insulin-like growth factor 1 receptor: implications in postnatal cardiac remodeling and cell survival. J Biol Chem *287*, 12913-12926.

Lelliott, C.J., Medina-Gomez, G., Petrovic, N., Kis, A., Feldmann, H.M., Bjursell, M., Parker, N., Curtis, K., Campbell, M., Hu, P.*, et al.* (2006). Ablation of PGC-1beta results in defective mitochondrial activity, thermogenesis, hepatic function, and cardiac performance. PLoS Biol *4*, e369.

Lin, J., Puigserver, P., Donovan, J., Tarr, P., and Spiegelman, B.M. (2002). Peroxisome proliferator-activated receptor gamma coactivator 1beta (PGC-1beta), a novel PGC-1-related transcription coactivator associated with host cell factor. J Biol Chem *277*, 1645-1648.

Lowell, B.B., and Spiegelman, B.M. (2000). Towards a molecular understanding of adaptive thermogenesis. Nature *404*, 652-660.

Osman, A. (2012). MicroRNAs in health and disease--basic science and clinical applications. Clin Lab *58*, 393-402.

Ouellet, V., Labbe, S.M., Blondin, D.P., Phoenix, S., Guerin, B., Haman, F., Turcotte, E.E., Richard, D., and Carpentier, A.C. (2012). Brown adipose tissue oxidative metabolism contributes to energy expenditure during acute cold exposure in humans. J Clin Invest *122*, 545-552.

Rottiers, V., and Naar, A.M. (2012). MicroRNAs in metabolism and metabolic disorders. Nat Rev Mol Cell Biol *13*, 239-250.

Sladek, R., Bader, J.A., and Giguere, V. (1997). The orphan nuclear receptor estrogen-related receptor alpha is a transcriptional regulator of the human medium-chain acyl coenzyme A dehydrogenase gene. Mol Cell Biol *17*, 5400-5409.

Song, G., Sharma, A.D., Roll, G.R., Ng, R., Lee, A.Y., Blelloch, R.H., Frandsen, N.M., and Willenbring, H. (2010). MicroRNAs control

hepatocyte proliferation during liver regeneration. Hepatology *51*, 1735-1743.

Sonoda, J., Mehl, I.R., Chong, L.W., Nofsinger, R.R., and Evans, R.M. (2007). PGC-1beta controls mitochondrial metabolism to modulate circadian activity, adaptive thermogenesis, and hepatic steatosis. Proc Natl Acad Sci U S A *104*, 5223-5228.

Tallquist, M.D., and Soriano, P. (2000). Epiblast-restricted Cre expression in MORE mice: a tool to distinguish embryonic vs. extra-embryonic gene function. Genesis *26*, 113-115.

Tranter, M., Helsley, R.N., Paulding, W.R., McGuinness, M., Brokamp, C., Haar, L., Liu, Y., Ren, X., and Jones, W.K. (2011). Coordinated post-transcriptional regulation of Hsp70.3 gene expression by microRNA and alternative polyadenylation. J Biol Chem *286*, 29828-29837.

Vianna, C.R., Huntgeburth, M., Coppari, R., Choi, C.S., Lin, J., Krauss, S., Barbatelli, G., Tzameli, I., Kim, Y.B., Cinti, S.*, et al.* (2006). Hypomorphic mutation of PGC-1beta causes mitochondrial dysfunction and liver insulin resistance. Cell Metab *4*, 453-464.

Villena, J.A., Hock, M.B., Chang, W.Y., Barcas, J.E., Giguere, V., and Kralli, A. (2007). Orphan nuclear receptor estrogen-related receptor alpha is essential for adaptive thermogenesis. Proc Natl Acad Sci U S A *104*, 1418-1423.

Wang, P., Gu, Y., Zhang, Q., Han, Y., Hou, J., Lin, L., Wu, C., Bao, Y., Su, X., Jiang, M.*, et al.* (2012). Identification of resting and type I IFN-activated human NK cell miRNomes reveals microRNA-378 and microRNA-30e as negative regulators of NK cell cytotoxicity. J Immunol *189*, 211-221.

TABLES AND FIGURES

Figure 5.1. Generation of the mir-378 conditional knockout mouse and the mir-378 total knockout mouse

(**A**) Design of targeting construct for the generation of the mir-378 conditional knockout mouse, mir378CKO, and the mir-378 total knockout mouse, mir378TKO. A LoxP site-flanked neomycin cassette (Neo) is introduced downstream of mir-378, along with one LoxP site just upstream of mir-378. Cre-mediated deletion of the Neo cassette only produces the conditional knockout (Disrupted Allele I). Total collapse of the LoxP sites deletes mir-378 to generate the total knockout (Disrupted Allele II). Exon 1 of the mir-378 host gene *Ppargc1b* is indicated by a blue box. (**B**) Confirmation of the insertion of the targeted allele in ES cells. WT, wild type ES cells; +/T, ES cells heterozygous for the targeted allele, T. Left panel, validation using primers F1 and R. Expected size of WT band is 4.35kb; targeted allele is 6.3kb. Right, validation using primers F2 and R. No WT band expected, band at 5kb expected for targeted allele. Location of primers shown in (A) on Targeted Allele diagram. (**C**) Confirmation of LoxP collapse by PCR from genomic DNA. Top panels show the deletion of the Neo cassette only (left) generating the mir378CKO (Disrupted Allele I) and deletion of both mir378 and the Neo cassette (right) generating the mir378TKO (Disrupted Allele II). Primers f and r1 were used. Arrow indicates band generated by conditional knockout allele. Lower left panel proves, using primers f and r2, that mir378 is still present in the genome of Disrupted Allele I. Location of primers shown in (A) on Targeted Allele diagram. KO, knockout; HET, heterozygote; WT, wild type. (**D**) Basal expression levels of miR-378* and miR-378 in WT mouse tissues as determined by qRT-PCR. U6 served as the internal control, and values were normalized to the average of the lowest expressing tissue, testes. (**E**) Relative expression levels of miR-378* (left), miR-378 (central), and *Ppargc1b* (right) confirm that miR-378* and miR-378 are not expressed in mir378TKO mice (from now on, mir378KO), while host gene *Ppargc1b*

retains normal expression levels. SnoRNA412 serves as an internal control for miRNA expression; *Arbp* serves as an internal control for mRNA expression.

Figure 5.1

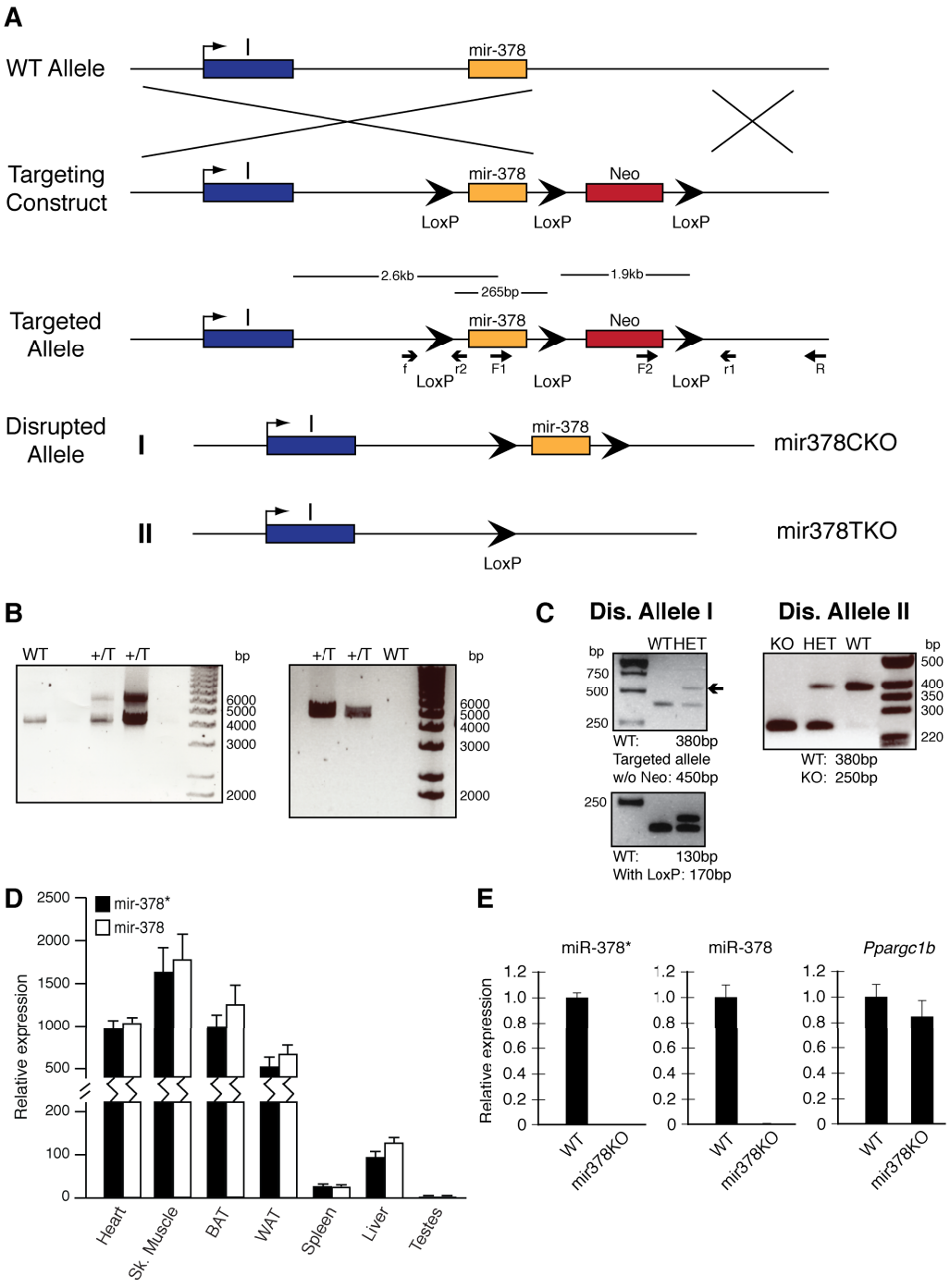
A
WT Allele
mir-378
Targeting Construct
mir-378
Neo
LoxP
LoxP
LoxP
2.6kb
265bp
1.9kb
Targeted Allele
mir-378
Neo
f
LoxP
r2
F1
LoxP
F2
LoxP
r1
R
Disrupted Allele
I
mir-378
mir378CKO
II
LoxP
mir378TKO
B
WT
+/T
+/T
bp
6000
5000
4000
3000
2000
+/T
+/T
WT
bp
6000
5000
4000
3000
2000
C
Dis. Allele I
Dis. Allele II
bp
WT
HET
750
500
250
WT: 380bp
Targeted allele w/o Neo: 450bp
250
WT: 130bp
With LoxP: 170bp
KO
HET
WT
bp
500
400
350
300
220
WT: 380bp
KO: 250bp
D
mir-378*
mir-378
Relative expression
2500
2000
1500
1000
500
200
100
0
Heart
Sk. Muscle
BAT
WAT
Spleen
Liver
Testes
E
miR-378*
miR-378
Ppargc1b
Relative expression
1.2
1.0
0.8
0.6
0.4
0.2
0
WT
mir378KO

Figure 5.2. Phenotyping screen of different tissues suggests role for mir-378 in brown adipose tissue

(**A**) Total body weight and tissue weights, including interscapular brown adipose tissue (BAT), interscapular white adipose tissue (WAT), Heart, Skeletal Muscle (sk. muscle), Spleen, Testes, Liver and Lungs, from male matched littermate WT and mir378 KO mice. Tissue weight data normalized to total body weight. (**B**) Histological analysis of same tissues from mice in (A). H&E staining. Images at 20X magnification unless indicated otherwise. Unpaired student's *t* test was used for evaluation of statistical significance. *P< 0.05.

Figure 5.2

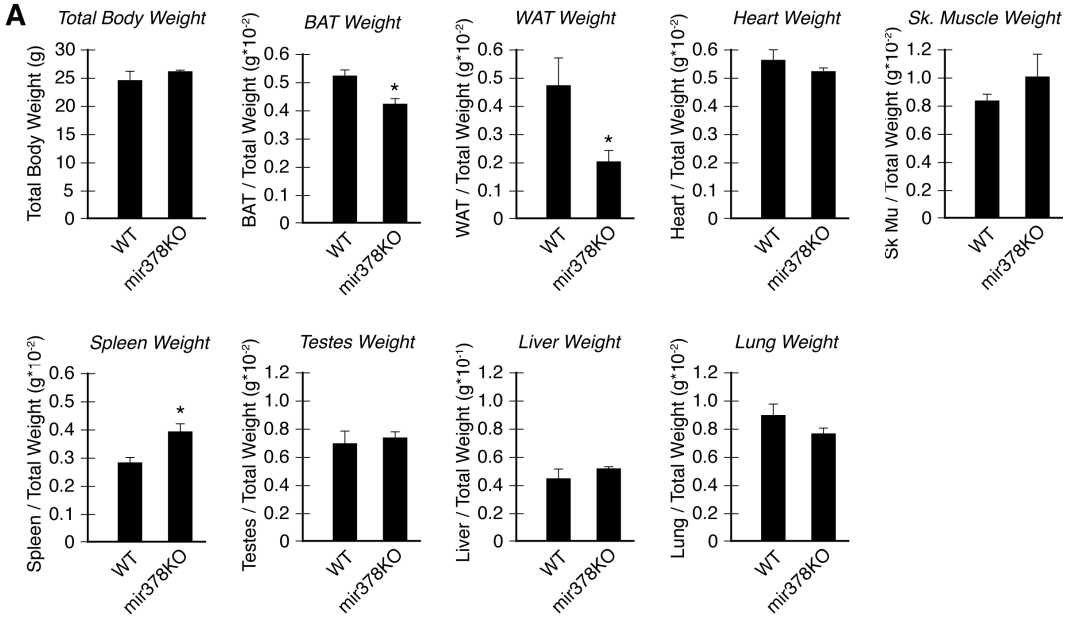
A
Total Body Weight
Total Body Weight (g)
BAT Weight
BAT / Total Weight (g*10-2)
WAT Weight
WAT / Total Weight (g*10-2)
Heart Weight
Heart / Total Weight (g*10-2)
Sk. Muscle Weight
Sk Mu / Total Weight (g*10-2)
Spleen Weight
Spleen / Total Weight (g*10-2)
Testes Weight
Testes / Total Weight (g*10-2)
Liver Weight
Liver / Total Weight (g*10-1)
Lung Weight
Lung / Total Weight (g*10-2)
WT
mir378KO

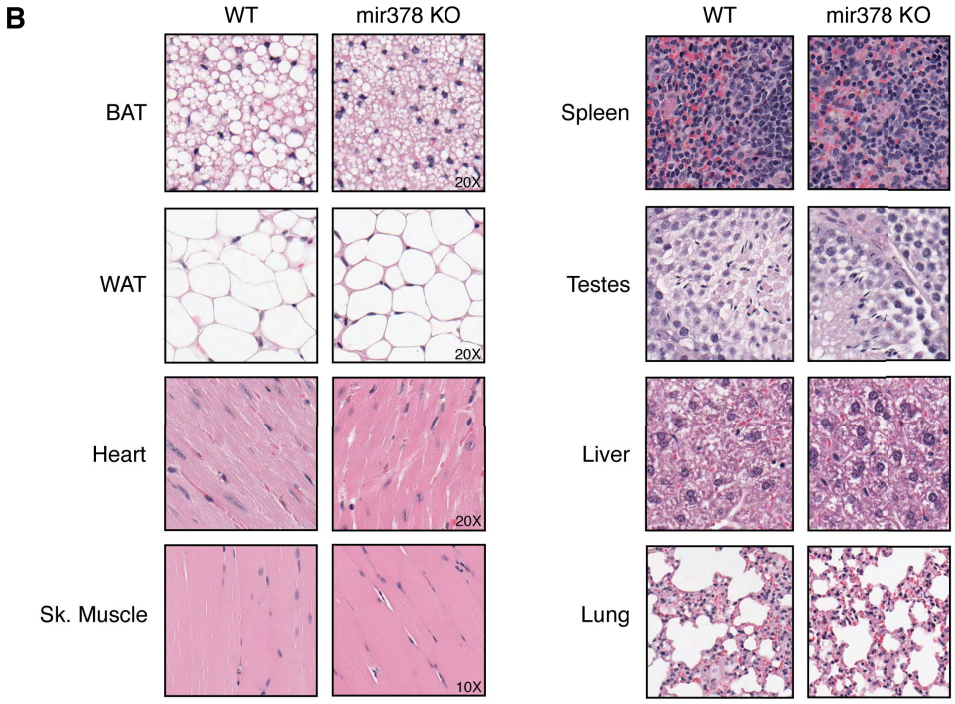
B
WT
mir378 KO
BAT
WAT
Heart
Sk. Muscle
Spleen
Testes
Liver
Lung
20X
10X

Figure 5.3. Basal adipose tissue defects in male mir378KO mice.

(**A**) mir378KO mice exhibit less WAT and BAT than WT mice. Photographs of inguinal WAT (iWAT) and BAT from male mice. (**B**) Electron microscopy of BAT reveals defects in lipid droplet integrity in mir378KO mice. (**C**) Mitochondrial DNA content. (**D**) BAT of mir378KO mice displays a reduction in gene expression of key genes responsible for BAT function, as determined by qRT-PCR. Arbp was used as an internal control. n = 5. Unpaired student's t test was used for evaluation of statistical significance. *P< 0.05, **P< 0.01.

Figure 5.3

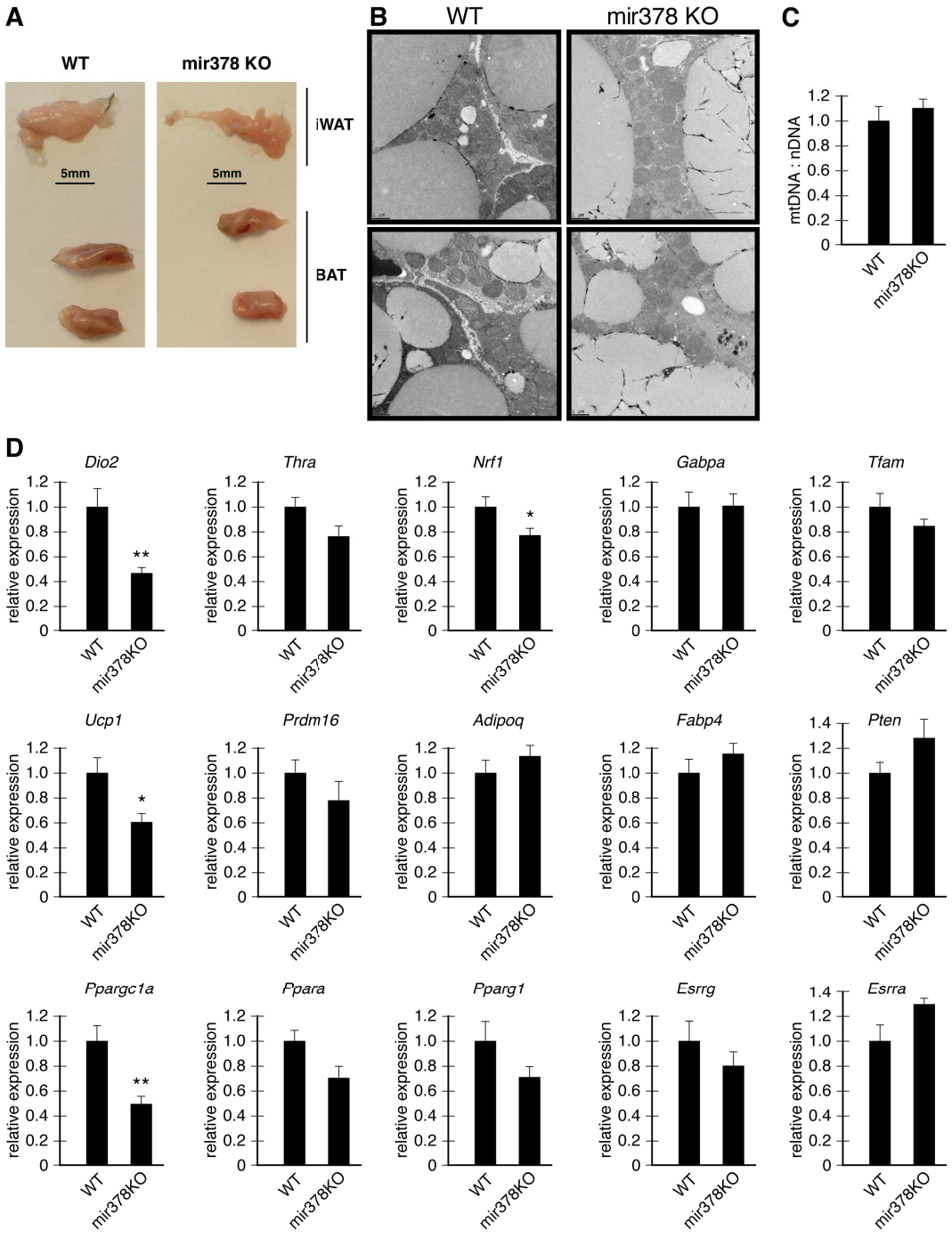
A
WT
mir378 KO
5mm
5mm
iWAT
BAT
B
WT
mir378 KO
C
mtDNA : nDNA
WT
mir378KO
D
Dio2
Thra
Nrf1
Gabpa
Tfam
Ucp1
Prdm16
Adipoq
Fabp4
Pten
Ppargc1a
Ppara
Pparg1
Esrrg
Esrra
relative expression
WT
mir378KO

Figure 5.4. Adipose and cardiac tissue analysis of female WT and mir378KO mice.

(**A**) Histological analysis of BAT from female mice. H&E staining. Images at 20X magnification. (**B**) Histological analysis of WAT from female mice. H&E staining. Images at 20X magnification. (**C**) Histological analysis of the heart of female mice. H&E staining. Images at 20X (top panels) and 1.8X (bottom panels) magnification. (**D**) BAT of female mir378KO mice displays different gene expression defects than male mice, as determined by qRT-PCR. Arbp was used as an internal control. WT, n = 4; mir378KO, n = 3. Unpaired student's *t* test was used for evaluation of statistical significance.

Figure 5.4

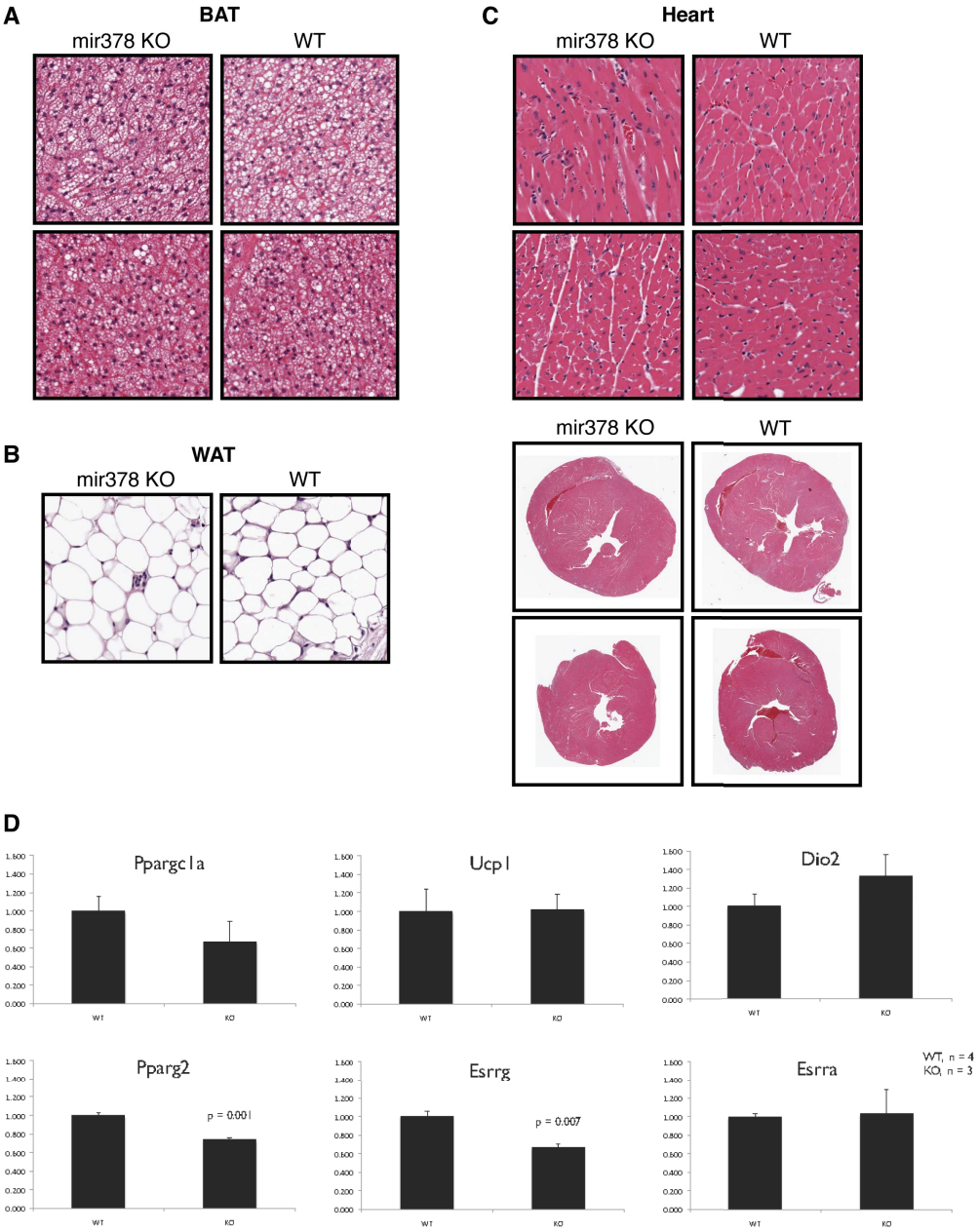
A
BAT
mir378 KO
WT
B
WAT
mir378 KO
WT
C
Heart
mir378 KO
WT
mir378 KO
WT
D
Ppargc1a
Ucp1
Dio2
Pparg2
p = 0.001
Esrrg
p = 0.007
Esrra
WT, n = 4
KO, n = 3
WT
KO

CHAPTER VI: General Discussion

The PGC-1/ERR pathway has been established as a major regulatory pathway controlling metabolic gene expression. However, the metabolic function of this pathway in breast cancer was largely unknown. At the start of this thesis work, miRNA discovery was relatively new and, therefore, very little was known about miR-378* function. Furthermore, nothing was known about miRNA regulation of the PGC-1/ERR pathway.

The general goal of this thesis was to elucidate the role of the PGC-1/ERR pathway in breast cancer cell metabolism. Establishing the direct link between miR-378* and this pathway early on motivated the study of these novel molecular relationships.

6.1 miR-378* fine-tuning of the Warburg effect and the PGC-1/ERR pathway

In Chapter II, we identified a direct molecular link between PGC-1β and ERRγ, miR-378*, which allowed us to uncover a relevance to the metabolic function of both ERR and miR-378* in breast cancer cells. This work identified that a miRNA is capable of inducing the Warburg effect, thereby becoming one of the first examples of miRNA involvement in cancer cell metabolism. Furthermore, this is the first study to implicate the ERRs directly in cancer cell metabolism. The specificity of action of miR-378* on ERRγ but not on ERRα established an important functional difference between ERR isoforms in the same context and conditions. Furthermore, only PGC-1β and not PGC-1α contains an intronic miRNA, the mir-378 hairpin, the relevance of which for PGC-1 biological function had, until this work, not been investigated. The careful elucidation of these molecular relationships in Chapter II, while expanding the understanding

of the PGC-1/ERR pathway, simultaneously hightlights the complexity of nuance of metabolic regulation in cancer cells.

In fact, ERRγ not only binds the same regulatory sites as ERRα within target promoters but also can do so as both homo- or heterodimeric species with ERRα (Dufour et al., 2007a). Therefore, the repertoire of ERRγ direct target genes is essentially the same as that of ERRα in the tissue studied to date, the mouse heart (Alaynick et al., 2007a; Dufour et al., 2007a) and, in Chapter II, human breast cancer cells. However, we have shown in Chapter II that, in the same biological context, ERRα and ERRγ regulate the expression of many genes in the TCA cycle in different manners. In the context of human breast cancer cells, ERRα contributes to the suppression of oxidative metabolism which is simultaneously promoted by ERRγ. This is supported by later work in Drosophila demonstrating that the ortholog of the ERR family of nuclear receptors directs a metabolic transition during development supporting a proliferative program essential for developmental growth of the organism, thus indicating that ERR regulation of a metabolic shift is broadly conserved (Tennessen et al., 2011). Taken together, our work in Chapter II suggests a level of mechanistic complexity in ERR regulation of OXPHOS which was previously predominantly unexplored at the molecular level.

A technical note about the miRNA detection methods applied throughout this and the subsequent data chapters: the work in this thesis utilized Applied Biosystems Taqman miRNA detection assays for the detection of relative expression levels of miR-378* and miR-378. These assays were the most well-established assays commercially available at the time of assay optimization during the work of this thesis. Furthermore, in order to be able to compare results from different conditions as directly as possible, once chosen as the method of detection and considering the absence of indications that the assay chosen was problematic (it remains consistently used in miRNA literature), there was an inherent value in continuing to use the same detection techniques throughout the work of

this thesis. The Taqman miRNA detections assays detect only mature miRNA (not the precursor), and do so with single-base discrimination. The miRNA-specific looped RT primer ensures that only the mature miRNA is reverse transcribed. A reporter dye system ensures specific product amplification. As miR-378* is currently considered a unique mature miRNA, with no other known miRNA bearing a similar sequence, Taqman probe miRNA detection specificity is unlikely to pose a problem for interpretation of data from such miRNA detection assays used to detect miR-378* levels. However, as miR-378 was discovered recently to have multiple varients in human and mouse differing in sequence by one to two nucleotides, Taqman probe specificity may be considered for this miRNA. The precise ability of the Taqman miRNA assays to distinguish between miRNA with sequences differing by only one or two nucleotides, such as miRNA in the the large let-7 family, alleviates the concern that the miR-378 assay (to detect miR-378a) may cross react with other miR-378 miRNA family members. Furthermore, Figure 5.1E shows the detection of a complete loss of miR-378 expression as determined by Taqman miRNA assay. This result proves that the Taqman miR-378 (miR-378a) detection assay does not recognizes the other miR-378 family members, as they were not genetically deleted in this mouse model and should, therefore, still be expressed. Either all other miR-378s (b-d) are definitively not detected by this Taqman assay, corresponding to what is predicted based on the known assay specificity, and/or the other miR-378s are not expressed at all in the brown adipose tissue. In the latter case, this would implicate miR-378 (miR-378a) as the only functional miR-378 in the brown adipose tissue. This itself would be an important functional finding. Using Taqman assays to detect miR-378b-d in these samples would resolve the ambiguity between these two potential explanations.

On a similar technical note, *in-situ* hybridization in Chapter II was performed using Exiqon double-DIG labeled Locked Nucleic Acid (LNA) probes. First, Exiqon LNA probes have been well established across

multiple applications to be highly specific between different miRNA of similar sequences including those with one or two nucleotide differences in sequence. Moreover, this robust sequence specificity allows these LNA probes to be used commercially for the detection of SNPs. Second, the methylene bridge of the LNA constrains the conformation of the probe, resulting in more rapid and increased stability, and correspondingly enhanced affinity, of the resulting duplex with its target. The double-DIG label (on both the 5' and 3' ends of the *in-situ* hybridization LNA probe) combined with the probe-specific Tm confers further specificity for the mature miRNA target and minizes the noise from nonspecific background. Finally, the work in Chapter II applied LNA probes to detect miR-378* by *in-situ* hybridization, and while miR-378 was discovered recently to have multiple variants in human, miR-378* is still considered a unique mature miRNA which originates only from one region of the genome. This fact, combined with the sequence sensitivity of the LNA technology, provides great confidence that the results presented in Chapter II are in fact based on specific detection of mature miR-378* in breast cancer tissue.

Finally, the specificity of small RNA probes and the importance of sequence precision for miRNA function also pertain to the gain- and loss-of-function experiments carried out in Chapters II and III. While these chapters study the function of miR-378* predominantly in human cells where there are, as of recently, 11 miR-378 paralogs with similar but distinct sequences, miR-378* is unique within the human genome. Furthermore, the miRNA mimics and inhibitors used to modulate miR-378* levels are highly specific tools (as discussed above). Taken together, the molecular and biological effects observed in response to experiments applying these tools certainly reveal the effects of specifically miR-378* and not miR-378 which, regardless of its paralogs, is composed of a completely different sequence than miR-378*.

6.2 miR-378* directly links the ERR and AMPK pathways

Chapter III links the PGC-1/ERR pathway, through miR-378*, to AMPK pathway activity. While a relationship between ERRα and AMPK has been established in the cardiac context, where there is indication of a feedback loop such that ERRα acts upstream of AMPK activity (Dufour et al., 2007a) and vice versa (Hu et al., 2011), a direct molecular mechanism explaining these functional responses has yet to be established. Interestingly, we found that miR-378* functions to simultaneously target ERRγ and AMPK pathway activity (through CAMKK2), directly linking these two important metabolic pathways in breast cancer cells and expanding the breadth of miR-378* function in cancer cell metabolism. While these results do not explain the established link between ERRα and AMPK in the heart, they do raise several interesting points. First, it would be interesting to understand why, in a breast cancer context, CAMKK2 rather than the established tumor suppressor, LKB1, is the mechanism through which oncogenic miR-378* regulates AMPK pathway activity. Such mechanistic specificity is interesting, especially in that it is reminiscent of the ERR isoform targeting specificity exhibited by miR-378*. Considering, as we have uncovered in Chapter II, that miR-378* targeting of ERRγ and not ERRα has important metabolic functional consequences, it is tempting to speculate that miR-378* specific targeting of CAMKK2 and not LKB1 may have similarly important biological consequences for breast cancer cell metabolic function.

6.3 AMPK is inhibited by breast cancer oncogenes

Second, considering that we have established that miR-378* functions downstream of the breast cancer oncogene ERBB2 and that

miR-378* expression increases with breast cancer progression in the human disease, it is natural to consider miR-378* as an oncogenic miRNA in breast cancer. By extension, its negative regulation of ERRγ provides further evidence that ERRγ expression correlates with good prognosis, an observation which had remained largely unexplained (Ariazi et al., 2002b). Similarly, negative regulation of AMPK activity by miR-378* in a breast cancer cell context links AMPK activity with breast cancer. While the role of LKB1 as an *in-vivo* tumor suppressor has clearly established a role for AMPK pathway activity in cancer (Ollila and Makela, 2011), relevance of this pathway in breast cancer is currently less clear. Therefore, the placement of AMPK downstream of oncogenic miR-378* strengthens the link between this important metabolic pathway and breast cancer and, by extension, even suggests a link between AMPK and ERBB2. It is not yet clear if AMPK levels are modulated in a biologically-relevant manner in breast cancer, so the link between ERBB2, miR-378* and the AMPK pathway identified is Chapters II and III of this thesis may be a valuable indicator that AMPK levels could be misregulated in breast cancer just as it could guide investigators toward the proper breast cancer subtypes to investigate such hypotheses. Functionally, it makes sense that oncogenic signalling would inactivate AMPK activity. This would allow cells to escape the control of cell growth exerted by AMPK, as AMPK functions to activate catabolic energy-generating pathways while turning off biomass-generating anabolic pathways which support cancerous cell proliferation (Hardie, 2011). It will be exciting to follow the discoveries to come about AMPK in breast cancer cell metabolism. It is clear from the work of this thesis that regulation of the AMPK pathway by miR-378* is a relevant part of such study which should not be neglected. Furthermore, the total and conditional knockout mouse models generated in Chapter V could prove to be valuable tools with which to study and validate AMPK pathway function in tumorigenesis including ERBB2-induced models of mammary tumorigenesis.

6.4 Metabolic pathway fine-tuning extends to post-translational modifications

Third, the indication from our metabolomics data that the mir-378 hairpin reduces the availability of products necessary for O-GlcNAcylation raises interesting ideas about the extent of mir-378 function. It is possible that, in such, the mir-378 hairpin is capable of regulating post-translational modification. As discussed in Chapter III, there are multiple avenues through which mir-378 could affect the O-GlcNAc pathway. miR-378* may directly target OGT, the enzyme responsible for transferring the glucose-containing moiety onto target proteins. Or, considering that the AMPK pathway has been implicated as an upstream regulator of the O-GlcNAc pathway, miR-378* control of AMPK pathway activity may contribute to the explanation. It is also possible that the mir-378 hairpin functions through an entirely different mechanism, perhaps through control of ERRγ or other factors upstream of this pathway. All of these possibilities require further investigation.

Considering that the O-GlcNAc pathway relies on available cellular glucose to be shuttled away from glycolysis in order to be utilized in this post-translational modification pathway, it seems reasonable that the mir-378 hairpin, already identified by our work to precisely regulate the balance between metabolic pathways, could be implicated in regulating the balance between glucose-utilizing pathways. Importantly, the metabolomics results were obtained from cells grown in high-glucose media. As such, and considering the absence of differences in cellular glucose levels observed by metabolomics, this suggests that the mir-378 hairpin regulates the hexosamine biosynthesis pathway in a manner independent of nutrient availability signals. However, nutrient availability is a major component of breast cancer cell growth *in-vivo*, and it will, therefore, be necessary and interesting to study the relationship between

the mir-378 hairpin and the O-GlcNAc pathway *in-vivo* and outside of the context of excess glucose availability. It will be quite exciting to better understand the relationships between this miRNA and these metabolic pathways, including the novel idea that the mir-378 hairpin can regulate metabolite-based post-translational modification. These ideas are yet another reminder of the delicate complexity of metabolic regulation in cancer.

6.5 *In-vivo* cancer metabolism

Chapters IV and V rely on mouse model approaches to study ERR and the mir-378 hairpin *in-vivo*, undertaken with the ultimate goal of better understanding the metabolic roles of these molecules in cancer. Studying the ERRα-/- mouse model in the background of mammary tumorigenesis allowed us to identify an unexpected component of metabolic function in cancer progression; the relevance of ERRα in resisting the onset of cancer cachexia. This observation leads to several important conclusions. First, the idea that ERRα is implicated in cachexia is entirely new. Considering the established metabolic function of ERRα, and that cachexia is a disease of metabolic derangements, in hindsight, which is always 20/20, it seems logical that ERRα could be implicated in this disease. However, to observe unexpectedly and first-hand the wasting of these animals throughout disease progression in contrast to their plump wildtype counterparts was quite a striking event. Second, the extension of the idea that a metabolic regulator such as ERR is necessary for resistance to cachexia suggests that ablation or inhibition of other metabolic regulators may also be important components of cachexia. By extension, animal models for these factors may also prove to be useful tools for studying this disease. Third, with these results we have identified what is perhaps one of the first genetic-based models of cancer cachexia. While disease onset in our model occurred at around 6 months of age and the duration of

disease progression was approximately 3 months, which is considered moderately aggressive for a genetic model, it is actually rather slow in comparison with the available cachexia models where aggressive cancer cells are injected into mice that reach disease endpoint approximately 6 weeks later. There are several major benefits to a genetic model of cachexia, including the ability to study less aggressive forms of the disease and without the necessity to inject foreign material. Foremost, this disease has been notoriously difficult to study, as it is fundamentally systemic and, therefore, requires the use of *in-vivo* models, yet identification of appropriate mouse models has proven frustratingly limited. Therefore, the identification of successful mouse models of cancer cachexia such as ours is likely to prove very useful for the field. Finally, these results provide an important warning about the application of ERRα inhibitors in the treatment of breast cancer. While this protein acts as an oncogene at the onset of mammary tumorigenesis and would, therefore, be an appealing target for breast cancer therapies, our work suggests that the temporal application of systemic ERRα inhibitors should be considered with care.

There are also several questions remaining to be answered about the role of ERRα in this disease. First and foremost, it will be important to identify if the elevated inflammation originating at the site of the tumors is the cause of the cachexia induced by the absence of ERRα, or if the absence of this protein in metabolic tissues is at fault. This is an important question which could be answered using a classical model of cachexia such as the Lewis Lung Carcinoma cell model, where highly inflammatory cancer cells would be injected into mice of either wildtype or ERRα-/- genetic backgrounds. This type of experiment would induce cachexia in an ERRα-/- background but with equivalent levels of inflammation between the wildtype controls and the ERRα-/- mice of interest, and would provide valuable information about the contribution of ERRα-/--induced inflammation to the onset of cachectic symptoms. It would also be

interesting to identify the underlying mechanism behind the elevated inflammation in the ERRα-/- tumors. ERRα function in macrophages has already been established (Sonoda et al., 2007c), raising questions about the cell type origin of the elevated inflammation observed in the ERRα-/- tumors. Is there augmented recruitment of specific types of inflammatory cells in the ERRα-/- tumors? If so, which ones? And what is the underlying mechanism and explanation for this? Furthermore, the study on ERRα function in macrophages implicated PGC-1β in the explanation for the observed phenotype. Considering that we have proven that the mir-378 hairpin is co-expressed with PGC-1β, does this imply a function for the mir-378 hairpin in ERR-related immune response? Finally, it is noteworthy that the ERRα-/- mouse model studied in Chapter IV exhibited a major depletion in fat deposits in response to cancer progression, whereas the skeletal muscle was largely resistant to breakdown of a similar scale. ERR is known to have an important role in both fat and muscle, raising questions about why ERRα-/- adipose tissue is so much more vulnerable to the systemic effects of cancer than ERRα-/- skeletal muscle of the same animals. While several interesting questions remain, it is clear that our study in Chapter IV has identified a novel and clinically-relevant compenent to ERRα function in breast cancer.

Chapter V was originally undertaken to generate a mir-378 mouse model that could be used to study the *in-vivo* role of this miRNA in breast cancer. The conditional knockout mouse model generated in Chapter V will be a valuable tool for studying mir-378 hairpin function in breast cancer, as it will allow for the specific deletion of the mir-378 hairpin from mammary epithelial cells when crossed to MMTV-driven models of mammary tumorigenesis. While extremely powerful and interesting, these experiments are very long-term, especially considering the necessity to backcross our new mouse line to pure FVB background in order to study it in combination with a model of mammary tumorigenesis. Therefore, in the meantime, considering the absence of *in-vivo* information about the mir-

378 hairpin and our knowledge about its importance in metabolic function, we chose to study the basal phenotypes of the mir-378 hairpin total knockout mouse model. This allowed us to identify basal adipose phenotypes, particularly in the brown adipose tissue, as well as gender-specific cardiac phenotypes. These observations correspond to the known functions of the host gene, PGC-1β, placing even more relevance on the teamwork between these two molecules. It will be fascinating to uncover the *in-vivo* fine-tuning relationships between mir-378 and its host gene. Recent evidence from other groups which was reviewed above has also implicated mir-378 in adipocyte and cardiac function. Therefore, it is clear that our mouse models generated in Chapter V will be valuable tools for the precise elucidation of the functions of the mir-378 hairpin in each tissue and disease context in which it will be studied.

CONCLUSION

We have contributed extensively to the understanding of the ERR/PGC-1 pathway, including the identification of a role for this pathway in breast cancer cell metabolism. We have, furthermore, uncovered that the role of ERR in breast cancer extends beyond the primary tumor and, in fact, also contributes to the systemic response to disease burden. By identifying the relationship of miR-378* to the PGC-1/ERR pathway, we have expanded the understanding of its molecular core. We have also contributed greatly to the understanding of miR-378* function by identifying three direct targets and several biological functions in normal and disease physiology, as well as by generating two mouse models which will allow for further elegant study of this interesting small molecule.

REFERENCES

Ariazi, E.A., Clark, G.M., and Mertz, J.E. (2002). Estrogen-related receptor alpha and estrogen-related receptor gamma associate with unfavorable and favorable biomarkers, respectively, in human breast cancer. Cancer research *62*, 6510-6518.

Dufour, C.R., Wilson, B.J., Huss, J.M., Kelly, D.P., Alaynick, W.A., Downes, M., Evans, R.M., Blanchette, M., and Giguere, V. (2007). Genome-wide orchestration of cardiac functions by the orphan nuclear receptors ERRalpha and gamma. Cell metabolism *5*, 345-356.

Hardie, D.G. (2011). AMP-activated protein kinase: an energy sensor that regulates all aspects of cell function. Genes & development *25*, 1895-1908.

Hu, X., Xu, X., Lu, Z., Zhang, P., Fassett, J., Zhang, Y., Xin, Y., Hall, J.L., Viollet, B., Bache, R.J.*, et al.* (2011). AMP activated protein kinase-alpha2 regulates expression of estrogen-related receptor-alpha, a metabolic transcription factor related to heart failure development. Hypertension *58*, 696-703.

Ollila, S., and Makela, T.P. (2011). The tumor suppressor kinase LKB1: lessons from mouse models. J Mol Cell Biol *3*, 330-340.

Sonoda, J., Laganiere, J., Mehl, I.R., Barish, G.D., Chong, L.W., Li, X., Scheffler, I.E., Mock, D.C., Bataille, A.R., Robert, F.*, et al.* (2007). Nuclear receptor ERR alpha and coactivator PGC-1 beta are effectors of IFN-gamma-induced host defense. Genes & development *21*, 1909-1920.

Tennessen, J.M., Baker, K.D., Lam, G., Evans, J., and Thummel, C.S. (2011). The Drosophila estrogen-related receptor directs a metabolic switch that supports developmental growth. Cell metabolism *13*, 139-148.

CHAPTER VII: Contribution to Original Research

Chapter II

- I identified that the breast cancer oncogene ERBB2 promotes the expression of the *PPARGC1b* locus, and that the intronic miRNA, mir-378, is co-expressed with this transcript.
- I have shown that miR-378* directly targets ERRγ (but not ERRα) and GABPA and modulates the expression of metabolic genes in breast cancer cells in an ERR-isoform specific manner.
- I established that miR-378* induces the Warburg effect in mouse mammary and human breast cancer cells.
- I have shown that the expression of miR-378* correlates with the progression of human breast cancer.

Chapter III

- I identified that miR-378* directly targets CAMKK2, an upstream kinase of AMPK.
- I established that miR-378*, through its regulation of CAMKK2, represses AMPK pathway activity in breast cancer cells.
- I identified that the mir-378 hairpin causes a reduction in UDP-GlcNAc levels, the glucose-derived metabolite used as a substrate for O-GlcNAc post-translational modification of proteins, implicating mir-378 in the regulation of post-translational modification.

Chapter IV

- I observed that the absence of ERRα in a mouse model of ERBB2-induced mammary tumorigenesis delays tumor onset but accelerates disease progression after onset.

- I quantified that tumor-bearing ERRα-/- mice fail to maintain the normal progression of body weight observed in ERRα+/+ animals.
- I found that tumors from ERRα-/- mice exhibited elevated levels of inflammation.
- I identified metabolic derangements in the serum, skeletal muscle and adipose tissue of tumor-bearing ERRα-/- mice.
- Taken together, these observations led me to conclude that the absence or pharmacological inhibition of ERRα predisposes the host to cancer cachexia.

Chapter V

- I generated two mir-378 mouse models, a total knockout and a conditional knockout model.
- I screened 8 tissues for phenotypes and identified basal differences in WAT, BAT and Spleen weight in the mir-378 total knockout mice.
- I identified basal BAT phenotypes by histology, electron microscopy, and gene expression analysis, suggesting an *in-vivo* role for mir-378 in thermogenesis.

APPENDIX I

Figure A.2.1. miR-378* does not significantly affect mitochondrial content.

BT-474 cells were analyzed by FACS analysis for mitochondrial content after staining with MitoTracker dyes as indicated. Results from non-stained cells are shown in **A-C**, and results from cells stained simultaneously with MitoTracker Red and Green (co-stained) are shown in **D-E**. The effects of miR-378* (**A**), a miR-378* inhibitor (miR-378* inhib) (**B, D**) or siESRRG (**C, E**) on mitochondrial content are shown, as compared to transfection with a miRNA Mimic control, a miRNA inhibitor control or a scramble siRNA, respectively.

Figure A.2.1

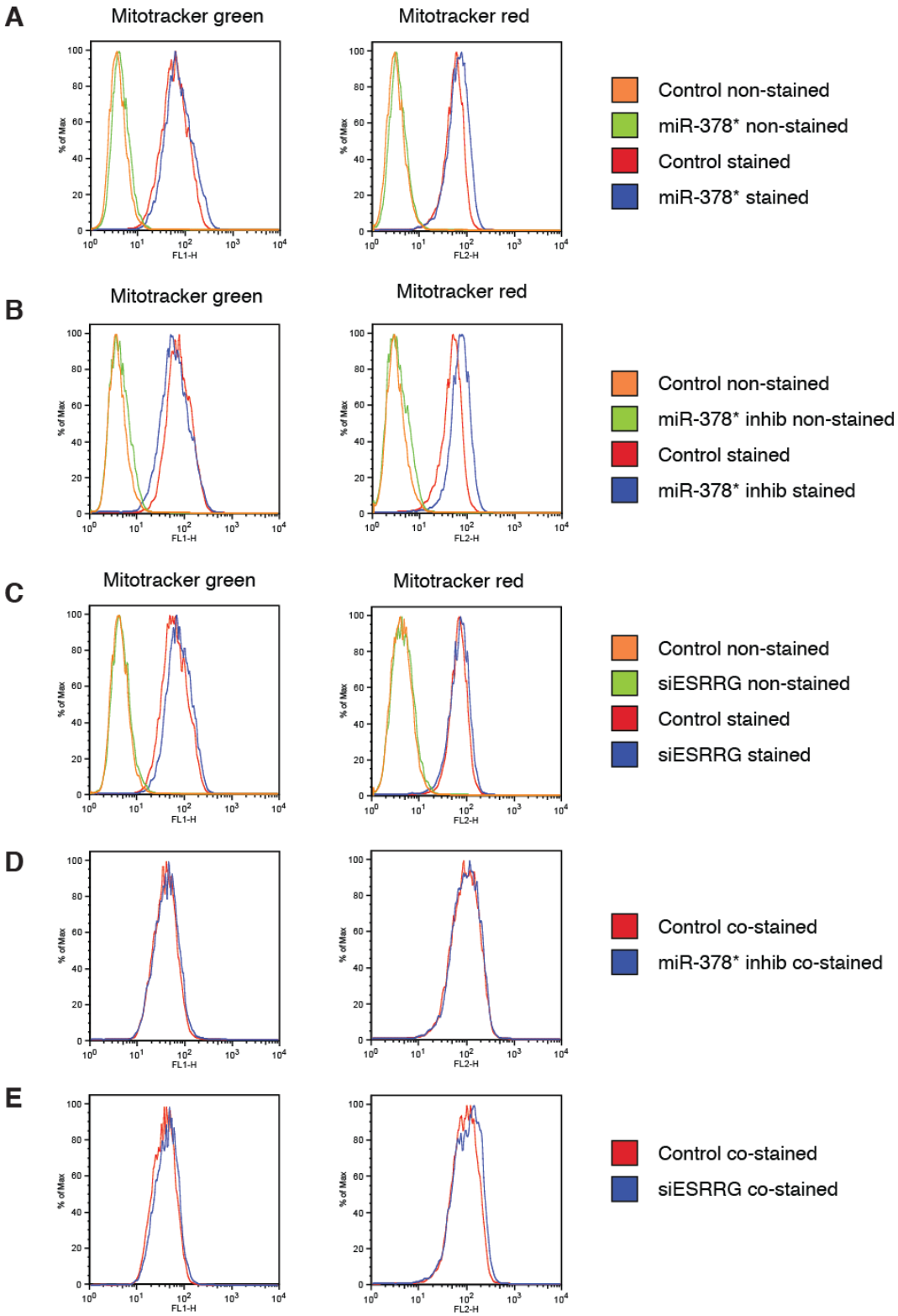
A
Mitotracker green
Mitotracker red
% of Max
FL1-H
FL2-H
Control non-stained
miR-378* non-stained
Control stained
miR-378* stained
B
Mitotracker green
Mitotracker red
Control non-stained
miR-378* inhib non-stained
Control stained
miR-378* inhib stained
C
Mitotracker green
Mitotracker red
Control non-stained
siESRRG non-stained
Control stained
siESRRG stained
D
Control co-stained
miR-378* inhib co-stained
E
Control co-stained
siESRRG co-stained

Figure A.2.2. Genes regulating the glutamine pathway are largely unaffected by miR-378*.

mRNA expression analysis of glutamine pathway genes in BT-474 cells in response to transient transfection of miR-378* (**A**) or a miR-378* inhibitor (**B**) as compared to a control miRNA Mimic or a miRNA inhibitor control, respectively, as determined by qRT-PCR and normalized to *TUBA1A* and *18S* internal controls. *P<0.05.

Figure A.2.2

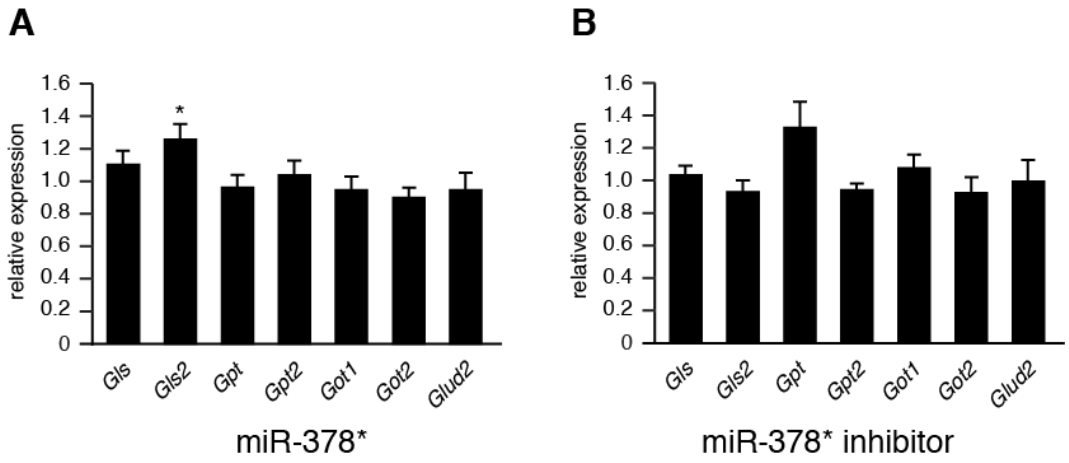
A
B
relative expression
1.6
1.4
1.2
1.0
0.8
0.6
0.4
0.2
0
*
Gls
Gls2
Gpt
Gpt2
Got1
Got2
Glud2
miR-378*
miR-378* inhibitor

Table A.2.1. Primers used for cloning miR-378* target regions into a luciferase reporter

Legend:

Bolded lower-case letters are restriction sites (Xba1) added for cloning.

Underlined upper-case letters are the miR-378* seed sequence target site.

Underlined and bolded upper-case letters are the mutated bases within the miR-378* target regions.

Numbers refer to the position of the base within the target gene's 3'UTR (1 is the first (5') base in the 3'UTR), and indicate the start of the miR-378* seed sequence region within the target 3'UTR.

"Mutb4" indicates that the 4th base in the miRNA target region seed sequence was mutated.

Primers are indicated following the model:

Gene 3'UTR position #

Forward (F) primer

Reverse (R) primer

Human primers used for cloning the miR-378* target regions into a luciferase reporter:

ESRRG 3'UTR position 1310

F-***ctaga***ACTGCACATGAGATATAGATCCGTAGAATTGTCAGGAGTGCACCTCTCTACTTG***t***

R-***ctaga***CAAGTAGAGAGGTGCACTCCTGACAATTCTACGGATCTATATCTCATGTGCAGT**t**

ESRRG 3'UTR position 1310 mutb4

F-**ctaga**ACTGCACATGAGATATAGATCCGTAGAATTGTCA**T**GAGTGCACCTCTCTACTTG**t**

R-**ctaga**CAAGTAGAGAGGTGCACTC**A**TGACAATTCTACGGATCTATATCTCATGTGCAGT**t**

ESRRG 3'UTR position 2011

F-***ctaga***GAATTAGAGACAATATTGGATGTACAATTCCTCAGGAGACTACAGTAGTATATT***t***

R-**ctaga**AATATACTACTGTAGTCTCCTGAGGAATTGTACATCCAATATTGTCTCTAATTC**t**

ESRRG 3'UTR position 2011 mutb4

F-***ctaga***GAATTAGAGACAATATTGGATGTACAATTCCTCA**T**GAGACTACAGTAGTATATT***t***

R-**ctaga**AATATACTACTGTAGTCTC**A**TGAGGAATTGTACATCCAATATTGTCTCTAATTC**t**

GABPA 3'UTR position 250

F-***ctaga***GAAGGCAGGTTCATTGTGGAATAGTTTAACAGTCAGGAAGGCTAAACTGGTCAG***t***

R-**ctaga**CTGACCAGTTTAGCCTTCCTGACTGTTAAACTATTCCACAATGAACCTGCCTTC**t**

GABPA 3'UTR position 250 mutb4

F-***ctaga***GAAGGCAGGTTCATTGTGGAATAGTTTAACAGTC**C**GGAAGGCTAAACTGGTCAG***t***

R-**ctaga**CTGACCAGTTTAGCCTTCC**G**GACTGTTAAACTATTCCACAATGAACCTGCCTTC**t**

Mouse primers used for cloning the miR-378* target regions into a luciferase reporter:

Esrrg 3'UTR position 2025

F-***ctaga***AGAATTAGAGACAGTATTGGATGTATACTTCCTCAGGAGACTACAGTAGTATAT***t***

R-***ctaga***ATATACTACTGTAGTCTCCTGAGGAAGTATACATCCAATACTGTCTCTAATTCT*t*

Esrrg 3'UTR position 2025 mutb4

F-***ctaga***AGAATTAGAGACAGTATTGGATGTATACTTCCTCA**T**GAGACTACAGTAGTATAT***t***

R-***ctaga***ATATACTACTGTAGTCTC**A**TGAGGAAGTATACATCCAATACTGTCTCTAATTCT***t***

Esrrg 3'UTR position 3074

F-***ctaga***TTTCCAGCAAGACCGTTTAGTTAATGCCAGCTGTCAGGAAGATACCAAGGTGTA***t***

R-***ctaga***TACACCTTGGTATCTTCCTGACAGCTGGCATTAACTAAACGGTCTTGCTGGAAA***t***

Esrrg 3'UTR position 3074 mutb4

F-***ctaga***TTTCCAGCAAGACCGTTTAGTTAATGCCAGCTGTC**C**GGAAGATACCAAGGTGTA***t***

R-***ctaga***TACACCTTGGTATCTTCC**G**GACAGCTGGCATTAACTAAACGGTCTTGCTGGAAA***t***

Esrrg 3'UTR position 3704

F-***ctaga***TTCAGATATGTAACTCAAATTATTATGCCTTTCAGGAGGATGGTAGAACAATAT***t***

R-***ctaga***ATATTGTTCTACCATCCTCCTGAAAGGCATAATAATTTGAGTTACATATCTGAA***t***

Esrrg 3'UTR position 3704 mutb4

F-***ctaga***TTCAGATATGTAACTCAAATTATTATGCCTTTCA**T**GAGGATGGTAGAACAATAT***t***

R-***ctaga***ATATTGTTCTACCATCCTC**A**TGAAAGGCATAATAATTTGAGTTACATATCTGAA***t***

Gabpa 3'UTR position 250

F-***ctaga***AGAGCAGGTTCATCGGGGTAGTTTGCTAACAGTCAGGAAAGCTAAACTGGTCAG***t***

R-***ctaga***CTGACCAGTTTAGCTTTCCTGACTGTTAGCAAACTACCCCGATGAACCTGCTCT***t***

Gabpa 3'UTR position 250 mutb4

F-***ctaga***AGAGCAGGTTCATCGGGGTAGTTTGCTAACAGTC**C**GGAAAGCTAAACTGGTCAG***t***

R-***ctaga***CTGACCAGTTTAGCTTTCC**G**GACTGTTAGCAAACTACCCCGATGAACCTGCTCT***t***

Table A.2.2. Primers Used for Real-Time PCR on Chromatin IP Samples

Short name	Full gene name	Primer sequence	
Negative control region located 4 kb upstream of the ESRRA start site		GTGGCCCACAGGTGTCGCTCAAGTCTTC	F
		GGATGCAGTGTCCTTCTCCCCCAGATTG	R
CS	citrate synthase	TAGATTTTATTAGCCCACTTGTCC	F
		GCATGAATAAAGCAGCCAAGTGAG	R
ACO2	aconitase 2	CCAACTTCTCGTGTACCTGTCCCGGTTG	F
		CAAAAAGAAGAAAGAGGTGCCTCCGCTC	R
IDH1	isocitrate dehydrogenase 1	AGGACATGCAAACCCCAAGACCTG	F
		CAGTGCTGAGTGTACTCGGTGGGA	R
IDH3A	isocitrate dehydrogenase 3 alpha	TCTCCTTGACAGCTCAGATGCCAG	F
		TCATTTGCTATGTGACCTTGGGAA	R
IDH3B	isocitrate dehydrogenase 3 beta	GGGCGAAGGAGCGGAGAGTTTGTC	F
		ACCTCTCCATGCCCCAGGGTTCCC	R
OGDH	oxoglutarate (alpha-ketoglutarate) dehydrogenase	CTAGGCTGGAAGGAGTCCTGC	F
		GCTTAACCTTGCCAAAGAGAGCTGG	R
DLST	dihydrolipoamide S-succinyltransferase	GTTGAATGAGTTGACCTTGTTGTGGGCTTTC	F
		CAAGGCTTTTAAGCTCTCTTGTCTTGGGTTATG	R
SUCLA2	succinate-CoA ligase, ADP-forming, beta	CTGACCCAGCCCTTAGTCCG	F
		CTCAGCCCACCGTGCCAGAC	R
SDHB	succinate dehydrogenase complex, subunit B	GAGCATCCCTGTCAAGTTATCTTT	F
		AATGTCTGGATTCAAATTCTGGTT	R
SDHD	succinate dehydrogenase complex, subunit D	GGTTCACCCAGCATTTCCTCTTCC	F
		AAGACCCCTCACCTCGGCCTCCTA	R
FH	fumarate hydratase	CCAGCCGCAGCCTTAGCTTC	F
		GGAATCTCTCCCGCCAAGTC	R
MDH2	mitochondrial malate dehydrogenase	CATAGTATGGACAAACCGAGGCTA	F
		GCCAAGTCAAGCACTGTTAAGACA	R
LDHD	D-lactate dehydrogenase	GGGAGAGAAGAGAAGTCCTCTGGAGG	F
		CACTCTACACCCACCCACAGTTGCC	R
ESRRA	Estrogen-related	CCATCCGAGTGGAATTTGAGTCCTAAAG	F

	receptor alpha		
		GAACCGTAGACCCAGTAGCCCCACAGAG	R
GABPA	GA binding protein transcription factor, α	CGTTCTGCCTAAGTAGCCTAGACGCTCC C	F
		GGGCAACCCAAGGTCAGGC	R

Table A.2.3. RT-PCR Primers for human genes

Short gene name	Full gene name	Primer sequence	Primer type (F=forward R=reverse)
Figures 2.1 and 2.9:			
RPS18 (18S)	ribosomal protein S18	GATGGGCGGCGGAAAATAG	F
		GCGTGGATTCTGCATAATGGT	R
PPARGC1B	peroxisome proliferator-activated receptor gamma coactivator-1-β	CCAAGACCAGCAGCTCCTACGG	F
		AGTTGGGTCGCTTTGTGACAAG	R
PPARGC1B	peroxisome proliferator-activated receptor gamma coactivator-1β	GTACATTCAAAATCTCTCCAGCGACATG	F
		GAGGGCTCGTTGCGCTTCCTCAGGGCAG	R
Figures 2.2 and 2.9:			
RPLP0	ribosomal protein P0	TTAAACCCTGCGTGGCAATCC	F
		GCCCATCAGCACCACGACCTT	R
TUBA1A	α tubulin 1a	AACTTATCACAGGCAAAGAAGATG	F
		GCCATAATCAACTGAGAGACGTTC	R
RPS18 (18S)	ribosomal protein S18	GATGGGCGGCGGAAAATAG	F
		GCGTGGATTCTGCATAATGGT	R
ESRRA	estrogen-related receptor α	GCTGCCCTGCTGCAACTAGTG	F
		GCCGCCGCTCAGCACCCCCTC	R
ESRRB	estrogen-related receptor β	CCAAGAGGCAGCATGTGCATT	F
		GCTCTGATCCCTGCTTGTGAA	R
ESRRG	estrogen-related receptor γ	CTGGTAAAGAAATACAAGAGCATGAAGC	F
		CAGCATCTTGCCAGCTCGACGAGGGTCT	R
GABPA	GA binding protein transcription factor, α	GAACAACAGATGAATGAAATAGTTACAA	F
		CTAGCAAAAACTGCCATAGTTGGATTTG	R
Figures 2.4 and 2.9:			
TUBA1A	α tubulin 1a	AACTTATCACAGGCAAAGAAGATG	F
		GCCATAATCAACTGAGAGACGTTC	R
RPS18 (18S)	ribosomal protein S18	GATGGGCGGCGGAAAATAG	F
		GCGTGGATTCTGCATAATGGT	R
CS	citrate synthase	CAACTCAGGACGGGTTGTTCCAGG	F
		GTAGTAATTCATCTCCGTCATGCC	R

ACO2	aconitase 2	GATCCACGAGACCAACCTGAAGAA	F
		CCTTCATTCTGTTGAGGGCACTGC	R
IDH1	isocitrate dehydrogenase 1	ACCAATCCCATTGCTTCCATTTTT	F
		TCAAGTTTTCTCCAAGTTTATCCA	R
IDH3A	isocitrate dehydrogenase 3 alpha	ACATCCTTAGTGACTTGTGTGCAG	F
		GCATTGCCTCCCAAATCTTTTGTC	R
IDH3B	isocitrate dehydrogenase 3 beta	GATGTGCTTGTGATGCCCAATCTC	F
		GTGATACTCAAGATTAAGATGCCG	R
OGDH	oxoglutarate (α-ketoglutarate) dehydrogenase	AGATCATCCGTCGGCTGGAGATGG	F
		CTTCTCAGAGGACCACTTCCGCTG	R
DLST	dihydrolipoamide S-succinyltransferase	GTTCAGAACATCGGGAGAAAATGA	F
		GTTCCTGCAAGGCAAAGGCTGAGG	R
SUCLA2	succinate-CoA ligase, ADP-forming, beta	GGGCTGCTGCTCAGGTTCTGGGAAGTTC	F
		GTGCCTTTATCACGACATCTTTTGAACC	R
SDHB	succinate dehydrogenase complex, subunit B	CAGCTACTGGTGGAACGGAGACAA	F
		CCCTGGATTCAGACCCTTAGGACA	R
SDHD	succinate dehydrogenase complex, subunit D	CCACCATTCTGGCTCCAAGGCTGC	F
		CAGCTTTCTGCAAGGCATCCCCAT	R
FH	fumarate hydratase	CCATGTTGCTGTCACTGTCGGAGG	F
		CATACCCTATATGAGGATTGAGAG	R
MDH2	mitochondrial malate dehydrogenase	GCTCTGCCACCCTCTCCATG	F
		TTTGCCGATGCCCAGGTTCTTCTC	R
GABPA	GA binding protein transcription factor, α	GAACAACAGATGAATGAAATAGTTACAA	F
		CTAGCAAAAACTGCCATAGTTGGATTTG	R
HK2	Hexokinase 2	GCTGTGGTGGACAGGATACGAGAA	F
		CGCCGCCCCCTTCCCGCTGCCATC	R
LDHA	Lactate dehydrogenase A	GACCTACGTGGCTTGGAAGATAAGTGGT	F
		AATCTGGGTGCAGAGTCTTCAGAGAGAC	R
LDHB	Lactate dehydrogenase B	CTCATTGCACCAGTTGCGGAAG	F
		CATCCACAAGAGCAAGTTCATCAGC	R
LDHC	Lactate dehydrogenase C	GGACTGTCTGTGATGGATTTGGTAGG	
		GTGTTTCTGCACTCTTCTTGAAAAGGG	
LDHD	Lactate dehydrogenase D	CTTCCACTGCATCCTGCTGGTCAAC	F
		GGAACTTGTGGGCTAAGTGCTCAGACC	R

Figure A.2.2:

GLUD2	Glutamate dehydrogenase 2	GTACAGTGAAGCTGGTGTGACCTT	F
		TCTCCTTAACGGGCTGATTTGGAT	R
GLS	Glutaminase	TGCTGCATATACTGGAGATGTGTC	F
		TGTCCAAAGTGCAGTGCTTCATCC	R

GLS2	Glutaminase 2	TGGATATGGAACAGAAAGACTATG	F
		AAGCAGTTTGACCACCTCCAGATG	R
GPT	Glutamic-pyruvate transaminase	CGCAGTGCAGGTGGATTACTAC	F
		GAAGGCGAAGCGGATCACGG	R
GPT2	Glutamic-pyruvate transaminase 2	CAAAGCTGTGGAGGCTGCTCAGGC	F
		AGGAAGTTGATGTGGAAGTCTT	R
GOT1	Glutamic-oxaloacetic transaminase 1	GACAATAGCCTAAATCACGAGTATC	F
		CGCTAAGAAATCAGCTCCAATTCG	R
GOT2	Glutamic-oxaloacetic transaminase 2	ACAATGGCTGCAAGAAGTGAAAGT	F
		TTTTGTCATGTAGATGGAGAACTC	R

Table A.2.4. RT-PCR Primers for mouse genes

Short gene name	Full gene name	Primer sequence	
Figure 2.5:			
Arbp (Rplp0)	ribosomal protein, large, P0	GCAGCAGATCCGCATGTCGCTCCG	F
		GAGCTGGCACAGTGACCTCACACGG	R
Ppargc1b	peroxisome proliferator-activated receptor gamma coactivator-1-β	CAGCCAGTACAGCCCCGATG	F
		GGTGTGTCGCCTTCATCCAG	R
Esrrg	estrogen-related receptor γ	CTCCAGCACCATCGTAGAGGATC	F
		GATCTCACATTCATTCGTGGCTG	R
Gabpa	GA binding protein transcription factor, α	GGTGACGAGATGGGCTGCTGCACTGGAA	F
		CTTGGTTGAGACTACATAATTCTCTTCC	R
Cs	citrate synthase	GTGCCCAATATCCTCTTAGAGCAAGGGA	F
		CACACCCAGTGCCCGAGACACTCCAAAC	R
Fh1	fumarate hydratase	AGGCTACTGGGAGATGCTTCAGTGTCCT	F
		GTTTCCTTTAAGGTTGATCCGTTCTTGT	R
Sdhb	succinate dehydrogenase complex, subunit B	ACCCCTTCTCTGTCTACCGCTGCCACAC	F
		GTTGACAGGCACACTCAGCACGGACTGG	R
Figure 2.8:			
Ppargc1b exon 1, 2/3	peroxisome proliferator-activated receptor gamma coactivator-1-β	CTCTGACACGCAGGGTGGGGACTC	F
		ATTCTCACTGTCAATCTGGAAGAG	R
Ppargc1b exon 4, 5	peroxisome proliferator-activated receptor gamma coactivator-1-β	AGACCAGCCTCAGTTCCAGAAGTC	F
		ATCCTCCCCCACCTCCTCCTCCTC	R
Ppargc1b exon 7, 8	peroxisome proliferator-activated receptor gamma coactivator-1-β	CTTGGCAAGAAGAGCTTTGAGGAG	F
		TGGGGTGGCTGTGAGCGGAAGAGC	R

Figure A.3.1. *CAMKK2* mRNA is not affected by miR-378

(**A**) Transient transfection of naïve BT-474 cells with miR-378 inhibitor (miR-378-i) does not affect *CAMKK2* mRNA transcript level as compared to control inhibitor (ctrl-i).

Figure A.3.1

A

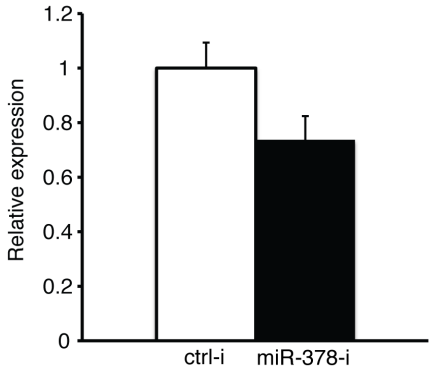

Table A.3.1. RT-PCR Primers

Short gene name	Primer sequence	Primer type (F=forward R=reverse)
RPS18 (18S)	GATGGGCGGCGGAAAATAG	F
	GCGTGGATTCTGCATAATGGT	R
PPARGC1B	CCAAGACCAGCAGCTCCTACGG	F
	AGTTGGGTCGCTTTGTGACAAG	R
ESRRG	CTGGTAAAGAAATACAAGAGCATGAAGC	F
	CAGCATCTTGCCAGCTCGACGAGGGTCT	R
CAMKK2	CACCCGAGTCGCTCTCTGAGAC	F
	CAGGTCCTTCAAGTC CTCAGCTATGT	R

Table A.3.2. Primers used for cloning miR-378* target regions into a luciferase reporter

Legend:

Underline indicates seed sequence

Italics indicates restriction site (Xba1)

Bold indicates mutated base within targeted seed region

Numbers refer to the position of the base within the target gene's 3'UTR (1 is the first (5') base in the 3'UTR), and indicate the start of the miR-378* seed sequence region within the target 3'UTR.

“Mutb4” indicates that the 4th base in the miRNA target region seed sequence was mutated.

Primers are indicated following the model:

Gene 3’UTR position #

Forward (F) primer

Reverse (R) primer

Human primers used for cloning the miR-378* target regions into a luciferase reporter:

CAMKK2 3’UTR position 597

F-*ctaga*AAGGATTTTTAAATTTTTTATGGGTAGAATTGTAGTCAGGAAAACAGAAAG*t*

R-*ctaga*CTTTCTGTTTTCCTGACTACAATTCTACCCATAAAAAATTTAAAAATCCTT*t*

CAMKK2 3’UTR position 597 mutb4

F-*ctaga*AAGGATTTTTAAATTTTTTATGGGTAGAATTGTAGTC**C**GGAAAACAGAAAG*t*

R-*ctaga*CTTTCTGTTTTCC**G**GACTACAATTCTACCCATAAAAAATTTAAAAATCCTT*t*

Figure A.4.1. Non-amino acid metabolites differentially regulated in serum and skeletal muscle of Neu ERRα-/- mice.

(**A**) Serum metabolite levels identified by metabolomics are expressed as fold from values obtained from Neu ERRα-/- mice normalized to values obtained from Neu WT mice. White bars indicate measurements from tumor-free mice, black bars represent data from tumor-bearing mice. n=4. (**B**) Skeletal muscle metabolite levels are expressed as fold from values obtained from Neu ERRα-/- mice normalized to values from Neu WT mice. n=5. Unpaired Student's *t* test was used for evaluation of statistical significance. *P< 0.05, **P< 0.01.

Figure A.4.1

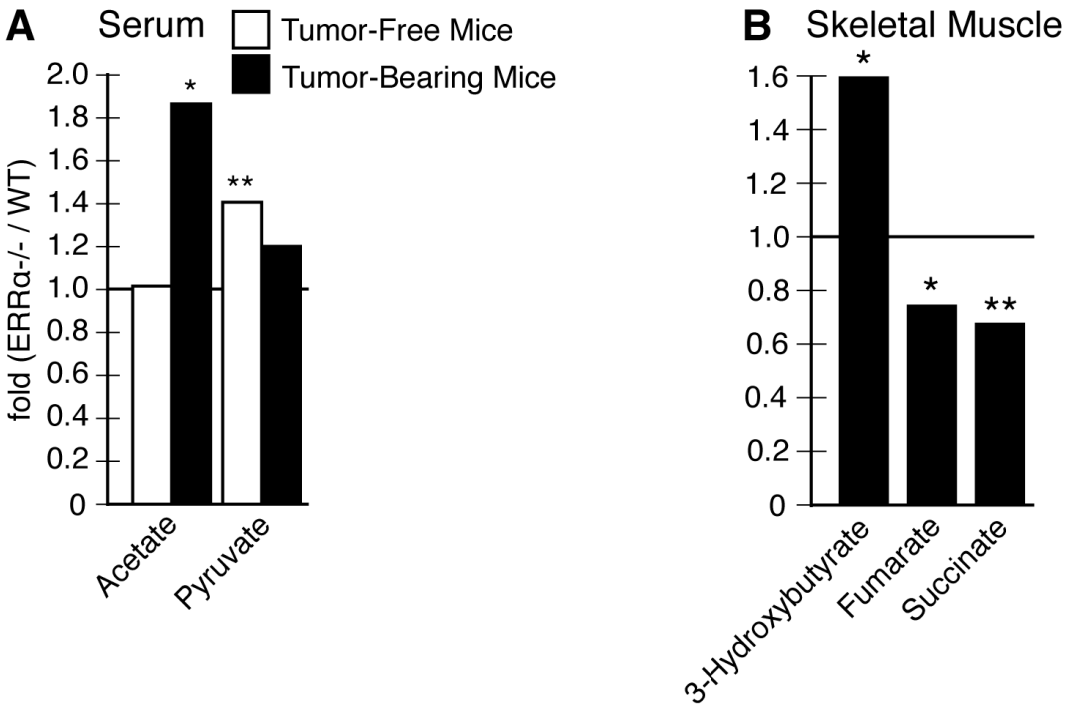
A
Serum
Tumor-Free Mice
Tumor-Bearing Mice
fold (ERRα-/- / WT)
2.0
1.8
1.6
1.4
1.2
1.0
0.8
0.6
0.4
0.2
0
*
**
Acetate
Pyruvate
B
Skeletal Muscle
1.6
1.4
1.2
1.0
0.8
0.6
0.4
0.2
0
*
*
**
3-Hydroxybutyrate
Fumarate
Succinate

Table A.4.1. RT-PCR Primers

Short gene name	Primer sequence	Primer type (F=forward R=reverse)
Arbp (Rplp0)	GCAGCAGATCCGCATGTCGCTCCG	F
	GAGCTGGCACAGTGACCTCACACGG	R
Hprt	GCCCCAAAATGGTTAAGGTT	F
	CAAGGGCATATCCAACAACA	R
Ifit1	GAGAGCAGAGAGTCAAGGCAGGTT	F
	TCTCACTTCCAAATCAGGTATGTC	R
Tnfsf9	CCAACACTACACAACAGGGCTCTC	F
	TGTGTTTGTGAATGTTGGACTGAG	R
Fos	TACGGACTCCCCACCCAGTCTGCT	F
	TGGCAATCTCAGTCTGCAACGC	R
Vegfa	ACCAAAGAAAGACAGAACAAAGCC	F
	CAAAGTGCTCCTCGAAGAGTCTCC	R
Irs2	GCCACAGTTCAGAGACCTTTTCCTC	F
	CCAGGGTACTGCTGCCTTCACTGC	R
Pik3c2g	CCCTGAATGAAGAGCTTTCCAAGGAG	F
	GGGTTCAGAGGAAGATGGCAAGTC	R
Atg10	CAGATAGGCGATGGCTGGGAATG	F
	CGTCACTTCAGAATCATCCATTGGTAGC	R
Becn1	GCTGGACAAGCTCAAGAAAACCAATG	F
	GCATGGAGCAGCAGCACTGTCTG	R
Bnip3	CAGCGTTCCAGCCTCCGTCTC	F
	GGTGTCTGGGAGCGAGGTGGG	R
Ctsf	GATGGCTCCACTCTTCAAGGACTTC	F
	GGTGATCCCATACTGAGCTGTGCC	R
Ctsl	GTCCTCTGCTTGGGAACAGCCTTAG	F
	CGTGCTGCCCGTTGCTGTATTC	R
Fbxo32	CACTGGTGCAGAGAGTCGGCAAGTC	F
	GGCAGGTCGGTGATCGTGAGG	R
Mstn	CACGGAAACAATCATTACCATGCCTACAG	F
	GAGTCTCAGGATTTGCACAAACACTGTTG	R
Cebpb	CAAGAAGACGGTGGACAAGCTGAG	F
	GAACAAGTTCCGCAGGGTGCTG	R
Fabp4	GATGCCTTTGTGGGAACCTGGAAGC	F
	GTGACCAAATCCCCATTTACGCTGATG	R
Lep	GCAGTGCCTATCCAGAAAGTCCAG	F
	GAGGACCTGTTGATAGACTGCCAGAG	R
Lepr	GTTCAGGAGTCTGGAGTGACTGGA	F
	GTTGGAGAAGGTAACTTTGCTAAC	R
Lpl	GGACACTTGTCATCTCATTCCTGG	F
	GCTGACACTGGATAATGTTGCTGG	R

Nrip1	GAACACATCCAGGAGGTGCG	F
	CATCATCTTTCGTTGCTCACC	R
Plin1	GTTCCTCCTGCCACCAGACAAG	F
	GGTGCTGACCCTCCTCACAAG	R
Gr	TCTGTATGAAAACCTTACTGCTTC	F
	AATTCAATACTCATGGACTTATCC	R
Cebpa	GCATCTGCGAGCACGAGACG	F
	CCTTCTCCTGCTGTCGGCTGTG	R
CD36	TTGCGACATGATTAATGGCACAGA	F
	CAAAGGCATTGGCTGGAAGAACAA	R
Klb	AGATCCGAAAGTACTACTTGGAGA	F
	GGCTGACCACACGCAGGACTTCTG	R

Figure A.5.1. Cardiac tissue analysis by electron microscopy of male WT and mir378KO mice.

Electron microscopy images at 8800X (top panels) and 19500X magnifications (bottom panels).

Figure A.5.1

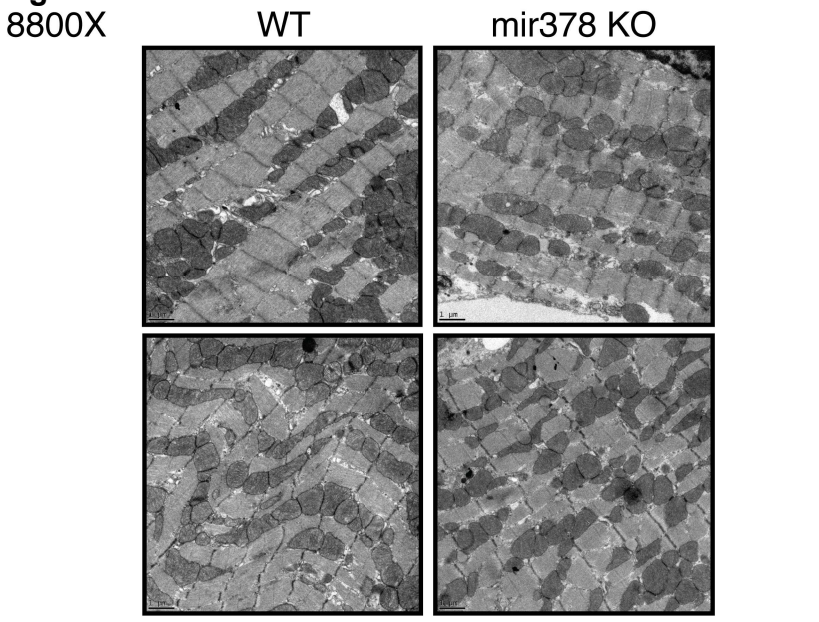

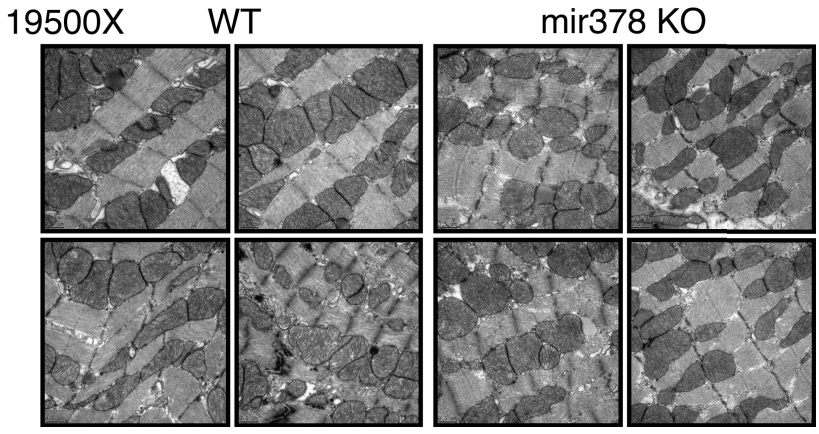

Table A.5.1. RT-PCR Primers

gene name	Primer sequence	Primer type (F=forward R=reverse)
Fig. 5.1B F1, R	CTGACTCCAGGTCCTGTGTGTTAC	F1
	GCCCTTTGCACATCAGACTTCAAG	R
Fig. 5.1B F2, R	ATCAGGATGATCTGGACGAAGAGC	F2
	GCCCTTTGCACATCAGACTTCAAG	R
Genotyping for Fig. 5.1C top panels, (f, r1)	CCACCCCCTTTTAACTTAATCACG	f
	GATGGAGAAACACGGCTGGAGAGT	r1
Genotyping for Fig. 5.1C lower panel, (f, r2)	GGGTGATCTTTGCCGGGCCAACTT	f
	CCTCTTCCCCAACTGTAAAATGAG	r2
Arbp (Rplp0)	GCAGCAGATCCGCATGTCGCTCCG	F
	GAGCTGGCACAGTGACCTCACACGG	R
Ppargc1b	CAGCCAGTACAGCCCCGATG	F
	GGTGTGTCGCCTTCATCCAG	R
Dio2	CATGCTGACCTCAGAAGGGCTG	F
	CTGAACCAAAGTTGACCACCAGTG	R
Thra	GCCAATGTCCCCTGAAAAGC	F
	GCAGCCCTCACAAGTGATACAGC	R
Nrf1	CCATGTAGCCACGTACACTGAGCACAG	F
	CGTTTCCGTTTCTTCCCTGTTGCCAC	R
Gabpa	GCACATTACGACCATTTCAGACGAGACC	F
	CTTGGGGACCGTTGCACTTTAGCTG	R
Tfam	CCAGGAGGCAAAGGATGATTCG	F
	CCAACTTCAGCCATCTGCTCTTCCC	R
Ucp1	CATCACCTTCCCGCTGGACAC	F
	CACACCTCCAGTCATTAAGCC	R
Prdm16	GGGTAGAAAAGCGGAAGGTGGC	F
	CTTCATGGCTGCAAAGCTCTCC	R
Adipoq	CGTGATGGCAGAGATGGCACTCC	F
	GCGATACACATAAGCGGCTTCTCC	R
Fabp4	GATGCCTTTGTGGGAACCTGGAAGC	F
	GTGACCAAATCCCCATTTACGCTGATG	R
Pten	GGCGGGAGGACAAGTTCA	F
	GGTTTCCTCTGGTCCTGG	R
Ppargc1a	CAGTCCTTCCTCCATGCCTG	F
	GGGTTTGTTCTGATCCTGTGG	R
Ppara	CGTTCTGTGACATCATGGAACCC	F
	GTGTCATCTGGATGGTTGCTCTGC	R
Pparg1	GAAAGAAGCGGTGAACCACTGATATTC	F
	CACAGAGCTGATTCCGAAGTTGGTG	R

Pparg2	GAGATTCTCCTGTTGACCCAGAGC	F
	GATGTCAAAGGAATGCGAGTGGTCTTC	R
Esrrg	CTCCAGCACCATCGTAGAGGATC	F
	GATCTCACATTCATTCGTGGCTG	R
Esrra	CCAGAGGTGGACCCTTTGCCTTTC	F
	CACCAGCAGATGCGACACCAGAG	R

APPENDIX II

Molecular and Genetic Crosstalks Between mTOR and ERRα are Key Determinants of Rapamycin-induced Non-Alcoholic Fatty Liver

Cédric Chaveroux[1], Lillian J. Eichner[1,5], Catherine R. Dufour[1,4], Aymen Shatnawi[1], Guillaume Bourque[4], Nahum Sonenberg[1,2] and Vincent Giguère[1,2,3,*]

[1]Rosalind and Morris Goodman Cancer Research Centre, McGill University, 1160 Pine Avenue West, Montreal, QC, H3A 1A3, Canada.
[2]Departments of Biochemistry, [3]Medicine and Oncology, [4]Human Genetics, McGill University, Montréal, PQ H3G 1Y6, Canada.
[5]These authors contributed equally to this work.

*Correspondence: vincent.giguere@mcgill.ca

Short title: ERRα/mTOR metabolic axis in liver

Keywords: ChIP-sequencing; estrogen related receptor; lipogenesis; metabolomics; TCA cycle; ubiquitin

Contact: Dr. Vincent Giguère
Email: vincent.giguere@mcgill.ca
Tel.: 514-398-5899

SUMMARY

mTOR and ERRα are key regulators of common metabolic processes, including lipid homeostasis. However, it is currently unknown whether these two factors cooperate in the control of metabolism. ChIP-sequencing analyses of mouse liver reveal that mTOR binds to regulatory regions of genes on a genome-wide scale, including enrichment at genes shared with ERRα that are involved in the TCA cycle and lipid biosynthesis. Genetic ablation of ERRα and rapamycin treatment, alone or in combination, alter the expression of these genes and induce the accumulation of TCA metabolites. As a consequence, both genetic and pharmacological inhibition of ERRα activity exacerbates hepatic hyperlipidemia observed in rapamycin-treated mice. We further show that mTOR regulates ERRα activity through transcriptional control of the ubiquitin-proteasome pathway and ubiquitin-mediated degradation of ERRα. Our work not only uncovers novel mechanisms of mTOR action in metabolism but highlights the existence of a potent mTOR/ERRα metabolic regulatory axis with significant clinical impact.

HIGHLIGHTS

- ChIP-sequencing reveals mTOR as a global transcriptional regulator of metabolic genes
- Identification of comprehensive ERRα/mTOR functional crosstalk in metabolic control
- Genetic or pharmacological inhibition of ERRα exacerbates the development of rapamycin-induced fatty liver
- mTOR controls ERRα activity via a ubiquitin/proteasome-dependent mechanism

INTRODUCTION

The mammalian target of rapamycin (mTOR), a phosphatidylinositol 3-kinase (PI3K)-related serine/threonine kinase, plays a major role in cell growth, proliferation and survival, in part by controlling mRNA translation (Averous and Proud, 2006; Heinz et al., 2010; Wullschleger et al., 2006). This kinase is strongly expressed in tissues with high-energy demands and its activity is closely linked to PI3K signaling (Willems et al., 2012). mTOR is the core component of two distinct complexes: mTORC1 (complex 1) and mTORC2 (complex 2). mTORC1 is considered to be a central integrator of a wide range of physiological cues such as amino acid levels, growth factors, energy status, genotoxic stress and oxygen levels in order to promote cellular growth and proliferation (Gulati and Thomas, 2007). The majority of these different stimuli (except amino acids) signals to mTORC1 through the modulation of Tuberous sclerosis complex 1 and 2 (TSC1/2) activity (Gulati et al., 2008; Laplante and Sabatini, 2012). mTORC1 is also the only complex sensitive to acute rapamycin treatment and has been shown to control protein synthesis via the S6 kinase/S6 axis and 4E-BP1 phosphorylation (Sonenberg and Hinnebusch, 2009).

At a physiological level, the mTORC1 signaling pathway has been described to play an important role in the control of energy metabolism, in particular, lipid biosynthesis (Inoki et al., 2012). This notion has emerged from observations of clinical trials involving rapamycin or rapalogs administration. Multiple well-known side-effects of these drugs have been

reported including the development of hyperlipidemia and hypercholesterolemia and activation of gluconeogenesis in liver, a major organ for lipid biosynthesis (Houde et al., 2010; Levy et al., 2006; Morrisett et al., 2002). Furthermore, rodents treated with rapamycin and rapalogs develop non-alcoholic fatty livers (NAFL) associated with elevated free fatty acid (FFA) levels (Patsenker et al., 2011; Pearce, 1983). It is thought that the mechanism by which inhibitors of mTOR generate an increase in lipogenesis involves of a multitude of factors that includes PPARγ, SREBP1 and/or lipin1 (Laplante and Sabatini, 2009; Peterson et al., 2011). These factors can interplay with each other to regulate the lipogenic gene program.

Aside from the well-established role of mTOR as a kinase in phosphorylation signaling cascades, recent studies show that mTOR can shuttle between the cytoplasm and nucleus and act as a direct transcriptional regulator of gene expression (Bachmann et al., 2006; Kim and Chen, 2000; Rosner and Hengstschlager, 2008; Walsh et al., 2012; Zhang et al., 2002). Standard chromatin immunoprecipitation (ChIP) studies revealed that mTOR is recruited to DNA and can interact with various transcription factors such as YY1 and MAF1 to modulate gene expression at a transcriptional level (Cunningham et al., 2007; Kantidakis et al., 2010). Although the first *de novo* mTOR target genes identified by standard ChIP were polymerase (pol) III-dependent genes, mTOR was later shown to also bind to the gene encoding dystrophin, a protein

associated with muscle integrity, and two genes encoding proteins involved in mitochondrial function, namely cytochrome C and the coactivator PGC-1α (Cunningham et al., 2007; Kantidakis et al., 2010; Risson et al., 2009; Shor et al., 2010; Tsang et al., 2010). Although these findings suggested a distinct mechanism by which mTOR could regulate energy metabolism, the limited number of mTOR target genes identified thus far currently prevents a full appreciation of the importance of the potential role of mTOR as a transcriptional regulator.

Estrogen-related receptor α (ERRα, NR3B1) is an orphan nuclear receptor identified through sequence similarities with that of the estrogen receptor (Giguère et al., 1988). In the absence of a known ligand, ERRα activity is modulated through interaction with cofactors such as PGC-1α and β, RIP140 and Prox1 (Deblois and Giguère, 2011; Villena and Kralli, 2008). The identification of the first ERRα target gene, *Acadm,* encoding medium-chain acyl coenzyme A, suggested a potential role for ERRα in the control of lipid metabolism (Sladek et al., 1997a; Vega and Kelly, 1997). Mice lacking ERRα are lean and resistant to weight gain under a high-fat diet (Luo et al., 2003). Furthermore, several studies demonstrated ERRα as a major regulator of mitochondrial function and glucose homeostasis (Eichner and Giguère, 2011; Giguere, 2008a). These observations have reinforced the concept that ERRα is an essential factor in the control of energy metabolism and has been proposed as a

therapeutic target for the treatment of metabolic disorders such as diabetes (Giguere, 2008a; Patch et al., 2011b).

While mTOR and ERRα are considered as key regulators of metabolism, particularly in mitochondrial function and lipid homeostasis, it is currently unknown to which extent the two signaling pathways intersect. Herein, we first demonstrate that mTOR, in a manner analogous to ERRα, targets metabolic genes on a genome-wide scale. mTOR is then shown to positively regulate ERRα expression and activity via transcriptional control of the ubiquitin pathway. We further show that the mTOR/ERRα axis is of physiological significance as it plays a key role in the development of rapamycin-induced NAFL.

RESULTS

ChIP-sequencing reveals a molecular network linking mTOR and ERRα to the TCA cycle and lipid metabolism

We first sought to explore whether mTOR plays a global or more restricted role as a transcriptional regulator and to investigate its potential interplay with the ERRα regulatory pathway. Two independent mTOR and ERRα ChIP-sequencing analyses were performed using chromatin obtained from mouse livers (Supplemental Tables S1 and S2). Analysis of the datasets revealed 9469 peaks bound by mTOR. The distribution of these binding events across the genome is shown in Figure 1A. Considering a likely role of mTOR as a transcriptional regulator of pol III genes, we initially

investigated the extent of mTOR recruitment to pol III-driven genes by comparing our mTOR ChIP-seq dataset with a recently published pol III ChIP-seq dataset (Carriere et al., 2012). Comparison of the two datasets revealed that 44% of the pol III bound RNA-encoding genes are also bound by mTOR with a preference for co-localization in intergenic regions (Figure S1A). Our analysis demonstrates a striking preference for shared pol III/mTOR occupancy of 4.5S RNAs (100%) and tRNAs (76%) compared to SINEs (3%) (Table S3). Standard ChIP analysis validates that mTOR is indeed recruited to different classes of RNA-encoding genes bound by pol III (Figure S1B and C). Next, we examined the mTOR ChIP-seq dataset for mTOR binding to pol II-transcribed genes. Standard ChIP analysis validation of a subset of these genes is shown in Figure S2A. 4055 of the 9469 mTOR bound peaks which are associated with 54% (2969) of the unique genes identified are found within +/- 10 kb of the transcriptional start sites (TSSs) of genes (Figure 1B). These binding events have a strong preference for a region surrounding +/- 1kb of TSSs of genes (Figures 1B and S2B). Ingenuity Pathway Analysis (IPA) software analysis of mTOR target genes revealed a strong enrichment in physiological functions related to protein metabolism and turnover. More specifically, mTOR targets the protein ubiquitination pathway, assembly of RNA pol III complex and tryptophan metabolism (Figure 1C). In addition, we found a significant enrichment of genes involved in the PI3K/AKT, Wnt/β-catenin and insulin receptor signaling pathways. These results are consistent with the described role of mTORC1 in protein synthesis and

molecular pathways known to be connected to mTORC1 signaling (Dellinger et al., 2012; Zhou et al., 2011; Zoncu et al., 2011). In addition, mTOR is significantly recruited at genes involved in oxidative phosphorylation (OXPHOS) (Figure 1C). Prototypic binding profiles illustrating mTOR recruitment to *Polr3e*, a component of RNA polymerase III, *Pten* and *Tsc1* whose gene products are crucial to the PI3K/AKT/mTOR signaling pathway, and *Cox5b* encoding an enzyme of the mitochondrial respiratory chain, are shown in Figure 1D. Known and *de novo* motif finding analyses were performed on the entire mTOR ChIP-seq dataset, as well as using binding peaks restricted to within +/- 10 kb and +/- 1 kb of the TSSs of genes. However, we were unable to identify with high confidence a consensus motif specifically associated with mTOR binding events.

Mouse liver ERRα ChIP-seq analyses identified 23226 peaks significantly enriched for the sequence TCAAGGTCA, the known ERRα consensus binding motif (Sladek et al., 1997a) (Figure S3A). Nearly 50% of the peaks were found within intronic regions with a substantial preference for the first intron close to the TSS (Figures S3A and B). 8077 of the ERRα bound peaks are found within +/- 10kb of the TSSs of genes corresponding to 43% (2373) of the unique genes identified (Figure S3C). Next, we investigated the potential cross-talk between ERRα and mTOR by comparing the two ChIP-seq datasets. Our analysis revealed a non-significant overlap in binding peaks (175) implying that ERRα and mTOR

do not interact physically with each other on DNA (Figure 1E). In contrast, the comparative study revealed that a significantly large proportion of genes (3687, ~2/3 of the mTOR target genes) are commonly targeted by ERRα and mTOR, indicating that these factors regulate common biological functions. As shown in Figure 1F, IPA analysis revealed a large number of targets shared by ERRα and mTOR involved in metabolic processes including OXPHOS, TCA cycle, glycolysis/gluconeogenesis and lipid metabolism.

We next sought to determine the impact of mTOR and ERRα signaling on the hepatic expression of a subset of these genes involved in the TCA cycle and lipogenesis (Figure 2A). Interestingly, our results uncovered three different classes of genes based on their response to rapamycin inhibition of mTOR and/or ablation of ERRα. First, we identified genes that are only affected by the loss of ERRα that includes *Sdhd* and *Suclg2* whose gene products are enzymes of the TCA cycle (Figure 2B). Second, *Gpam* and *Elovl6,* whose gene products are implicated in the lipogenic pathway, were classified as being only sensitive to rapamycin (Figure 2C). Rapamycin treatment resulted in increased mRNA levels of these two genes irrespective of the genotype of the mice. Finally, *Sdhb* and *Fasn,* whose gene products are involved in the TCA cycle and lipid biosynthesis pathway, respectively, were classified based on their responsiveness to both ERRα and mTOR modulation (Figure 2D). In particular, livers of ERRα-null mice were found to have nearly 2.5X more

Fasn levels compared to WT and these mRNA levels nearly doubled again in the presence of rapamycin. The increased *Fasn* transcript levels in ERRα KO mice by rapamycin indicates that other transcription factors could also play a role in the control of this gene. We thus explored the expression levels of several transcription factors associated with ERRα and/or mTOR signaling known to play a role in energy metabolism (Figures 2E and S4). Strikingly, the effects of rapamycin treatment and/or loss of ERRα on *Pparg* expression is similar to that observed for *Fasn* (Figure 2E). Furthermore, while rapamycin treatment did not affect *Srebf1* (encoding Srebp1) levels, those were nearly tripled in ERRα-null mice.

Loss of ERRα activity results in impaired TCA cycle activity and exacerbates rapamycin-induced NAFL

We next explored the biological consequence of the loss of both mTOR and ERRα signaling in mouse liver. First, we examined that impact on TCA cycle activity by quantifying TCA cycle intermediates in liver. To this end, we used a metabolomics approach combining GC/MS (citrate, cis-aconitate, α-oxoglutarate, fumarate and malate) and NMR (succinate) studies to measure six intermediates of the TCA cycle (Figure 3, inside graphs). In addition, the expression level of one gene for every step of the TCA cycle was measured (Figure 3, boxed graphs). Of note, most of these genes belong to the sub-group of genes responding to both rapamycin and the absence of ERRα (Figure 2D). Treatment of wild-type mice with

rapamycin did not significantly affect the levels of the TCA intermediates measured. In contrast, ERRα-null mice exhibit higher levels of citrate and cis-aconitate (Figure 3). Furthermore, rapamycin treatment in ERRα-null mice resulted in increased levels of cis-aconitate and succinate with a trend for higher 2-oxo-glutarate levels compared to untreated ERRα KO mice. Interestingly, intermediates did not accumulate in later stages of the TCA cycle and no further accumulation of citrate was observed. The repressed gene expression profiles in the ERRα KO livers of the enzymes corresponding to the transitions from citrate through to fumarate suggests that the specific metabolite accumulation observed may indicate the outcome of an ERRα-dependent blunted TCA cycle between these steps. Taken together, and again considering that citrate does not accumulate in a rapamycin-dependent fashion, this data suggests that rapamycin treatment in ERRα KO mice results, instead, in increased incorporation of citrate into FFAs.

To test this hypothesis, histological and biochemical analyses were performed on the corresponding livers. Hematoxylin and eosin (H&E) and Oil Red O staining showed the development of larger vesicles and an accumulation of lipids in ERRα KO livers compared to wild-type in response to rapamycin (Figure 4A). The effects of the drug and ERRα genotype on the mTOR signaling pathway and ERRα expression were verified by Western Blot analysis (Figure 4B). As expected, rapamycin treatment strongly reduced the phosphorylation of the ribosomal S6

protein in both genotypes. There were no noticeable differences in basal S6 phosphorylation between the wild-type and the KO mice suggesting that the loss of ERRα does not affect the mTORC1-signaling pathway. Furthermore, we found that the phosphorylation of AKT, a target of mTORC2, was higher in all of the rapamycin treated mice which is consistent with this phenomenon as previously noted in the liver (Sarbassov et al., 2006). Surprisingly, rapamycin treatment in wild-type mice nearly completely abolished ERRα protein levels (Figure 4B), in a manner which cannot be explained by the modest decrease in *Esrra* transcript level (Figure S4). These observations suggest that rapamycin affects ERRα expression most dominantly at the post-translational level. Although no significant difference in basal liver FFAs were identified in ERRα-null livers, ERRα KO mice treated with rapamycin exhibited a greater hepatic FFA content compared to rapamycin treated wild-type mice (Figure 4C). In contrast, no differences in liver cholesterol levels were observed between the four groups (Figure 4D). Taken together with the metabolomic data (Figure 3), these observations indicate that citrate may be reoriented to serve as a substrate for the lipogenesis pathway. To further support this notion, mRNA levels of the gene encoding ATP citrate lyase (*Acly*) which is responsible for converting citrate into acetyl-CoA at the first committed step of the lipogenic pathway, were found to be highest in ERRα-null mice treated with rapamycin (Figure 4E). To further validate our findings that rapamycin treatment in mice deficient in ERRα activity

worsens the development of NAFL, mice were injected with rapamycin and/or compound 29 (C29), a recently developed ERRα inverse agonist (Patch et al., 2011b). Similarly to our observations in mice with a genetic ablation of ERRα, larger vesicles and higher accumulation of lipids were found in livers of co-treated mice (Figure 4F).

mTOR signaling controls ERRα expression and transcriptional activity

The observation that the expression of ERRα is regulated in a rapamycin-sensitive manner led us to investigate the molecular link between mTORC1 signaling and ERRα transcriptional activity. At the mRNA level, treatment of the Hepa 1-6 mouse cell line with siRNAs against mTOR resulted in a modest but significant reduction (~20%) in ERRα transcript levels (Figure 5A). The corresponding Western blot analysis confirmed that silencing mTOR affects both mTORC1 and mTORC2 kinase activities with the observed reduction in S6 and AKT phosphorylation, respectively (Figure 5B). Consistent with what we observed previously in livers of rapamycin treated mice, ERRα protein expression was strongly abrogated in cells lacking mTOR (Figure 5B). Similar results were obtained in a human cell line (HeLa) infected with a shRNA directed against mTOR (Figure 5C). Hepa 1-6 cells treated with rapamycin display a similar

decrease in ERRα mRNA levels to that observed previously with siRNAs against mTOR (Figure 5D). Interestingly, rapamycin treatment also resulted in a strong decrease in ERRα protein levels in these cells (Figure 5E). Next, we sought to determine if the effects of rapamycin on ERRα also altered recruitment of ERRα to its target genes. Indeed, we observed a decrease in ERRα recruitment to its own promoter, *Esrra,* as well as to that of two metabolic targets, *Ogdh* and *Idh3a*, in Hepa 1-6 cells treated with rapamycin (Figure 5F). The ChIP results parallel the reduction in the mRNA levels of these genes in Hepa 1-6 cells (Figure 5G) or mouse liver (Figure 3) exposed to rapamycin. To further validate the influence of mTORC1 on ERRα expression, we tested the effects of manipulating mTORC1 activity by either a genetic approach or physiological stimuli. Constitutive activation of mTORC1 signaling in TSC2-null MEFs results in an increase in ERRα levels (Figure 5H) while inhibition of mTORC1 activity via starvation of Hepa 1-6 cells of either amino acids or glucose abolished ERRα expression in those cells (Figure 5I).

Rapamycin induces ubiquitin/proteasome-mediated ERRα degradation

We next explored the underlying mechanism responsible for the striking decrease in ERRα protein expression in response to rapamycin inhibition of mTOR signaling. We hypothesized that post-translational mechanisms were of importance as the robust decrease in ERRα protein expression

observed after rapamycin treatment cannot be attributed to the modest reduction in mRNA levels alone. To test whether mTOR inhibition contributes to ERRα degradation via a ubiquitin-dependent mechanism, we first examined the effect of mTOR silencing on whole cell protein ubiquitination (Figure 6A). mTOR knock-down resulted in decreased phosphorylation of S6, mTOR and ERRα protein levels associated with a higher amount of ubiquitinated proteins compared to the cells transfected with siCtrl. In the presence of rapamycin, nuclear ERRα disappeared after drug treatment (Figure 6B). Note that rapamycin treatment resulted in decreased P-S6 in both cytoplasmic and nuclear fractions. In parallel, we noticed an accumulation of ubiquitinated proteins in both cellular fractions in response to the mTOR inhibitor. These data indicate that mTOR inhibition leads to an activation of the ubiquitin pathway in hepatocytes. We next determined the turnover of ERRα in hepatocytes. Cycloheximide treatment shows that the ERRα protein has a relatively short half-life (~4 hr) as compared to actin, the levels of which levels remained constant during this time period (Figure 6C). We then asked if inhibiting the proteasome using MG132 can rescue the rapamycin-induced inhibition of ERRα protein expression. Indeed, MG132 treatment of Hepa 1-6 cells results in a significant accumulation of ubiquitinated proteins and leads to ERRα stabilization (Figure 6D) an increase in ubiquitinated ERRα (Figure 6E). Interestingly, MG132 treatment was also found to protect against rapamycin induced ERRα protein degradation and rescued rapamycin

inhibition of S6 phosphorylation (Figure 6F). This result provides further evidence that ERRα is eliminated by the proteasome in a rapamycin-sensitive manner.

Next, we investigated whether mTOR regulates the protein ubiquitination pathway, the most significantly enriched canonical pathway for mTOR ChIP-seq target genes identified by IPA software (Figure 1C). Binding peak profiles of mTOR for the genes *Ubb* and *Stub1*, also known as CHIP, encoding ubiquitin B and an E3-ubiquitin protein ligase, respectively, are shown in Figure 6G. Ubb is involved in the direct process of protein ubiquitination. However, the molecular mechanisms controlling its expression still remain unclear (Chadwick et al., 2012). On the other hand, CHIP plays a key role in targeting chaperone bound substrates for proteasomal degradation. These proteins include the estrogen receptor α and the recently identified CHIP substrate, LKB1, an important kinase involved in the regulation of AMPK activity (Fan et al., 2005; Gaude et al., 2012). To determine whether mTOR regulates the expression of *Ubb* and *Stub1*, we first show that mTOR recruitment to the *Ubb* and *Stub1* genes is rapamycin-sensitive (Figure 6H). Second, Hepa 1-6 cells treated with either siRNAs directed against mTOR (Figure 6I) or rapamycin (Figure 6J) led to an up-regulation in both *Ubb* and *Stub1* expression. Our data indicate that mTOR is a repressor of the protein ubiquitination pathway and that inhibition of mTOR signaling leads to an increase in ubiquitinated proteins including ERRα and, as a consequence, their degradation

mediated by the proteasome. Taken together, our results demonstrate that mTOR signaling controls ERRα degradation by regulating the non-lysosomal ubiquitin/proteasome system at the transcriptional level. A model depicting this process is shown in Figure 6K.

DISCUSSION

In the study, we have investigated the metabolic gene networks controlled by mTOR and ERRα in the liver. ERRα is well-known to play a pivotal role in the control of energy metabolism and, like mTOR, is a potential therapeutic target for the treatment of diabetes and obesity. The work presented herein reveals that mTOR and ERRα bind and control the expression of a large set of both unique and common genes implicated in mitochondrial function and the lipid biosynthesis pathway. Furthermore, we show that rapamycin inhibition of mTOR leads to the degradation of ERRα through a proteasome-dependent mechanism, indicating that ERRα is integrated into the mTOR signaling pathway as a downstream mediator. The finding that rapamycin represses ERRα expression provides an additional molecular link between mTOR and ERRα in the control of energy metabolism. Our data suggest that the metabolic side effects that occur in response to rapamycin treatment are mediated in part through the reduction in ERRα expression. The physiological relevance of this finding is that the complete absence or pharmacological inhibition of ERRα activity exacerbates the development of rapamycin-induced NAFL. A

model highlighting the mechanisms and physiological implications of these findings is presented in Figure 7.

The absence of ERRα in mouse liver results in a significant dysregulation of the expression of genes involved in the TCA cycle and lipogenic pathways. The combination of rapamycin and loss of ERRα activity results in a truncated TCA cycle directing citrate to be used as a preferential substrate for the synthesis of lipids associated with the increase in *Fasn* and *Acly* levels. A defect in glucose handling or redistribution of lipids from adipose storage to the liver could also play a role in the observed lipid accumulation in response to rapamycin treatment. Although ERRα is recruited to and can regulate genes of the glycolysis/gluconeogenesis pathway, and loss of ERRα correlates with improved insulin sensitivity and glucose tolerance in rodent models (Charest-Marcotte et al., 2010b; Dufour et al., 2011; Patch et al., 2011b), absence of ERRα had no effect on rapamycin-induced glucose intolerance in mice (data not shown). In addition, rapamycin has been shown to reduce lipoprotein lipase-mediated lipid clearance from white adipose tissue and decrease TAG secretion from the liver (Blanchard et al., 2012). Thus, exacerbation of NAFL observed in our co-treated mice is most likely based primarily on *de novo* lipid biosynthesis in the liver.

The mTOR-signaling pathway is one of the major molecular mechanisms controlling protein synthesis and energy metabolism. Recent studies have attributed a nuclear function to mTOR in the transcriptional

control of metabolic genes and protein synthesis. However, only a few target genes have been identified to date and the physiological pathways governed by this novel transcriptional mechanism remained largely unknown. To help elucidate the role of mTOR in gene regulation, ChIP-seq analyses of mTOR were performed in mouse liver. Our data shows that mTOR specifically targets a large subset of pol III-transcribed genes (e.g tRNAs and 4.5S RNAs), supporting its role in protein translation. In addition, mTOR targets a wide-range of pol II-driven gene programs involved in immune signaling, insulin receptor signaling, cancer signaling pathways, the ubiquitin/proteasome pathway as well as OXPHOS and fatty acid metabolism. The mechanisms by which mTOR regulates transcription of these gene networks remains to be elucidated. However, it has been previously shown that mTOR can act as a transcriptional cofactor through phosphorylation of specific transcription factors (e.g. MAF1 and YY1) (Blattler et al., 2012a; Shor et al., 2010). The observation that a clear consensus motif associated with mTOR binding events in the mouse liver genome could not be identified with high confidence supports the concept that mTOR is a pluripotent cofactor that does not work with a specific DNA-binding transcription factor.

Our results demonstrate that ERRα is a nuclear receptor functioning downstream of the mTOR signaling pathway and may participate in the mTOR-dependent response towards nutrient availability and energy sensing. We show that rapamycin treatment, which is known

to mimic amino acid-like starvation (Peng et al., 2002), modulates ERRα metabolic target genes (e.g. *Idh3a* and *Ogdh*), supporting a role for ERRα as a component of the mTOR signaling pathway. However, it is clear that many genes were affected solely by the rapamycin treatment and were not dependent on the presence or absence of ERRα. These results indicate that other pathways are involved in the hepatic lipidemia appearance. Among them, it is well known that mTOR controls energy metabolism through the regulation of SREBP-1. *In vitro* analyses report an increase in SREBP-1 activity along with the induction of lipogenic genes in a mTORC1 and AKT-dependent manner (Porstmann et al., 2008; Yamauchi et al., 2011). Likewise, studies using adipocyte cell lines demonstrated that mTOR inhibition reduced the mRNA and protein levels of PPARγ. In our work, although rapamycin treatment triggered *Pparg* expression, it did not affect *Srebp1* expression despite a higher level of P-AKT. These results are consistent with published data obtained from adipose tissues of rats treated with rapamycin (Blanchard et al., 2012). Interestingly, we found that ERRα-null mice display a strong basal elevation in *Pparg* and *Srebp1* expression that could collectively participate in the induction of the lipogenic program observed following rapamycin administration in these mice. YY1 is also another important transcription factor shown to play a role in the development of rapamycin-induced diabetic-like syndrome. Rapamycin treatment induces dephosphorylation of YY1, a direct target of mTOR kinase activity in the nucleus, leading to a reduction in the

expression of genes involved in the insulin/IGF signaling (Blattler et al., 2012a; Blattler et al., 2012b). On the other hand, loss of YY1 protects against rapamycin-induced insulin resistance (Blattler et al., 2012a). Since our data also demonstrate a protective role of ERRα in rapamycin-induced NAFL, it would be of interest to dissect the possible crosstalk between ERRα and YY1 in the liver.

An unanticipated finding of our study is that rapamycin regulates ERRα activity by targeting the receptor for degradation. Our results demonstrate that ERRα is degraded by the non-lysosomal ubiquitin/proteasome system in response to rapamycin and that this effect can be reversed by the proteasome inhibitor MG132. In particular, ChIP-seq and functional analyses revealed that mTOR is recruited to a significant number of genes involved in this process and show that it can repress a subset of these genes, providing a molecular mechanism for the observed rapamycin-induced ERRα degradation in the proteasome. Indeed, rapamycin inhibition of mTOR can promote ubiquitin-conjugation and the degradation of proteins such as Cyclin D1/3 and nitric oxide synthetase (iNOS) (Chotechuang et al., 2011; Dong et al., 2005; Garcia-Morales et al., 2006; Harston et al., 2011; Jin et al., 2009). Our work now directly implicates mTOR in this process as a negative transcriptional regulator of the ubiquitination pathway and, together with its known repressive action on autophagy (Codogno and Meijer, 2005; Kim et al., 2011; Yu et al., 2010b), enhances its ability to repress protein degradation.

Results presented in our report have an important clinical relevance, as analogs of rapamycin (e.g. sirolimus) are commonly used to treat cancer or as immuno-suppressants to help prevent the rejection of organ transplants (Geissler et al., 2008; McMahon et al., 2011; Yuan et al., 2009). A significant number of patients treated with these molecules develop associated side effects including insulin resistance and hepatic hyperlipidemia also referred to as a diabetes-like syndrome (Houde et al., 2010; Levy et al., 2006; Morrisett et al., 2002). Therefore, a better control of glucose homeostasis in these rapamycin-treated individuals has been proposed, in particular by employing antidiabetic drugs as therapeutic strategies to prevent rapalog-induced diabetes (Blattler et al., 2012a; Yang et al., 2012). Prior to this study, the use of selective ERRα antagonists to improve insulin sensitivity (e.g. compound 29) may have been considered to help counteract these side effects (Handschin and Mootha, 2005; Patch et al., 2011b). However, genetic and pharmacologic evidence presented herein suggest that treating patients with agents inhibiting ERRα, in combination with mTOR inhibitors, would exacerbate the development of NAFL. Therefore, considering that ERRα-dependent control of metabolic gene programs is rapamycin-sensitive, strategies aimed at enhancing rather than repressing ERRα activity appears to be a viable therapeutic avenue to relieve hepatic hyperlipidemia and steatosis observed in patients treated with mTOR inhibitors.

EXPERIMENTAL PROCEDURES

Animals

Two- to 3-month old male wild-type and ERR$\alpha^{-/-}$ mice in a C57BL/6J genetic background were housed and fed standard chow in an animal facility at McGill University. Mice were administered daily with 10 mg/kg of rapamycin (LC Laboratories, R-5000) and/or 10 mg/kg of Compound 29 or vehicles by intraperitoneal injections for a period of 7 or 10 days as previously described (Patch et al., 2011b; Sarbassov et al., 2006). For all experiments, livers were isolated from mice (n=8-9) sacrificed by cervical dislocation at Zeitgeber time (ZT) 4. All manipulations were performed in accordance with the McGill Facility Animal Care Committee and the Canadian Council on Animal Care.

Cell culture and reagents

Hepa 1-6, HeLa, TSC2$^{+/+}$ and TSC2$^{-/-}$ MEFS (Pollizzi et al., 2009) were cultured in Dulbecco's modified Eagle's medium (DMEM) supplemented with 10% FBS, sodium pyruvate, L-glutamine, and antibiotics and were maintained in 5% CO_2 at 37°C. Cells were treated with 80 nM rapamycin (Calbiochem, 553211), 100 µg/ml cycloheximide (Sigma-Aldrich, C4859) or 20 µM MG132 (Calbiochem, 474791). For rescue experiments, MG132 was added 24 hr post rapamycin addition and cells were collected 24 hr later. For nutrients and serum supplementations, cells were cultured in minimum essential medium (MEM) for 48 hr and then the media was

changed for complete DMEM or lacking glucose (Invitrogen, 11966-025) or amino acids (Deval et al., 2008) for a period of 24 hr.

Biochemistry measurements

Hepatic lipids were extracted by homogenization of 100 mg of liver powder with 2 mL of CM buffer (2 volumes of chloroform/1 volume of methanol) with shaking for 15 min at room temperature (RT). After centrifugation at 10,000×g for 10 min, supernatants were collected and 0.2 volumes of 0.9% NaCl were added. FFAs in liver were assessed by using a triglyceride assay kit (Cayman chemical, 10010303-96). Total cholesterol was measured using a Cholesterol/Cholesteryl Ester Quantification Kit (Abcam, ab65359).

Metabolomics Analysis

Metabolomics studies were performed at the Metabolomics Core Facility at McGill University. Briefly, metabolites were extracted from pulverized liver samples using modified Folch extraction. NMR data were acquired on a 500MHz Inova NMR system whereas GC/MS data were collected on an Agilent 7693MSD (both from Agilent Technologies). See online supplemental experimental procedures for further details.

Standard ChIP and ChIP-sequencing

For ChIP-based experiments, specific ERRα (Epitomics, 2131-1) and

mTOR (Abcam, ab32028) antibodies were used and an anti-rabbit IgG antibody (Santa Cruz, sc-2027) as a control. For ChIP-seq studies, mouse liver chromatin and protein A Dynabeads (Invitrogen) were utilized. ChIP-seq DNA libraries, sequencing and peak identification were performed at the Génome Québec Innovation Centre. ChIP-seq bed files have been deposited in the NCBI Gene Expression Omnibus. ERRα and mTOR ChIP enrichments were quantified by qPCR analysis using specific primers and normalized to the average enrichments obtained using 2 control primer sets amplifying non ERRα and mTOR bound genomic regions (Supplementary Tables S4 and S5). For a more detailed description, see online supplemental experimental procedures.

Binding Motif Analyses

In vivo binding sequences from mTOR and ERRα mouse liver ChIP-seq peak files were retrieved from UCSC Genome Database (mm9, July 2007). Unbiased motif analysis was performed using HOMER (Heinz et al., 2010) to identify statistically overrepresented motifs using default parameters.

Ingenuity Pathways Analysis of ChIP-seq Target Genes

Analysis of mTOR and ERRα ChIP-seq target genes found within +/- 10 kb of the TSS's of genes for significant biological pathways was done using Ingenuity Pathways Analysis software (Ingenuity® Systems,

www.ingenuity.com). Canonical pathways analysis identified significant pathways for the Ingenuity's Pathways Analysis library of canonical pathways. Fisher's exact test was used to calculate p-values determining the probability that the association between genes in the dataset and the canonical pathway is explained by chance alone.

RNA Isolation, Reverse Transcription and qRT-PCR

Total RNA from cells and liver was isolated using the RNeasy Mini Kit (Qiagen). cDNA was made from 2 μg of RNA by reverse transcription with Oligo(dT) primer, dNTPs, 5X 1st strand buffer, DTT, RNase inhibitor, and Superscript II RNase H Reverse Transcriptase (Invitrogen). cDNA was amplified by qRT-PCR using specific primers (Supplemental Table S6), a QuantiTect SYBR Green PCR Kit (Qiagen) and a LightCycler instrument (Roche) following the Qiagen software protocol.

Histology, Immunoprecipitation and Western Blotting, **siRNA and Lentiviral shRNA Silencing**

See online supplemental experimental procedures.

SUPPLEMENTAL INFORMATION

Supplemental information includes 4 Figures, 6 Tables, and Supplemental Experimental Procedures and References.

ACKNOWLEDGMENTS

The authors are grateful to Dr. Fafournoux (INRA de Theix, France) for the gift of media with and without amino acids. We thank Dr. Kwiatkowski (Harvard Medical School, Massachusetts) for the gift of $TSC2^{-/-}$ MEFs. We acknowledge members of the histology core facility of the Goodman Cancer Research Centre (GCRC) at McGill University. We thank C. Ouellet for mouse husbandry, M. Caron for bioinformatics analyses, M. Ghahremani for technical assistance and D.W.K. Tsang, B.D. Fonseca and G. Deblois for helpful discussions. NMR experiments were recorded at the Québec/Eastern Canada High Field NMR Facility, supported by the Natural Sciences and Engineering Research Council of Canada, the Canada Foundation for Innovation (CFI), the Ministère de la recherche en science et technologie du Québec. We thank Dr. Daina Avizonis of the Metabolomic core facility of the GCRC, also funded by the CFI. This work was supported by grants from the Canadian Institutes for Health Research (MOP-84227, MOP-111144) and a Program Project Grant from the Terry Fox Foundation (TFF-116128) to V.G. and N.S. The authors declare no conflict of interest.

Averous, J., and Proud, C.G. (2006). When translation meets transformation: the mTOR story. Oncogene *25*, 6423-6435.

Bachmann, R.A., Kim, J.H., Wu, A.L., Park, I.H., and Chen, J. (2006). A nuclear transport signal in mammalian target of rapamycin is critical for its cytoplasmic signaling to S6 kinase 1. J Biol Chem *281*, 7357-7363.

Blanchard, P.G., Festuccia, W.T., Houde, V.P., St-Pierre, P., Brule, S., Turcotte, V., Cote, M., Bellmann, K., Marette, A., and Deshaies, Y. (2012). Major involvement of mTOR in the PPARγ-induced stimulation of adipose tissue lipid uptake and fat accretion. J Lipid Res *53*, 1117-1125.

Blattler, S.M., Cunningham, J.T., Verdeguer, F., Chim, H., Haas, W., Liu, H., Romanino, K., Ruegg, M.A., Gygi, S.P., Shi, Y.*, et al.* (2012a). Yin Yang 1 deficiency in skeletal muscle protects against rapamycin-induced diabetic-like symptoms through activation of insulin/IGF signaling. Cell Metab *15*, 505-517.

Blattler, S.M., Verdeguer, F., Liesa, M., Cunningham, J.T., Vogel, R.O., Chim, H., Liu, H., Romanino, K., Shirihai, O.S., Vazquez, F.*, et al.* (2012b). Defective mitochondrial morphology and bioenergetic function in mice lacking the transcription factor YY1 in skeletal muscle. Mol Cell Biol *ePub June 18 2012*.

Carriere, L., Graziani, S., Alibert, O., Ghavi-Helm, Y., Boussouar, F., Humbertclaude, H., Jounier, S., Aude, J.C., Keime, C., Murvai, J.*, et al.* (2012). Genomic binding of Pol III transcription machinery and relationship with TFIIS transcription factor distribution in mouse embryonic stem cells. Nucleic Acids Res *40*, 270-283.

Chadwick, L., Gentle, L., Strachan, J., and Layfield, R. (2012). Review: unchained maladie - a reassessment of the role of Ubb(+1) -capped polyubiquitin chains in Alzheimer's disease. Neuropathol Appl Neurobiol *38*, 118-131.

Charest-Marcotte, A., Dufour, C.R., Wilson, B.J., Tremblay, A.M., Eichner, L.J., Arlow, D.H., Mootha, V.K., and Giguere, V. (2010a). The homeobox protein Prox1 is a negative modulator of ERR{alpha}/PGC-1{alpha} bioenergetic functions. Genes & development *24*, 537-542.

Chotechuang, N., Azzout-Marniche, D., Bos, C., Chaumontet, C., Gaudichon, C., and Tome, D. (2011). Down-regulation of the ubiquitin-proteasome proteolysis system by amino acids and insulin involves the adenosine monophosphate-activated protein kinase and mammalian target of rapamycin pathways in rat hepatocytes. Amino Acids *41*, 457-468.

Cunningham, J.T., Rodgers, J.T., Arlow, D.H., Vazquez, F., Mootha, V.K., and Puigserver, P. (2007). mTOR controls mitochondrial oxidative function through a YY1-PGC-1α transcriptional complex. Nature *450*, 736-740.

Deblois, G., and Giguere, V. (2011). Functional and physiological genomics of estrogen-related receptors (ERRs) in health and disease. Biochimica et biophysica acta *1812*, 1032-1040.

Dellinger, T.H., Planutis, K., Tewari, K.S., and Holcombe, R.F. (2012). Role of canonical Wnt signaling in endometrial carcinogenesis. Expert Rev Anticancer Ther *12*, 51-62.

Deval, C., Talvas, J., Chaveroux, C., Maurin, A.C., Mordier, S., Cherasse, Y., Parry, L., Carraro, V., Jousse, C., Bruhat, A.*, et al.* (2008). Amino-acid limitation induces the GCN2 signaling pathway in myoblasts but not in myotubes. Biochimie *90*, 1716-1721.

Dong, J., Peng, J., Zhang, H., Mondesire, W.H., Jian, W., Mills, G.B., Hung, M.C., and Meric-Bernstam, F. (2005). Role of glycogen synthase kinase 3β in rapamycin-mediated cell cycle regulation and chemosensitivity. Cancer Res *65*, 1961-1972.

Dufour, C.R., Levasseur, M.-P., Pham, N.H.H., Eichner, L.J., Wilson, B.J., Charest-Marcotte, A., Duguay, D., Poirier-Héon, J.-F., Cermakian, N., and Giguère, V. (2011). Genomic convergence among ERRα, Prox1 and Bmal1 in the control of metabolic clock outputs. PLoS Genet *7*, e1002143.

Eichner, L.J., and Giguère, V. (2011). Estrogen-related receptors (ERRs): a new dawn in the control of mitochondrial gene networks. Mitochondrion *11*, 544-552.

Fan, M., Park, A., and Nephew, K.P. (2005). CHIP (carboxyl terminus of Hsc70-interacting protein) promotes basal and geldanamycin-induced degradation of estrogen receptor-alpha. Mol Endocrinol *19*, 2901-2914.

Garcia-Morales, P., Hernando, E., Carrasco-Garcia, E., Menendez-Gutierrez, M.P., Saceda, M., and Martinez-Lacaci, I. (2006). Cyclin D3 is down-regulated by rapamycin in HER-2-overexpressing breast cancer cells. Mol Cancer Therapeutics *5*, 2172-2181.

Gaude, H., Aznar, N., Delay, A., Bres, A., Buchet-Poyau, K., Caillat, C., Vigouroux, A., Rogon, C., Woods, A., Vanacker, J.M.*, et al.* (2012). Molecular chaperone complexes with antagonizing activities regulate stability and activity of the tumor suppressor LKB1. Oncogene *31*, 1582-1591.

Geissler, E.K., Schlitt, H.J., and Thomas, G. (2008). mTOR, cancer and transplantation. Am J Transplant *8*, 2212-2218.

Giguere, V. (2008a). Transcriptional control of energy homeostasis by the estrogen-related receptors. Endocr Rev *29*, 677-696.

Giguere, V., Yang, N., Segui, P., and Evans, R.M. (1988). Identification of a new class of steroid hormone receptors. Nature *331*, 91-94.

Gulati, P., Gaspers, L.D., Dann, S.G., Joaquin, M., Nobukuni, T., Natt, F., Kozma, S.C., Thomas, A.P., and Thomas, G. (2008). Amino acids activate mTOR complex 1 via Ca2+/CaM signaling to hVps34. Cell Metab *7*, 456-465.

Gulati, P., and Thomas, G. (2007). Nutrient sensing in the mTOR/S6K1 signalling pathway. Biochem Soc Trans *35*, 236-238.

Handschin, C., and Mootha, V.K. (2005). Estrogen-related receptor α (ERRα): A novel target in type 2 diabetes. Drug Discovery Today: Therapeutic Strategies *2*, 151-156.

Harston, R.K., McKillop, J.C., Moschella, P.C., Van Laer, A., Quinones, L.S., Baicu, C.F., Balasubramanian, S., Zile, M.R., and Kuppuswamy, D. (2011). Rapamycin treatment augments both protein ubiquitination and Akt activation in pressure-overloaded rat myocardium. Am J Physiol Heart Circ Physiol *300*, H1696-1706.

Heinz, S., Benner, C., Spann, N., Bertolino, E., Lin, Y.C., Laslo, P., Cheng, J.X., Murre, C., Singh, H., and Glass, C.K. (2010). Simple combinations of lineage-determining transcription factors prime cis-regulatory elements required for macrophage and B cell identities. Mol Cell *38*, 576-589.

Houde, V.P., Brule, S., Festuccia, W.T., Blanchard, P.G., Bellmann, K., Deshaies, Y., and Marette, A. (2010). Chronic rapamycin treatment causes glucose intolerance and hyperlipidemia by upregulating hepatic gluconeogenesis and impairing lipid deposition in adipose tissue. Diabetes *59*, 1338-1348.

Inoki, K., Kim, J., and Guan, K.L. (2012). AMPK and mTOR in cellular energy homeostasis and drug targets. Annu Rev Pharmacol Toxicol *52*, 381-400.

Jin, H.K., Ahn, S.H., Yoon, J.W., Park, J.W., Lee, E.K., Yoo, J.S., Lee, J.C., Choi, W.S., and Han, J.W. (2009). Rapamycin down-regulates inducible nitric oxide synthase by inducing proteasomal degradation. Biol Pharm Bull *32*, 988-992.

Kantidakis, T., Ramsbottom, B.A., Birch, J.L., Dowding, S.N., and White, R.J. (2010). mTOR associates with TFIIIC, is found at tRNA and 5S rRNA genes, and targets their repressor Maf1. Proc Natl Acad Sci U S A *107*, 11823-11828.

Kim, J., Kundu, M., Viollet, B., and Guan, K.L. (2011). AMPK and mTOR regulate autophagy through direct phosphorylation of Ulk1. Nat Cell Biol *13*, 132-141.

Kim, J.E., and Chen, J. (2000). Cytoplasmic-nuclear shuttling of FKBP12-rapamycin-associated protein is involved in rapamycin-sensitive signaling and translation initiation. Proc Natl Acad Sci U S A *97*, 14340-14345.

Laplante, M., and Sabatini, D.M. (2009). An emerging role of mTOR in lipid biosynthesis. Curr Biol *19*, R1046-1052.

Laplante, M., and Sabatini, D.M. (2012). mTOR Signaling. Cold Spring Harb Perspect Biol *4*.

Levy, G., Schmidli, H., Punch, J., Tuttle-Newhall, E., Mayer, D., Neuhaus, P., Samuel, D., Nashan, B., Klempnauer, J., Langnas, A.*, et al.* (2006). Safety, tolerability, and efficacy of everolimus in de novo liver transplant recipients: 12- and 36-month results. Liver Transpl *12*, 1640-1648.

Luo, J., Sladek, R., Carrier, J., Bader, J.-A., Richard, D., and Giguère, V. (2003). Reduced fat mass in mice lacking orphan nuclear receptor estrogen-related receptor α. Mol Cell Biol *23*, 7947-7956.

McMahon, G., Weir, M.R., Li, X.C., and Mandelbrot, D.A. (2011). The evolving role of mTOR inhibition in transplantation tolerance. J Am Soc Nephrol *22*, 408-415.

Morrisett, J.D., Abdel-Fattah, G., Hoogeveen, R., Mitchell, E., Ballantyne, C.M., Pownall, H.J., Opekun, A.R., Jaffe, J.S., Oppermann, S., and Kahan, B.D. (2002). Effects of sirolimus on plasma lipids, lipoprotein levels, and fatty acid metabolism in renal transplant patients. J Lipid Res *43*, 1170-1180.

Patch, R.J., Searle, L.L., Kim, A.J., De, D., Zhu, X., Askari, H.B., O'Neill, J.C., Abad, M.C., Rentzeperis, D., Liu, J.*, et al.* (2011b). Identification of diaryl ether-based ligands for estrogen-related receptor α as potential antidiabetic agents. J Med Chem *54*, 788-808.

Patsenker, E., Schneider, V., Ledermann, M., Saegesser, H., Dorn, C., Hellerbrand, C., and Stickel, F. (2011). Potent antifibrotic activity of mTOR inhibitors sirolimus and everolimus but not of cyclosporine A and tacrolimus in experimental liver fibrosis. J Hepatol *55*, 388-398.

Pearce, J. (1983). Fatty acid synthesis in liver and adipose tissue. The Proceedings of the Nutrition Society *42*, 263-271.

Peng, T., Golub, T.R., and Sabatini, D.M. (2002). The immunosuppressant rapamycin mimics a starvation-like signal distinct from amino acid and glucose deprivation. Mol Cell Biol *22*, 5575-5584.

Peterson, T.R., Sengupta, S.S., Harris, T.E., Carmack, A.E., Kang, S.A., Balderas, E., Guertin, D.A., Madden, K.L., Carpenter, A.E., Finck, B.N.*, et al.* (2011). mTOR complex 1 regulates lipin 1 localization to control the SREBP pathway. Cell *146*, 408-420.

Pettersson, K., Svensson, K., Mattsson, R., Carlsson, B., Ohlsson, R., and Berkenstam, A. (1996). Expression of a novel member of estrogen response element-binding nuclear receptors is restricted to the early stages of chorion formation during mouse embryogenesis. Mechanisms of development *54*, 211-223.

Pollizzi, K., Malinowska-Kolodziej, I., Doughty, C., Betz, C., Ma, J., Goto, J., and Kwiatkowski, D.J. (2009). A hypomorphic allele of Tsc2 highlights the role of TSC1/TSC2 in signaling to AKT and models mild human TSC2 alleles. Hum Mol Genet *18*, 2378-2387.

Porstmann, T., Santos, C.R., Griffiths, B., Cully, M., Wu, M., Leevers, S., Griffiths, J.R., Chung, Y.L., and Schulze, A. (2008). SREBP activity is regulated by mTORC1 and contributes to Akt-dependent cell growth. Cell Metab *8*, 224-236.

Risson, V., Mazelin, L., Roceri, M., Sanchez, H., Moncollin, V., Corneloup, C., Richard-Bulteau, H., Vignaud, A., Baas, D., Defour, A.*, et al.* (2009). Muscle inactivation of mTOR causes metabolic and dystrophin defects leading to severe myopathy. J Cell Biol *187*, 859-874.

Rosner, M., and Hengstschlager, M. (2008). Cytoplasmic and nuclear distribution of the protein complexes mTORC1 and mTORC2: rapamycin triggers dephosphorylation and delocalization of the mTORC2 components rictor and sin1. Hum Mol Genet *17*, 2934-2948.

Sarbassov, D.D., Ali, S.M., Sengupta, S., Sheen, J.H., Hsu, P.P., Bagley, A.F., Markhard, A.L., and Sabatini, D.M. (2006). Prolonged rapamycin treatment inhibits mTORC2 assembly and Akt/PKB. Mol Cell *22*, 159-168.

Shor, B., Wu, J., Shakey, Q., Toral-Barza, L., Shi, C., Follettie, M., and Yu, K. (2010). Requirement of the mTOR kinase for the regulation of Maf1 phosphorylation and control of RNA polymerase III-dependent transcription in cancer cells. J Biol Chem *285*, 15380-15392.

Sladek, R., Bader, J.-A., and Giguère, V. (1997a). The orphan nuclear receptor estrogen-related receptor α is a transcriptional regulator of the human medium-chain acyl coenzyme A dehydrogenase gene. Mol Cell Biol *17*, 5400-5409.

Sonenberg, N., and Hinnebusch, A.G. (2009). Regulation of translation initiation in eukaryotes: mechanisms and biological targets. Cell *136*, 731-745.

Tsang, C.K., Liu, H., and Zheng, X.F. (2010). mTOR binds to the promoters of RNA polymerase I- and III-transcribed genes. Cell Cycle *9*, 953-957.

Vega, R.B., and Kelly, D.P. (1997). A role for estrogen-related receptor α in the control of mitochondrial fatty acid β-oxidation during brown adipocyte differentiation. J Biol Chem *272*, 31693-31699.

Villena, J.A., and Kralli, A. (2008). ERRα: a metabolic function for the oldest orphan. Trends Endocrinol Metab *19*, 269-276.

Walsh, S., Flanagan, L., Quinn, C., Evoy, D., McDermott, E.W., Pierce, A., and Duffy, M.J. (2012). mTOR in breast cancer: differential expression in triple-negative and non-triple-negative tumors. Breast *21*, 178-182.

Willems, L., Tamburini, J., Chapuis, N., Lacombe, C., Mayeux, P., and Bouscary, D. (2012). PI3K and mTOR signaling pathways in cancer: new data on targeted therapies. Curr Oncol Rep *14*, 129-138.

Wullschleger, S., Loewith, R., and Hall, M.N. (2006). TOR signaling in growth and metabolism. Cell *124*, 471-484.

Yamauchi, Y., Furukawa, K., and Hamamura, K. (2011). Positive feedback loop between PI3K-Akt-mTORC1 signaling and the lipogenic pathway boosts Akt signaling: induction of the lipogenic pathway by a melanoma antigen. Cancer Res *71*, 4989-4997.

Yang, S.B., Lee, H.Y., Young, D.M., Tien, A.C., Rowson-Baldwin, A., Shu, Y.Y., Jan, Y.N., and Jan, L.Y. (2012). Rapamycin induces glucose intolerance in mice by reducing islet mass, insulin content, and insulin sensitivity. J Mol Med *90*, 575-585.

Yu, L., McPhee, C.K., Zheng, L., Mardones, G.A., Rong, Y., Peng, J., Mi, N., Zhao, Y., Liu, Z., Wan, F.*, et al.* (2010b). Termination of autophagy and reformation of lysosomes regulated by mTOR. Nature *465*, 942-946.

Yuan, R., Kay, A., Berg, W.J., and Lebwohl, D. (2009). Targeting tumorigenesis: development and use of mTOR inhibitors in cancer therapy. J Hematol Oncol *2*, 45.

Zhang, X., Shu, L., Hosoi, H., Murti, K.G., and Houghton, P.J. (2002). Predominant nuclear localization of mammalian target of rapamycin in normal and malignant cells in culture. J Biol Chem *277*, 28127-28134.

Zhou, Q., Lui, V.W., and Yeo, W. (2011). Targeting the PI3K/Akt/mTOR pathway in hepatocellular carcinoma. Future Oncol *7*, 1149-1167.

Zoncu, R., Efeyan, A., and Sabatini, D.M. (2011). mTOR: from growth signal integration to cancer, diabetes and ageing. Nat Rev Mol Cell Biol *12*, 21-35

LEGENDS TO FIGURES

Figure 1. ChIP-sequencing identifies mTOR as a transcriptional regulator of diverse signaling and metabolic pathways

(A) Mapping of mouse liver mTOR ChIP-seq peaks across the genome. TTS (transcription termination site) represents binding peaks found -100 bp to + 1kb relative to the nearest TSS.

(B) Histogram illustrating the distribution of mTOR ChIP-seq peaks +/- 10 kb relative to the TSS of the nearest gene. Peaks were combined into 1000 bp bins. Inner histogram shows peaks +/- 1 kb relative to the TSS of the nearest gene. Peaks were combined into 100 bp bins.

(C) Subset of significantly enriched canonical pathways identified by IPA analysis of mTOR ChIP-seq targets found within +/- 10 kb relative to the TSS of the nearest gene.

(D) ChIP-seq binding profiles of the mTOR bound genes *Polr3e, Tsc1*, *Pten* and *Cox5b*.

(E) Venn diagrams illustrating the overlap in number of binding peaks and unique genes identified in the ERRα and mTOR mouse liver ChIP-seq datasets.

(F) Number of ChIP-seq targets bound by either ERRα (red), mTOR (blue) or both (green) within metabolic pathways identified by IPA analysis are shown. *$p < 0.05$.

Figure 2. Cross-talk between mTOR and ERRα in the transcriptional control of the TCA cycle and lipogenesis

(A) Schematic illustrating the ChIP-seq targets bound by either ERRα (red), mTOR (blue) or both (green) implicated in the TCA cycle and lipid biosynthesis.

(B) qRT-PCR analysis of metabolic genes that are ERRα-responsive in livers isolated from WT and ERRα-null mice treated with or without rapamycin for 7 days. Data are normalized to *Hprt* levels. Error bars represent ± SEM. Student's t test, *p < 0.05.

(C) qRT-PCR analysis of metabolic genes that are rapamycin(?)-responsive.

(D) qRT-PCR analysis of metabolic genes that are responsive to both ERRα and mTOR.

(E) qRT-PCR analysis of metabolic transcription factors that are responsive to ERRα and/or mTOR.

Figure 3. Metabolic cross-talk between mTOR and ERRα in the production of TCA cycle intermediates

Quantification of TCA cycle intermediates by either GC/MS or NMR analyses of livers collected from wild-type and ERRα KO mice administered rapamycin (10 mg/kg) or vehicle on a daily basis by intraperitoneal injection during a 7-day period. qRT-PCR analysis was performed on the same livers used for metabolomics studies and one TCA

cycle gene at every step in the cycle is shown as boxed graphs. qRT-PCR data are normalized to *Hprt* levels. Error bars represent ± SEM. Student's t test, *p < 0.05.

Figure 4. Rapamycin-induced NAFL is exacerbated in mice lacking ERRα or by pharmacological inhibition of ERRα

(A) Representative H&E and Oil Red O staining of livers collected from wild-type and ERRα KO mice administered rapamycin (10 mg/kg) or vehicle on a daily basis by intraperitoneal injection during a 7-day period.

(B) Western blot analysis of total ERRα, phospho-S6 kinase (S235/S236) and phospho-AKT (S473) levels in mouse livers collected from wild-type and ERRα KO mice treated with or without rapamycin for 7 days. Actin levels are shown as a loading control.

(C) Measurement of hepatic free fatty acids of wild-type and ERRα-null mice following a 7-day treatment of rapamycin or vehicle. Error bars represent ± SEM. Student's t test, *p < 0.05.

(D) Measurement of hepatic cholesterol of wild-type and ERRα-null mice as in (C).

(E) qRT-PCR analysis of *Acly* levels in mouse livers collected from wild-type and ERRα KO mice treated with or without rapamycin for 7 days. Error bars represent ± SEM. Student's t test, *p < 0.05.

(F) Representative H&E and Oil Red O staining of livers collected from wild-type mice administered rapamycin (10 mg/kg), the ERRα inverse

agonist compound 29 (10 mg/kg) or both on a daily basis by intraperitoneal injection during a 10-day period.

Figure 5. ERRα expression and activity is positively regulated by the mTOR signaling pathway

(A) qRT-PCR expression analysis of *mTOR* and *Esrra* following treatment of Hepa 1-6 cells with a pool of siRNAs against mTOR for 96 hr. Data are normalized to *Hprt* levels. Error bars represent ± SEM. Student's t test, *p < 0.05.

(B) Western blot analysis of total ERRα, mTOR, phospho-S6 kinase (S235/S236) and phospho-AKT (S473) in Hepa 1-6 cells treated with a pool of siRNAs for 96 hr against mTOR. Actin levels are shown as a loading control.

(C) Western blot analysis shows loss of ERRα protein levels in HeLa cells infected with an shRNA targeting mTOR for 72 hr. Actin levels are shown as a loading control.

(D) *Esrra* mRNA expression levels in Hepa 1-6 cells cells treated with 80 nM of rapamycin or vehicle for 48 hr. Data are normalized to *Hprt* levels. Error bars represent ± SEM. Student's t test, *p < 0.05.

(E) Total ERRα, phospho-S6 kinase (S235/S236) and phospho-AKT (S473) protein levels in Hepa 1-6 cells in response to a 48 hr treatment of rapamycin. Actin levels are shown as a loading control.

(F) Standard ChIP analysis of ERRα target genes in Hepa 1-6 cells treated with 80 nM of rapamycin or vehicle as a control for 48 hr.

(G) qRT-PCR analysis of *Esrra*, *Ogdh* and *Idh3a* expression in Hepa 1-6 cells treated with 80 nM of rapamycin or vehicle for 48 hr. Data are normalized to *Hprt* levels. Error bars represent ± SEM. Student's t test, *p < 0.05.

(H) Activation of mTOR signaling in TSC2-null MEFs results in increased ERRα and phospho-S6 kinase (S235/S236) protein levels as determined by Western blot analysis. Actin levels are shown as a loading control.

(I) Western blot analysis shows loss of ERRα and phospho-S6 kinase (S235/S236) protein levels in Hepa 1-6 cells following a 24 hr starvation of total amino acids or glucose. Actin levels are shown as a loading control.

Figure 6. Rapamycin treatment leads to mTOR mediated degradation of ERRα via a ubiquitin/proteasomal-dependent mechanism

(A) Western blot analysis of total ubiquitinated proteins, mTOR, phospho-S6 kinase (S235/S236) and ERRα in Hepa 1-6 cells treated with a pool of siRNAs against mTOR. Actin levels are shown as a loading control.

(B) Western blot analysis of ERRα, phospho-S6 kinase (S235/S236) and ubiquitinated proteins in nuclear and cytoplasmic fractions of Hepa 1-6 cells treated with 80 nM of rapamycin or vehicle for 48 hr. Lamin B1 and tubulin levels are shown as loading controls for nuclear and cytoplasmic fractions, respectively.

(C) Western blot analysis of ERRα expression in Hepa 1-6 cells treated with cycloheximide at the indicated time points. Actin levels are shown as a loading control.

(D) Hepa 1-6 cells were treated with or without the proteasome inhibitor, MG132 (20 μM) for 24 hr. Western blot analysis shows an accumulation of ubiquitinated proteins and ERRα in the presence of MG132. Actin levels are shown as a loading control.

(E) Immunoprecipitation studies show ERRα ubiquitination in Hepa 1-6 cells treated with MG132 for 24 hr. Actin levels are shown as a loading control.

(F) Western blot analysis shows that MG132 treatment rescues rapamycin mediated inhibition of ERRα and phospho-S6 kinase (S235/S236) levels in Hepa 1-6 cells.

(G) ChIP-seq mTOR binding profiles for the genes *Ubb* and *Stub1* (*CHIP*).

(H) Standard ChIP analysis of mTOR target genes in Hepa 1-6 cells treated with 80 nM of rapamycin or vehicle as a control for 48 hr.

(I) Q-RT-PCR analysis of *Ubb* and *Stub1* (*CHIP*) mRNA levels in Hepa 1-6 cells treated with siRNAs against mTOR. Data are normalized to *Hprt* levels. Error bars represent ± SEM. Student's t test, *$p < 0.05$.

(J) Loss of mTOR signaling in Hepa 1-6 cells via rapamycin treatment leads to a reduction in both *Ubb* and *Stub1* (*CHIP*) mRNA levels. Error bars represent ± SEM. Student's t test, *$p < 0.05$.

(K) Schematic representation highlighting the molecular link between rapamycin, mTOR, ERRα and the ubiquitin/proteasome system.

Figure 7. Model illustrating transcriptional crosstalk between mTOR and ERRα and its role in the development and severity of rapamycin-induced NAFL

In a normal liver, mTOR positively regulates ERRα expression by repressing the ubiquitin/proteasome pathway. mTOR and ERRα both regulate the basal transcription of genes controlling the TCA cycle and lipid synthesis pathway. In the presence of rapamycin, repression of mTOR-dependent genes involved in the ubiquitin/proteasome pathway is relieved, leading to the degradation of ERRα. As a consequence, genes regulating lipid synthesis are induced, resulting in the development of NAFL. The complete loss of ERRα expression or inhibition of its activity by C29, in combination with rapamycin treatment results in diminished TCA cycle gene expression and a further increase in lipogenic genes. Our findings suggest a model in which accumulation of citrate from the TCA cycle shuttles into the fatty acid synthesis pathway, leading to the development of an exacerbated fatty liver.

Figure 1

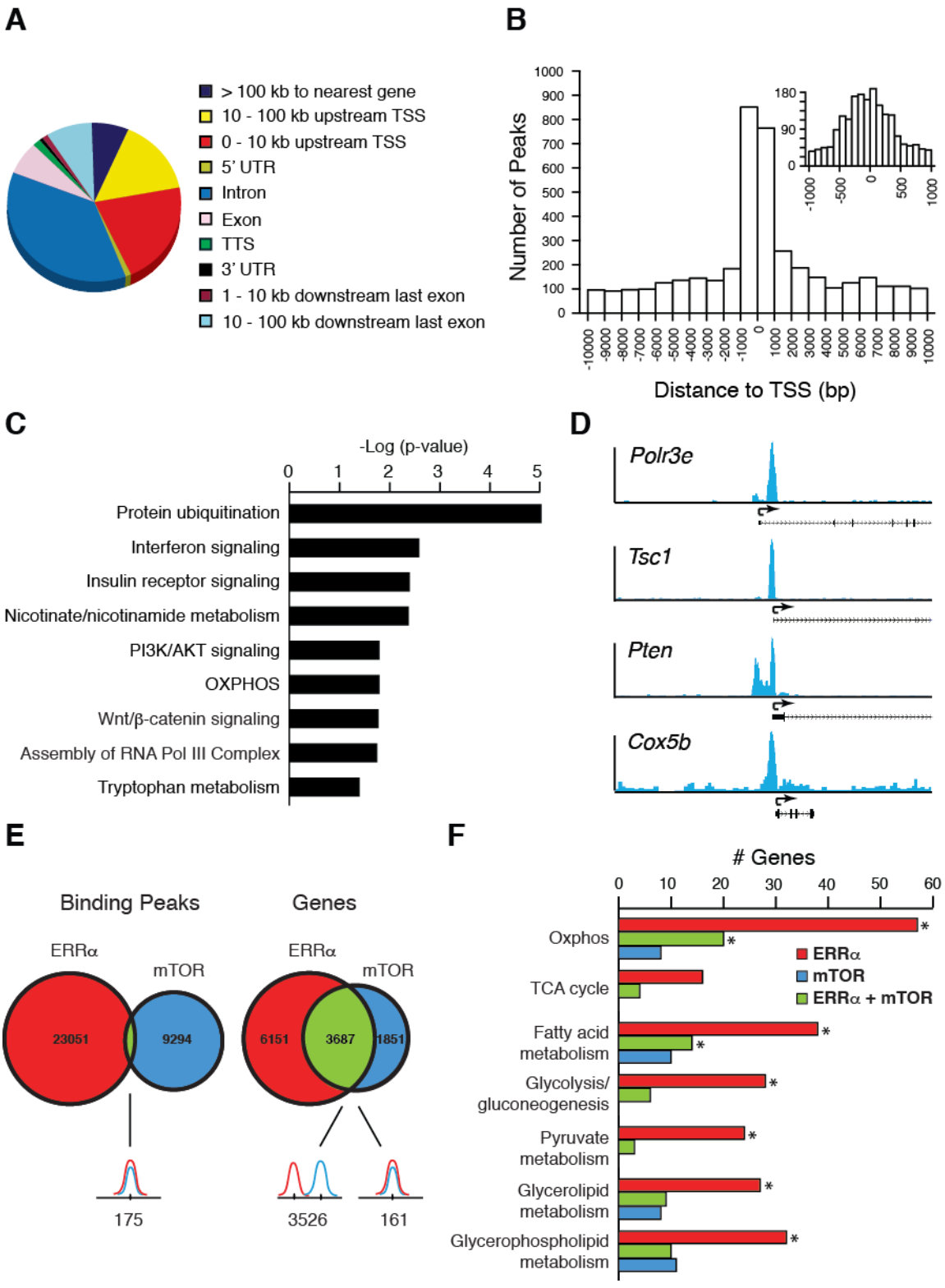
A
> 100 kb to nearest gene
10 - 100 kb upstream TSS
0 - 10 kb upstream TSS
5' UTR
Intron
Exon
TTS
3' UTR
1 - 10 kb downstream last exon
10 - 100 kb downstream last exon
B
Number of Peaks
Distance to TSS (bp)
C
-Log (p-value)
Protein ubiquitination
Interferon signaling
Insulin receptor signaling
Nicotinate/nicotinamide metabolism
PI3K/AKT signaling
OXPHOS
Wnt/β-catenin signaling
Assembly of RNA Pol III Complex
Tryptophan metabolism
D
Polr3e
Tsc1
Pten
Cox5b
E
Binding Peaks
Genes
ERRα
mTOR
23051
9294
6151
3687
1851
175
3526
161
F
Genes
Oxphos
TCA cycle
Fatty acid metabolism
Glycolysis/ gluconeogenesis
Pyruvate metabolism
Glycerolipid metabolism
Glycerophospholipid metabolism
ERRα
mTOR
ERRα + mTOR

Figure 2

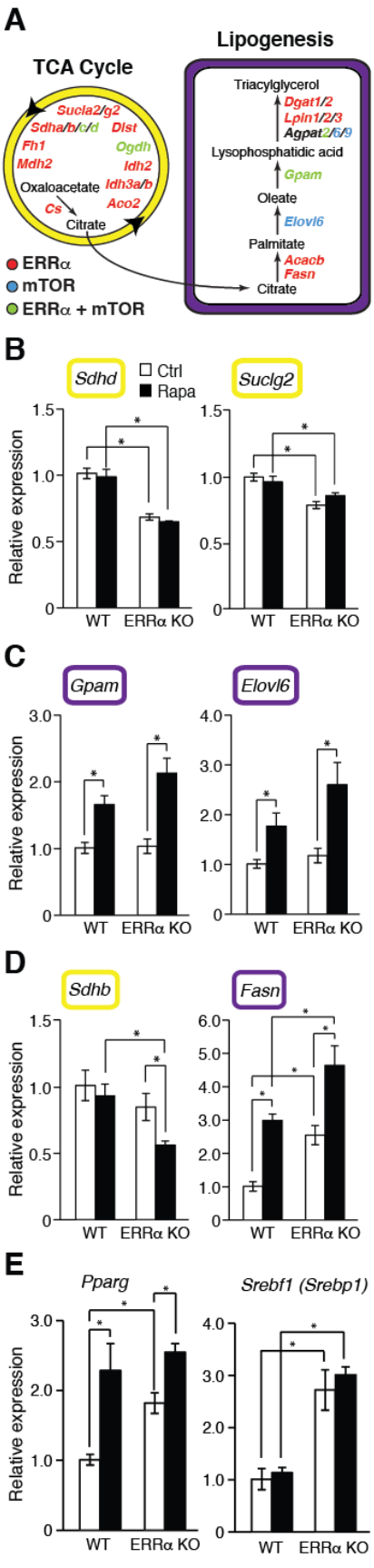
A
Lipogenesis
TCA Cycle
Sucla2/g2
Sdha/b/c/d
Dlst
Fh1
Ogdh
Mdh2
Idh2
Oxaloacetate
Idh3a/b
Aco2
Cs
Citrate
Triacylglycerol
Dgat1/2
Lpin1/2/3
Agpat2/6/9
Lysophosphatidic acid
Gpam
Oleate
Elovl6
Palmitate
Acacb
Fasn
Citrate
ERRα
mTOR
ERRα + mTOR
B
Sdhd
Ctrl
Rapa
Suclg2
Relative expression
WT
ERRα KO
C
Gpam
Elovl6
D
Sdhb
Fasn
E
Pparg
Srebf1 (Srebp1)

Figure 3

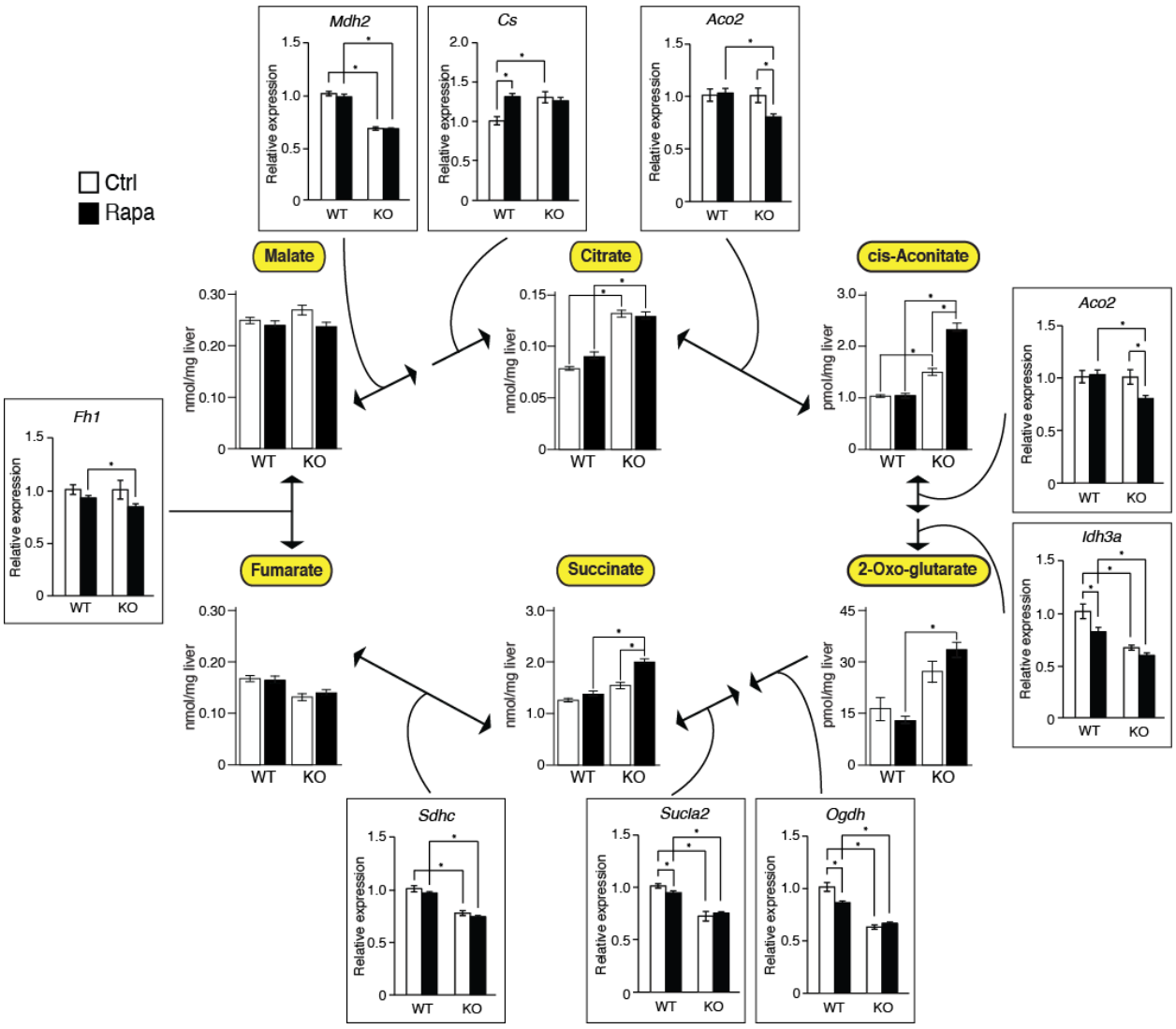
Ctrl
Rapa
Mdh2
Cs
Aco2
Malate
Citrate
cis-Aconitate
Fh1
Aco2
Idh3a
Fumarate
Succinate
2-Oxo-glutarate
Sdhc
Sucla2
Ogdh
Relative expression
nmol/mg liver
pmol/mg liver
WT
KO

Figure 4

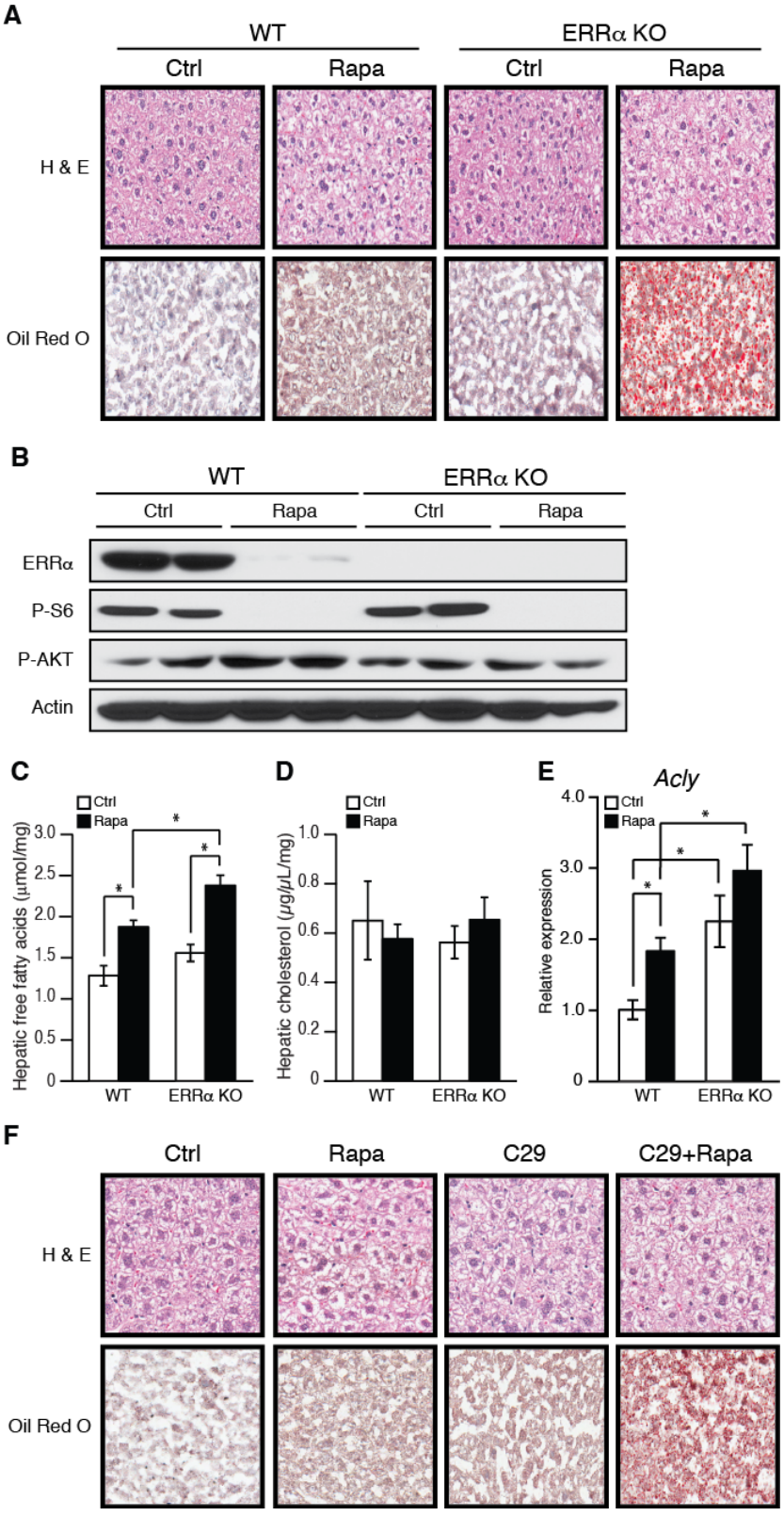
A
WT
ERRα KO
Ctrl
Rapa
Ctrl
Rapa
H & E
Oil Red O
B
WT
ERRα KO
Ctrl
Rapa
Ctrl
Rapa
ERRα
P-S6
P-AKT
Actin
C
Ctrl
Rapa
Hepatic free fatty acids (μmol/mg)
3.0
2.5
2.0
1.5
1.0
0.5
0
WT
ERRα KO
D
Ctrl
Rapa
Hepatic cholesterol (μg/μL/mg)
1.0
0.8
0.6
0.4
0.2
0
WT
ERRα KO
E
Acly
Ctrl
Rapa
Relative expression
4.0
3.0
2.0
1.0
0
WT
ERRα KO
F
Ctrl
Rapa
C29
C29+Rapa
H & E
Oil Red O

Figure 5

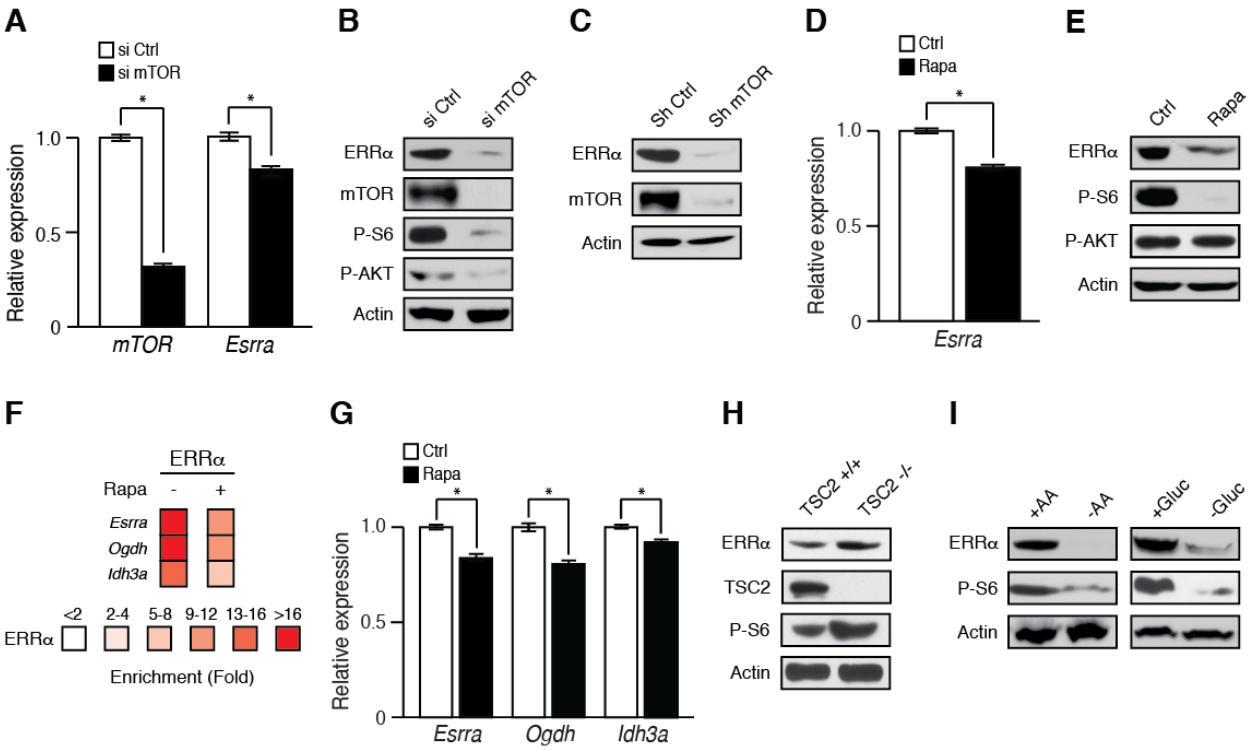
A
si Ctrl
si mTOR
Relative expression
1.0
0.5
0
mTOR
Esrra
B
si Ctrl
si mTOR
ERRα
mTOR
P-S6
P-AKT
Actin
C
Sh Ctrl
Sh mTOR
ERRα
mTOR
Actin
D
Ctrl
Rapa
Relative expression
Esrra
E
Ctrl
Rapa
ERRα
P-S6
P-AKT
Actin
F
ERRα
Rapa
Esrra
Ogdh
Idh3a
<2
2-4
5-8
9-12
13-16
>16
Enrichment (Fold)
G
Ctrl
Rapa
Relative expression
Esrra
Ogdh
Idh3a
H
TSC2 +/+
TSC2 -/-
ERRα
TSC2
P-S6
Actin
I
+AA
-AA
+Gluc
-Gluc
ERRα
P-S6
Actin

Figure 6

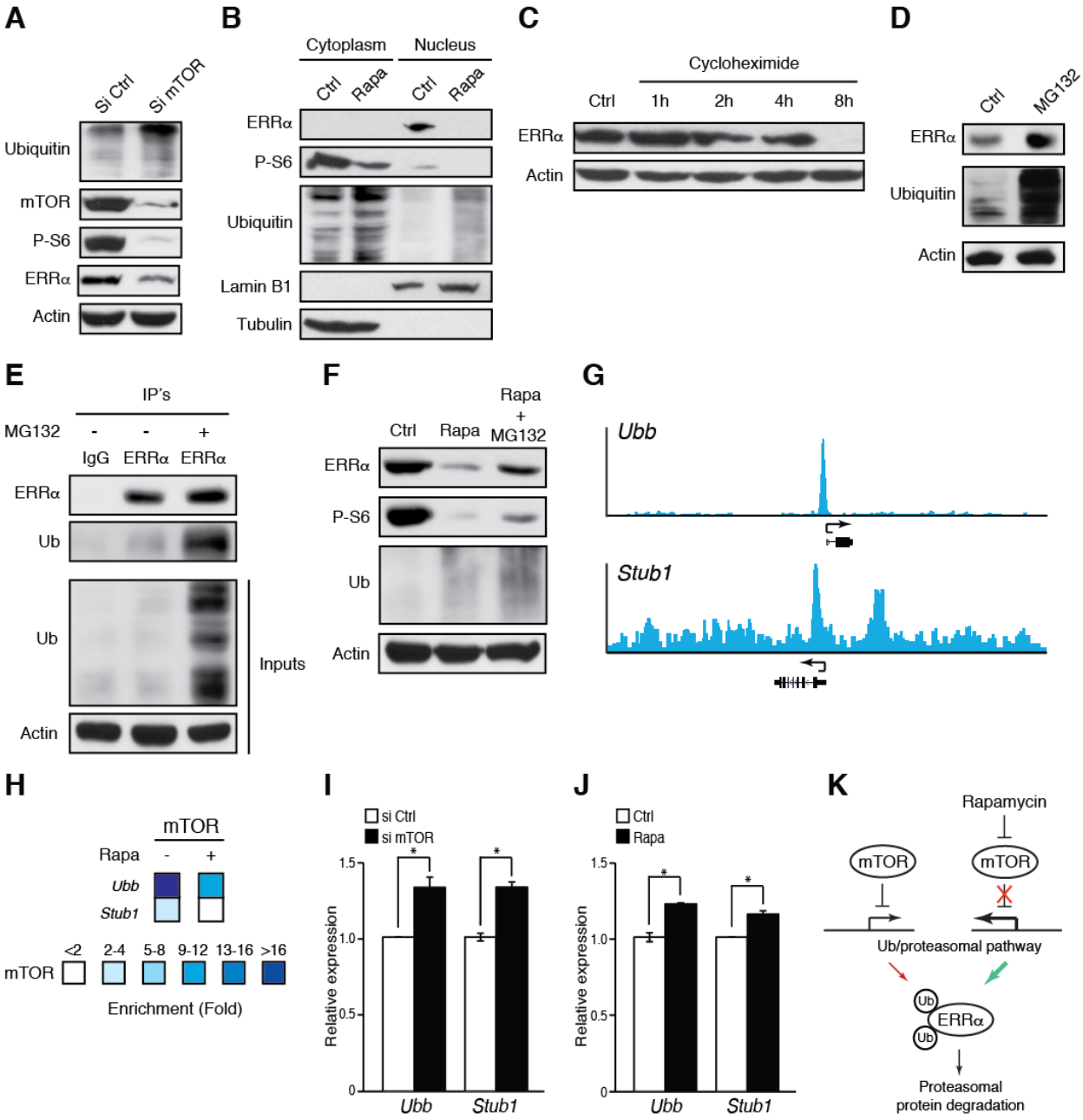
A
Si Ctrl
Si mTOR
Ubiquitin
mTOR
P-S6
ERRα
Actin
B
Cytoplasm
Nucleus
Ctrl
Rapa
Ctrl
Rapa
ERRα
P-S6
Ubiquitin
Lamin B1
Tubulin
C
Cycloheximide
Ctrl
1h
2h
4h
8h
ERRα
Actin
D
Ctrl
MG132
ERRα
Ubiquitin
Actin
E
IP's
MG132
-
-
+
IgG
ERRα
ERRα
ERRα
Ub
Ub
Actin
Inputs
F
Ctrl
Rapa
Rapa + MG132
ERRα
P-S6
Ub
Actin
G
Ubb
Stub1
H
mTOR
Rapa
-
+
Ubb
Stub1
<2
2-4
5-8
9-12
13-16
>16
mTOR
Enrichment (Fold)
I
si Ctrl
si mTOR
Relative expression
1.5
1.0
0.5
0
Ubb
Stub1
J
Ctrl
Rapa
Relative expression
1.5
1.0
0.5
0
Ubb
Stub1
K
Rapamycin
mTOR
mTOR
Ub/proteasomal pathway
Ub
ERRα
Ub
Proteasomal protein degradation

Figure 7

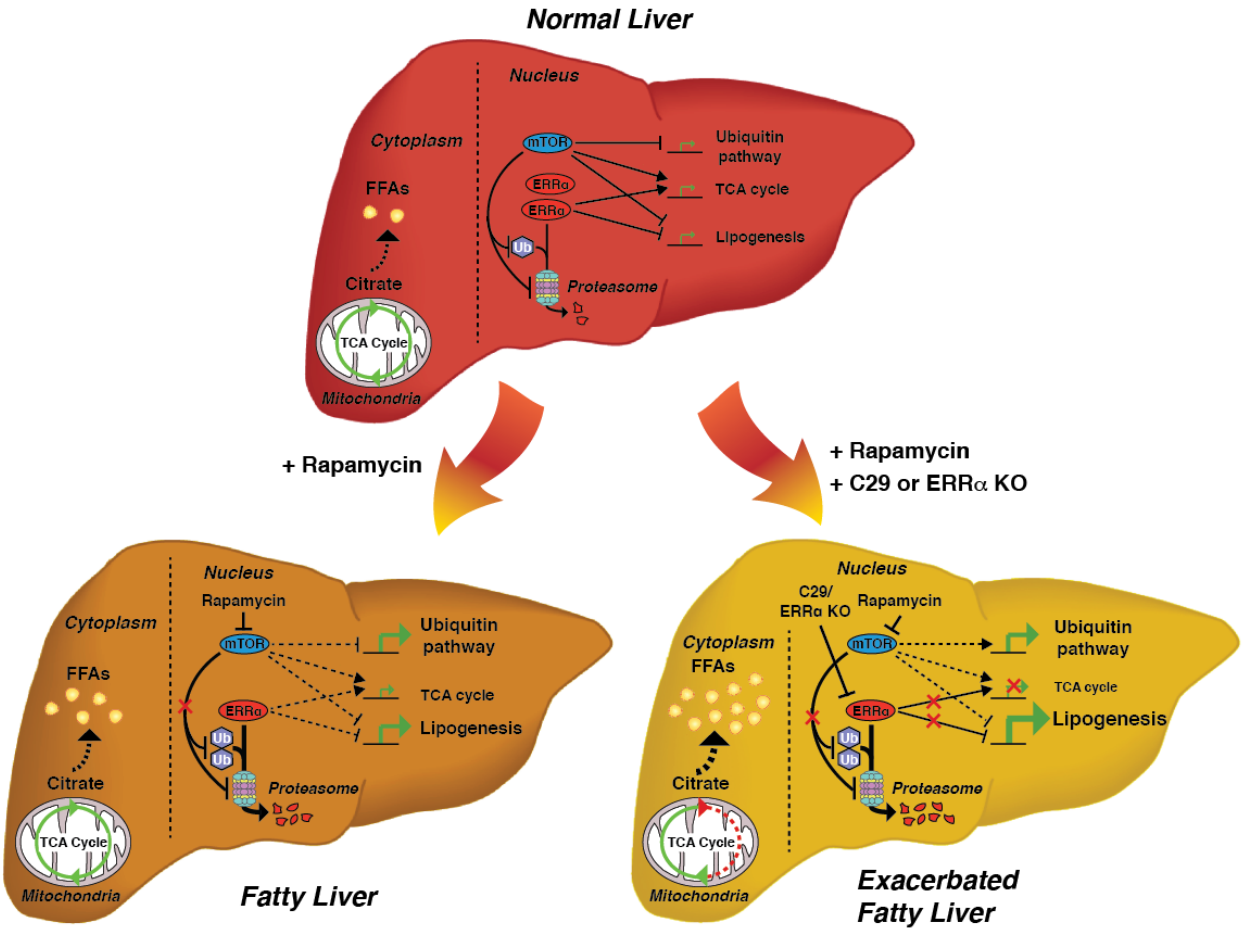
Normal Liver
Nucleus
Cytoplasm
FFAs
Citrate
TCA Cycle
Mitochondria
mTOR
ERRα
ERRα
Ub
Proteasome
Ubiquitin pathway
TCA cycle
Lipogenesis
+ Rapamycin
+ Rapamycin
+ C29 or ERRα KO
Nucleus
Rapamycin
Cytoplasm
FFAs
Citrate
TCA Cycle
Mitochondria
mTOR
ERRα
Ub
Ub
Proteasome
Ubiquitin pathway
TCA cycle
Lipogenesis
Fatty Liver
Nucleus
C29/ ERRα KO
Rapamycin
Cytoplasm
FFAs
Citrate
TCA Cycle
Mitochondria
mTOR
ERRα
Ub
Ub
Proteasome
Ubiquitin pathway
TCA cycle
Lipogenesis
Exacerbated Fatty Liver